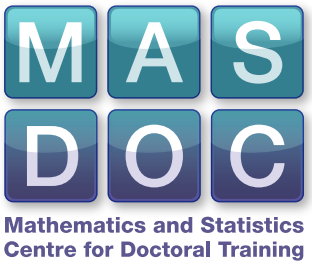

A Diffuse Interface Model of Surfactants in Multi-Phase Flow

by

Oliver Dunbar

Thesis

Submitted for the degree of

Doctor of Philosophy

Mathematics Institute

The University of Warwick

September 2017

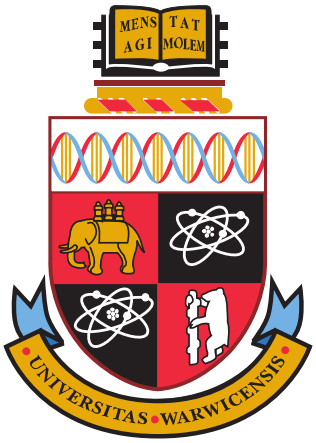

Contents

List of Tables

List of Figures

Acknowledgments

I am indebted to both of my supervisors Björn Stinner and Andreas Dedner for their guidance, honesty, and at times their considerable patience. I would also like to thank my examiners James Sprittles and Vanessa Styles, who had the perseverance to read, correct and examine me on this thesis, and to Dwight Barkley for advising on the examination and for chairing my personal advisory committee in the last 3 years. Also to all others with whom I have consulted, and worked with, or those who have helped proofread my thesis, I thank you.

I also would like to thank my parents Chris and Alistair and my sister Charlotte, I am overwhelmed by their persistent love and support. As well as their frequent supplies of vegetables, honey, eggs, and generally hilarious company.

I would like to thank all my friends of MASDOC and at Warwick who have made life as a PhD student into a true pleasure. Those in my cohort deserve a special credit, in order of proximity to my desk, thank you to John, Jack, Jamie, Adam, Yulong, Luke, Rodolfo, and Matt. Also to the lost MASDOC'er Jake who has remained a great friend.

To Rebecca, the girl who has kept me sane by pretending to listen for hours on end about the hardships of a PhD life, who has given me so much love and support in these last few months, which have kept me on track and happy through all the stress. I love you, and thank you.

I would like to thank the MASDOC centre and all of its staff and the training it provided, and to the Mathematics department for their wine and Statistics department for their coffee. Finally, I would like to thank EPSRC and as this work was supported by their catchily entitled grant EP/H023364/1 enabling all of this research to come to fruition.

Declarations

This thesis is submitted to the University of Warwick in support of my application for the degree of Doctor of Philosophy. It has been composed by myself and has not been submitted in any previous application for any degree.

The work has been carried out by myself. There has been collaboration in Chapter 2 with Björn Stinner, and I was given support for the code development from Andreas Dedner. The use of code packages and numerical libraries from other developers has been well documented in Chapter 1.

Figure 1.1 in the introduction was originally from

`http://people.maths.ox.ac.uk/griffit4/micelle_schematic.jpg`

Abstract

We investigate a free boundary problem arising in fluid dynamics, by modelling multiple incompressible fluids over subdomains with different material quantities, and in the presence of surface tension reducing chemicals known as surfactants. We construct a free energy for this system, and we require it obey the second law of thermodynamics, leading to the formulation of an energy minimisation problem (the sharp problem). This problem is degenerate, so we regularise it by constructing a new energy of Ginzburg-Landau type, parametrised by a (small) constant $\epsilon > 0$ and when $\epsilon \to 0$ the sharp problem is recovered in the sense of $\Gamma-$convergence. This multi-phase energy is formed from a multiwell potential and gradient term, and the minimisers are known as phase field variables. The phase field variables approximate characteristic functions of the subdomains, and the model is rewritten as functions of them. Beneficially, the energy analysis can be repeated as before to obtain a diffuse interface model.

We construct and perform numerical analysis of a novel discretisation scheme for a Cahn-Hilliard Navier-Stokes system. Here we create a fractional-theta coupling scheme which is importantly proved to be of second order in time. The key property of this scheme is that it uses weighted operator splitting to separate the different nonlinearities that appear in a Cahn-Hilliard Navier-Stokes system. That is, the Cahn-Hilliard multiwell potential, the incompressibility condition and the convection. We discuss stability and the extension to surfactants. We implement the novel scheme in DUNE (Distributed Unified Numerics Environment), a finite element package and use simulation to run tests to validate the stability and consistency of the schemes, convergence of the diffuse interface model with respect to its parametrisation, and flexibility for the code development.

Chapter 1

Introduction

1.1 General introduction

Surfactants (surface active agents) are chemicals which are identified by their ability to lower the surface tension along the interfaces between different fluids. The reduction of surface forces is caused by the chemical structure of the molecules: they are amphiphilic, that is, they have a hydrophilic (water attractive) head and hydrophobic (water repulsive) tail. It is therefore beneficial for the surfactant to adsorb to fluid-fluid interfaces, that is, to form an oriented, single molecule thick layer there. Figure 1.1 displays this process and furthermore shows the tendency of surfactants to self assemble into complex bulk structures such as micelles. At high concentrations they may also self assemble to form bilayers [86], vesicles, and even liquid crystal lattices [132], these structures minimize contact between the repulsive tails and the surrounding solution. The behaviour and formation of the single layers along fluid interfaces can vary widely due to solubility of the surfactant in the fluids, and the interactions between the molecules such as electrostatic forces of polar surfactants. Having formed these monolayers, the surfactant cannot bond as strongly to other molecules as the pre-existing liquid-liquid bonds can. It requires less energy to break these bonds, and the surface tension is reduced. The chemistry of these products are widely known, for example, these are explained in the introductory chapters of [78, 99].

The importance of manipulation of surface tension can be seen in the change of force balance within the fluid. Consider a regime where surface forces dominate a fluid's evolution. If a surfactant is then added, inertial or viscous forces may dominate over the now reduced surface tension (possibly by several orders of magnitude, see [110]) leading to different drivers of evolution and hence an altered macroscopic behaviour. A good review of Marangoni forces, the induced dynamics due to concentration gradients across liquid surface films, can be found in [3], other effects such as droplet breakup/tip streaming in

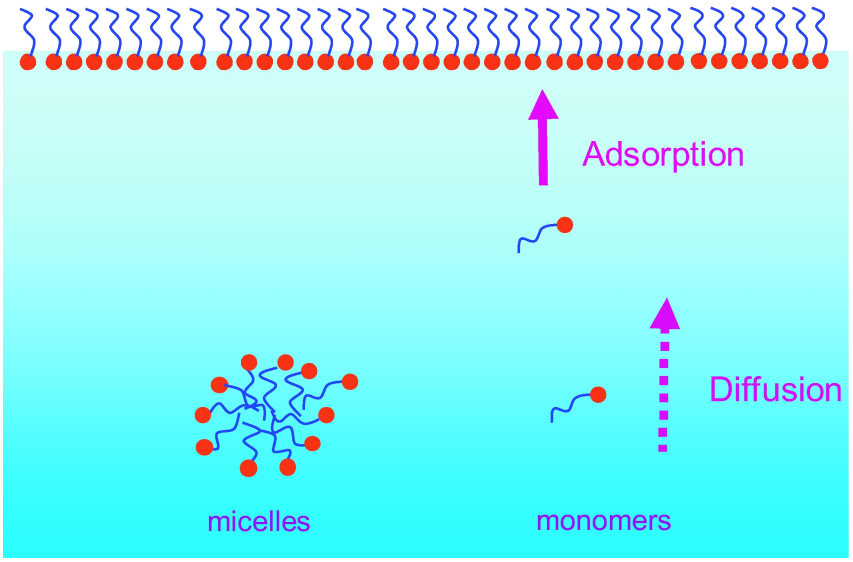

Figure 1.1: *Schematic displaying surfactant molecular structure, and behaviour in solution including the adsorption monolayer formation. The image source is given in the Declaration.*

[123], and some examples of the surfactants that induce these behaviours in [111].

Surfactants can occur naturally and are vital to a wide range of physical, chemical and biological systems [125]. Material scientists may also synthesize surfactants from natural (fatty acids and alcohols) or petrochemical ingredients. The ability to control the chemical structure and concentrations of the surfactants in a solvent, has lead to a wealth of commercial products, such as detergents, dispersents, wetting agents, emulsifiers (for example in oil recovery [115]), and in industries such as agrochemicals, pharmaceuticals and cosmetics. A more complete view of the vast scale of applications for different species of surfactant is given in [125].

This thesis focuses on activity of surfactants in a system of more than two fluids. In many of the industries mentioned, there are applications involving these systems. For example there is great interest in surfactant effects to water-in-oil-in-water emulsions, in the food industry for naturally occuring emulsions [83], or in pharmaceutical or cosmetic industries for prolonging drug release [87, 74]. Surfactants used in enhanced oil recovery are introduced to stabilize foaming for ternary solutions [107] or non aqueous solutions [51].

Many surfactant induced phenomena have been examined experimentally in material science. More recently in applied mathematics, the simulation of these systems has become possible through developments of mathematical tools and computational techniques for multiple fluids [63] and for coupled bulk-surface problems. These coupled problems

model a system of fluids, each described by the incompressible Navier-Stokes equations in isothermal conditions, and demarcated by material parameters such as mass density ρ and dynamic viscosity η ([63]).

In order for Newton's laws to hold, these equations are supplemented with derived interfacial force conditions where two fluids meet, and some contact line force conditions if three of these dividing interfaces meet at a triple junction. From this mathematical perspective, the aforementioned effects of surfactants on their environment are modelled, through the form of force balancing conditions and their dependence upon the concentration of adsorbed surfactant at the fluid-fluid interfaces.

1.2 Thesis contributions

The objective of this thesis is to provide new developments towards modelling surfactants in multi-phase flow in two core areas.

First, we construct a diffuse interface model extending [54] (which investigated two phase flow with surfactant) to three or more phases. We emphasize the inclusion of surfactants dissolved in three fluids and adsorbed along interfaces between them. In some applications surfactant mixtures are used [109], for simplicity we shall only model a single species of surfactant, however it is a straightforward generalization to multiple surfactants and is remarked upon when relevant. We also present numerical simulations to support some analytic results.

Second, we propose a new numerical timestepping scheme for multi-phase flow with surfactant based on the idea of a fractional time splitting introduced in [26]. The numerical investigation tackles stability and consistency. Supported by numerical benchmarking against several test problems, it demonstrates the scope and accuracy of the scheme. We also assess the validity of the model we construct in this way, by looking at both qualitative and quantitative simulation for benchmarks of multi-phase fluid with surfactant.

The fundamental mathematical technique we apply is known as phase field modelling [8]. This is a method for approximating a system with several interacting (usually time dependent) subdomains that cover a domain of interest by replacing the separating hypersurfaces between domains with thin interfacial layers of a (small) positive interface width, denoted by ε throughout. These are described by a phase field variable (or order parameter) which distinguishes between different phases. In the bulk phases, the phase field variable takes a near-constant value, and in the interfacial layers, it smoothly changes value between the different constants. A good introduction to these "diffuse" methods for fluid flow can be found [8].

1.2.1 Diffuse interface model of surfactants in multi-phase flow

Many methods exist for accounting for different classes of surfactants. For insoluble surfactants, which are modelled with no bulk presence, one can describe their evolution and behaviour purely from their interfacial concentrations. Here, research directions are directed to methods which accurately and efficiently predict the interface evolution. In particular techniques that exploit the fact that the interface dimension is one less than the bulk, and treat the surfactant efficiently with a surface partial differential equation. One popular idea is that the interface can be tracked explicitly with marker particles (Lagrangian points [45]), that is, the computational mesh tracks the interface. These may be coupled with a Navier-Stokes solver, such as an embedded boundary method [84]. One may also use tracking for the interface but solve for the surfactant using a finite volume method [68, 88]. Another field of investigation is for solving problems over a fixed grid and employ techniques to capture or reconstruct the interface, such as volume of fluid methods [73] (relying on volume conservation to construct the interface), level set methods [138] (a level set of a function represents the interface [101, 102]) or novel fixed grid methods such as segment projection methods [79] (the interface is segmented and parametrised by simple functions on chosen coordinate planes). Finally, one may use a carefully chosen smoothing function that preserves key mathematical structure, and replaces the (sharp) hypersurface with a (diffuse) thin interfacial region. This technique is known as a phase field model or diffuse interface model [92], with a more general discussion in [8]. One particular benefit of this method over any others mentioned (including the level set formulation), is that the approximation it provides to the free boundary problem is more mathematically grounded. In particular there is much stronger notion of convergence as our interfacial region shrinks to a hypersurface, and this allows for the recovery of the equations for the entire free boundary problem. We shall utilize this latter method in this thesis, and the corresponding asymptotic analysis which characterises the recovery will be presented in a forthcoming article [42].

Methods have also been developed for soluble surfactants, that is, where the surfactant is present as both an interfacial quantity as a monolayer concentration, and a bulk quantity dissolved in one or more of the fluids. The difficulty of this extension is twofold: we must both solve for the bulk surfactants and the behaviours they may exhibit (such as structure formation [132]), and we must account for kinetics of the surfactant adsorption-desorption process (the formation of a monolayer along a fluid-fluid boundary). In different scenarios, either factor may dominate in influencing the system dynamics. Typically the surfactant is modelled by a surface PDE at the interfaces and also a bulk PDE within each fluid region where it is soluble. These are coupled by boundary conditions related to the kinetics of the adsorption-desorption process. In early attempts, the surfactant was accounted for only on the interface, under the assumption that sorption dynamics were dominated by

diffusion and assumption that the concentration of surfactant was near constant in the bulk [75]. Developments have lead to solving in the bulk regions too. This can be handled with explicit tracking [32, 98], redistributing mesh methods [14] or embedded boundary methods [80] as in the insoluble surfactant case, assuming an equilibrium relation for the sorption. The fixed grid reconstructions and interface capturing methods have also been developed in this direction - see, for example level set methods [139] and the phase field methods [46, 127, 92].

Despite the high accuracy of the explicit tracking methods, fixed grid capturing methods are widely studied as well, as they allow for more complex dynamic geometrical features to be accounted for naturally. In particular, they may describe fluid systems which undergo topological changes. This is because the information pertaining to the geometry of the problem is contained within fields and equations and not within the mesh grids or computational set up. Problems of geometry then become problems in partial differential equation theory, and so the library of techniques for differential equations can be utilized to solve them.

We discuss phase field methods in this thesis, and in this case the aforementioned fields known as *phase field variables* are subjected to the Allen-Cahn or Cahn-Hilliard equations (orginally in [30, 29]). The reformulation not only approximates the geometry of the original problem but also the accompanying energy framework. In fact, it has been known [96] that the system energy for the phase field model (or *diffuse interface model*) will converge (in the sense of Γ-Convergence [24]) to the system energy of the model it approximates (the *sharp interface model*) as the width of the interfacial region tends to 0. In particular, this means that the minimisers of the diffuse interface model energy will converge strongly to minimisers of the sharp interface model energy. This fact potentially provides significant benefit over other interface capturing approaches, as it increases the amount of information that is recoverable through the interface representation, for example, by preforming an asymptotic analysis. For application of this technique to a Stefan problem see [49], and for examples of recovered equations from curvature driven evolution see [52].

The governing equations of the previous techniques required an equilibrium relation known as an isotherm (for example [85], which connected the surface and bulk fields. Analysis [136, 39, 40] and experiments [76] have shown that this assumption implies that the rate of any kinetic properties (for example orientation of molecules or effects of intermolecular charge forces) can be quick relative to the timescale of diffusion when forming the surfactant monolayer at interfaces. This is a good approximation for certain non-ionic surfactants out of mixture, however for ionic surfactants, or larger molecule surfactants, this equilibrium is not immediately satisfied. The relevant extension to the free energy framework is presented in [126] and refined regarding energy formulation and asymptotic

analysis in [54], where a thermodynamically consistent model for soluble surfactant in two phase flow is considered.

Extending work in [54], we generalize the model of a binary flow found in [1] to the multi-phase (i.e three or more phases) case and include the presence of a soluble surfactant. In particular we use a vector phase field (diffuse interface) model construction and focus our study on the modelling of contact lines or triple junctions where three fluid-fluid interfaces meet. The model for the $M \geq 3$ phases we consider is that of a vector Cahn-Hilliard type system, which is a partial differential equation over the domain, for order paramaters (phase field variables) $\varphi_\varepsilon = (\varphi_\varepsilon^{(1)}, \ldots, \varphi_\varepsilon^{(M)})$, parametrized by an interfacial layer width ε. Their motion is governed by two features of the energy framework. The first is a smooth multi-well potential that ensures the lowest energy states will take the form where φ_ε approximates $\boldsymbol{e}_k$ (the k^{th} standard basis vector) in the fluid region (or "phase") k. The second energetic feature is a multi-phase gradient energy that ensures the phase field variables are regularized enough so that they smoothly transition between values $\boldsymbol{e}_i$ and $\boldsymbol{e}_j$ across interfacial layers or contact regions between 3 phases.

We describe fluid flow through the language of continuum mechanics, that is, from a macroscopic scale - treating molecular effects as negligible. Studying from this viewpoint involves finding the velocity $\boldsymbol{v}(\boldsymbol{x}, t)$, the pressure $p(\boldsymbol{x}, t)$ at any point in the fluid volume $\boldsymbol{x} \in \Omega \subset \mathbb{R}^d$, $d = 2, 3$ and time interval $t \in [0, T]$. The individual flows (i.e phases) are assumed incompressible, and so the fluid density $\rho(\boldsymbol{x}, t)$ is assumed constant within the bulk region of each fluid. The phase fields φ_ε describe the geometry, thus the density variation originates from the dependence $\rho \equiv \rho(\varphi_\varepsilon)$, acting as an interpolation over interfacial layers between bulk density values. Other material quantities that are constant in each fluid phase, such as viscosity, are attributed a similar dependency $\eta \equiv \eta(\varphi_\varepsilon)$.

The limiting model when $\varepsilon \to 0$, known as the sharp interface model, also involves a natural free energy framework. It is a classical description of the system where one assumes that the interfaces between fluids can be represented as hypersurfaces and is the basis of front tracking approximation methods. It is derived using the same procedure as for the phase field model: We postulate balance equations for the fluids. These are supplemented with corresponding interface force balance equations between phases i and j by opposing surface tension forces $\sigma_{i,j}$ (as in [103]) with bulk fluid pressures and viscous stresses. We then use the system energy to derive constitutive assumptions and suitable boundary conditions to close the system and ensure thermodynamic consistency. This consistency is the agreement of the model with the second law of thermodynamics, that is, the decay of the global system energy over time.

The surfactants are accounted for through the surface tension $\sigma_{i,j} \equiv \sigma_{i,j}(c^{(i,j)})$ which depends on the surface concentration $c^{(i,j)}$ of surfactant. The converse coupling

arises as the surfactants are themselves subject to fluid transport, and will depend on the geometry of the interfaces. To derive the corresponding approximating phase field model for the surfactants, we are motivated by the work of [6] and [54] which we extend to multiple phases. The equivalence between distributional forms for interfaces and contact lines, with using characteristic test functions of these features allows us to reform our surfactant concentration equations in the latter form. We regularize the characteristic functions, using the carefully chosen distributions, and then construct surfactant dependent free energies which also satisfy energy decay laws under corresponding conditions. This flexible approach allows for solubility of the surfactant in one or more phases, and receives benefits of the phase field formulation described earlier.

In Chapter 2 we first present our sharp interface description of the problem in Section 2.1. We use mass and momentum balance equations to derive the governing equations, and close the system with appropriate boundary conditions and constitutive assumptions that lead to a thermodynamically consistent system seen in Section 2.1.8. In Section 2.1.9 we consider the particular case of local equilibrium of the surfactant potential around interfaces and present the resulting model in this case in Section 2.1.10. Finally we state some choices for the adsorption isotherms under this equilibrium. In Section 2.2 we present the diffuse interface description of the problem. We follow similar methods as in the sharp interface case and arrive once more at a thermodynamically consistent system seen in Section 2.2.5. We then proceed with the diffuse approximation of the case of local equilibrium of the surfactant potential and present this model in Section 2.2.7. We finally list some possible choices for mobilities and multiwell potentials for the phase field model in Section 2.2.8.

1.2.2 A scheme for multi-phase flow

The notion that a fluid interface could have a nonzero thickness, and this thickness could be determined by an equation of state due to a density profile, dates back to the work of Rayleigh and van der Waals [112, 113]. The theory was built upon by Korteweg [82], to construct constitutive laws for the fluid stress tensor in terms of density and density gradients. The ideas were then reformulated by Cahn and Hilliard [30, 29], with regards to a more general construct of a phase field variable. One of the earliest approaches for modelling binary fluids through this phase field approach was the so called "model H" introduced by [71] which used a Cahn-Hilliard equation with a (soft enforcing) smooth phase field potential for the phase field coupled to the Navier-Stokes equations with constant mass density for the fluid mechanics. This construction was formulated with a restriction on the mass density of the fluids, and more recently was shown to obey a form of the second law of thermodynamics by [67]. A significant branch of research over the past two decades has

lead to the extension of this original model to include varying mass densities [93], and more recently to enforce divergence free velocities ([41, 20]) and also frame indifference and thermodynamic consistency [1]. These properties greatly improve the quality of numerical schemes which can be constructed for these models.

Many schemes in the literature currently available for multi-phase flow, are based on robust schemes for the phase field systems, to which the fluids scheme is then attached. In practice, the fluid mechanics becomes very expensive to solve accurately especially with large Reynold's numbers [134] or large density variations between different phases. We take a different approach. We inspect the literature ([89]) for a reliable scheme for general incompressible fluids, and this we then develop into an accurate and efficient scheme for multi-phase flow, which is shown to be stable in several diverse test problems. We now describe the current state of the field for these types of fluid systems.

A large class of methods for incompressible flows are corrective schemes (velocity or pressure), created by Chorin [33, 34] and Temam [128, 129]. In pressure correction, the most basic scheme comprise two substeps. In the first step, one solves for a velocity field while treating the pressure with some degree of extrapolation (perhaps using a previous timestep as the approximation). In the second step, one projects the computed velocity into a desired solution space - a divergence free Sobolev space.

Numerical boundary layers limit this accuracy to first order, unless one takes more complex forms of the scheme ([64]) and use more previous timesteps for extrapolation. The benefits of these schemes are to separate the treatment of the two core difficulties of the incompressible Navier-Stokes: the incompressibility constraint and the inertial effects. Velocity correction methods are similar (in fact, regarding error analysis, they are equivalent), but the substep order is reversed compared with the pressure correction. Evidence suggests they are more stable than pressure correction for second order or higher accuracy [116, 77], though typically less easy to implement. They still contain boundary layers which limits accuracy. Consistent [65], and Gauge-Uzawa [100] methods eliminate artificial splitting errors and results are compared in [64].

There have been generalizations of these splitting techniques for variable density flows for finite differences by [16, 5], and, additionally, for finite volumes and finite elements [50, 66]. A novel form of the Navier-Stokes equations is presented in [66], which conserves kinetic energy in the discrete setting. This property has lead to the development of an unconditionally stable scheme for three phase Cahn-Hilliard-Navier-Stokes in [95]. The difficulty addressed in this thesis is to create a coupling scheme which allows for the Cahn-Hilliard system to be transported by a non divergence free velocity field, and for this scheme to ensure decay of the discrete system energy over time. More recently Gauge-Uzawa methods have been developed to deal with variable density. In [108] the authors

have obtained some results for convergence and stability even for higher density ratios. A two phase flow scheme has been constructed using these techniques by Shen and Yang in [117, 118, 119].

We wish to investigate another promising class of splitting methods, which solve time discrete initial value problems by splitting the physical time interval into subintervals and solving different problems over different subintervals. These can be thought of similar to Strang splitting [124], and a good introduction can be found in [60]. The key assumption of these schemes are that the system operator F can be decomposed into $F = F_1 + F_2$, where F_1 and F_2 are mathematically simpler objects than F. In the incompressible Navier-Stokes, these will be an operator for the incompressibility (a Stokes type operator) and a convection type operator for the inertial term (a Burgers type operator). The simplest case of these splittings, is the Peaceman-Rachford scheme [104], where one splits the n^{th} time interval $[n\Delta t, (n+1)\Delta t]$ of size Δt into two equally sized subintervals about the midpoint $(n + \frac{1}{2})\Delta t$. The Peaceman-Rachford scheme [104] solves for a solution with F_1 taken implicitly and F_2 taken explicitly in the first half-step, then F_2 taken implicitly and F_1 taken explicitly in the second step. One can demonstrate from eigenvalue analysis that this scheme is very accurate, of second (almost third) order accuracy [60] in time, however there are issues with slow convergence similarly observed in a Crank-Nicholson scheme (which is in fact a particular case of the Peaceman-Rachford scheme), making it an inappropriate choice for stiff systems.

A promising scheme from this field (with praise in [134]) is the *fractional theta scheme* . This scheme contains three substeps, $[n\Delta t, (n+\theta)\Delta t]$, $[(n+\theta)\Delta t, (n+1-\theta)\Delta t]$ and $[(n + 1 - \theta)\Delta t, (n + 1)\Delta t]$. Solving for the variable u, the split system operator $F(u) = F_1(u) + F_2(u)$ forms the fractional scheme as follows:

1. $[n\Delta t, (n + \theta)\Delta t]$, length $\theta\Delta t$, solve the substep $t^n \to t^{n+\theta}$,

$$\frac{u^{n+\theta} - u^n}{\theta\Delta t} + \mathcal{F}_1(u^{n+\theta}) + \mathcal{F}_2(u^n) = 0 \tag{1.1}$$

2. $[(n + \theta)\Delta t, (n + 1 - \theta)\Delta t]$, length $(1 - 2\theta)\Delta t$, solve the substep $t^{n+\theta} \to t^{n+1-\theta}$,

$$\frac{u^{n+1-\theta} - u^{n+\theta}}{(1 - 2\theta)\Delta t} + \mathcal{F}_2(u^{n+1-\theta}) + \mathcal{F}_1(u^{n+\theta}) = 0 \tag{1.2}$$

3. $[(n + 1 - \theta)\Delta t, (n + 1)\Delta t]$, length $\theta\Delta t$, solve the substep $t^{n+1-\theta} \to t^{n+1}$,

$$\frac{u^{n+1} - u^{n+1-\theta}}{\theta\Delta t} + \mathcal{F}_1(u^{n+1}) + \mathcal{F}_2(u^{n+1-\theta}) = 0 \tag{1.3}$$

So the operator F_1 is treated implicitly-explicitly-implicitly over the timestep, and F_2 is treated explicitly-implicitly-explicitly. With correct choice of θ one can obtain second order accuracy, strong A-stability, and thus demonstrate robustness regarding stiff systems. This method has been applied to the Navier-Stokes equations by [26] and a finite element method for the spatial discretisation has been analyzed by [81] and [97] for fixed densities. The stability and accuracy of the scheme have been demonstrated in numerical simulations, such as [134]. Some of the good properties of the scheme can be shown through a link with the Augmented Lagrangian formulation for saddle point problems [61].

We present a variable density form of the scheme, and show it still satisfies second order accuracy with the correct choice of theta. We further couple it to a Cahn-Hilliard system by using a technique found in [36]. For this coupled system we perform a stability analysis in the case of matched densities. In the variable density case we show consistency and verify this complication does not yield loss of accuracy.

In Chapter 3 we present the abstract fractional-theta scheme and then develop the operator splitting for the fixed density two phase Cahn-Hilliard Navier-Stokes scheme for the weak time discrete problem in Section 3.1.2. We present the fully discrete scheme in Section 3.2.1, and investigate stability for the discrete energy in Section 3.2.3. Extensions to multiple phases and variable density are formed in Section 3.3 and Section 3.4. The proof that the variable density scheme is of second order accuracy in time is in Section 3.4.2.

1.2.3 Benchmark testing

We additionally provide validation to our modelling framework and our numerical schemes by using simulation benchmarks for qualitative and quantitative verification in Chapter 4.

We assess the scheme by validating the second order accuracy in time proved in Chapter 3 and to commenting on stability in Section 4.2. We construct a relaxing liquid lens problem for three fluids of variable density and comparison of discrete solutions to a reference solution on a very fine time step resolution gives us orders of convergence, which we find to be of second order for the velocity.

To assess the validity of the diffuse interface model constructed in Chapter 2, we investigate the convergence of the surfactant equations as the interfacial width parameter ε tends to 0. We demonstrate this in Section 4.3.1 by setting up a test problem in which a flow of surfactant travelling through a stable, relaxed, triple junction. We compare this to the solution of the corresponding sharp interface solution and observe the convergence. We also present a qualitative simulation for the convergence as ε is reduced of the marangoni effect on a triple junction, for a liquid lens in Section 4.3.3. We find that if the interfacial width is large then interfacial effects are more dominant over inertial effects in the bulk, we also find the solutions converge as the interfacial width is reduced. As multi-phase flow

with soluble surfactant is still novel for phase field descriptions, this provides insight into the size of ε which may be required in for accurate results. We finally demonstrate the flexibility of the scheme by considering a rising coupled droplet in three space dimensions with surfactant in Section 4.4. Here we use a qualitative example to demonstrate the effects of surfactant presence on a variable density multi-phase flow. We run two experiments, with and without surfactants and observe the changes in behaviour of the droplets that are captured by the simulation. In particular the surfactants induce a topological change as the coupled droplet decouples into two disjoint droplets.

The reader is additionally directed to the YouTube channel, where I have records of some of the videos from simulations in the thesis.

`https://www.youtube.com/channel/UC0K4vFNJzPyiHofVOU8aAJg`

1.2.4 Software development

The software element to this thesis required substantial effort, and thus, the tools used throughout were of vital importance. This section highlights the key software that was developed and used of for the duration of the project. Documentation and cleanup of this code will shortly be completed, for other users.

The implementation for the numerical schemes were performed using the Dune-Fem toolbox, part of DUNE(-2.5) Distributed and Unified Numerics Environment. DUNE is a modular software for solving partial differential equations using methods such as finite elements, finite volumes and finite differences, of which we use the first extensively in our code. We direct the reader to `www.dune-project.org/modules/dune-fem/` for the current software webpage, and cite [38] for an overview of the core principals of this module and accompanying Dune-Fem-Howto module with accompanying documentation for some example code. The Navier-Stokes solver is already in use by other members of DUNE development team. The version control and writing of software was managed by creating a git repository on GitLab and creating a new module where the software and some supporting documents are kept.

We utilize some external software in the finite element simulations. For grid management we use ALUGrid, through the module Dune-ALUGrid [4], which provides the parallelizable adaptive grids that are used in the grid construction. Also linked in are some external solvers (direct and iterative) for linear systems and corresponding preconditioners. These use the flexible PETSc interface [12, 11, 13], where we make use of the UMFPACK SuiteSparse package [37] for serial problems, the MUMPS direct matrix solver [7], and the HYPRE BoomerAMG preconditioner [47] for parallel problems .

For the visualisations throughout this thesis, ParaView [10] is used to display the so-

lutions from the simulation, and for graphical output, I have used GNUPlot. I have written some finite difference simulations (for example in the epsilon convergence tests) in MATLAB and credit is due to the MATLAB and Statistics Toolbox Release 2014a-2016b, The MathWorks, Inc., Natick, Massachusetts, United States.

Chapter 2

Models

We begin by deriving a model for multi-phase flow with surfactant. It is an extension of the work [54] which studied two phase flow with surfactant. Firstly, we fix the notation and terminology of the thesis. Then we derive a model using local balance laws of mass and momentum, giving rise to a free energy formulation of the problem. By considering a suitable free energy, we can pose constitutive assumptions and find closing conditions and natural boundary conditions for our problem. The summary of this sharp interface model will be described in Section 2.1.8. We also note an important version of the model, when it is under the assumption of local chemical equilibrium, which will ease the numerical simulation. This is summarised in Section 2.1.10.

We approximate the sharp interface model (2.58) – (2.67) with a phase field methodology. The construction of the phase field model follows similarly to the derivation of the sharp interface model, and these links will be noted throughout. The balance laws, free energy formulation and choices of constitutive assumptions are detailed in subsequent Sections 2.1.2 to Section 2.1.5 and the summary of the diffuse model approximating (2.58) – (2.67) can be found in Section 2.2.5. Under a local chemical equilibrium at interfaces, the model (2.82) – (2.90), also has a diffuse interface counterpart. This is detailed in Section 2.2.7.

The ending of this chapter deals with some more specific choices of key potentials associated to the diffuse model, and within the chapter we additionally give some examples of isotherms describing different equilibrium regimes for the model (2.82) – (2.90) .

2.1 Sharp interface model

2.1.1 Notation and preliminaries

Let $\Omega \subset \mathbb{R}^d$, $d \in \{2,3\}$, be a bounded domain and $I = (0,T)$, $T \in [0,\infty)$ be a time interval. Assume that Ω is partitioned by moving hypersurfaces $\Gamma^{(i,j)}(t)$ into M time dependent open subdomains $\Omega^{(k)}(t)$, $i,j,k \in \{1,\dots,M\}$. Intersections of three hypersurfaces are denoted by $T^{(i,j,k)}(t)$ and form triple points ($d=2$) or form triple lines ($d=3$) ending in quadruple points $Q^{(i,j,k,l)}(t)$, $i,j,k,l \in \{1,\dots,M\}$. For simplicity, with regards to $T^{(i,j,k)}$ we will only talk about *triple junctions* in the following. Similarly, on the external boundary $\partial\Omega$ there are triple points or lines $T^{(i,j,ext)}(t)$ with quadruple points $Q^{(i,j,k,ext)}(t)$ if $d=3$. The unit normal on $\Gamma^{(i,j)}(t)$ pointing out of $\Omega^{(i)}(t)$ into $\Omega^{(j)}(t)$ is denoted by $\boldsymbol{\nu}^{(i,j)}(t)$ and by $\boldsymbol{\nu}_\Omega$ on $\partial\Omega$. For the conormal of $\Gamma^{(i,j)}(t)$ in $T^{(i,j,k)}(t)$ pointing into $\Omega^{(k)}(t)$ we write $\boldsymbol{\mu}^{(i,j,k)}(t)$, and we write $\boldsymbol{\mu}^{(i,j,ext)}(t)$ for it on $\partial\Omega$. Figure 2.1 is a sketch of a configuration as we have it in mind. Henceforth, for brevity, we omit writing the time dependence of these objects.

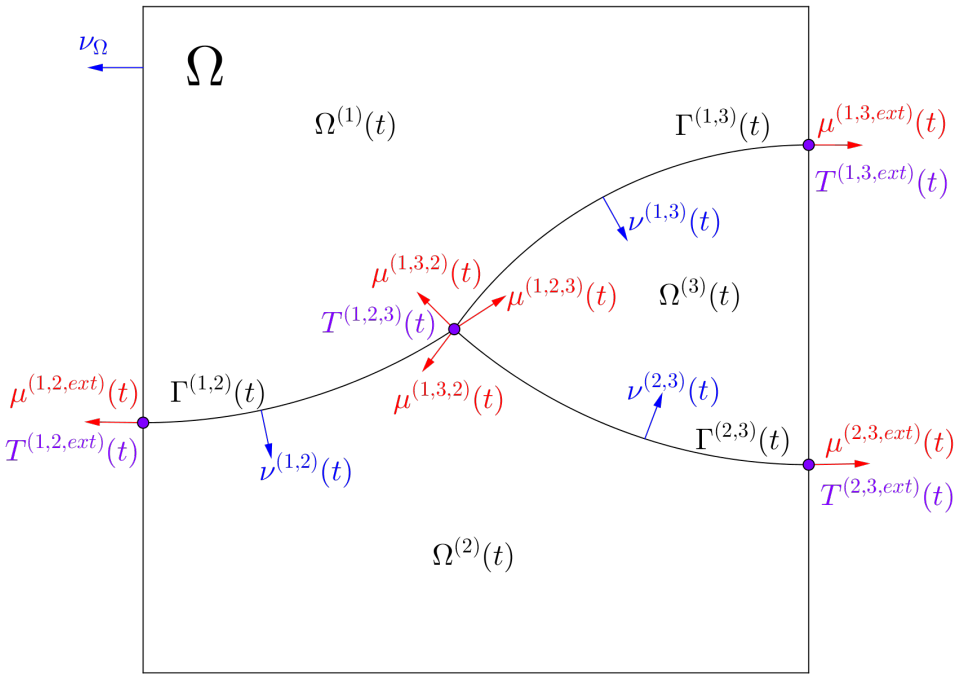

Figure 2.1: *We display geometric features of a domain Ω partitioned into three time dependent subdomains $\Omega^{(i)}(t)$, separated by interfaces $\Gamma^{(i,j)}(t)$ which meet at a triple junction $T^{(i,j,k)}(t)$ and at the boundaries $T^{(i,j,ext)}(t)$. For completeness we display the normals and conormals to the interfaces*

The whole configuration is transported by a continuous velocity field $\boldsymbol{v} : [0,T) \times$

$\Omega \to \mathbb{R}^d$, i.e., for each point $x \in \Omega^{(i)}(t)$ there is a point $x_0 \in \Omega^{(i)}(0)$ such that $x = \zeta(t)$ where $\zeta : [0,t] \to \mathbb{R}^d$ is the solution to $\partial_{\tilde{t}}\zeta(\tilde{t}) = \boldsymbol{v}(\tilde{t}, \zeta(\tilde{t}))$ with initial value $\zeta(0) = x_0$, and similarly for the interfaces, triple junctions, and quadruple points. We assume the fluids are immiscible, and so interfaces are impermeable. An implication of the properties of $\boldsymbol{v}$ is that

$$[\boldsymbol{v}]_i^j = 0, \quad u^{(i,j)} = \boldsymbol{v} \cdot \boldsymbol{\nu}^{(i,j)} \qquad \text{on } \Gamma^{(i,j)}, \tag{2.1}$$

where $[\cdot]_i^j = (\cdot)^{(j)} - (\cdot)^{(i)}$ stands for the jump from domain $\Omega^{(i)}$ into $\Omega^{(j)}$ across the interface $\Gamma^{(i,j)}$ and $u^{(i,j)}$ is the normal velocity of $\Gamma^{(i,j)}$ in direction $\boldsymbol{\nu}^{(i,j)}$. The match of tangential components of the velocity is typically required for stable viscous fluid-fluid interfaces [15], although recently it has been shown that polymer fluids are modelled with slip conditions [105]. Furthermore

$$\boldsymbol{u}^{(i,j,k)} = \boldsymbol{P}_{(T^{(i,j,k)})^\perp}\boldsymbol{v} \qquad \text{in } T^{(i,j,k)}, \tag{2.2}$$

where $\boldsymbol{u}^{(i,j,k)}$ is the normal velocity of $T^{(i,j,k)}$ and $\boldsymbol{P}_{(T^{(i,j,k)})^\perp}$ is the projection to the plane normal to $T^{(i,j,k)}$.

Further notation concerns the material velocity for a field $w : [0,T) \times \Omega \to \mathbb{R}$,

$$\partial_t^{\bullet(\boldsymbol{v})} w \coloneqq \partial_t w + \boldsymbol{v} \cdot \nabla w. \tag{2.3}$$

Thanks to the above assumption that velocity transports the interfaces, this operator is well-defined for fields restricted to a hypersurface $\Gamma^{(i,j)}$. We denote the surface derivative and divergence along the hypersurface $\Gamma^{(i,j)}$ by $\nabla_{\Gamma^{(i,j)}}$ and $\nabla_{\Gamma^{(i,j)}}\cdot$, respectively. Some useful identities such as a transport identity on evolving surfaces and integration by parts formula on surfaces are provided in Chapter 6.

2.1.2 Balance equations

$M \in \mathbb{N}$ represents the number of fluids we consider in our system. They are assumed to be immiscible, incompressible, and Newtonian, and each fluid occupies a subdomain $\Omega^{(i)}(t)$. Denoting by $\overline{\rho}^{(i)}$ the mass density of fluid $i \in \{1, \dots, M\}$, the mass and linear momentum balances in $\Omega^{(i)}$ read

$$\nabla \cdot \boldsymbol{v} = 0, \tag{2.4}$$

$$\partial_t(\overline{\rho}^{(i)}\boldsymbol{v}) + \nabla \cdot (\overline{\rho}^{(i)}\boldsymbol{v} \otimes \boldsymbol{v}) = \nabla \cdot \boldsymbol{T}^{(i)}, \tag{2.5}$$

with a symmetric stress tensor $\boldsymbol{T}^{(i)}$. The symmetry allows for motion to be accounted fully by the balance of linear momentum and angular momentum can be neglected.

For simplicity we only consider a single surfactant. Its bulk and surface mass densities are denoted by $c^{(i)}(t) : \Omega^{(i)}(t) \to \mathbb{R}$ and $c^{(i,j)}(t) : \Gamma^{(i,j)} \to \mathbb{R}$, respectively. We consider only mass balance equations for surfactant and effects on the ambient fluids' mass and momentum are neglected. This assumes that we model only a dilute surfactant solution, and is taken implicitly in much of the literature, for example [19, 138, 137]. A range of applications for dilute surfactant can be explored in [125]. There are also applications with high surfactant concentration where this modelling assumption is unsuitable, see [125, 83].

Following the derivation in [54] the surfactant mass balance equations read

$$\partial_t^{\bullet(\boldsymbol{v})} c^{(i)} = -\nabla \cdot \boldsymbol{j}_c^{(i)}, \qquad \text{in } \Omega^{(i)}(t), \tag{2.6}$$

$$\partial_t^{\bullet(\boldsymbol{v})} c^{(i,j)} + c^{(i,j)} \nabla_{\Gamma^{(i,j)}} \cdot \boldsymbol{v} = -\nabla_{\Gamma^{(i,j)}} \cdot \boldsymbol{j}_c^{(i,j)} + q_{\mathrm{AD}}^{(i,j)} \qquad \text{in } \Gamma^{(i,j)}(t), \tag{2.7}$$

where $\boldsymbol{j}_c^{(\cdot)}$ and $\boldsymbol{j}_c^{(\cdot,\cdot)}$ are associated bulk and surface diffusive fluxes and $q_{\mathrm{AD}}^{(i,j)}$ is the adsorption desorption flux. We determine the form of this sorption flux and a closing condition for the triple junction in the following calculation.

Let $V(t) \subset \Omega$ be an arbitrary material test volume, with $V \cap \partial\Omega = \emptyset$. Let $\boldsymbol{\nu}_V(\boldsymbol{x}, t)$ be the external unit normal of of $V(t)$ and $\boldsymbol{\mu}_V^{(i,j)}(\boldsymbol{x}, t)$ be the external conormal of $V(t) \cap \Gamma^{(i,j)}(t)$ in $\partial V(t) \cap \Gamma^{(i,j)}(t)$. Let $c^{(i)}, c^{(i,j)}$ represent the concentration of surfactant dissolved into fluids $\Omega^{(i)}$ and interfaces $\Gamma^{(i,j)}$. This implicitly assumes the surfactants are soluble in fluid regions and may adsorb to all interfaces (discussion of this assumption is found in Remark 2.1.1).

We integrate the balance equations (2.6) and (2.7) and sum over all $\Omega^{(\cdot)}$, $\Gamma^{(\cdot,\cdot)}$:

$$\sum_i \int_{V(t)\cap\Omega^{(i)}(t)} (\partial_t^{\bullet(\boldsymbol{v})} c^{(i)} + c^{(i)} \nabla \cdot \boldsymbol{v}) + \sum_{i<j} \int_{V(t)\cap\Gamma^{(i,j)}(t)} (\partial_t^{\bullet(\boldsymbol{v})} c^{(i,j)} + c^{(i,j)} \nabla_{\Gamma^{(i,j)}} \cdot \boldsymbol{v}) \tag{2.8}$$

$$= \sum_i \int_{V(t)\cap\Omega^{(i)}(t)} -\nabla \cdot \boldsymbol{j}_c^{(i)} + \sum_{i<j} \int_{V(t)\cap\Gamma^{(i,j)}(t)} (-\nabla_{\Gamma^{(i,j)}} \cdot \boldsymbol{j}_c^{(i,j)} + q_{\mathrm{AD}}^{(i,j)}). \tag{2.9}$$

We have used incompressibility of the fluid (2.4) here. Now we apply the Reynold's Transport Theorem (6.1) and the Surface Transport Theorem (6.2) to the integrals in (2.8):

$$\frac{\mathrm{d}}{\mathrm{d}t}\Big(\sum_i \int_{V(t)\cap\Omega^{(i)}(t)} c^{(i)} + \sum_{i<j} \int_{V(t)\cap\Gamma^{(i,j)}(t)} c^{(i,j)} \Big),$$

and we apply the Divergence Theorem to the integral of $\boldsymbol{j}_c^{(i)}$ in (2.9) to obtain:

$$-\sum_i \int_{\partial V(t)\cap\partial\Omega^{(i)}(t)} \boldsymbol{j}_c^{(i)}\cdot\boldsymbol{\nu}_V - \sum_{i<j}\int_{V(t)\cap\Gamma^{(i,j)}(t)} (\boldsymbol{j}_c^{(i)}\cdot\boldsymbol{\nu}^{(i,j)} + \boldsymbol{j}_c^{(j)}\cdot\boldsymbol{\nu}^{(j,i)}),$$

and finally we apply the Surface Divergence Theorem (6.4) to the integral of $\boldsymbol{j}_c^{(i,j)}$ in (2.9) to obtain:

$$\begin{aligned}&\sum_{i<j}\int_{V(t)\cap\Gamma^{(i,j)}(t)} q_{\mathrm{AD}}^{(i,j)} - \sum_{i<j}\int_{\partial V(t)\cap\Gamma^{(i,j)}(t)} \boldsymbol{j}_c^{(i,j)}\cdot\boldsymbol{\mu}_V^{(i,j)}\\ &-\sum_{i<j<k}\int_{V(t)\cap T^{(i,j,k)}(t)} (\boldsymbol{j}_c^{(i,j)}\cdot\boldsymbol{\mu}^{(i,j,k)} + \boldsymbol{j}_c^{(j,k)}\cdot\boldsymbol{\mu}^{(j,k,i)} + \boldsymbol{j}_c^{(k,i)}\cdot\boldsymbol{\mu}^{(k,i,j)}).\end{aligned}$$

As the flux $\boldsymbol{j}_c^{(i,j)}$ is tangential, the curvature term vanishes $\boldsymbol{j}_c^{(i,j)}\cdot\boldsymbol{\kappa}^{(i,j)} = 0$. Overall we obtain:

$$\frac{\mathrm{d}}{\mathrm{d}t}\Big(\sum_i\int_{V(t)\cap\Omega^{(i)}(t)} c^{(i)} + \sum_{i<j}\int_{V(t)\cap\Gamma^{(i,j)}(t)} c^{(i,j)}\Big) \tag{2.10}$$

$$= -\sum_i\int_{\partial V(t)\cap\partial\Omega^{(i)}(t)} \boldsymbol{j}_c^{(i)}\cdot\boldsymbol{\nu}_V - \sum_{i<j}\int_{\partial V(t)\cap\Gamma^{(i,j)}(t)} \boldsymbol{j}_c^{(i,j)}\cdot\boldsymbol{\mu}_V^{(i,j)} \tag{2.11}$$

$$+\sum_{i<j}\int_{V(t)\cap\Gamma^{(i,j)}(t)} (q_{\mathrm{AD}}^{(i,j)} - [\boldsymbol{j}_c^{(\cdot)}]_j^i\cdot\boldsymbol{\nu}^{(i,j)}) \tag{2.12}$$

$$-\sum_{i<j<k}\int_{V(t)\cap T^{(i,j,k)}(t)} (\boldsymbol{j}_c^{(i,j)}\cdot\boldsymbol{\mu}^{(i,j,k)} + \boldsymbol{j}_c^{(j,k)}\cdot\boldsymbol{\mu}^{(j,k,i)} + \boldsymbol{j}_c^{(k,i)}\cdot\boldsymbol{\mu}^{(k,i,j)}), \tag{2.13}$$

due to $V\cap\partial\Omega = \emptyset$, we do not admit any boundary integrals. The identity reads that the (instantaneous) change of surfactant mass in the material volume $V(t)$ (2.10) is given by the surfactant mass flux across $\partial V(t)$ (2.11). In the absence of source or sinks, we wish for the mass of surfactant to be conserved over the test volume. Therefore we require that there is no creation or destruction of surfactant during the adsorption-desorption process. With this in mind, we can determine a form of the sorption fluxes from (2.12):

$$q_{\mathrm{AD}}^{(i,j)} = \boldsymbol{j}_c^{(i)}\cdot\boldsymbol{\nu}^{(i,j)} + \boldsymbol{j}_c^{(j)}\cdot\boldsymbol{\nu}^{(j,i)} = [\boldsymbol{j}_c^{(\cdot)}]_j^i\cdot\boldsymbol{\nu}^{(i,j)}. \tag{2.14}$$

We additionally define the more convenient one-sided sorption flux $q_{\mathrm{ad}}^{(i,j)}$ from domain $\Omega^{(i)}$ to interface $\Gamma^{(i,j)}$ through

$$q_{\mathrm{ad}}^{(i,j)} \coloneqq \boldsymbol{j}_c^{(i)}\cdot\boldsymbol{\nu}^{(i,j)}, \tag{2.15}$$

so $q_{\text{AD}}^{(i,j)} = q_{\text{ad}}^{(i,j)} + q_{\text{ad}}^{(j,i)}$. From (2.13), we assume the diffusive surface fluxes obey:

$$\boldsymbol{j}_c^{(i,j)} \cdot \boldsymbol{\mu}^{(i,j,k)} + \boldsymbol{j}_c^{(j,k)} \cdot \boldsymbol{\mu}^{(j,k,i)} + \boldsymbol{j}_c^{(k,i)} \cdot \boldsymbol{\mu}^{(k,i,j)} = 0 \quad \text{in } T^{(i,j,k)}. \tag{2.16}$$

We define a one-sided sorption flux $q_{\text{ad}}^{(i,j,k)}$ interface $\Gamma^{(i,j)}$ to $T^{(i,j,k)}$ by,

$$q_{\text{ad}}^{(i,j,k)} \coloneqq \boldsymbol{j}_c^{(i,j)} \cdot \boldsymbol{\mu}^{(i,j,k)}. \tag{2.17}$$

The assumption (2.16) states that no surfactant mass is created, destroyed or stored in the triple points if $d = 2$ nor in triple lines or quadruple points if $d = 3$. The triple junction contribution of (2.13) vanishes.

Remark 2.1.1. *We have assumed for* (2.10) – (2.13) *that the surfactant is soluble in each fluid and adsorbs to all interfaces between fluids. However surfactants may be insoluble in some region $\Omega^{(k)}$ or may not adsorb to some interface $\Gamma^{(k,l)}$. This is often due to the compatibility of structures in the fluids and surfactants. Empirically it is measured by the hydrophile-lipophile balance (HLB) described in [78, 62] which assesses the strength of the hydrophilic subgroups of a surfactant against the lipophilic subgroup of the surfactant. For example, adding low HLB surfactants to an oil-water mixture causes water droplets to disperse in oil; a water-in-oil emulsion. Adding high HLB surfactants causes an oil-in-water emulsion. Fortunately the model can easily take into account insolubility (see Remark 2.1.5), S and we will show in the following section, that one may simply set $c^{(i)} = 0$ or $c^{(i,j)} = 0$ in the relevant fluid regions or interfaces.*

2.1.3 Free energy

In order to close the balance equations and relate the fluxes to the conserved fields we consider an energetic framework. With regards to the surfactant we postulate bulk free energies $g_i(c^{(i)})$ and surface free energies $\gamma_{i,j}(c^{(i,j)})$ which are strictly convex, i.e. $g_i''(c^{(i)}) > 0$ and $\gamma_{i,j}''(c^{(i,j)}) > 0$. The total free energy including the kinetic free energy then is

$$E \coloneqq \sum_i \int_{\Omega^{(i)}} \left(\frac{\overline{\rho}^{(i)}}{2} |\boldsymbol{v}|^2 + g_i(c^{(i)}) \right) + \sum_{i<j} \int_{\Gamma^{(i,j)}} \gamma_{i,j}(c^{(i,j)}). \tag{2.18}$$

Related to the surface free energy we define the *surface tension*

$$\sigma_{i,j}(c^{(i,j)}) \coloneqq \gamma_{i,j}(c^{(i,j)}) - c^{(i,j)} \gamma_{i,j}'(c^{(i,j)}). \tag{2.19}$$

This is well defined due to convexity of $\gamma_{i,j}$. We now perform a similar derivation as in Section 2.1.2 for this energy E. Let $V(t) \subset \Omega$ be an arbitrary material test volume with

$\partial V \cap \partial\Omega = \emptyset$; boundary conditions for the problem will be briefly discussed in Section 2.1.7. Let $\boldsymbol{\nu}_V(\boldsymbol{x},t)$ be the external unit normal of of $V(t)$ and $\boldsymbol{\mu}_V^{(i,j)}(\boldsymbol{x},t)$ be the external conormal of $V(t)\cap\Gamma^{(i,j)}(t)$ in $\partial V(t)\cap\Gamma^{(i,j)}(t)$.

For brevity we drop the $(\boldsymbol{x},t)$ dependence in the notation. Due to the transport identities (6.1) and (6.2) and the incompressibility of the fluids (2.4):

$$\begin{aligned}
&\frac{\mathrm{d}}{\mathrm{d}t}\left(\sum_i\int_{V\cap\Omega^{(i)}}\left(\frac{\overline{\rho}^{(i)}}{2}|\boldsymbol{v}|^2+g_i(c^{(i)})\right)+\sum_{i<j}\int_{V\cap\Gamma^{(i,j)}}\gamma_{i,j}(c^{(i,j)})\right)\\
=&\sum_i\int_{V\cap\Omega^{(i)}}(\overline{\rho}^{(i)}\boldsymbol{v}\cdot\partial_t^{\bullet(\boldsymbol{v})}\boldsymbol{v}+g_i'(c^{(i)})\partial_t^{\bullet(\boldsymbol{v})}c^{(i)})\\
&+\sum_{i<j}\int_{V\cap\Gamma^{(i,j)}}(\gamma_{i,j}'\partial_t^{\bullet(\boldsymbol{v})}c^{(i,j)}+\gamma_{i,j}\nabla_{\Gamma^{(i,j)}}\cdot\boldsymbol{v}),
\end{aligned}\tag{2.20}$$

We insert the balance law (2.5) (noting (2.4)) to replace the velocity term, and the balance law (2.6) to replace the bulk concentration term. Hereafter we drop the argument of g_i:

$$\begin{aligned}
&\sum_i\int_{V\cap\Omega^{(i)}}(\overline{\rho}^{(i)}\boldsymbol{v}\cdot\partial_t^{\bullet(\boldsymbol{v})}\boldsymbol{v}+g_i'(c^{(i)})\partial_t^{\bullet(\boldsymbol{v})}c^{(i)})\\
=&\sum_i\int_{V\cap\Omega^{(i)}}\big(\boldsymbol{v}\cdot(\nabla\cdot\boldsymbol{T}^{(i)})+g_i'(-\nabla\cdot\boldsymbol{j}_c^{(i)})\big),
\end{aligned}\tag{2.21}$$

we further insert the balance law (2.7) (noting the definitions (2.15) and (2.19)) to replace the surface concentration terms in the second integral. Hereafter we drop the argument of $\gamma_{i,j}$:

$$\begin{aligned}
&\sum_{i<j}\int_{V\cap\Gamma^{(i,j)}}(\gamma_{i,j}'\partial_t^{\bullet(\boldsymbol{v})}c^{(i,j)}+\gamma_{i,j}\nabla_{\Gamma^{(i,j)}}\cdot\boldsymbol{v})\\
=&\sum_{i<j}\int_{V\cap\Gamma^{(i,j)}}\Big(\gamma_{i,j}'\big(-\nabla_{\Gamma^{(i,j)}}\cdot\boldsymbol{j}_c^{(i,j)}+[\boldsymbol{j}_c^{(\cdot)}]_j^i\cdot\boldsymbol{\nu}^{(i,j)}\big)+\sigma_{i,j}\nabla_{\Gamma^{(i,j)}}\cdot\boldsymbol{v}\Big).
\end{aligned}\tag{2.22}$$

Define $\boldsymbol{D}(\boldsymbol{v}) = \frac{1}{2}(\nabla \boldsymbol{v} + (\nabla \boldsymbol{v})^{\perp})$. Sum (2.21) and (2.22). Use the symmetry of $\boldsymbol{T}^{(i)}$, and applying (6.4) and $\boldsymbol{j}_c^{(i,j)} \cdot \boldsymbol{\kappa}^{(i,j)} = 0$ (the flux is tangential). Then,

$$
\begin{aligned}
&\sum_i \int_{V\cap\Omega^{(i)}} \big(\boldsymbol{v}\cdot(\nabla\cdot\boldsymbol{T}^{(i)}) + g_i'(-\nabla\cdot\boldsymbol{j}_c^{(i)})\big) \\
&+ \sum_{i<j}\int_{V\cap\Gamma^{(i,j)}} \Big(\gamma_{i,j}'\big(-\nabla_{\Gamma^{(i,j)}}\cdot\boldsymbol{j}_c^{(i,j)} + [\boldsymbol{j}_c^{(\cdot)}]_j^i\cdot\boldsymbol{\nu}^{(i,j)}\big) + \sigma_{i,j}\nabla_{\Gamma^{(i,j)}}\cdot\boldsymbol{v}\Big) \\
=&\sum_i\Big(\int_{V\cap\Omega^{(i)}}(-\boldsymbol{D}(\boldsymbol{v})\colon\boldsymbol{T}^{(i)} + \nabla g_i'\cdot\boldsymbol{j}_c^{(i)}) + \int_{\partial V\cap\Omega^{(i)}}(\boldsymbol{T}^{(i)}\boldsymbol{v} - g_i'\boldsymbol{j}_c^{(i)})\cdot\boldsymbol{\nu}_V\Big) \\
&+ \sum_i\sum_{j\neq i}\int_{V\cap\Gamma^{(i,j)}}(\boldsymbol{T}^{(i)}\boldsymbol{v} - g_i'\boldsymbol{j}_c^{(i)})\cdot\boldsymbol{\nu}^{(i,j)} \\
&+ \sum_{i<j}\int_{V\cap\Gamma^{(i,j)}}\big(\nabla_{\Gamma^{(i,j)}}\gamma_{i,j}'\cdot\boldsymbol{j}_c^{(i,j)} + [\gamma_{i,j}'\boldsymbol{j}_c^{(\cdot)}]_j^i\cdot\boldsymbol{\nu}^{(i,j)} - \nabla_{\Gamma^{(i,j)}}\sigma_{i,j}\cdot\boldsymbol{v} - \sigma_{i,j}\boldsymbol{\kappa}^{(i,j)}\cdot\boldsymbol{v}\big) \\
&+ \sum_{i<j}\Big(\int_{\partial V\cap\Gamma^{(i,j)}}(\gamma_{i,j}'\boldsymbol{j}_c^{(i,j)} + \sigma_{i,j}\boldsymbol{v})\cdot\boldsymbol{\mu}_V^{(i,j)} \\
&+ \sum_{k\neq i,j}\int_{V\cap T^{(i,j,k)}}(-\gamma_{i,j}'\boldsymbol{j}_c^{(i,j)} + \sigma_{i,j}\boldsymbol{v})\cdot\boldsymbol{\mu}^{(i,j,k)},
\end{aligned}
$$

with the external conormal $\boldsymbol{\mu}_V^{(i,j)}$, rewriting the double sums we obtain the following form for (2.20)

$$
\begin{aligned}
&\frac{\mathrm{d}}{\mathrm{d}t}\left(\sum_i\int_{V\cap\Omega^{(i)}}\left(\frac{\overline{\rho}^{(i)}}{2}|\boldsymbol{v}|^2 + g_i(c^{(i)})\right) + \sum_{i<j}\int_{V\cap\Gamma^{(i,j)}}\gamma_{i,j}(c^{(i,j)})\right) \\
=&\sum_i\int_{V\cap\Omega^{(i)}}(-\boldsymbol{D}(\boldsymbol{v})\colon\boldsymbol{T}^{(i)} + \nabla g_i'\cdot\boldsymbol{j}_c^{(i)}) + \sum_{i<j}\int_{V\cap\Gamma^{(i,j)}}\nabla_{\Gamma^{(i,j)}}\gamma_{i,j}'\cdot\boldsymbol{j}_c^{(i,j)} && (2.23)\\
&+ \sum_{i<j}\int_{V\cap\Gamma^{(i,j)}}\big[(\gamma_{i,j}' - g_{(\cdot)}')\boldsymbol{j}_c^{(\cdot)}\big]_j^i\cdot\boldsymbol{\nu}^{(i,j)} && (2.24)\\
&+ \sum_{i<j}\int_{V\cap\Gamma^{(i,j)}}\big([\boldsymbol{T}^{(\cdot)}]_j^i\boldsymbol{\nu}^{(i,j)} - \nabla_{\Gamma^{(i,j)}}\sigma_{i,j} - \sigma_{i,j}\boldsymbol{\kappa}^{(i,j)}\big)\cdot\boldsymbol{v} && (2.25)\\
&+ \sum_{i<j<k}\int_{V\cap T^{(i,j,k)}}\big(\sigma_{i,j}\boldsymbol{\mu}^{(i,j,k)} + \sigma_{j,k}\boldsymbol{\mu}^{(j,k,i)} + \sigma_{k,i}\boldsymbol{\mu}^{(k,i,j)}\big)\cdot\boldsymbol{v} && (2.26)\\
&- \sum_{i<j<k}\int_{V\cap T^{(i,j,k)}}\big(\gamma_{i,j}'\boldsymbol{j}_c^{(i,j)}\cdot\boldsymbol{\mu}^{(i,j,k)} + \gamma_{j,k}'\boldsymbol{j}_c^{(j,k)}\cdot\boldsymbol{\mu}^{(j,k,i)} + \gamma_{k,i}'\boldsymbol{j}_c^{(k,i)}\cdot\boldsymbol{\mu}^{(k,i,j)}\big) \\
& && (2.27)
\end{aligned}
$$

$$+\sum_i \int_{\partial V\cap\Omega^{(i)}} \big((\boldsymbol{T}^{(i)}\boldsymbol{\nu}_V)\cdot\boldsymbol{v} - g_i'\boldsymbol{j}_c^{(i)}\cdot\boldsymbol{\nu}_V\big) \tag{2.28}$$

$$+\sum_{i<j} \int_{\partial V\cap\Gamma^{(i,j)}} \big(-\gamma_{i,j}'\boldsymbol{j}_c^{(i,j)}\cdot\boldsymbol{\mu}_V^{(i,j)} + \sigma_{i,j}\boldsymbol{\mu}_V^{(i,j)}\cdot\boldsymbol{v}\big). \tag{2.29}$$

2.1.4 Dynamic sorption

The adsorption-desorption dynamics of the surfactant at interfaces is an important governing factor to the overall dynamics of the system, and this can be observed by the phase field approximation we will construct in Section 2.2. The variation in these dynamics which we investigate in particular are the differences when the rate of adsorption-desorption is on a comparable timescale to other system motions (discussed here), and when the rate of adsorption-desorption on some or all interfaces is on a fast timescale compared with the other system dynamics (discussed in Section 2.1.9).

We are directed by the free energy calculation in Section 2.1.3, as we wish the energy to be dissipative (upto external forcing) to make consitutive assumptions ensuring this. In particular, (2.24) and (2.27) direct us to make assumptions on the surfactant fluxes.

In the interface $\Gamma^{(i,j)}$, due to (2.24), we assume that:

$$\alpha_{i,j}\boldsymbol{j}_c^{(i)}\cdot\boldsymbol{\nu}^{(i,j)} = -(\gamma_{i,j}'(c^{(i,j)}) - g_i'(c^{(i)})), \tag{2.30}$$

where $\alpha_{i,j}\geq 0$ for each $i<j$ pair, may be a function of $(c^{(i)}, c^{(i,j)})$. In general we permit that $\alpha_{i,j}\neq\alpha_{j,i}$, that is, the adsorption rate of surfactant from $\Omega^{(i)}$ into $\Gamma^{(i,j)}$ can differ from the adsorption rate of surfactant from $\Omega^{(j)}$ into $\Gamma^{(i,j)}$. We can interpret $\alpha_{i,j}\geq 0$ as a factor which relates the adsorption (desorption) at the interface $\Gamma^{(i,j)}$ from (into) the bulk to the deviation from chemical equilibrium.

In the triple junction$T^{(i,j,k)}$, due to (2.27), we assume that:

$$\boldsymbol{j}_c^{(i,j)}\cdot\boldsymbol{\mu}^{(i,j,k)} \coloneqq \beta_{j,k\leftrightarrow i,j}(\gamma_{i,j}'(c^{(i,j)}) - \gamma_{j,k}'(c^{(j,k)})) + \beta_{k,i\leftrightarrow i,j}(\gamma_{i,j}'(c^{(i,j)}) - \gamma_{k,i}'(c^{(k,i)})), \tag{2.31}$$

where the coefficients $\beta_{i,j\leftrightarrow A,B}\geq 0$ satisfy the following symmetries

$$\beta_{i,j\leftrightarrow A,B} = \beta_{A,B\leftrightarrow i,j}, \qquad \beta_{A,B\leftrightarrow i,j} = \beta_{B,A\leftrightarrow i,j}, \qquad \beta_{A,B\leftrightarrow i,j} = \beta_{A,B\leftrightarrow j,i}.$$

for $(A,B)\in\{(j,k),(k,i)\}$.

One can see in the Appendix 6.2 how these choices achieve the desired properties. The choice assumes a linear relation between fluxes, which is not physically derived, but does allow for interpretation that the $\beta_{i,j\leftrightarrow A,B}\geq 0$ can be viewed as a factor relating surfactant flux at a junction from interface $\Gamma^{(i,j)}$ to $\Gamma^{(A,B)}$ to the deviation from equilibrium.

Other more complex choices satisfying the symmetries and positivity could be constructed this investigation is outside the scope of our current study.

Further investigation of the calculations in Section 2.1.3, the terms in (2.23) motivate us to assume the surfactant fluxes have the form

$$\boldsymbol{j}_c^{(i)} = -M_c^{(i)} \nabla g_i'(c^{(i)}) \qquad \text{in } \Omega^{(i)}, \tag{2.32}$$

$$\boldsymbol{j}_c^{(i,j)} = -M_c^{(i,j)} \nabla_{\Gamma^{(i,j)}} \gamma_{i,j}'(c^{(i,j)}) \qquad \text{in } \Gamma^{(i,j)}, \tag{2.33}$$

with mobilities $M_c^{(i)} \geq 0$ and $M_c^{(i,j)} \geq 0$ that may be functions of the $c^{(i)}$ and the $c^{(i,j)}$ respectively. The g_i' and $\gamma_{i,j}'$ are exactly the chemical potentials of the bulk and interfacial surfactants, thus the evolution of the surfactant is determined primarily by the gradients of the chemical potentials.

Remark 2.1.2. *We may regain Fick's law for diffusivities of the surfactant by choosing the mobilities:*

$$M_c^{(i)} := -\mathcal{D} \frac{1}{g_i''(c^{(i)})} \text{ in the bulk, and } M_c^{(i,j)} := -\mathcal{D} \frac{1}{\gamma_{i,j}''(c^{(i,j)})} \text{ on the interface.}$$

for a positive constant diffusivity $\mathcal{D}$. Indeed, the chain rule implies

$$\boldsymbol{j}_c^{(i)} = -\mathcal{D} \frac{g_i''(c^{(i)}) \nabla c^{(i)}}{g_i''(c^{(i)})} = -\mathcal{D} \nabla c^{(i)}, \quad \text{and similarly,} \quad \boldsymbol{j}_c^{(i,j)} = -\mathcal{D} \nabla c^{(i,j)}.$$

2.1.5 Further constitutive assumptions

We now may make an assumption on the stress tensor $\boldsymbol{T}^{(\cdot)}$ found in (2.5):

$$\boldsymbol{T}^{(i)} = -p\boldsymbol{I} + 2\eta^{(i)} \boldsymbol{D}(\boldsymbol{v}), \tag{2.34}$$

where $\boldsymbol{I}$ denotes the identity. The rate of strain tensor $\boldsymbol{D}$ gives a sign to ensure the dissipation of the free energy term in (2.23), while the fluid pressure p, is seen as a lagrange multiplier to enforce incompressibility (2.4) without effect the energy dissipation.

At the interfaces $\Gamma^{(i,j)}$ we assume, due to the term (2.25), that the force balance at the interface is given by

$$[\boldsymbol{T}^{(\cdot)}]_j^i \boldsymbol{\nu}^{(i,j)} = \sigma_{i,j}(c^{(i,j)}) \boldsymbol{\kappa}^{(i,j)} + \nabla_{\Gamma^{(i,j)}} \sigma_{i,j}(c^{(i,j)}), \tag{2.35}$$

which means that the stresses exerted by the fluids adjacent to the interfaces are counterbalanced by intrinsic forces, namely the surface tension forces $\sigma_{i,j} \boldsymbol{\kappa}^{(i,j)}$ (curvature $\boldsymbol{\kappa}^{(i,j)}$) and the *Marangoni forces* $\nabla_{\Gamma^{(i,j)}} \sigma_{i,j}$.

In the triple points or lines, due to the term (2.26), we assume the following balances of capillary forces:

$$\sigma_{i,j}(c^{(i,j)})\boldsymbol{\mu}^{(i,j,k)} + \sigma_{j,k}(c^{(j,k)})\boldsymbol{\mu}^{(j,k,i)} + \sigma_{k,i}(c^{(k,i)})\boldsymbol{\mu}^{(k,i,j)} = 0. \tag{2.36}$$

This triple junction condition is also known as *Young's law*, see [57] for a discussion in the context of general anisotropic surface energies. In particular, it determines the angles at which the three phases meet in the triple junction. In the case $d = 3$ the condition (2.36) also fully determines the configuration and angles at the quadruple junctions $Q^{(i,j,k,l)}$, see [27] , Section 3, for a discussion.

Condition (2.36) is a local mechanical equilibrium condition which may not always hold true. One such case of this is in wetting or spreading phenomena, which are of great relevance in many applications. Therefore this assumption limits the model to the cases where this does not occur.

Remark 2.1.3. *Wetting is characterised by* wetting *or* spreading *functions [69]*

$$S^{(i,j,k)} := \sigma_{i,j}(c^{(i,j)}) - \big(\sigma_{i,k}(c^{(i,k)}) + \sigma_{j,k}(c^{(j,k)})\big). \tag{2.37}$$

If (2.37) *is positive, it is energetically favourable for a thin layer of fluid k to exist between fluids i and j. This causes existence of stable interfaces $\Gamma^{(i,k)}$, $\Gamma^{(j,k)}$ and unstable $\Gamma^{(i,j)}$ which disappears after suitably long times. In this case the condition* (2.36) *then cannot be satisfied but other closing conditions, for instance, involving precursor films have to be postulated [106]. We will not cover the spreading case in the free boundary problem and the subsequent asymptotic analysis but note that some phase field models are able to capture the behaviour (see [21, 22]).*

Accounting for all constitutive assumptions (2.68), (2.69), (2.32), (2.33), (2.30),

(2.31), (2.35), and (2.36) we obtain from (2.23) – (2.29) that

$$\frac{\mathrm{d}}{\mathrm{d}t}\left(\sum_i \int_{V\cap\Omega^{(i)}} \left(\frac{\overline{\rho}^{(i)}}{2}|\boldsymbol{v}|^2 + g_i(c^{(i)})\right) + \sum_{i<j}\int_{V\cap\Gamma^{(i,j)}} \gamma_{i,j}(c^{(i,j)})\right) \tag{2.38}$$

$$= -\sum_i \int_{V\cap\Omega^{(i)}} (2\eta^{(i)}|\boldsymbol{D}(\boldsymbol{v})|^2 + M_c^{(i)}|\nabla g_i'(c^{(i)})|^2) \tag{2.39}$$

$$-\sum_{i<j}\int_{V\cap\Gamma^{(i,j)}} M_c^{(i,j)}|\nabla_{\Gamma^{(i,j)}}\gamma_{i,j}'(c^{(i,j)})|^2 \tag{2.40}$$

$$-\sum_{i<j}\int_{V\cap\Gamma^{(i,j)}} \frac{1}{\alpha_{i,j}}(\gamma_{i,j}'(c^{(i,j)} - g_i'(c^{(i)}))^2 + \frac{1}{\alpha_{j,i}}(\gamma_{i,j}'(c^{(i,j)}) - g_j'(c^{(i)}))^2 \tag{2.41}$$

$$\begin{aligned}-\sum_{i<j<k}\int_{V\cap T^{(i,j,k)}} &\beta_{k,i\leftrightarrow i,j}(\gamma_{i,j}'(c^{(i,j)}) - \gamma_{k,i}'(c^{(k,i)}))^2 \\ &+ \beta_{k,i\leftrightarrow j,k}(\gamma_{j,k}'(c^{(j,k)}) - \gamma_{k,i}'(c^{(k,i)}))^2 \\ &+ \beta_{j,k\leftrightarrow i,j}(\gamma_{i,j}'(c^{(i,j)}) - \gamma_{j,k}'(c^{(j,k)}))^2\end{aligned} \tag{2.42}$$

$$-\sum_i \int_{\partial V\cap\Omega^{(i)}} M_c^{(i)} g_i'(c^{(i)})\nabla g_i'(c^{(i)})\cdot\boldsymbol{\nu}_V \tag{2.43}$$

$$-\sum_{i<j}\int_{\partial V\cap\Gamma^{(i,j)}} M_c^{(i,j)}\gamma_{i,j}'(c^{(i,j)})\nabla_{\Gamma^{(i,j)}}\gamma_{i,j}'(c^{(i,j)})\cdot\boldsymbol{\mu}_V^{(i,j)} \tag{2.44}$$

$$+\sum_i \int_{\partial V\cap\Omega^{(i)}} (\boldsymbol{T}^{(i)}\boldsymbol{v})\cdot\boldsymbol{\nu}_V + \sum_{i<j}\int_{\partial V\cap\Gamma^{(i,j)}} \sigma_{i,j}(c^{(i,j)})\boldsymbol{v}\cdot\boldsymbol{\mu}_V^{(i,j)}. \tag{2.45}$$

The terms in (2.39) and (2.40) are dissipative contributions to the change of energy. Terms (2.41) and (2.42) are the bulk-interface and interface-interface sorption dissipation terms respectively. Finally, (2.45) represents the work done on V by the external fluid, and (2.43) and (2.44) list the loss (or gain) of energy due to the surfactant mass fluxes across ∂V.

2.1.6 Distributional form

Our derivation of the surfactant equations is constructed using methods of conservation of local balance laws over arbitrary test volumes. This is a well recognised form of the equations, however we shall additionally rewrite the surfactant equations in a formulation using distributions. In this form it is easier to motivate forms for the phase field equations for the surfactant. In [6], the author has shown for the two phase case, there is an equivalence between balance laws written as a differential (in)equality, in a distributional form and in an integral form over test volumes. We wish to extend the result of [6] to $M \geq 3$ phases for

our surfactant equations, with particular focus on the triple junctions.

We shall derive the distributional form of the equation (2.7), along with (2.30) and (2.31) for $c^{(i,j)}$. The distributional form for (2.6) is similarly found, so we shall omit these calculations. The procedure will be to integrate the strong form of the interfacial surfactant equation (2.7) against any test function $\zeta \in C_0^\infty((0,T)\times\Omega)$.

Remark 2.1.4. *Depending on the choice of the space of ζ's, one can obtain different features of the equation, it is standard first to take $\zeta \in C_0^\infty((0,T)\times\Omega)$, which will remove the boundary and initial conditions from consideration. Typically one would then repeat the calculations with, for example, $\zeta \in C_g^\infty((0,T)\times\Omega)$ where g represents the Dirichlet boundary data $\zeta|_{\partial\Omega} = g$, which will aid recovery of boundary conditions. We do not present these calculations.*

Integrate (2.7) against $\zeta \in C_0^\infty((0,T)\times\Omega)$:

$$0 = \int_0^T \int_{\Gamma^{(i,j)}} \Big(\partial_t^{\bullet(\boldsymbol{v})}(c^{(i,j)}) + c^{(i,j)} \nabla_{\Gamma^{(i,j)}} \cdot \boldsymbol{v} + \nabla_{\Gamma^{(i,j)}} \cdot \boldsymbol{j}_c^{(i,j)} - \boldsymbol{j}_c^{(i)} \cdot \boldsymbol{\nu}^{(i,j)} - \boldsymbol{j}_c^{(j)} \cdot \boldsymbol{\nu}^{(j,i)} \Big) \zeta.$$

Integrating by parts, and noting that $\boldsymbol{j}_c^{(i,j)}$ is tangential along $\Gamma^{(i,j)}$, so $\boldsymbol{j}_c^{(i,j)} \cdot \nabla_{\Gamma^{(i,j)}} \zeta = \boldsymbol{j}_c^{(i,j)} \cdot \nabla \zeta$, gives:

$$\begin{aligned} 0 = & \int_0^T \int_{\Gamma^{(i,j)}} (\partial_t^{\bullet(\boldsymbol{v})}(c^{(i,j)}\zeta) + c^{(i,j)} \zeta \nabla_{\Gamma^{(i,j)}} \cdot \boldsymbol{v}) - c^{(i,j)} \partial_t^{\bullet(\boldsymbol{v})}(\zeta) - \boldsymbol{j}_c^{(i,j)} \cdot \nabla \zeta \\ & - \int_0^T \int_{\Gamma^{(i,j)}} \Big(\boldsymbol{j}_c^{(i)} \cdot \boldsymbol{\nu}^{(i,j)} + \boldsymbol{j}_c^{(j)} \cdot \boldsymbol{\nu}^{(j,i)} \Big) \zeta + \int_0^T \int_{\partial\Gamma^{(i,j)}} \zeta \boldsymbol{j}_c^{(i,j)} \cdot \boldsymbol{\mu}^{(i,j)}, \end{aligned}$$

where $\boldsymbol{\mu}^{(i,j)}$ is the external unit conormal for $\Gamma^{(i,j)}$. By (6.2), we obtain that:

$$\begin{aligned} 0 = & \int_0^T \frac{\mathrm{d}}{\mathrm{d}t} \Big(\int_{\Gamma^{(i,j)}} c^{(i,j)} \zeta \Big) - \int_0^T \int_{\Gamma^{(i,j)}} c^{(i,j)} \partial_t^{\bullet(\boldsymbol{v})}(\zeta) + \boldsymbol{j}_c^{(i,j)} \cdot \nabla \zeta \\ & - \int_0^T \int_{\Gamma^{(i,j)}} \Big(\boldsymbol{j}_c^{(i)} \cdot \boldsymbol{\nu}^{(i,j)} + \boldsymbol{j}_c^{(j)} \cdot \boldsymbol{\nu}^{(j,i)} \Big) \zeta + \int_0^T \int_{\partial\Gamma^{(i,j)}} \zeta \boldsymbol{j}_c^{(i,j)} \cdot \boldsymbol{\mu}^{(i,j)}. \end{aligned}$$

Using zero boundary conditions of the test function we get:

$$\begin{aligned} 0 = & - \int_0^T \int_{\Gamma^{(i,j)}} c^{(i,j)} (\partial_t \zeta + \boldsymbol{v} \cdot \nabla \zeta) + \boldsymbol{j}_c^{(i,j)} \cdot \nabla \zeta \\ & - \int_0^T \int_{\Gamma^{(i,j)}} \Big(\boldsymbol{j}_c^{(i)} \cdot \boldsymbol{\nu}^{(i,j)} + \boldsymbol{j}_c^{(j)} \cdot \boldsymbol{\nu}^{(j,i)} \Big) \zeta + \int_0^T \sum_{k \neq i,j} \int_{T^{(i,j,k)}} \zeta \boldsymbol{j}_c^{(i,j)} \cdot \boldsymbol{\mu}^{(i,j,k)}. \end{aligned}$$

Define the distributions $\delta_{\Gamma^{(i,j)}} = (L^1 \otimes \mathcal{H}^d) \llcorner \Gamma^{(i,j)}$ and $\tau_{T^{(i,j,k)}} = (L^1 \otimes \mathcal{H}^d) \llcorner T^{(i,j,k)}$ by,

$$\langle \delta_{\Gamma^{(i,j)}}, f \rangle = \int_0^T \int_{\Gamma^{(i,j)}(t)} f(\boldsymbol{x}, t) \, \mathrm{d}\mathcal{H}^{d-1}(\boldsymbol{x}) \, \mathrm{d}L^1(t), \tag{2.46}$$

and,

$$\langle \tau_{T^{(i,j,k)}}, f \rangle = \int_0^T \int_{T^{(i,j,k)}(t)} f(\boldsymbol{x}, t) \, \mathrm{d}\mathcal{H}^{d-2}(\boldsymbol{x}) \, \mathrm{d}L^1(t), \tag{2.47}$$

for any $f \in D_0^\infty((0,T) \times \Omega)$. We have shown in distribution that,

$$\begin{aligned} 0 = {} & \partial_t(\delta_{\Gamma^{(i,j)}} c^{(i,j)}) + \nabla \cdot \left(\delta_{\Gamma^{(i,j)}}(c^{(i,j)} \boldsymbol{v} + \boldsymbol{j}_c^{(i,j)})\right) \\ & - \delta_{\Gamma^{(i,j)}}(\boldsymbol{j}_c^{(i)} \cdot \boldsymbol{\nu}^{(i,j)} + \boldsymbol{j}_c^{(j)} \cdot \boldsymbol{\nu}^{(j,i)}) + \sum_{k \neq i,j} \tau_{T^{(i,j,k)}}(\boldsymbol{j}_c^{(i,j)} \cdot \boldsymbol{\mu}^{(i,j,k)}), \end{aligned} \tag{2.48}$$

where, due to assumptions (2.30) and (2.31), we take:

$$\delta_{\Gamma^{(i,j)}} \boldsymbol{j}_c^{(i)} \cdot \boldsymbol{\nu}^{(i,j)} = \delta_{\Gamma^{(i,j)}} \Big(- \frac{1}{\alpha_{i,j}} (\gamma'_{i,j}(c^{(i,j)}) - g'_i(c^{(i)})) \Big), \tag{2.49}$$

$$\begin{aligned} \tau_{T^{(i,j,k)}} \boldsymbol{j}_c^{(i,j)} \cdot \boldsymbol{\mu}^{(i,j,k)} = {} & \tau_{T^{(i,j,k)}} \Big(\beta_{j,k \leftrightarrow i,j} (\gamma'_{i,j}(c^{(i,j)}) - \gamma'_{j,k}(c^{(j,k)})) \\ & + \beta_{k,i \leftrightarrow i,j} (\gamma'_{i,j}(c^{(i,j)}) - \gamma'_{k,i}(c^{(k,i)})) \Big). \end{aligned} \tag{2.50}$$

With corresponding distribution $\chi_{\Omega^{(i)}} = (L^1 \otimes \mathcal{H}^d) \llcorner \Omega^{(i)}$, defined by

$$\langle \chi_{\Omega^{(i)}}, f \rangle = \int_0^T \int_{\Omega^{(i)}(t)} f(\boldsymbol{x}, t) \, \mathrm{d}\mathcal{H}^d(\boldsymbol{x}) \, \mathrm{d}L^1(t), \tag{2.51}$$

we reformulate (2.6) as,

$$0 = \partial_t(\chi_{\Omega^{(i)}} c^{(i)}) + \nabla \cdot (\chi_{\Omega^{(i)}}(c^{(i)} \boldsymbol{v} + \boldsymbol{j}_c^{(i)})) + \sum_{j \neq i} \delta_{\Gamma^{(i,j)}} \boldsymbol{j}_c^{(i)} \cdot \boldsymbol{\nu}^{(i,j)}. \tag{2.52}$$

We will use these forms to motivate the surfactant equations used in the phase field modelling methodology in Section 2.2.1. Now we shall discuss boundary conditions.

2.1.7 Boundary conditions

By considering test volumes $V(t)$ in the calculation found in Section 2.1.3 with $\partial V(t) \cap \partial\Omega \neq \emptyset$ we can assess the impact of the boundary conditions on the PDEs considered. In particular the terms (2.45), (2.43) and (2.44) motivate the following boundary conditions.

With regards to the velocity, we assume impenetrable boundaries

$$\boldsymbol{v} \cdot \boldsymbol{\nu}_\Omega = 0 \quad \text{on } \partial\Omega, \tag{2.53}$$

i.e., the velocity is tangential on $\partial\Omega$. We obtain a stress-free boundary condition, due to the first term (2.45), by imposing the condition

$$\boldsymbol{T}^{(i)} \cdot \boldsymbol{\nu}_{\partial\Omega} = 0 \quad \text{on } \partial\Omega. \tag{2.54}$$

Defining $\boldsymbol{P}_{\partial\Omega} = \boldsymbol{I} - \boldsymbol{\nu}_\Omega \otimes \boldsymbol{\nu}_\Omega \in \mathbb{R}^{d\times d}$ as the projection of $\mathbb{R}^d$ to the tangential space in each point of $\partial\Omega$, and looking at the second term (2.45), we impose the condition at interfaces $\Gamma^{(i,j)}$:

$$\boldsymbol{P}_{\partial\Omega}\boldsymbol{\mu}_\Omega^{(i,j)} = 0 \quad \text{on } \partial\Omega \cap \Gamma^{(i,j)}. \tag{2.55}$$

This ensures the interfaces intersect with $\partial\Omega$ with a $90°$ angle. No-flux conditions for both the bulk and the surface surfactant are natural conditions due to (2.43) and (2.44), and due to the boundary condition (2.53), these reduce to

$$\boldsymbol{j}_c^{(i)} \cdot \boldsymbol{\nu}_\Omega = 0 \quad \text{on } \partial\Omega \cap \partial\Omega^{(i)}, \tag{2.56}$$

$$\boldsymbol{j}_c^{(i,j)} \cdot \boldsymbol{\mu}_\Omega^{(i,j)} = 0 \quad \text{on } \partial\Omega \cap \partial\Gamma^{(i,j)}. \tag{2.57}$$

Depending on the application, other boundary conditions may be of relevance. Instead of (2.53) and (2.54) one could consider a Dirichlet condition for $\boldsymbol{v}$, so long as the boundary data satisfies the incompressibility constraint. In the case of in-flow or out-flow (2.56) then will read $(c^{(i)}\boldsymbol{v} + \boldsymbol{j}_c^{(i)}) \cdot \boldsymbol{\nu}_\Omega = 0$ (which is more clearly seen by viewing the distributional form (2.52)) and similarly for (2.57). For the surfactant a Dirichlet or a Robin condition may be of interest, too, and can easily be expressed in terms of the $c^{(i)}$ and the $c^{(i,j)}$. In all of these cases of non-natural boundary conditions the terms in (2.45) and (2.44) with $V(t) = \Omega$ will not vanish, in general, but may be interpreted as work done by the boundary condition.

2.1.8 Summary of sharp interface model with general sorption

We summarise the equations governing the evolution of the multi-phase flow with surfactant. The problem consists in finding a continuous velocity field $\boldsymbol{v}$, a pressure p and

surfactant concentrations $c^{(i)}$, $c^{(i,j)}$ such that in the domains $\Omega^{(i)}$

$$\nabla \cdot \boldsymbol{v} = 0, \tag{2.58}$$

$$\partial_t(\overline{\rho}^{(i)}\boldsymbol{v}) + \nabla \cdot (\overline{\rho}^{(i)}\boldsymbol{v} \otimes \boldsymbol{v}) = \nabla \cdot \big(-p\boldsymbol{I} + 2\eta^{(i)}\boldsymbol{D}(\boldsymbol{v})\big), \tag{2.59}$$

$$\partial_t^{\bullet(\boldsymbol{v})} c^{(i)} = \nabla \cdot \big(M_c^{(i)} \nabla g_i'(c^{(i)})\big), \tag{2.60}$$

in the interfaces $\Gamma^{(i,j)}$

$$u^{(i,j)} = \boldsymbol{v} \cdot \boldsymbol{\nu}^{(i,j)}, \ \ [\boldsymbol{v}] = 0, \tag{2.61}$$

$$[-p\boldsymbol{I} + 2\eta^{(\cdot)}\boldsymbol{D}(\boldsymbol{v})]_j^i \boldsymbol{\nu}^{(i,j)} = \sigma_{i,j}(c^{(i,j)})\boldsymbol{\kappa}^{(i,j)} + \nabla_{\Gamma^{(i,j)}}\sigma_{i,j}(c^{(i,j)}), \tag{2.62}$$

$$\alpha_{i,j} M_c^{(i)} \nabla g_i'(c^{(i)}) \cdot \boldsymbol{\nu}^{(i,j)} = (\gamma_{i,j}'(c^{(i,j)}) - g_i'(c^{(i)})), \tag{2.63}$$

$$\begin{aligned} \partial_t^{\bullet(\boldsymbol{v})} c^{(i,j)} + c^{(i,j)} \nabla_{\Gamma^{(i,j)}} \cdot \boldsymbol{v} = {} & \nabla_{\Gamma^{(i,j)}} \cdot \big(M_c^{(i,j)} \nabla_{\Gamma^{(i,j)}} \gamma_{i,j}'(c^{(i,j)})\big) \\ & + \frac{1}{\alpha_{i,j}}(g_i'(c^{(i)}) - \gamma_{i,j}'(c^{(i,j)})) \\ & + \frac{1}{\alpha_{j,i}}(g_j'(c^{(j)}) - \gamma_{i,j}'(c^{(i,j)})) \end{aligned} \tag{2.64}$$

and in the triple junctions $T^{(i,j,k)}$

$$\boldsymbol{u}^{(i,j,k)} = \boldsymbol{P}_{(T^{(i,j,k)})^\perp} \boldsymbol{v}, \tag{2.65}$$

$$\begin{aligned} -M_c^{(i,j)} \nabla_{\Gamma^{(i,j)}} \gamma_{i,j}'(c^{(i,j)}) \cdot \boldsymbol{\mu}^{(i,j,k)} = {} & \beta_{j,k\leftrightarrow i,j}(\gamma_{i,j}'(c^{(i,j)}) - \gamma_{j,k}'(c^{(j,k)})) \\ & + \beta_{k,i\leftrightarrow i,j}(\gamma_{i,j}'(c^{(i,j)}) - \gamma_{k,i}'(c^{(k,i)})), \end{aligned} \tag{2.66}$$

$$\begin{aligned} 0 = {} & \sigma_{i,j}(c^{(i,j)})\boldsymbol{\mu}^{(i,j,k)} + \sigma_{j,k}(c^{(j,k)})\boldsymbol{\mu}^{(j,k,i)} \\ & + \sigma_{k,i}(c^{(k,i)})\boldsymbol{\mu}^{(k,i,j)}. \end{aligned} \tag{2.67}$$

These equations then are completed with suitable initial conditions and boundary conditions as discussed in Section 2.1.7.

Remark 2.1.5. *In reference to the previous Remark 2.1.1 note that, we have implicitly assumed that there is always a mass of surfactant present in the whole domain, and so assuming that the surfactants are soluble in each fluid and may be adsorbed to any interface. However, one may account for insolubilities of any $c^{(i)}$'s by dropping the corresponding bulk equations* (2.60) *and any g_i terms in* (2.64)*. Similarly, one may account for the non adsorbant $c^{(i,j)}$ by dropping the corresponding interface equations* (2.64) *and dropping the $\gamma_{i,j}$ terms in the triple junctions.*

2.1.9 Instantaneous sorption

We investigate the case where adsorption-desorption dynamics of the surfactant at the interfaces and triple junction is on a fast timescale. It may then be considered as instantaneous at the time scale of the interface and fluid flow dynamics. Here we take for simplicity the case where this occurs at all interfaces and triple junctions. The statements and assumptions may be easily adapted for where surfactant chemisty is taken instantaneous at some interfaces and junctions, but elsewhere is noninstantaneous as before.

The local equilibrium conditions at the interfaces, that arise from the instantaneous sorption, result in *isotherms* [43]. These are static relationships (at constant temperature) between the surfactant concentration in a sublayer close to an interface, with the interfacial surfactant concentration. They are empirical and attempt to describe factors of the local chemistry at interfaces, we describe these further, with examples, in Section 2.1.11

In terms of the chemical potentials g_i' and $\gamma_{i,j}'$ the equilibrium conditions read

$$g_i'(c^{(i)}) = g_j'(c^{(j)}) = \gamma_{i,j}'(c^{(i,j)}) \quad \text{in } \Gamma^{(i,j)}, \tag{2.68}$$

and they can be obtained by setting $\alpha_{i,j} = 0$ in (2.30). In addition, we assume a local chemical equilibrium at the triple junctions:

$$\gamma_{i,j}'(c^{(i,j)}) = \gamma_{j,k}'(c^{(j,k)}) = \gamma_{k,i}'(c^{(k,i)}) \quad \text{in } T^{(i,j,k)}, \tag{2.69}$$

which can be obtained by letting $\beta_{i,j\leftrightarrow A,B} \to \infty$ in (2.31). Thus, if we assume that these equilibria are satisfied at all interfaces and triple junctions, then the chemical potential defined by:

$$q \coloneqq \begin{cases} g_i'(c^{(i)}) & \text{in } \Omega^{(i)}, \\ \gamma_{i,j}'(c^{(i,j)}) & \text{in } \Gamma^{(i,j)} \end{cases} \tag{2.70}$$

is a continuous function on Ω.

The consequences of local equilibrium (2.68) – (2.70) have a significant effect on the energy analysis. If one performs the energy dissipation calculations of Section 2.1.5, the term (2.41) vanishes due to (2.68). Similarly, the term (2.42) vanishes due to (2.69).

As free energies are convex as functions of the concentrations, the new description (2.68)-(2.70) allows for them to be locally inverted to express surfactant bulk and surface concentrations in terms of q:

$$c^{(i,j)}(q) = (\gamma_{i,j}')^{-1}(q), \quad c^{(i)}(q) = (g_i')^{-1}(q). \tag{2.71}$$

We can then also express the surface tension as a function of q:

$$\tilde{\sigma}_{i,j}(q) \coloneqq \sigma_{i,j}(c^{(i,j)}(q)) = \gamma_{i,j}(c^{(i,j)}(q)) - q\, c^{(i,j)}(q). \tag{2.72}$$

Similarly, for the surfactant fluxes:

$$\begin{aligned}
\boldsymbol{j}_c^{(i)} &= -M_c^{(i)} \nabla q && \text{in } \Omega^{(i)}, && (2.73)\\
\boldsymbol{j}_c^{(i,j)} &= -M_c^{(i,j)} \nabla_{\Gamma^{(i,j)}} q && \text{in } \Gamma^{(i,j)}, && (2.74)\\
[\boldsymbol{T}^{(\cdot)}]_j^i \boldsymbol{\nu}^{(i,j)} &= \tilde{\sigma}_{i,j}(q) \boldsymbol{\kappa}^{(i,j)} + \nabla_{\Gamma^{(i,j)}} \tilde{\sigma}_{i,j}(q) && \text{in } \Gamma^{(i,j)}, && (2.75)\\
0 &= \tilde{\sigma}_{i,j}(q) \boldsymbol{\mu}^{(i,j,k)} + \tilde{\sigma}_{j,k}(q) \boldsymbol{\mu}^{(j,k,i)} + \tilde{\sigma}_{k,i}(q) \boldsymbol{\mu}^{(k,i,j)} && \text{in } T^{(i,j,k)}. && (2.76)
\end{aligned}$$

This results in changes in the free energy evolution. From (2.38)-(2.44) we obtain

$$\begin{aligned}
&\frac{\mathrm{d}}{\mathrm{d}t} \left(\sum_i \int_{V \cap \Omega^{(i)}} \left(\frac{\overline{\rho}^{(i)}}{2} |\boldsymbol{v}|^2 + g_i(c^{(i)}(q)) \right) + \sum_{i<j} \int_{V \cap \Gamma^{(i,j)}} \gamma_{i,j}(c^{(i,j)}(q)) \right) && (2.77)\\
&= - \sum_i \int_{V \cap \Omega^{(i)}} (2\eta^{(i)} |\boldsymbol{D}(\boldsymbol{v})|^2 + M_c^{(i)} |\nabla q|^2) - \sum_{i<j} \int_{V \cap \Gamma^{(i,j)}} M_c^{(i,j)} |\nabla_{\Gamma^{(i,j)}} q|^2 && (2.78)\\
&\quad + \sum_i \int_{\partial V \cap \Omega^{(i)}} M_c^{(i)} q \nabla q \cdot \boldsymbol{\nu}_V && (2.79)\\
&\quad + \sum_{i<j} \int_{\partial V \cap \Gamma^{(i,j)}} M_c^{(i,j)} q \nabla_{\Gamma^{(i,j)}} q \cdot \boldsymbol{\mu}_V^{(i,j)}. && (2.80)\\
&\quad + \sum_i \int_{\partial V \cap \Omega^{(i)}} (\boldsymbol{T}^{(i)} \boldsymbol{v}) \cdot \boldsymbol{\nu}_V + \sum_{i<j} \int_{\partial V \cap \Gamma^{(i,j)}} \sigma_{i,j} \boldsymbol{v} \cdot \boldsymbol{\mu}_V^{(i,j)}. && (2.81)
\end{aligned}$$

2.1.10 Summary of sharp interface model with instantaneous sorption

Let us summarise the equations governing the evolution of the multi-phase flow with surfactant. The problem consists in finding a continuous velocity field $\boldsymbol{v}$, a pressure p and, due to (2.68),(2.69) a *continuous* chemical potential q, such that in the domains $\Omega^{(i)}$

$$\begin{aligned}
\nabla \cdot \boldsymbol{v} &= 0, && (2.82)\\
\partial_t(\overline{\rho}^{(i)} \boldsymbol{v}) + \nabla \cdot (\overline{\rho}^{(i)} \boldsymbol{v} \otimes \boldsymbol{v}) &= \nabla \cdot \big(- p\boldsymbol{I} + 2\eta^{(i)} \boldsymbol{D}(\boldsymbol{v}) \big), && (2.83)\\
\partial_t^{\bullet(\boldsymbol{v})} c^{(i)}(q) &= \nabla \cdot \big(M_c^{(i)} \nabla q \big), && (2.84)
\end{aligned}$$

in the interfaces $\Gamma^{(i,j)}$

$$u^{(i,j)} = \boldsymbol{v} \cdot \boldsymbol{\nu}^{(i,j)}, \tag{2.85}$$

$$[-p\boldsymbol{I} + 2\eta^{(\cdot)}\boldsymbol{D}(\boldsymbol{v})]^i_j \boldsymbol{\nu}^{(i,j)} = \tilde{\sigma}_{i,j}(q)\boldsymbol{\kappa}^{(i,j)} + \nabla_{\Gamma^{(i,j)}}\tilde{\sigma}_{i,j}(q), \tag{2.86}$$

$$\begin{aligned}\partial_t^{\bullet(\boldsymbol{v})} c^{(i,j)}(q) + c^{(i,j)}(q)\nabla_{\Gamma^{(i,j)}} \cdot \boldsymbol{v} &= \nabla_{\Gamma^{(i,j)}} \cdot \left(M_c^{(i,j)} \nabla_{\Gamma^{(i,j)}} q\right) \\ &\quad + \left[M_c^{(\cdot)} \nabla q\right]^i_j \cdot \boldsymbol{\nu}^{(i,j)}\end{aligned} \tag{2.87}$$

and in the triple junctions $T^{(i,j,k)}$

$$\boldsymbol{u}^{(i,j,k)} = \boldsymbol{P}_{(T^{(i,j,k)})^\perp} \boldsymbol{v}, \tag{2.88}$$

$$\begin{aligned}0 &= M_c^{(i,j)} \nabla_{\Gamma^{(i,j)}} q \cdot \boldsymbol{\mu}^{(i,j,k)} + M_c^{(j,k)} \nabla_{\Gamma^{(j,k)}} q \cdot \boldsymbol{\mu}^{(j,k,i)} \\ &\quad + M_c^{(k,i)} \nabla_{\Gamma^{(k,i)}} q \cdot \boldsymbol{\mu}^{(k,i,j)},\end{aligned} \tag{2.89}$$

$$0 = \tilde{\sigma}_{i,j}(q)\boldsymbol{\mu}^{(i,j,k)} + \tilde{\sigma}_{j,k}(q)\boldsymbol{\mu}^{(j,k,i)} + \tilde{\sigma}_{k,i}(q)\boldsymbol{\mu}^{(k,i,j)}. \tag{2.90}$$

These equations then are completed with suitable initial conditions and boundary conditions as discussed in Section 2.1.7, where once again surfactant mass densities and fluxes are expressed in terms of q.

Remark 2.1.6. *In the case of instantaneous adsorption in only some of the interfaces and triple junctions, the equations are modified by setting $\alpha_{i,j} = 0$ and sending $\beta_{i,j\leftrightarrow A,B} \to \infty$ in only the terms under equilibrium. This leads to a mixture of boundary conditions at interfaces: continuity of q imposed at interfaces in local equilibrium; jump conditions* (2.63) *imposed at interfaces out of equilibrium; finally, one sided jump conditions where the interface has a local equilibrium into just one of the neighbouring phases. Similarly for the triple junction boundary conditions.*

The distributional form is simplified from the introduction of the variable q, and by adding equations (2.48) and (2.52) over all the respective interface and bulk regions $\Omega^{(i)}$, $\Gamma^{(i,j)}$:

$$\partial_t^{\bullet(\boldsymbol{v})}\Big(\sum_i \chi_{\Omega^{(i)}} c^{(i)}(q) + \sum_{i<j} \delta_{\Gamma^{(i,j)}} c^{(i,j)}(q)\Big) = -\nabla \cdot \Big(\sum_i \chi_{\Omega^{(i)}} \boldsymbol{j}_c^{(i)} + \sum_{i<j} \delta_{\Gamma^{(i,j)}} \boldsymbol{j}_c^{(i,j)}\Big). \tag{2.91}$$

Remark 2.1.7. *In the case of instantaneous adsorption in only some of the interfaces and triple junctions here, one would simply sum over all the regions under a local equilibrium condition. The distributional form in other regions would be described with separate equations, as with* (2.48) *and* (2.52)*.*

2.1.11 Isotherm relations for instantaneous sorption

The assumption of instantaneous sorption around an interface leads to an local equilibrium between the surfactant chemical potentials in the bulk and on the interface, described by (2.68). The equilibrium relation is given by an appropriate *sorption isotherm*, associating the $c^{(i)}(q)$ to the $c^{(i,j)}(q)$ through a constant temperature time independent relationship. The different isotherms are empirical and chosen to represent particular chemical behaviours which the surfactants may undergo. The simplest and most commonly used relationships for nonionic surfactants are given below [44]. We describe the relations using an adsorption rate coefficient K, and $c_{\max}^{(i,j)}$, the surface tension of a surface with no surfactant present is given by σ_0. We additionally provide the corresponding free energies $\gamma_{i,j} - \sigma_0$ and g_i:

The Henry Isotherm:

$$Kc^{(i)} = \frac{c^{(i,j)}}{c_{\max}^{(i,j)}}. \tag{2.92}$$

This linear isotherm is motivated formally by Henry's gas law, which states (in our context) that the interfacial coverage of surfactant depends linearly on the concentration of bulk surfactant. The bulk and surface free energy associated with this isotherm are given by the Gibbs' adsorption equation in isothermal equilibrium (see Volume III Chapter 5 of [2]) which states,

$$g_i'(c^{(i)}) = B\ln(Kc^{(i)}), \tag{2.93}$$

for constant B (dependent only on temperature). Using the equilibrium relations (2.68), (2.70) and (2.92) we obtain:

$$g_i(c^{(i)}(q)) = BKc^{(i)}(q)\Big(\ln(Kc^{(i)}(q)) - 1\Big) = \exp\Big(\frac{q}{B}\Big)\Big(q - B\Big) \tag{2.94}$$

$$\gamma_{i,j}(c^{(i,j)}(q)) - \sigma_0 = \frac{B}{c_{\max}^{(i,j)}}c^{(i,j)}(q)\Big(\ln\Big(\frac{c^{(i,j)}(q)}{c_{\max}^{(i,j)}}\Big) - 1\Big) = \exp\Big(\frac{q}{B}\Big)\Big(q - B\Big). \tag{2.95}$$

The Langmuir Isotherm [85]:

$$Kc^{(i)} = \frac{c^{(i,j)}}{c_{\max}^{(i,j)} - c^{(i,j)}}. \tag{2.96}$$

This nonlinear isotherm introduces a maximum coverage of the interface in surfactant. The surface is still assumed homogeneous regarding adsorption, the rate is given proportional to the available sites with respect to the maximal concentration. The bulk and surface free

energy associated with this isotherm are given by,

$$g_i(c^{(i)}(q)) = BKc^{(i)}(q)\Big(\ln(Kc^{(i)}(q)) - 1\Big) = \exp\Big(\frac{q}{B}\Big)\Big(q - B\Big) \tag{2.97}$$

$$\begin{aligned}\gamma_{i,j}(c^{(i,j)}(q)) - \sigma_0 &= B\Big(\frac{c^{(i,j)}(q)}{c^{(i,j)}_{\max} - c^{(i,j)}(q)} \ln\Big(\frac{c^{(i,j)}(q)}{c^{(i,j)}_{\max} - c^{(i,j)}(q)}\Big) \\ &\qquad + c^{(i,j)}_{\max} \ln(c^{(i,j)}_{\max} - c^{(i,j)}(q))\Big) \\ &= \exp\Big(\frac{q}{B}\Big)q + Bc^{(i,j)}_{\max} \ln\Big(\frac{c^{(i,j)}_{\max}}{1 + \exp\big(\frac{q}{B}\big)}\Big)\Big).\end{aligned} \tag{2.98}$$

A Quadratic Isotherm:

We also make use of a nonphysical isotherm relation in implementation for demonstrative purposes. The bulk and surface free energy are given by:

$$g_i(c^{(i)}(q)) = \frac{1}{2}\beta_i(c^{(i)}(q))^2 = \frac{1}{2}\frac{q^2}{\beta_i} \tag{2.99}$$

$$\gamma_{i,j}(c^{(i,j)}(q)) - \sigma_0 = \frac{1}{2}\beta_{i,j}(c^{(i,j)})^2 = \frac{1}{2}\frac{q^2}{\beta_{i,j}} \tag{2.100}$$

for $\beta_i > 0$, $\beta_{i,j} > 0$ chosen constants. For convenience we also state the corresponding surface tension $\tilde{\sigma}_{i,j}(q)$ and bulk excess free energy $\tilde{\lambda}_{i,j}(q)$ in this :

$$\tilde{\sigma}_{i,j}(q) = \sigma_0 - \frac{1}{2}\frac{q^2}{\beta_{i,j}}, \qquad \tilde{\lambda}_{i,j}(q) = -\frac{1}{2}\frac{q^2}{\beta_i}. \tag{2.101}$$

2.2 Diffuse interface model

The goal is now to derive a phase field model to approximate the free boundary problem which was presented in Section 2.1. As in [54] we postulate abstract balance equations for the mass of the mass and momentum of the fluid, the mass of surfactant and the newly introduce phase field variables, and close them within an energetic framework by postulating a suitable free energy density. The phase field model for multi-phase flow is based on [1] which is extended to multiple phases.

2.2.1 Phase field approach and balance equations

As introduced in Chapter 1, we begin by defining a small length scale $\varepsilon > 0$, the *interfacial thickness parameter*, which will characterise the length scales of interfacial layers between

the different fluids (or more precisely, the different *phases* of a fluid domain). It is a fundamental parameter of the approximation, thus we shall use it as an index for all newly defined variables depending on ε. As usual in phase field approaches to multi-phase problems we introduce one phase field variable for each phase (here, the immiscible fluids) which serves to model its presence. Denoting by $\rho_\varepsilon^{(i)}$ the mass density of fluid i we define the phase field variables by

$$\varphi_\varepsilon^{(i)} \coloneqq \frac{\rho_\varepsilon^{(i)}}{\overline{\rho}^{(i)}}, \quad i = 1, \dots, M. \tag{2.102}$$

As the fluids are immiscible one will expect that $\rho_\varepsilon^{(i)} \approx \overline{\rho}^{(i)}$ in the domain of fluid i and $\rho_\varepsilon^{(i)} \approx 0$ elsewhere, with values in between only in the thin layers between the fluid domains where the fluids mix.

We assume that the phase field obeys the following constraint:

$$\sum_{i=1}^{M} \varphi_\varepsilon^{(i)} = 1. \tag{2.103}$$

This assumption is that there there is no excess volume of mixing in these layers. In a small control volume V, the masses of the fluids are given by $M^{(i)} = \rho_\varepsilon^{(i)} V$. No excess volume of mixing means that V coincides with the sum of the volumes $V^{(i)} = M^{(i)}/\overline{\rho}^{(i)}$ occupied by the same masses of pure fluids, $V = \sum_i V^{(i)}$ (dividing by V yields (2.103)).

Remark 2.2.1. *One can pick different fields for the order parameters $\varphi_\varepsilon^{(i)}$, such as the $\rho_\varepsilon^{(i)}$ or the mass concentrations $\rho_\varepsilon^{(i)}/\rho_\varepsilon$. The essential requirement is that the mass densities $\rho_\varepsilon^{(i)}$ and the total mass density ρ_ε can be expressed in terms of the $\varphi_\varepsilon^{(i)}$.*

We introduce the *Gibbs' Simplex*

$$\Sigma^M \coloneqq \Big\{ u = (u_1, \dots, u_M) \in \mathbb{R}^M \ : \ \sum_{i=1}^{M} u_i = 1, \text{ where } 0 \le u_i \le 1 \Big\}, \tag{2.104}$$

as well as

$$T\Sigma^M \coloneqq \Big\{ u = (u_1, \dots, u_M) \in \mathbb{R}^M \ : \ \sum_{i=1}^{M} u_i = 0 \Big\}, \tag{2.105}$$

which can be naturally identified with the tangent space on Σ^M in each point, we thus have that $\varphi_\varepsilon = (\varphi_\varepsilon^{(1)}, \dots, \varphi_\varepsilon^{(M)}) \in \Sigma^M$. Note that the corners of the Gibbs' simplex correspond to the pure fluids as there one of the phase field variables equals one and all the others are zero. We write $\boldsymbol{e}_k = (\tilde{\delta}_{k,l})_{l=1}^M$, $k = 1, \dots, M$ for these corners, where $\tilde{\delta}_{k,l}$ stands for the Kronecker symbol. For later use we also introduce $\mathbf{1} = (1, \dots, 1) \in \mathbb{R}^M$ and note that vectors $u \in T\Sigma^M$ are characterised by $u \cdot \mathbf{1} = 0$.

Remark 2.2.2. *In practice, the hard constraint $\varphi_\varepsilon^{(i)} \in [0,1]$ often is dropped in favour of a soft penalisation. We allow values outside the interval $[0,1]$ but it is energetically unfavourable for $\varphi_\varepsilon^{(i)}$ to do this. This penalisation allows for higher regularity in the differential equations that govern the $\varphi_\varepsilon^{(i)}$'s.*

Denoting by $\boldsymbol{v}^{(i)}$ the velocity of mass particles of fluid i the mass balances for the fluids read

$$\partial_t \rho_\varepsilon^{(i)} + \nabla \cdot (\rho_\varepsilon^{(i)} \boldsymbol{v}^{(i)}) = 0. \tag{2.106}$$

In order to describe the motion of the fluid mixture we use the *volume averaged velocity*, (see remark 2.2.3):

$$\boldsymbol{v}_\varepsilon \coloneqq \sum_{i=1}^{M} \varphi_\varepsilon^{(i)} \boldsymbol{v}^{(i)}, \tag{2.107}$$

which is solenoidal: indeed, using (2.103), (2.102), and (2.106)

$$\nabla\cdot\boldsymbol{v}_\varepsilon = \partial_t\Big(\sum_{i=1}^{M}\varphi_\varepsilon^{(i)}\Big)+\nabla\cdot\Big(\sum_{i=1}^{M}\varphi_\varepsilon^{(i)}\boldsymbol{v}^{(i)}\Big) = \sum_{i=1}^{M}\frac{1}{\overline{\rho}^{(i)}}\big(\partial_t\rho_\varepsilon^{(i)}+\nabla\cdot(\rho_\varepsilon^{(i)}\boldsymbol{v}^{(i)})\big) = 0. \tag{2.108}$$

As in the previous section (see (2.3)) we use a *material derivative*

$$\partial_t^{\bullet(\boldsymbol{v}_\varepsilon)} w \coloneqq \partial_t w + \boldsymbol{v}_\varepsilon \cdot \nabla w, \tag{2.109}$$

here with respect to the velocity field $\boldsymbol{v}_\varepsilon$. The species mass balances (2.106) yield that

$$\partial_t^{\bullet(\boldsymbol{v}_\varepsilon)} \varphi_\varepsilon^{(i)} + \varphi_\varepsilon^{(i)} \nabla \cdot \boldsymbol{v}_\varepsilon = -\nabla \cdot \boldsymbol{j}_{\varphi_\varepsilon^{(i)}}, \tag{2.110}$$

$$\boldsymbol{j}_{\varphi_\varepsilon^{(i)}} = \varphi_\varepsilon^{(i)}(\boldsymbol{v}^{(i)} - \boldsymbol{v}_\varepsilon). \tag{2.111}$$

Note that, because of (2.108), the total mass density

$$\rho_\varepsilon \coloneqq \sum_{i=1}^{M} \varphi_\varepsilon^{(i)} \rho_\varepsilon^{(i)}, \tag{2.112}$$

satisfies the equation

$$\partial_t^{\bullet(\boldsymbol{v}_\varepsilon)} \rho_\varepsilon + \rho_\varepsilon \nabla \cdot \boldsymbol{v}_\varepsilon = -\nabla \cdot \overline{\boldsymbol{j}}_\varepsilon \quad \text{with } \overline{\boldsymbol{j}}_\varepsilon = \sum_{i=1}^{M} \overline{\rho}^{(i)} \boldsymbol{j}_{\varphi_\varepsilon^{(i)}}. \tag{2.113}$$

Remark 2.2.3. *We have chosen a framework as given by [1]. This constructs a divergence free (volume averaged) velocity, which is very useful for computations (for issues relating to compressibility in this case see [20, 41]). The sacrifice as we see is that we do not*

obtain a mass conservation for the fluids, but instead yield the dissipation shown in (2.113)*. There are other methods [20, 41], which prove more admissible for theoretical results [58], beginning with mass conservation of the fluids. The sacrifice is that the velocity (that is mass averaged) is not divergence free. These constructions arise when one is considering the interpolation* $\rho_\varepsilon(\varphi_\varepsilon)$ *not to be linear, but a harmonic interpolation. For example,* $M = 2$*:*
Linear interpolation:

$$\rho(\varphi_\varepsilon) = \overline{\rho}^{(1)}\varphi_\varepsilon + \overline{\rho}^{(2)}(1 - \varphi_\varepsilon), \tag{2.114}$$

Harmonic interpolation:

$$\frac{1}{\rho(\varphi_\varepsilon)} = \frac{\varphi_\varepsilon}{\overline{\rho}^{(1)}} + \frac{1 - \varphi_\varepsilon}{\overline{\rho}^{(2)}}. \tag{2.115}$$

The linear interpolation (2.114) *may lead to spurious unphysical densities* $\rho_\varepsilon(\varphi_\varepsilon) \leq 0$ *because the Cahn-Hilliard equation doesn't satisfy a maximum principle [90]. One can show however that* (2.115)*, due to* L^∞ *bounds of the solution [28], can ensure* $\rho_\varepsilon(\varphi_\varepsilon) > 0$*, which is a desirable property.*

We now assume that the inertia and the kinetic energy which are due to the motion of the fluids relative to the gross motion given in terms of $\boldsymbol{v}_\varepsilon$ is negligible. This allows us to continue to work in a framework based on local balance laws, and the second law of thermodynamics as detailed in [67]. Thus, rather than formulating momentum balances for the individual velocities $\boldsymbol{v}^{(i)}$ we will formulate the conservation of (linear) momentum in terms of $\boldsymbol{v}_\varepsilon$ and, within an energetic framework presented further below, make assumptions on the fluxes $\boldsymbol{j}_{\varphi_\varepsilon^{(i)}}$. With a stress tensor $\boldsymbol{T}_\varepsilon$ yet to be determined we postulate

$$\partial_t^{\bullet(\boldsymbol{v}_\varepsilon)}(\rho_\varepsilon \boldsymbol{v}_\varepsilon) + \rho_\varepsilon \boldsymbol{v}_\varepsilon \, \nabla \cdot \boldsymbol{v}_\varepsilon = \nabla \cdot \boldsymbol{T}_\varepsilon. \tag{2.116}$$

In Section 2.1.6 we discussed the distributional form of the surfactant equations in the bulk and interface regions. In order to approximate these forms of the surfactant equations using our diffuse interface model, we approximate the distributions $\delta_{\Gamma^{(i,j)}}$, $\tau_{T^{(i,j,k)}}$ and $\chi_{\Omega^{(i)}}$ with the help of the phase field variables. Let $\delta_{i,j}(\varphi_\varepsilon, \nabla\varphi_\varepsilon)$ denote an approximation to $\delta_{\Gamma^{(i,j)}}$ which will be picked later on (see (2.129)), and let

$$\xi_i(\varphi_\varepsilon) \coloneqq \begin{cases} 0 & \text{if } \varphi_\varepsilon \leq 0, \\ 1 & \text{if } \varphi_\varepsilon \geq 1, \\ \varphi_\varepsilon^2(3 - 2\varphi_\varepsilon) & \text{else,} \end{cases} \tag{2.117}$$

denote an approximation of the characteristic function $\chi_{\Omega^{(i)}}$. The forms that (2.117) can take are discussed in [122] and the effects on an asymptotic analysis is presented. For that analysis we require that the function ξ_i is monotone, and $\xi_i \in C^1(\Omega)$, with $\xi_i(p) = 0$,

$\xi_i(1-p) = 1\ \forall p \leq 0$ and derivative $\xi_i'(p) = 0$ if $p \in \{0,1\}$. The choice (2.117) fulfills these criteria. By $\tau_{i,j,k}(\varphi_\varepsilon, \nabla\varphi_\varepsilon)$ we denote an approximation to the distribution $\tau_{T^{(i,j,k)}}$, which will be discussed in Section 2.2.5.

For the general dynamic sorption case Section refsec:nonintad, we take the following ansatz for the form of balance of the surfactant mass densities $c_\varepsilon^{(i)}$, and $c_\varepsilon^{(i,j)}$ with corresponding mass fluxes $\boldsymbol{j}_{c,\varepsilon}^{(i)}$, $\boldsymbol{j}_{c,\varepsilon}^{(i,j)}$ and sorption fluxes $q_{\mathrm{ad},\varepsilon}^{(i,j)}$, $q_{\mathrm{ad},\varepsilon}^{(i,j,k)}$ over bulk and interfacial regions. It is constructed by substituting the distributions ξ_i, $\delta_{i,j}$, $\tau_{i,j,k}$ into (2.48) and (2.52) in the place of $\chi_{\Omega^{(i)}}$, $\chi_{\Gamma^{(i,j)}}$, $\chi_{T^{(i,j,k)}}$.

$$\begin{aligned}
&\partial_t^{\bullet(\boldsymbol{v}_\varepsilon)}\big(\delta_{i,j}(\varphi_\varepsilon,\nabla\varphi_\varepsilon)c_\varepsilon^{(i,j)}\big) + \delta_{i,j}(\varphi_\varepsilon,\nabla\varphi_\varepsilon)c_\varepsilon^{(i,j)}\nabla\cdot\boldsymbol{v}_\varepsilon + \nabla\cdot\big(\delta_{i,j}\boldsymbol{j}_{c,\varepsilon}^{(i,j)}\big)\\
&\qquad - \delta_{i,j}(\varphi_\varepsilon,\nabla\varphi_\varepsilon)(q_{\mathrm{ad},\varepsilon}^{(i,j)} + q_{\mathrm{ad},\varepsilon}^{(j,i)}) + \sum_{k\neq i,j}\tau_{i,j,k}(\varphi_\varepsilon,\nabla\varphi_\varepsilon)q_{\mathrm{ad},\varepsilon}^{(i,j,k)} = 0, \qquad (2.118)\\
&\partial_t^{\bullet(\boldsymbol{v}_\varepsilon)}\big(\xi_i(\varphi_\varepsilon)c_\varepsilon^{(i)}\big) + \xi_i(\varphi_\varepsilon^{(i)})c_\varepsilon^{(i)}\nabla\cdot\boldsymbol{v}_\varepsilon + \nabla\cdot\big(\xi_i(\varphi_\varepsilon^{(i)})\boldsymbol{j}_{c,\varepsilon}^{(i)}\big)\\
&\qquad + \sum_{j\neq i}\delta_{i,j}(\varphi_\varepsilon,\nabla\varphi_\varepsilon)q_{\mathrm{ad},\varepsilon}^{(i,j)} = 0. \qquad (2.119)
\end{aligned}$$

We make straightforward regularisations of the adsorption-desorption flux $q_{\mathrm{ad}}^{(i,j)}$ defined in (2.15) and (2.30) to define $q_{\mathrm{ad},\varepsilon}^{(i,j)}$. Similarly we regularise $q_{\mathrm{ad}}^{(i,j,k)}$ defined in (2.17) and (2.31) to define the flux $q_{\mathrm{ad},\varepsilon}^{(i,j,k)}$:

$$\begin{aligned}
q_{\mathrm{ad},\varepsilon}^{(i,j)} &= -\frac{1}{\alpha_{i,j}}(\gamma_{i,j}'(c_\varepsilon^{(i,j)}) - g_i'(c_\varepsilon^{(i)})), \qquad (2.120)\\
q_{\mathrm{ad},\varepsilon}^{(i,j,k)} &= \beta_{j,k\leftrightarrow i,j}(\gamma_{i,j}'(c_\varepsilon^{(i,j)}) - \gamma_{j,k}'(c_\varepsilon^{(j,k)})) + \beta_{k,i\leftrightarrow i,j}(\gamma_{i,j}'(c_\varepsilon^{(i,j)}) - \gamma_{k,i}'(c_\varepsilon^{(k,i)})), \qquad (2.121)
\end{aligned}$$

with coefficients $\alpha_{i,j}$ and $\beta_{i,j\leftrightarrow A,B}$ as in (2.30), (2.31).

Remark 2.2.4. *The above is a natural generalization of Model A in [54], based on the two-phase flow model by [1] to multiple phases and surfactant fields.*

In the same way, we study the case of instantaneous sorption, detailed in Section 2.1.9, we take the following ansatz for the regularisation of (2.91):

$$\begin{aligned}
&\partial_t^{\bullet(\boldsymbol{v}_\varepsilon)}\Big(\sum_i \xi_i(\varphi_\varepsilon^{(i)})c_\varepsilon^{(i)}(q_\varepsilon) + \sum_{i<j}\delta_{i,j}(\varphi_\varepsilon,\nabla\varphi_\varepsilon)c_\varepsilon^{(i,j)}(q_\varepsilon)\Big)\\
&\qquad + \Big(\sum_i \xi_i(\varphi_\varepsilon^{(i)})c_\varepsilon^{(i)}(q_\varepsilon) + \sum_{i<j}\delta_{i,j}(\varphi_\varepsilon,\nabla\varphi_\varepsilon)c_\varepsilon^{(i,j)}(q_\varepsilon)\Big)\nabla\cdot\boldsymbol{v}_\varepsilon\\
&\qquad\qquad + \nabla\cdot\Big(\sum_i \xi_i(\varphi_\varepsilon^{(i)})\boldsymbol{j}_{c,\varepsilon}^{(i)} + \sum_{i<j}\delta_{i,j}(\varphi_\varepsilon,\nabla\varphi_\varepsilon)\boldsymbol{j}_{c,\varepsilon}^{(i,j)}\Big) = 0. \qquad (2.122)
\end{aligned}$$

This is a generalisation of Model C in [54]. We will discuss the instantaneous sorption approximation later in Section 2.2.6.

Remark 2.2.5. *We could have dropped the terms with* $\nabla \cdot \boldsymbol{v}_\varepsilon$ *in* (2.110)*,* (2.116)*,* (2.119) *and* (2.118) *thanks to* (2.108)*. However, keeping track of them will give a clearer idea of pressure contributions to the stress tensor from the thermodynamic analysis in Section 2.2.3. In particular, we can identify interfacial terms which will prove beneficial in future asymptotic analysis.*

2.2.2 Free energy

The significance of the small parameter ε is how it features in a Ginzburg-Landau type energy for the phase field variables which serves to approximate the surface energies of the various possible interfaces. Let $\check{a} : \Sigma^M \times (T\Sigma^M)^d \to [0, \infty)$ be a gradient potential which is positive ($\check{a}(\varphi_\varepsilon, X) > 0$ whenever $X \neq 0$), even and two-homogeneous in the second argument ($\check{a}(\phi, \eta X) = \eta^2 \check{a}(\phi, X)$ for all $\eta \in \mathbb{R}$), and let $\check{w} : \Sigma^M \to [0, \infty]$ be a multi-well potential satisfying $\check{w}(\varphi_\varepsilon) = 0$ if and only if φ_ε is one of the corners of Σ^M. Under some more regularity and technical assumptions on $\check{a}$ and $\check{w}$ which we omit for brevity it is shown in [17] that, as $\varepsilon \to 0$,

$$\int_\Omega \Big(\varepsilon \check{a}(\varphi_\varepsilon, \nabla \varphi_\varepsilon) + \frac{1}{\varepsilon} \check{w}(\varphi_\varepsilon) \Big) \quad \to \quad \sum_{i<j} \int_{\Gamma^{(i,j)}} \check{\gamma}_{i,j}(\boldsymbol{\nu}^{(i,j)}), \tag{2.123}$$

in the sense of a Γ-limit. The relation between the potential and the surface energies is given by the minimisation problems (see [120, 55])

$$\check{\gamma}_{i,j}(\boldsymbol{\nu}^{(i,j)}) = \inf_p \Big\{ 2 \int_{-1}^{1} \sqrt{\check{w}(p) \check{a}(p, p' \otimes \boldsymbol{\nu}^{(i,j)})} dy \,\Big| \\ p : [-1,1] \to \Sigma^M \text{ Lipschitz }, \, p(-1) = \boldsymbol{e}_i, \, p(1) = \boldsymbol{e}_j \Big\}, \tag{2.124}$$

where $\boldsymbol{e}_i, \boldsymbol{e}_j \in \mathbb{R}^M$ are the corners of the Gibbs' simplex corresponding to the fluids i and j. Note that this formula holds for some anisotropic surface energies [57] (dependent on the direction $\boldsymbol{\nu}^{(i,j)}$ of the interface) but we here only consider isotropic surface energies.

For naïve choices of $\check{a}$ and $\check{w}$, minimisers lie in the interior of Σ^M rather than along the edge which connects $\boldsymbol{e}_i$ with $\boldsymbol{e}_j$. In numerical simulations so-called *third phase contributions* then can be observed within the thin interfacial layers [56]. While they may be considered unphysical, the main issue is that they make the recovery of given surface energies $\check{\gamma}_{i,j}$ difficult, see [121] for an outline of the problem. But suitable potentials have been discovered which avoid those interfacial third phase contributions (or satisfy the *consistency principle* introduced in [23] of reducing to a two-phase system given suitable initial

and boundary data). These potentials also enable the approximation of given surface energies $\check{\gamma}_{i,j}$, see [57, 56, 21, 23]. The choice of these potentials will be discussed further in Section 2.2.8, and observations into particular potential choices will be made within.

2.2.3 General sorption model

We build up on these works in order to approximate the energy (2.18). Consider the form

$$E_\varepsilon \coloneqq \int_\Omega e_\varepsilon, \quad e_\varepsilon \coloneqq \frac{\rho_\varepsilon}{2}|\boldsymbol{v}_\varepsilon|^2 + f(c_\varepsilon^{(\cdot)}, \varphi_\varepsilon) + \frac{1}{\varepsilon} w(c_\varepsilon^{(\cdot,\cdot)}, \varphi_\varepsilon) + \varepsilon a(c_\varepsilon^{(\cdot,\cdot)}, \varphi_\varepsilon, \nabla\varphi_\varepsilon), \tag{2.125}$$

with the contributions

$$f(c_\varepsilon^{(\cdot)}, \varphi_\varepsilon) \coloneqq \sum_i \xi_i(\varphi_\varepsilon^{(i)}) g_i(c_\varepsilon^{(i)}). \tag{2.126}$$

$$a(c_\varepsilon^{(\cdot,\cdot)}, \varphi_\varepsilon, \nabla\varphi_\varepsilon) \coloneqq \sum_{i<j} \gamma_{i,j}(c_\varepsilon^{(i,j)}) a_{i,j}(\varphi_\varepsilon, \nabla\varphi_\varepsilon), \tag{2.127}$$

$$w(c_\varepsilon^{(\cdot,\cdot)}, \varphi_\varepsilon) \coloneqq \sum_{i<j} \gamma_{i,j}(c_\varepsilon^{(i,j)}) \overline{w}_{i,j}(\varphi_\varepsilon), \tag{2.128}$$

See [57] for possible choices of the $a_{i,j}$ and the $\overline{w}_{i,j}$. We may then define,

$$\delta_{i,j}(\varphi_\varepsilon, \nabla\varphi_\varepsilon) \coloneqq \varepsilon a_{i,j}(\varphi_\varepsilon, \nabla\varphi_\varepsilon) + \frac{1}{\varepsilon}\overline{w}_{i,j}(\varphi_\varepsilon), \tag{2.129}$$

which will be the diffuse approximation of $\delta_{\Gamma^{(i,j)}}$ (in the sense of (2.123)) defined in (2.46).

As with the sharp interface model we require thermodynamic consistency in terms of the dissipation of the energy to be non-negative. We thus have to ensure that

$$\partial_t^{\bullet(\boldsymbol{v}_\varepsilon)} e_\varepsilon + e_\varepsilon \nabla\cdot\boldsymbol{v}_\varepsilon + \nabla\cdot\boldsymbol{j}_{e_\varepsilon} \leq 0, \tag{2.130}$$

where the free energy density e_ε is defined in (2.125) and its flux $\boldsymbol{j}_{e_\varepsilon}$ will be defined below. We recall the surface tension $\sigma_{i,j} = \gamma_{i,j}(c_\varepsilon^{(i,j)}) - \gamma'_{i,j} c_\varepsilon^{(i,j)}$ from (2.72) and define an analogous field for the bulk excess free energy by:

$$\lambda_k \coloneqq g_k(c_\varepsilon^{(k)}) - g_i'(c_\varepsilon^{(k)}) c_\varepsilon^{(k)}. \tag{2.131}$$

In the calculations hereafter we condense calculations with the following notation, for $\mathbf{a}, \mathbf{b}, \mathbf{c} \in \mathbb{R}^d$ and $\mathbf{M} \in \mathbb{R}^{d\times d}$:

$$(\mathbf{a}\cdot\mathbf{M})\cdot\mathbf{b} = \sum_{i,j} \mathbf{a}_i \mathbf{M}_{ij} \mathbf{b}_j, \quad \mathbf{a}\cdot(\nabla\cdot(\mathbf{b}\otimes\mathbf{c})) = \sum_{i,j} \mathbf{a}_i \partial_j(\mathbf{b}_i \mathbf{c}_j), \quad (\nabla\cdot\mathbf{M})\cdot\mathbf{a} = \sum_{i,j} \partial_i(\mathbf{M}_{ij})\mathbf{a}_j.$$

We first treat the kinetic energy terms. We rewrite $(*) = 2(*) - (*)$, we apply the product rule for two functions to the first term, and apply the product rule for three functions to the second term. This is seen in the following calculation:

$$
\begin{aligned}
&\partial_t^{\bullet(\boldsymbol{v}_\varepsilon)}\big(\frac{\rho_\varepsilon}{2}|\boldsymbol{v}_\varepsilon|^2\big)\\
&= 2\partial_t^{\bullet(\boldsymbol{v}_\varepsilon)}\big(\frac{\rho_\varepsilon}{2}|\boldsymbol{v}_\varepsilon|^2\big) - \partial_t^{\bullet(\boldsymbol{v}_\varepsilon)}\big(\frac{\rho_\varepsilon}{2}|\boldsymbol{v}_\varepsilon|^2\big)\\
&= 2\Big(\frac{\boldsymbol{v}_\varepsilon}{2}\cdot\partial_t^{\bullet(\boldsymbol{v}_\varepsilon)}\big(\rho_\varepsilon\boldsymbol{v}_\varepsilon\big) + \frac{\rho_\varepsilon\boldsymbol{v}_\varepsilon}{2}\cdot\partial_t^{\bullet(\boldsymbol{v}_\varepsilon)}\big(\boldsymbol{v}_\varepsilon\big)\Big)\\
&- \Big(\frac{\rho_\varepsilon\boldsymbol{v}_\varepsilon}{2}\cdot\partial_t^{\bullet(\boldsymbol{v}_\varepsilon)}\big(\boldsymbol{v}_\varepsilon\big) + \frac{\rho_\varepsilon\boldsymbol{v}_\varepsilon}{2}\cdot\partial_t^{\bullet(\boldsymbol{v}_\varepsilon)}\big(\boldsymbol{v}_\varepsilon\big) + \frac{|\boldsymbol{v}_\varepsilon|^2}{2}\cdot\partial_t^{\bullet(\boldsymbol{v}_\varepsilon)}\big(\rho_\varepsilon\big)\Big)\\
&= \boldsymbol{v}_\varepsilon\cdot\partial_t^{\bullet(\boldsymbol{v}_\varepsilon)}(\rho_\varepsilon\boldsymbol{v}_\varepsilon) - \frac{|\boldsymbol{v}_\varepsilon|^2}{2}\partial_t^{\bullet(\boldsymbol{v}_\varepsilon)}(\rho_\varepsilon).
\end{aligned}
$$

Insert the balance equations (2.116) and (2.113),

$$
\begin{aligned}
&\boldsymbol{v}_\varepsilon\cdot\partial_t^{\bullet(\boldsymbol{v}_\varepsilon)}(\rho_\varepsilon\boldsymbol{v}_\varepsilon) - \frac{|\boldsymbol{v}_\varepsilon|^2}{2}\partial_t^{\bullet(\boldsymbol{v}_\varepsilon)}(\rho_\varepsilon)\\
&= \boldsymbol{v}_\varepsilon\cdot(\nabla\cdot\boldsymbol{T}_\varepsilon) - \rho_\varepsilon|\boldsymbol{v}_\varepsilon|^2(\nabla\cdot\boldsymbol{v}_\varepsilon) - \frac{|\boldsymbol{v}_\varepsilon|^2}{2}(\nabla\cdot\overline{\boldsymbol{j}}_\varepsilon) + |\boldsymbol{v}_\varepsilon|^2(\nabla\cdot\overline{\boldsymbol{j}}_\varepsilon) + \frac{|\boldsymbol{v}_\varepsilon|^2}{2}\rho_\varepsilon(\nabla\cdot\boldsymbol{v}_\varepsilon).
\end{aligned}
\tag{2.132}
$$

We provide the differential identities:

$$
-\frac{|\boldsymbol{v}_\varepsilon|^2}{2}(\nabla\cdot\overline{\boldsymbol{j}}_\varepsilon) = -\nabla\cdot\Big(\frac{|\boldsymbol{v}_\varepsilon|^2}{2}\overline{\boldsymbol{j}}_\varepsilon\Big) + (\boldsymbol{v}_\varepsilon\cdot\nabla\boldsymbol{v}_\varepsilon)\cdot\overline{\boldsymbol{j}}_\varepsilon, \tag{2.133}
$$

$$
|\boldsymbol{v}_\varepsilon|^2(\nabla\cdot\overline{\boldsymbol{j}}_\varepsilon) = \boldsymbol{v}_\varepsilon\cdot(\nabla\cdot(\boldsymbol{v}_\varepsilon\otimes\overline{\boldsymbol{j}}_\varepsilon)) - (\boldsymbol{v}_\varepsilon\cdot\nabla\boldsymbol{v}_\varepsilon)\cdot\overline{\boldsymbol{j}}_\varepsilon, \tag{2.134}
$$

$$
\boldsymbol{v}_\varepsilon\cdot\big(\nabla\cdot\boldsymbol{T}_\varepsilon\big) = \nabla\cdot\big(\boldsymbol{T}_\varepsilon^{\perp}\boldsymbol{v}_\varepsilon\big) - \boldsymbol{T}_\varepsilon\colon\nabla\boldsymbol{v}_\varepsilon, \tag{2.135}
$$

$$
\boldsymbol{v}_\varepsilon\cdot\big(\nabla\cdot(\boldsymbol{v}_\varepsilon\otimes\overline{\boldsymbol{j}}_\varepsilon)\big) = \nabla\cdot\big((\boldsymbol{v}_\varepsilon\otimes\overline{\boldsymbol{j}}_\varepsilon)^{\perp}\boldsymbol{v}_\varepsilon\big) - (\boldsymbol{v}_\varepsilon\otimes\overline{\boldsymbol{j}}_\varepsilon)\colon\nabla\boldsymbol{v}_\varepsilon. \tag{2.136}
$$

Insert (2.133) and (2.134) into (2.132), to give the following equality:

$$
\begin{aligned}
&\boldsymbol{v}_\varepsilon\cdot(\nabla\cdot\boldsymbol{T}_\varepsilon) - \frac{|\boldsymbol{v}_\varepsilon|^2}{2}(\nabla\cdot\overline{\boldsymbol{j}}_\varepsilon) + |\boldsymbol{v}_\varepsilon|^2(\nabla\cdot\overline{\boldsymbol{j}}_\varepsilon) - \frac{|\boldsymbol{v}_\varepsilon|^2}{2}\rho_\varepsilon(\nabla\cdot\boldsymbol{v}_\varepsilon)\\
&= \boldsymbol{v}_\varepsilon\cdot(\nabla\cdot\boldsymbol{T}_\varepsilon) - \nabla\cdot\Big(\frac{|\boldsymbol{v}_\varepsilon|^2}{2}\overline{\boldsymbol{j}}_\varepsilon\Big) + (\boldsymbol{v}_\varepsilon\cdot\nabla\boldsymbol{v}_\varepsilon)\cdot\overline{\boldsymbol{j}}_\varepsilon + \boldsymbol{v}_\varepsilon\cdot\big(\nabla\cdot(\boldsymbol{v}_\varepsilon\otimes\overline{\boldsymbol{j}}_\varepsilon)\big)\\
&\quad - (\boldsymbol{v}_\varepsilon\cdot\nabla\boldsymbol{v}_\varepsilon)\cdot\overline{\boldsymbol{j}}_\varepsilon - \rho_\varepsilon\frac{|\boldsymbol{v}_\varepsilon|^2}{2}(\nabla\cdot\boldsymbol{v}_\varepsilon),
\end{aligned}
$$

then insert (2.135) and (2.136), for the equality:

$$\begin{aligned}
&\boldsymbol{v}_\varepsilon \cdot (\nabla \cdot \boldsymbol{T}_\varepsilon) - \nabla \cdot \Big(\frac{|\boldsymbol{v}_\varepsilon|^2}{2} \overline{\boldsymbol{j}}_\varepsilon \Big) + \boldsymbol{v}_\varepsilon \cdot \big(\nabla \cdot (\boldsymbol{v}_\varepsilon \otimes \overline{\boldsymbol{j}}_\varepsilon) \big) - \rho_\varepsilon \frac{|\boldsymbol{v}_\varepsilon|^2}{2} (\nabla \cdot \boldsymbol{v}_\varepsilon) \\
&= \nabla \cdot \Big((\boldsymbol{T}_\varepsilon^\perp + (\boldsymbol{v}_\varepsilon \otimes \overline{\boldsymbol{j}}_\varepsilon)^\perp) \boldsymbol{v}_\varepsilon - \frac{|\boldsymbol{v}_\varepsilon|^2}{2} \overline{\boldsymbol{j}}_\varepsilon \Big) - (\boldsymbol{T}_\varepsilon + \boldsymbol{v}_\varepsilon \otimes \overline{\boldsymbol{j}}_\varepsilon) \colon \nabla \boldsymbol{v}_\varepsilon - \rho_\varepsilon \frac{|\boldsymbol{v}_\varepsilon|^2}{2} (\nabla \cdot \boldsymbol{v}_\varepsilon).
\end{aligned} \tag{2.137}$$

We now deal with the free energy densities that depend on the bulk and interface surfactant concentration. However, for brevity, we drop dependence on the phase field and surfactant concentrations from the notation. For the other energy contribution,

$$\begin{aligned}
&\partial_t^{\bullet(\boldsymbol{v}_\varepsilon)} \big(f + \frac{1}{\varepsilon} w + \varepsilon a \big) \\
&\quad = \sum_i g_i' \partial_t^{\bullet(\boldsymbol{v}_\varepsilon)} (c_\varepsilon^{(i)}) \xi_i + g_i \xi_i' \partial_t^{\bullet(\boldsymbol{v}_\varepsilon)} \varphi_\varepsilon^{(i)} \\
&\qquad + \sum_{i<j} \gamma_{i,j}' \partial_t^{\bullet(\boldsymbol{v}_\varepsilon)} (c_\varepsilon^{(i,j)}) \tfrac{1}{\varepsilon} \overline{w}_{i,j} + \gamma_{i,j} \sum_k \tfrac{1}{\varepsilon} \partial_{\varphi_\varepsilon^{(k)}} \overline{w}_{i,j} \partial_t^{\bullet(\boldsymbol{v}_\varepsilon)} \varphi_\varepsilon^{(k)} \\
&\qquad + \sum_{i<j} \gamma_{i,j}' \partial_t^{\bullet(\boldsymbol{v}_\varepsilon)} (c_\varepsilon^{(i,j)}) \varepsilon a_{i,j} \\
&\qquad + \sum_{i<j} \gamma_{i,j} \sum_k \varepsilon \big(\partial_{\varphi_\varepsilon^{(k)}} a_{i,j} \partial_t^{\bullet(\boldsymbol{v}_\varepsilon)} \varphi_\varepsilon^{(k)} + \partial_{\nabla \varphi_\varepsilon^{(k)}} a_{i,j} \cdot \partial_t^{\bullet(\boldsymbol{v}_\varepsilon)} (\nabla \varphi_\varepsilon^{(k)}) \big) \\
&\quad = \sum_i g_i' \partial_t^{\bullet(\boldsymbol{v}_\varepsilon)} (c_\varepsilon^{(i)} \xi_i) + (g_i - g_i' c_\varepsilon^{(i)}) \xi_i' \partial_t^{\bullet(\boldsymbol{v}_\varepsilon)} \varphi_\varepsilon^{(i)} \\
&\qquad + \sum_{i<j} \gamma_{i,j}' \partial_t^{\bullet(\boldsymbol{v}_\varepsilon)} \big(c_\varepsilon^{(i,j)} (\tfrac{1}{\varepsilon} \overline{w}_{i,j} + \varepsilon a_{i,j}) \big) \\
&\qquad + \sum_{i<j} \big(\gamma_{i,j} - c_\varepsilon^{(i,j)} \gamma_{i,j}' \big) \sum_k \tfrac{1}{\varepsilon} \partial_{\varphi_\varepsilon^{(k)}} \overline{w}_{i,j} \partial_t^{\bullet(\boldsymbol{v}_\varepsilon)} \varphi_\varepsilon^{(k)} \\
&\qquad + \sum_{i<j} \big(\gamma_{i,j} - c_\varepsilon^{(i,j)} \gamma_{i,j}' \big) \sum_k \varepsilon \big(\partial_{\varphi_\varepsilon^{(k)}} a_{i,j} \partial_t^{\bullet(\boldsymbol{v}_\varepsilon)} \varphi_\varepsilon^{(k)} + \partial_{\nabla \varphi_\varepsilon^{(k)}} a_{i,j} \cdot \partial_t^{\bullet(\boldsymbol{v}_\varepsilon)} (\nabla \varphi_\varepsilon^{(k)}) \big).
\end{aligned} \tag{2.138}$$

We provide the differential identity:

$$\partial_t^{\bullet(\boldsymbol{v}_\varepsilon)} (\nabla \varphi_\varepsilon^{(k)}) = \nabla \partial_t^{\bullet(\boldsymbol{v}_\varepsilon)} \varphi_\varepsilon^{(k)} - (\nabla \boldsymbol{v}_\varepsilon)^\perp \nabla \varphi_\varepsilon^{(k)},$$

then inserting this and using the definitions (2.129) and (2.19):

$$\begin{aligned}
&\big(\gamma_{i,j} - c_\varepsilon^{(i,j)}\gamma'_{i,j}\big)\varepsilon\partial_{\nabla\varphi_\varepsilon^{(k)}} a_{i,j}\cdot\partial_t^{\bullet(\boldsymbol{v}_\varepsilon)}(\nabla\varphi_\varepsilon^{(k)})\big)\\
&\qquad = \sigma_{i,j}\partial_{\nabla\varphi_\varepsilon^{(k)}}\delta_{i,j}\cdot\big(\nabla\partial_t^{\bullet(\boldsymbol{v}_\varepsilon)}\varphi_\varepsilon^{(k)} - (\nabla\boldsymbol{v}_\varepsilon)^\perp\nabla\varphi_\varepsilon^{(k)}\big)\\
&\qquad = \nabla\cdot\big(\sigma_{i,j}\partial_{\nabla\varphi_\varepsilon^{(k)}}\delta_{i,j}\partial_t^{\bullet(\boldsymbol{v}_\varepsilon)}\varphi_\varepsilon^{(k)}\big) - \nabla\cdot\big(\sigma_{i,j}\partial_{\nabla\varphi_\varepsilon^{(k)}}\delta_{i,j}\big)\partial_t^{\bullet(\boldsymbol{v}_\varepsilon)}\varphi_\varepsilon^{(k)}\\
&\qquad\quad - \sigma_{i,j}\nabla\varphi_\varepsilon^{(k)}\otimes\partial_{\nabla\varphi_\varepsilon^{(k)}}\delta_{i,j} : \nabla\boldsymbol{v}_\varepsilon.
\end{aligned}$$

Therefore, we continue the calculation (2.138) using (2.19) and (2.131)

$$\begin{aligned}
&\partial_t^{\bullet(\boldsymbol{v}_\varepsilon)}\big(f + \frac{1}{\varepsilon}w + \varepsilon a\big) \qquad (2.139)\\
&\quad = \sum_i g_i'\partial_t^{\bullet(\boldsymbol{v}_\varepsilon)}(\xi_i c_\varepsilon^{(i)}) + \sum_{i<j}\gamma'_{i,j}\partial_t^{\bullet(\boldsymbol{v}_\varepsilon)}(\delta_{i,j}c_\varepsilon^{(i,j)})\\
&\qquad + \sum_i \lambda_i\xi_i'\partial_t^{\bullet(\boldsymbol{v}_\varepsilon)}\varphi_\varepsilon^{(i)}\\
&\qquad + \sum_{i<j}\sum_k\Big(\sigma_{i,j}\partial_{\varphi_\varepsilon^{(k)}}\delta_{i,j} - \nabla\cdot\big(\sigma_{i,j}\partial_{\nabla\varphi_\varepsilon^{(k)}}\delta_{i,j}\big)\Big)\partial_t^{\bullet(\boldsymbol{v}_\varepsilon)}\varphi_\varepsilon^{(k)}\\
&\qquad + \sum_{i<j}\sum_k\nabla\cdot\big(\sigma_{i,j}\partial_{\nabla\varphi_\varepsilon^{(k)}}\delta_{i,j}\partial_t^{\bullet(\boldsymbol{v}_\varepsilon)}\varphi_\varepsilon^{(k)}\big) - \sigma_{i,j}\nabla\varphi_\varepsilon^{(k)}\otimes\partial_{\nabla\varphi_\varepsilon^{(k)}}\delta_{i,j} : \nabla\boldsymbol{v}_\varepsilon,
\end{aligned}$$

which, when inserting the balance equations (2.118), (2.119) and (2.110), yields

$$\begin{aligned}
&\partial_t^{\bullet(\boldsymbol{v}_\varepsilon)}\big(f + \frac{1}{\varepsilon}w + \varepsilon a\big) \qquad (2.140)\\
&\quad = -\sum_i g_i'\Big(\nabla\cdot(\xi_i\boldsymbol{j}_{c,\varepsilon}^{(i)}) + \xi_i c_\varepsilon^{(i)}\nabla\cdot\boldsymbol{v}_\varepsilon + \sum_{j\neq i}\delta_{i,j}q_{\mathrm{ad},\varepsilon}^{(i,j)}\big)\Big)\\
&\qquad - \sum_{i<j}\gamma'_{i,j}\Big(\nabla\cdot(\delta_{i,j}\boldsymbol{j}_{c,\varepsilon}^{(i,j)}) + \delta_{i,j}c_\varepsilon^{(i,j)}\nabla\cdot\boldsymbol{v}_\varepsilon - \delta_{i,j}q_{\mathrm{ad},\varepsilon}^{(i,j)} - \delta_{j,i}q_{\mathrm{ad},\varepsilon}^{(j,i)}\Big)\\
&\qquad - \sum_{i<j}\gamma'_{i,j}\sum_{i<j<k}\tau_{i,j,k}q_{\mathrm{ad},\varepsilon}^{(i,j,k)}\\
&\qquad - \sum_i\lambda_i\xi_i'\left(\nabla\cdot\boldsymbol{j}_{\varphi_\varepsilon^{(i)}} + \varphi_\varepsilon^{(i)}\nabla\cdot\boldsymbol{v}_\varepsilon\right)\\
&\qquad - \sum_{i<j}\sum_k\Big(\sigma_{i,j}\partial_{\varphi_\varepsilon^{(k)}}\delta_{i,j} - \nabla\cdot\big(\sigma_{i,j}\partial_{\nabla\varphi_\varepsilon^{(k)}}\delta_{i,j}\big)\Big)(\nabla\cdot\boldsymbol{j}_{\varphi_\varepsilon^{(k)}} + \varphi_\varepsilon^{(k)}\nabla\cdot\boldsymbol{v}_\varepsilon)\\
&\qquad + \sum_{i<j}\sum_k\nabla\cdot\big(\sigma_{i,j}\partial_{\nabla\varphi_\varepsilon^{(k)}}\delta_{i,j}\partial_t^{\bullet(\boldsymbol{v}_\varepsilon)}\varphi_\varepsilon^{(k)}\big) - \sigma_{i,j}\nabla\varphi_\varepsilon^{(k)}\otimes\partial_{\nabla\varphi_\varepsilon^{(k)}}\delta_{i,j} : \nabla\boldsymbol{v}_\varepsilon
\end{aligned}$$

$$
\begin{aligned}
=&\nabla\cdot\Big[-\Big(\sum_i g_i'\xi_i\boldsymbol{j}_{c,\varepsilon}^{(i)}+\sum_{i<j}\gamma_{i,j}'\delta_{i,j}\boldsymbol{j}_{c,\varepsilon}^{(i,j)}\Big)\\
&\quad-\sum_k\Big(\lambda_k\xi_k'+\sum_{i<j}\big(\sigma_{i,j}\partial_{\varphi_\varepsilon^{(k)}}\delta_{i,j}-\nabla\cdot\big(\sigma_{i,j}\partial_{\nabla\varphi_\varepsilon^{(k)}}\delta_{i,j}\big)\big)\Big)\boldsymbol{j}_{\varphi_\varepsilon^{(k)}}\\
&\quad+\sum_k\sum_{i<j}\big(\sigma_{i,j}\partial_{\nabla\varphi_\varepsilon^{(k)}}\delta_{i,j}\partial_t^{\bullet(\boldsymbol{v}_\varepsilon)}\varphi_\varepsilon^{(k)}\big)\Big]\\
&+\sum_i\xi_i\nabla g_i'\cdot\boldsymbol{j}_{c,\varepsilon}^{(i)}+\sum_{i<j}\delta_{i,j}\nabla\gamma_{i,j}'\cdot\boldsymbol{j}_{c,\varepsilon}^{(i,j)}\\
&-\sum_{i\neq j}\Big(g_i'\delta_{i,j}q_{\mathrm{ad},\varepsilon}^{(i,j)}-\gamma_{i,j}'\delta_{i,j}q_{\mathrm{ad},\varepsilon}^{(i,j)}\Big)-\sum_{i<j}\gamma_{i,j}'\sum_{k\neq i,j}\tau_{i,j,k}q_{\mathrm{ad},\varepsilon}^{(i,j,k)}\\
&+\sum_k\Big(\lambda_k\xi_k'+\sum_{i<j}\big(\sigma_{i,j}\partial_{\varphi_\varepsilon^{(k)}}\delta_{i,j}-\nabla\cdot\big(\sigma_{i,j}\partial_{\nabla\varphi_\varepsilon^{(k)}}\delta_{i,j}\big)\big)\Big)\cdot\boldsymbol{j}_{\varphi_\varepsilon^{(k)}}\\
&-\Big[\sum_i\xi_i g_i'c_\varepsilon^{(i)}+\sum_{i<j}\delta_{i,j}\gamma_{i,j}'c_\varepsilon^{(i,j)}\Big]\nabla\cdot\boldsymbol{v}_\varepsilon\\
&-\Big[\sum_k\Big(\lambda_k\varphi_\varepsilon^{(k)}\xi_k'+\varphi_\varepsilon^{(k)}\sum_{i<j}\big(\sigma_{i,j}\partial_{\varphi_\varepsilon^{(k)}}\delta_{i,j}-\nabla\cdot\big(\sigma_{i,j}\partial_{\nabla\varphi_\varepsilon^{(k)}}\delta_{i,j}\big)\big)\Big)\Big]\nabla\cdot\boldsymbol{v}_\varepsilon\\
&-\sum_k\sum_{i<j}\sigma_{i,j}\nabla\varphi_\varepsilon^{(k)}\otimes\partial_{\nabla\varphi_\varepsilon^{(k)}}\delta_{i,j}:\nabla\boldsymbol{v}_\varepsilon. \qquad (2.141)
\end{aligned}
$$

Defining

$$
\begin{aligned}
\boldsymbol{j}_{e_\varepsilon}\coloneqq&-(\boldsymbol{T}_\varepsilon^{\perp}+(\boldsymbol{v}_\varepsilon\otimes\overline{\boldsymbol{j}}_\varepsilon)^{\perp})\boldsymbol{v}_\varepsilon-\frac{|\boldsymbol{v}_\varepsilon|^2}{2}\overline{\boldsymbol{j}}_\varepsilon\\
&+\Big(\sum_i g_i'\xi_i\boldsymbol{j}_{c,\varepsilon}^{(i)}+\sum_{i<j}\gamma_{i,j}'\delta_{i,j}\boldsymbol{j}_{c,\varepsilon}^{(i,j)}\Big)\\
&+\sum_k\Big(\lambda_k\xi_k'+\sum_{i<j}\big(\sigma_{i,j}\partial_{\varphi_\varepsilon^{(k)}}\delta_{i,j}-\nabla\cdot\big(\sigma_{i,j}\partial_{\nabla\varphi_\varepsilon^{(k)}}\delta_{i,j}\big)\big)\Big)\boldsymbol{j}_{\varphi_\varepsilon^{(k)}}\\
&-\sum_k\sum_{i<j}\big(\sigma_{i,j}\partial_{\nabla\varphi_\varepsilon^{(k)}}\delta_{i,j}\partial_t^{\bullet(\boldsymbol{v}_\varepsilon)}\varphi_\varepsilon^{(k)}\big),
\end{aligned}
$$

then we obtain from (2.137) and (2.141) that

$$
\begin{aligned}
&\partial_t^{\bullet(\boldsymbol{v}_\varepsilon)}e_\varepsilon+e_\varepsilon\nabla\cdot\boldsymbol{v}_\varepsilon+\nabla\cdot\boldsymbol{j}_{e_\varepsilon}\\
&=\sum_i\xi_i\nabla g_i'\cdot\boldsymbol{j}_{c,\varepsilon}^{(i)}+\sum_{i<j}\delta_{i,j}\nabla\gamma_{i,j}'\cdot\boldsymbol{j}_{c,\varepsilon}^{(i,j)} \qquad (2.142)\\
&-\sum_{i\neq j}(g_i'-\gamma_{i,j}')\delta_{i,j}q_{\mathrm{ad},\varepsilon}^{(i,j)}-\sum_{k\neq i,j}\gamma_{i,j}'\tau_{i,j,k}q_{\mathrm{ad},\varepsilon}^{(i,j,k)} \qquad (2.143)\\
&+\sum_k\Big(\lambda_k\xi_k'+\sum_{i<j}\big(\sigma_{i,j}\partial_{\varphi_\varepsilon^{(k)}}\delta_{i,j}-\nabla\cdot\big(\sigma_{i,j}\partial_{\nabla\varphi_\varepsilon^{(k)}}\delta_{i,j}\big)\big)\Big)\cdot\boldsymbol{j}_{\varphi_\varepsilon^{(k)}} \qquad (2.144)
\end{aligned}
$$

$$+\Big(\sum_i \xi_i\lambda_i + \sum_{i<j}\delta_{i,j}\sigma_{i,j}\Big)\nabla\cdot\boldsymbol{v}_\varepsilon \tag{2.145}$$

$$-\Big[\sum_k\Big(\lambda_k\varphi_\varepsilon^{(k)}\xi_k' + \varphi_\varepsilon^{(k)}\sum_{i<j}\big(\sigma_{i,j}\partial_{\varphi_\varepsilon^{(k)}}\delta_{i,j} - \nabla\cdot\big(\sigma_{i,j}\partial_{\nabla\varphi_\varepsilon^{(k)}}\delta_{i,j}\big)\big)\Big)\Big]\nabla\cdot\boldsymbol{v}_\varepsilon \tag{2.146}$$

$$-\Big(\boldsymbol{T}_\varepsilon + \boldsymbol{v}_\varepsilon\otimes\overline{\boldsymbol{j}}_\varepsilon + \sum_k\sum_{i<j}\sigma_{i,j}\nabla\varphi_\varepsilon^{(k)}\otimes\partial_{\nabla\varphi_\varepsilon^{(k)}}\delta_{i,j}\Big):\nabla\boldsymbol{v}_\varepsilon. \tag{2.147}$$

2.2.4 Constitutive assumptions and boundary conditions

The calculations resulting in (2.142) – (2.147) motivate the following assumptions to ensure non-negative dissipation of energy is nonnegative. First we choose the surfactant fluxes due to the terms of (2.142):

$$\begin{aligned}\boldsymbol{j}_{c,\varepsilon}^{(i)} &= -M_c^{(i)}\nabla g_i'(c_\varepsilon^{(i)}),\\ \boldsymbol{j}_{c,\varepsilon}^{(i,j)} &= -M_c^{(i,j)}\nabla\gamma_{i,j}'(c_\varepsilon^{(i,j)}),\end{aligned}$$

with mobilities $M_c^{(i)}$ and $M_c^{(i,j)}$ as in (2.32) and (2.33), respectively. Furthermore we assume that, due to (2.144):

$$\boldsymbol{j}_{\varphi_\varepsilon^{(k)}} \coloneqq -\sum_{l=1}^{M}\mathcal{L}^{(k,l)}\nabla\mu_\varepsilon^{(l)},$$

where,

$$\mu_\varepsilon^{(l)} \coloneqq \lambda_l\xi_l' + \sum_{i<j}\big(\sigma_{i,j}(c_\varepsilon^{(i,j)})\partial_{\varphi_\varepsilon^{(l)}}\delta_{i,j} - \nabla\cdot\big(\sigma_{i,j}(c_\varepsilon^{(i,j)})\partial_{\nabla\varphi_\varepsilon^{(l)}}\delta_{i,j}\big)\big), \tag{2.148}$$

with mobilities $\mathcal{L}^{(k,l)}$ that may depend on φ_ε and $c_\varepsilon^{(\cdot)}, c_\varepsilon^{(\cdot,\cdot)}$. $\mathcal{L}^{(k,l)}$ forms a symmetric positive semi-definite matrix, and satisfies

$$\sum_{k=1}^{M}\mathcal{L}^{(k,l)}(\varphi_\varepsilon, c_\varepsilon^{(\cdot)}, c_\varepsilon^{(\cdot,\cdot)}) = 0 \quad \forall\varphi_\varepsilon\in\Sigma^M, \text{ and } c_\varepsilon^{(\cdot)}\in\mathbb{R}^M,\ c_\varepsilon^{(\cdot,\cdot)}\in\mathbb{R}^{M,M}, \tag{2.149}$$

which ensures that (2.103) is fulfilled during the evolution. For the surfactant terms, we have already chosen the forms for $q_{\text{ad},\varepsilon}^{(i,j)}$, $q_{\text{ad},\varepsilon}^{(i,j,k)}$ in (2.120) and (2.121) respectively. These ensure that the terms in (2.143) have the correct sign. In fact, over a small test volume V these dissipative terms coincide with those obtained if we had written the integrals (2.41), (2.42) replacing $\delta_{\Gamma^{(i,j)}}$, $\tau_{T^{(i,j,k)}}$ with $\delta_{i,j}$,$\tau_{i,j,k}$. This validates our choice from the perspective of thermodynamic considerations.

Finally, by considering terms in (2.145) – (2.147), and the defintion (2.148), the

stress tensor is assumed to be:

$$\begin{aligned}\boldsymbol{T}_\varepsilon \coloneqq &\bar{\boldsymbol{T}}_\varepsilon - \boldsymbol{v}_\varepsilon \otimes \overline{\boldsymbol{j}}_\varepsilon - \sum_k \sum_{i<j} \sigma_{i,j} \nabla \varphi_\varepsilon^{(k)} \otimes \partial_{\nabla \varphi_\varepsilon^{(k)}} \delta_{i,j} \\ &+ \Big(\sum_k \big(\xi_k \lambda_k - \mu_\varepsilon^{(k)} \varphi_\varepsilon^{(k)} \big) + \sum_{i<j} \delta_{i,j} \sigma_{i,j} \Big) \boldsymbol{I},\end{aligned}$$

with the symmetric tensor:

$$\bar{\boldsymbol{T}}_\varepsilon \coloneqq -\tilde{p}_\varepsilon \boldsymbol{I} + 2\eta(\varphi_\varepsilon) \boldsymbol{D}(\boldsymbol{v}_\varepsilon),$$

with a pressure $\tilde{p}_\varepsilon$ and where $\eta(\varphi_\varepsilon)$ is a non-negative smooth interpolation function between the viscosities of the pure fluids, i.e., $\eta(\varphi_\varepsilon^{(1)}, \dots, \varphi_\varepsilon^{(M)}) = \eta^{(i)}$ if $\varphi_\varepsilon^{(i)} = 1$ (and then $\varphi_\varepsilon^{(j)} = 0$ for $j \neq i$ by (2.103)).

One can simplify the expression that is multiplying the identity tensor $\boldsymbol{I}$, by absorbing it into the pressure. We choose to not absorb the terms that are required in the asymptotic analysis to identify leading order terms in ε in interfacial regions (see the forthcoming [42]). One can also see this in the two phase case in [54]. Setting

$$p_\varepsilon \coloneqq \tilde{p}_\varepsilon - \sum_k \big(\mu_\varepsilon^{(k)} \varphi_\varepsilon^{(k)} - \xi_k \lambda_k \big),$$

we obtain

$$\begin{aligned}\boldsymbol{T}_\varepsilon = &-p_\varepsilon \boldsymbol{I} + 2\eta(\varphi_\varepsilon) \boldsymbol{D}(\boldsymbol{v}_\varepsilon) - \boldsymbol{v}_\varepsilon \otimes \overline{\boldsymbol{j}}_\varepsilon \\ &+ \sum_{i<j} \sigma_{i,j} \Big(\delta_{i,j} \boldsymbol{I} - \sum_k \nabla \varphi_\varepsilon^{(k)} \otimes \partial_{\nabla \varphi_\varepsilon^{(k)}} \delta_{i,j} \Big).\end{aligned} \tag{2.150}$$

Remark 2.2.6. *Notice that the term multiplying the identity tensor in* (2.150) *is the Korteweg stress [82]. This can be seen due to the definition of the phase field* (2.102) *is linear in the density $\rho_\varepsilon^{(i)}$, and due the definition of $\delta_{i,j}$* (2.129)*. In particular, if we take*

$$a_{i,j}(\varphi_\varepsilon, \nabla \varphi_\varepsilon) = a_{i,j}(\nabla \varphi_\varepsilon) = a_{i,j}(\nabla \varphi_\varepsilon^{(1)}, \dots, \nabla \varphi_\varepsilon^{(M)}) =: \tilde{a}_{i,j}(\nabla \rho_\varepsilon^{(1)}, \dots, \nabla \rho_\varepsilon^{(M)}),$$

and similarly denote

$$\overline{w}_{i,j}(\varphi_\varepsilon) =: \tilde{w}_{i,j}(\rho_\varepsilon^{(1)}, \cdots, \rho_\varepsilon^{(M)}).$$

Then, due to the two homogeneity of $a_{i,j}$ in $\nabla \varphi_\varepsilon^{(*)}$ (see Section 2.2.2), within each interfacial

region the bracketed stress term in (2.150) *can be viewed as*

$$\delta_{i,j}\boldsymbol{I} - \sum_k \nabla\varphi_\varepsilon^{(k)} \otimes \partial_{\nabla\varphi_\varepsilon^{(k)}}\delta_{i,j} = \Big(\sum_k \alpha_k|\nabla\rho_\varepsilon^{(k)}|^2 + \tilde{w}_{i,j}(\rho_\varepsilon^{(1)},\cdots,\rho_\varepsilon^{(M)})\Big)\boldsymbol{I} - \sum_k \beta_k \nabla\rho_\varepsilon^{(k)} \otimes \nabla\rho_\varepsilon^{(k)} \quad (2.151)$$

for constants a_k, β_k. This form expressed through the fluid density is now more recognisable as the Korteweg stress term.

Natural boundary conditions in $\partial\Omega$ arise from assuming a closed system so there are no mass and energy fluxes into or out of the domain. For the fluid flow they read as in the sharp interface model (2.53), (2.54),

$$\boldsymbol{v}_\varepsilon \cdot \boldsymbol{\nu}_\Omega = 0, \quad \text{on } \partial\Omega, \quad (2.152)$$

$$\boldsymbol{T}_\varepsilon \cdot \nu_\Omega = 0 \quad \text{on } \partial\Omega. \quad (2.153)$$

For the phase field, the natural conditions are

$$\boldsymbol{j}_{\varphi_\varepsilon^{(k)}} \cdot \boldsymbol{\nu}_\Omega = 0, \quad \text{on } \partial\Omega \quad (2.154)$$

$$\partial_{\nabla\varphi_\varepsilon^{(k)}}\delta_{i,j} \cdot \boldsymbol{\nu}_\Omega = 0, \quad \text{on } \partial\Omega \quad (2.155)$$

for all $k, l = 1, \ldots, M$ where (2.154) ensures a no-flux condition for the $\boldsymbol{j}_{\varphi_\varepsilon^{(k)}}$ and, (see the asymptotics presented in [54]) (2.155) is related to angles between the interface $\Gamma^{(i,j)}$ and the external boundary $\partial\Omega$. In order to guarantee a no-flux boundary condition for the surfactant mass one may assume that

$$\boldsymbol{j}_{c,\varepsilon}^{(i)} \cdot \boldsymbol{\nu}_\Omega = 0 \quad \text{on } \partial\Omega, \quad (2.156)$$

$$\boldsymbol{j}_{c,\varepsilon}^{(i,j)} \cdot \boldsymbol{\nu}_\Omega = 0 \quad \text{on } \partial\Omega. \quad (2.157)$$

2.2.5 Summary of diffuse interface model with general sorption

Summarising the phase field equations we have a Cahn-Hilliard type system for the phase fields of the form

$$\partial_t^{\bullet(\boldsymbol{v}_\varepsilon)}\varphi_\varepsilon^{(k)} = -\nabla \cdot \boldsymbol{j}_{\varphi_\varepsilon^{(k)}}, \quad (2.158)$$

$$\boldsymbol{j}_{\varphi_\varepsilon^{(k)}} = -\sum_l \mathcal{L}^{(k,l)}\nabla\mu_\varepsilon^{(l)}, \quad (2.159)$$

$$\mu_\varepsilon^{(l)} = \lambda_l\xi_l' + \sum_{i<j}\big(\sigma_{i,j}(c_\varepsilon^{(i,j)})\partial_{\varphi_\varepsilon^{(l)}}\delta_{i,j} - \nabla\cdot\big(\sigma_{i,j}(c_\varepsilon^{(i,j)})\partial_{\nabla\varphi_\varepsilon^{(l)}}\delta_{i,j}\big)\big), \quad (2.160)$$

for $k, l = 1, \dots, M$. It is coupled to a system of equations for the surfactant

$$\partial_t^{\bullet(\boldsymbol{v}_\varepsilon)}\Big(\xi_i c_\varepsilon^{(i)}\Big) = -\nabla\cdot(\xi_i \boldsymbol{j}_{c,\varepsilon}^{(i)}) - \sum_{j\colon j\neq i} \delta_{i,j} q_{\mathrm{ad},\varepsilon}^{(i,j)}, \tag{2.161}$$

$$\begin{aligned}\partial_t^{\bullet(\boldsymbol{v}_\varepsilon)}\Big(\delta_{i,j} c_\varepsilon^{(i,j)}\Big) &= -\nabla\cdot(\delta_{i,j}\boldsymbol{j}_{c,\varepsilon}^{(i,j)}) + \delta_{i,j} q_{\mathrm{ad},\varepsilon}^{(i,j)} + \delta_{j,i} q_{\mathrm{ad},\varepsilon}^{(j,i)} \\ &\quad + \sum_{i<j<k} \tau_{i,j,k} q_{\mathrm{ad},\varepsilon}^{(i,j,k)},\end{aligned} \tag{2.162}$$

$$\boldsymbol{j}_{c,\varepsilon}^{(i)} = -\xi_i M_c^{(i)} \nabla g_i', \qquad \boldsymbol{j}_{c,\varepsilon}^{(i,j)} = -\delta_{i,j} M_c^{(i,j)} \nabla \gamma_{i,j}', \tag{2.163}$$

$$q_{\mathrm{ad},\varepsilon}^{(i,j)} = -\frac{1}{\alpha_{i,j}}(\gamma_{i,j}'(c_\varepsilon^{(i,j)}) - g_i'(c_\varepsilon^{(i)})), \tag{2.164}$$

$$\begin{aligned}q_{\mathrm{ad},\varepsilon}^{(i,j,k)} &= \beta_{j,k\leftrightarrow i,j}(\gamma_{i,j}'(c_\varepsilon^{(i,j)}) - \gamma_{j,k}'(c_\varepsilon^{(j,k)})) \\ &\quad + \beta_{k,i\leftrightarrow i,j}(\gamma_{i,j}'(c_\varepsilon^{(i,j)}) - \gamma_{k,i}'(c_\varepsilon^{(k,i)})),\end{aligned} \tag{2.165}$$

while the fluid flow is subject to the Navier-Stokes system

$$\nabla\cdot\boldsymbol{v}_\varepsilon = 0, \tag{2.166}$$

$$\begin{aligned}\partial_t^{\bullet(\boldsymbol{v}_\varepsilon)}(\rho_\varepsilon \boldsymbol{v}_\varepsilon) &= \nabla\cdot\Big(-p_\varepsilon \boldsymbol{I} + 2\eta(\varphi_\varepsilon)\boldsymbol{D}(\boldsymbol{v}_\varepsilon) - \boldsymbol{v}_\varepsilon \otimes \sum_k \overline{\rho}^{(k)} \boldsymbol{j}_{\varphi_\varepsilon^{(k)}}\Big) \\ &\quad + \nabla\cdot\Big(\sum_{i<j}\sigma_{i,j}(c_\varepsilon^{(i,j)})\Big(\delta_{i,j}\boldsymbol{I} - \sum_k \nabla\varphi_\varepsilon^{(k)} \otimes \partial_{\nabla\varphi_\varepsilon^{(k)}}\delta_{i,j}\Big)\Big).\end{aligned} \tag{2.167}$$

For completion of the problem, boundary conditions as discussed in Section 2.2.4 and suitable initial conditions have to be imposed.

Remark 2.2.7. *We may reform the capilliary forcing of the Navier-Stokes equations using* (2.148)*. Starting with*

$$\begin{aligned}&\sum_k \mu_\varepsilon^{(k)} \nabla\varphi_\varepsilon^{(k)} \\ &= \sum_k \sum_{i<j} \Big(-\nabla\cdot(\sigma_{i,j}\partial_{\nabla\varphi_\varepsilon^{(k)}}\delta_{i,j})\nabla\varphi_\varepsilon^{(k)} + \sigma_{i,j}\partial_{\varphi_\varepsilon^{(k)}}\delta_{i,j}\nabla\varphi_\varepsilon^{(k)}\Big) + \lambda_k\xi_k'\nabla\varphi_\varepsilon^{(k)} \\ &= \sum_{i<j}\Big(-\nabla\cdot(\sigma_{i,j}\sum_k \partial_{\nabla\varphi_\varepsilon^{(k)}}\delta_{i,j})\nabla\varphi_\varepsilon^{(k)} + \sigma_{i,j}\sum_k \partial_{\varphi_\varepsilon^{(k)}}\delta_{i,j}\nabla\varphi_\varepsilon^{(k)}\Big) + \sum_k \lambda_k\nabla\xi_k \\ &= \sum_{i<j}\Big(\nabla\cdot(-\sigma_{i,j}\sum_k \nabla\varphi_\varepsilon^{(k)} \otimes \partial_{\nabla\varphi_\varepsilon^{(k)}}\delta_{i,j}) + \sigma_{i,j}\nabla\delta_{i,j}\Big) + \sum_k \lambda_k\nabla\xi_k \\ &= \nabla\cdot(\sum_{i<j}\sigma_{i,j}(\delta_{i,j}\boldsymbol{I} - \sum_k \nabla\varphi_\varepsilon^{(k)} \otimes \partial_{\nabla\varphi_\varepsilon^{(k)}}\delta_{i,j})) - \sum_{i<j}\delta_{i,j}\nabla\sigma_{i,j} + \sum_k \lambda_k\nabla\xi_k,\end{aligned}$$

and rearranging we find that

$$\nabla\cdot(\sum_{i<j}\sigma_{i,j}(\delta_{i,j}\boldsymbol{I}-\sum_{k}\partial_{\nabla\varphi_\varepsilon^{(k)}}\delta_{i,j}\otimes\nabla\varphi_\varepsilon^{(k)}))=\sum_k\mu_\varepsilon^{(k)}\nabla\varphi_\varepsilon^{(k)}+\sum_{i<j}\delta_{i,j}\nabla\sigma_{i,j}-\sum_k\lambda_k\nabla\xi_k,$$

which can be substituted into the momentum equation for Navier-Stokes to give:

$$\begin{aligned}\partial_t^{\bullet(\boldsymbol{v}_\varepsilon)}(\rho_\varepsilon\boldsymbol{v}_\varepsilon)=\nabla\cdot\Big(-p_\varepsilon\boldsymbol{I}+2\eta(\varphi_\varepsilon)\boldsymbol{D}(\boldsymbol{v}_\varepsilon)-\boldsymbol{v}_\varepsilon\otimes\sum_k\overline{\rho}^{(k)}\boldsymbol{j}_{\varphi_\varepsilon^{(k)}}\Big)\\+\sum_k\mu_\varepsilon^{(k)}\nabla\varphi_\varepsilon^{(k)}+\sum_{i<j}\delta_{i,j}\nabla\sigma_{i,j}-\sum_k\lambda_k\nabla\xi_k.\end{aligned}\tag{2.168}$$

The form (2.168) *is significantly easier to deal with during implementation compared with* (2.167)*, and more clearly demonstrates the origin and behaviour of the forces acting on the fluid.*

A possible form for $\tau_{i,j,k}$ that we could take is:

$$\tau_{i,j,k}\coloneqq C_{i,j,k}(\varphi_\varepsilon^{(i)})^2(\varphi_\varepsilon^{(j)})^2(\varphi_\varepsilon^{(k)})^2\tag{2.169}$$

for a suitable constant $C_{i,j,k}>0$. This is a bubble function that is only present, where all three phases i, j, k are present. Therefore it is positive in regions where there are third phase contributions along an interface. The study presented here focuses henceforth, in Section 2.2.6 and Chapter 4, in the case of local equilibrium. This leads to the surfactant equation (2.122) that does not feature such functions $\tau_{i,j,k}$. We shall leave the consideration of the form of the regularized distribution to future studies.

2.2.6 Instantaneous sorption

For the case of instantaneous sorption, we approximate the energy (2.18) by the following form:

$$E_\varepsilon\coloneqq\int_\Omega e_\varepsilon,\quad e_\varepsilon\coloneqq\frac{\rho_\varepsilon}{2}|\boldsymbol{v}_\varepsilon|^2+f(q_\varepsilon,\varphi_\varepsilon)+\frac{1}{\varepsilon}w(q_\varepsilon,\varphi_\varepsilon)+\varepsilon a(q_\varepsilon,\varphi_\varepsilon,\nabla\varphi_\varepsilon).\tag{2.170}$$

The free energy contributions $a(q_\varepsilon,\varphi_\varepsilon,\nabla\varphi_\varepsilon)$, $w(q_\varepsilon,\varphi_\varepsilon)$, $f(q_\varepsilon,\varphi_\varepsilon)$ are defined as in the general sorption case, (2.127), (2.128), (2.126), the difference being that we replace $c_\varepsilon^{(i)}$ and $c_\varepsilon^{(i,j)}$, with $c_\varepsilon^{(i)}(q_\varepsilon)$ and $c_\varepsilon^{(i,j)}(q_\varepsilon)$. We continue through calculations as in Section 2.2.3 to determine the flux $\boldsymbol{j}_{e_\varepsilon}$ satisfying (2.130). We first see that (2.137) remains unchanged. Then for the surfactant free energies, denote the instantaneous bulk field by:

$$\tilde{\lambda}_k(q_\varepsilon)\coloneqq g_k(c_\varepsilon^{(k)}(q_\varepsilon))-q_\varepsilon c_\varepsilon^{(k)}(q_\varepsilon).\tag{2.171}$$

The calculations prompt the energy flux definition,

$$\begin{aligned}\boldsymbol{j}_{e_\varepsilon} = &-(\boldsymbol{T}_\varepsilon^{\perp} + (\boldsymbol{v}_\varepsilon \otimes \overline{\boldsymbol{j}}_\varepsilon)^{\perp})\boldsymbol{v}_\varepsilon - \frac{|\boldsymbol{v}_\varepsilon|^2}{2}\overline{\boldsymbol{j}}_\varepsilon \\ &+ q_\varepsilon\big(\sum_i \xi_i \boldsymbol{j}_{c,\varepsilon}^{(i)} + \sum_{i<j}\delta_{i,j}\boldsymbol{j}_{c,\varepsilon}^{(i,j)}\big) \\ &+ \sum_k \Big(\tilde{\lambda}_k\xi_k' + \sum_{i<j}\big(\tilde{\sigma}_{i,j}\partial_{\varphi_\varepsilon^{(k)}}\delta_{i,j} - \nabla\cdot\big(\tilde{\sigma}_{i,j}\partial_{\nabla\varphi_\varepsilon^{(k)}}\delta_{i,j}\big)\big)\Big)\boldsymbol{j}_{\varphi_\varepsilon^{(k)}} \\ &- \sum_k\sum_{i<j}\big(\tilde{\sigma}_{i,j}\partial_{\nabla\varphi_\varepsilon^{(k)}}\delta_{i,j}\partial_t^{\bullet(\boldsymbol{v}_\varepsilon)}\varphi_\varepsilon^{(k)}\big),\end{aligned}$$

which gives the following energy dissipation:

$$\begin{aligned}&\partial_t^{\bullet(\boldsymbol{v}_\varepsilon)}e_\varepsilon + e_\varepsilon\nabla\cdot\boldsymbol{v}_\varepsilon + \nabla\cdot\boldsymbol{j}_{e_\varepsilon} \\ &\quad= \sum_i \xi_i\nabla q_\varepsilon\cdot\boldsymbol{j}_{c,\varepsilon}^{(i)} + \sum_{i<j}\delta_{i,j}\nabla q_\varepsilon\cdot\boldsymbol{j}_{c,\varepsilon}^{(i,j)} \\ &\qquad+ \sum_k\Big(\tilde{\lambda}_k\xi_k' + \sum_{i<j}\big(\tilde{\sigma}_{i,j}\partial_{\varphi_\varepsilon^{(k)}}\delta_{i,j} - \nabla\cdot\big(\tilde{\sigma}_{i,j}\partial_{\nabla\varphi_\varepsilon^{(k)}}\delta_{i,j}\big)\big)\Big)\cdot\boldsymbol{j}_{\varphi_\varepsilon^{(k)}} \\ &\qquad+ \Big[\sum_i\xi_i\tilde{\lambda}_i + \sum_{i<j}\delta_{i,j}\tilde{\sigma}_{i,j}\Big]\nabla\cdot\boldsymbol{v}_\varepsilon \\ &\qquad- \Big[\sum_k\Big(\tilde{\lambda}_k\varphi_\varepsilon^{(k)}\xi_k' + \varphi_\varepsilon^{(k)}\sum_{i<j}\big(\tilde{\sigma}_{i,j}\partial_{\varphi_\varepsilon^{(k)}}\delta_{i,j} - \nabla\cdot\big(\tilde{\sigma}_{i,j}\partial_{\nabla\varphi_\varepsilon^{(k)}}\delta_{i,j}\big)\big)\Big)\Big]\nabla\cdot\boldsymbol{v}_\varepsilon \\ &\qquad- \Big(\boldsymbol{T}_\varepsilon + \boldsymbol{v}_\varepsilon\otimes\overline{\boldsymbol{j}}_\varepsilon + \sum_k\sum_{i<j}\tilde{\sigma}_{i,j}\nabla\varphi_\varepsilon^{(k)}\otimes\partial_{\nabla\varphi_\varepsilon^{(k)}}\delta_{i,j}\Big) : \nabla\boldsymbol{v}_\varepsilon. \qquad (2.172)\end{aligned}$$

Equation (2.172) motivates the following constitutive assumptions to ensure energy dissipation:

$$\begin{aligned}\boldsymbol{j}_{c,\varepsilon}^{(i)} &\coloneqq -M_c^{(i)}\nabla q_\varepsilon, \\ \boldsymbol{j}_{c,\varepsilon}^{(i,j)} &\coloneqq -M_c^{(i,j)}\nabla q_\varepsilon.\end{aligned}$$

The mass flux of the phase field $\boldsymbol{j}_{\varphi_\varepsilon^{(k)}}$, and the fluid stress tensor $\boldsymbol{T}_\varepsilon$ differ notationally as $c_\varepsilon^{(\cdot)} \coloneqq c_\varepsilon^{(\cdot)}(q_\varepsilon)$, $c_\varepsilon^{(\cdot,\cdot)} \coloneqq c_\varepsilon^{(\cdot,\cdot)}(q_\varepsilon)$ from (2.71).

Finally, the boundary conditions (2.152)-(2.155) remain but we substitute (2.156) with:

$$0 = \nabla q_\varepsilon\cdot\boldsymbol{\nu}_\Omega. \qquad (2.173)$$

2.2.7 Summary of diffuse interface model with instantaneous sorption

Summarising we have a Cahn-Hilliard type system for the phase fields of the form:

$$\partial_t^{\bullet(\boldsymbol{v}_\varepsilon)}\varphi_\varepsilon^{(k)} = -\nabla\cdot\boldsymbol{j}_{\varphi_\varepsilon^{(k)}}, \tag{2.174}$$

$$\boldsymbol{j}_{\varphi_\varepsilon^{(k)}} = -\sum_l \mathcal{L}^{(k,l)}\nabla\mu_\varepsilon^{(l)}, \tag{2.175}$$

$$\mu_\varepsilon^{(l)} = \tilde{\lambda}_l\xi_l' + \sum_{i<j}\big(\tilde{\sigma}_{i,j}\partial_{\varphi_\varepsilon^{(l)}}\delta_{i,j} - \nabla\cdot\big(\tilde{\sigma}_{i,j}\partial_{\nabla\varphi_\varepsilon^{(l)}}\delta_{i,j}\big)\big), \tag{2.176}$$

for $k,l=1,\dots,M$. It is coupled to an equation for the surfactant:

$$\partial_t^{\bullet(\boldsymbol{v}_\varepsilon)}\Big(\sum_i \xi_i c_\varepsilon^{(i)}(q_\varepsilon) + \sum_{i<j}\delta_{i,j}c_\varepsilon^{(i,j)}(q_\varepsilon)\Big) = -\nabla\cdot\boldsymbol{j}_{q_\varepsilon}, \tag{2.177}$$

$$\boldsymbol{j}_{q_\varepsilon} = -\Big(\sum_i \xi_i M_c^{(i)}\nabla q_\varepsilon + \sum_{i<j}\delta_{i,j}M_c^{(i,j)}\nabla q_\varepsilon\Big), \tag{2.178}$$

while the fluid flow is subject to the Navier-Stokes system:

$$\nabla\cdot\boldsymbol{v}_\varepsilon = 0, \tag{2.179}$$

$$\begin{aligned}\partial_t^{\bullet(\boldsymbol{v}_\varepsilon)}(\rho_\varepsilon\boldsymbol{v}_\varepsilon) = {}&\nabla\cdot\Big(-p\boldsymbol{I} + 2\eta(\varphi_\varepsilon)\boldsymbol{D}(\boldsymbol{v}_\varepsilon) - \boldsymbol{v}_\varepsilon\otimes\sum_k\overline{\rho}^{(k)}\boldsymbol{j}_{\varphi_\varepsilon^{(k)}}\Big)\\ &+\nabla\cdot\Big(\sum_{i<j}\tilde{\sigma}_{i,j}\Big(\delta_{i,j} - \sum_k\nabla\varphi_\varepsilon^{(k)}\otimes\partial_{\nabla\varphi_\varepsilon^{(k)}}\delta_{i,j}\Big)\boldsymbol{I}\Big).\end{aligned} \tag{2.180}$$

For completion of the problem, boundary conditions as discussed in Section 2.2.6 and suitable initial conditions have to be imposed.

2.2.8 Forms of the energy functional

We observed in Section 2.2.2 that due to [120, 55], the Ginzburg-Landau energy density satisfies the reduced minimization problem (2.124). Following the work of [121] we require further admissibility conditions on the multiwell potential and gradient parts of the energy density to ensure there is a form of model reduction away from triple junctions. In particular, we require that within any interfacial region between two phases and away from a junction, there are contributions from a third phase present.

Multiwell potential admissibility criteria:

$$\breve{w}(\varphi_\varepsilon)\geq 0, \quad \breve{w}(\varphi_\varepsilon) = 0 \;\Leftrightarrow\; \varphi_\varepsilon\in\{e_1,\dots,e_M\}, \tag{2.181}$$

$$\breve{w}(t\boldsymbol{e}_i + (1-t)\boldsymbol{e}_j) = \overline{w}_{i,j}t^2(1-t)^2 \quad \forall t\in[0,1],\ \forall i,j\in\{1,\dots,M\}, \tag{2.182}$$

where $\boldsymbol{e}_k$ are the corners of the Gibbs' simplex Σ^M (2.104) .

Gradient energy admissibility criteria:

$$\check{a}(\varphi_\varepsilon, A) \geq 0, \quad \check{a}(\varphi_\varepsilon, \eta A) = \eta^2 \check{a}(\varphi_\varepsilon, A), \quad \forall \varphi_\varepsilon \in \Sigma^M, A \in (T\Sigma^M)^d, \eta \in \mathbb{R}, \tag{2.183}$$

and the following function,

$$\check{a}_{i,j}(\boldsymbol{\nu}^{(i,j)}) := \check{a}(t\boldsymbol{e}_i + (1-t)\boldsymbol{e}_j, (\boldsymbol{e}_j - \boldsymbol{e}_i) \otimes \boldsymbol{\nu}^{(i,j)}), \tag{2.184}$$

is independent of $t \in [0,1],\ \forall i, j \in \{1, \ldots, M\}$.

The admissibility criteria allow the minimization problem (2.124) to be rewritten as

$$\check{\gamma}_{i,j}(\boldsymbol{\nu}^{(i,j)}) = \inf_{\psi} \Big\{ \int_{\mathbb{R}} \check{a}(\psi, \partial_z \psi \otimes \boldsymbol{\nu}^{(i,j)}) + \check{w}(\psi) dz \,\Big|\, \psi : \mathbb{R} \to \Sigma^M \text{ Lipschitz }, \lim_{z \to -\infty} \psi(z) = \boldsymbol{e}_i, \lim_{z \to \infty} \psi(z) = \boldsymbol{e}_j \Big\}. \tag{2.185}$$

In [121] the author proves that a function $\check{\psi}$ of the form

$$\check{\psi}(z) = \chi(z)\boldsymbol{e}_i + (1 - \chi(z))\boldsymbol{e}_j, \quad \text{where} \quad \chi(z) = \frac{1}{2}\Big(1 + \tanh\Big(\sqrt{\frac{\check{w}_{i,j}}{\check{a}_{i,j}(\boldsymbol{\nu}^{(i,j)})}}\frac{z}{2}\Big)\Big),$$

satisfies the Euler-Lagrange equations associated to the minimisation problem (2.124). If $\check{\psi}$ is also a solution to (2.185) then one can recover the surface energy:

$$\check{\gamma}_{i,j}(\boldsymbol{\nu}^{(i,j)}) = \frac{1}{3}\sqrt{\check{a}_{i,j}(\boldsymbol{\nu}^{(i,j)})\check{w}_{i,j}}.$$

In general it is nontrivial to construct the functions a and w satisfying the minimization problem (2.124) or even (2.185), see [121]; it is easier to find specific forms $\check{a}$, $\check{w}$ for a, w, which satisfy the admissibility criteria (2.181)-(2.184).

Choice of Stinner

The general choices made in [121], are given as follows:

$$a(\varphi_\varepsilon, \nabla\varphi_\varepsilon) = \sum_{i<j} b_{i,j}(s_{i,j}(\varphi_\varepsilon^{(i)} \nabla \varphi_\varepsilon^{(j)} - \varphi_\varepsilon^{(j)} \nabla \varphi_\varepsilon^{(i)}))^2,$$

where $b_{i,j} > 0$ with $b_{i,j} = b_{j,i}$, and $s_{i,j} : \mathbb{R}^d \to \mathbb{R}$, a 1-homogenous function with $s_{i,j}(\nu) > 0$, for $\nu \in S^{d-1}$, is an admissible gradient energy density,

$$w(\varphi_\varepsilon) = 9 \sum_{i<j} b_{i,j} (\varphi_\varepsilon^{(i)})^2 (\varphi_\varepsilon^{(j)})^2 \Big(1 + \sum_{k \neq i,j} \varphi_\varepsilon^{(k)}\Big) + \sum_{i<j<k} b_{i,j,k} (\varphi_\varepsilon^{(i)})^2 (\varphi_\varepsilon^{(j)})^2 (\varphi_\varepsilon^{(k)})^2.$$

This is a sixth order polynomial potential which is an admissible multiwell potential. For large enough $b_{ijk} > 0$, additionally one can remove the "third phase contributions" discussed in Section 2.2.2 for $M = 3$ phases.

Remark 2.2.8. *For $M \geq 4$ we observe the presence of other phases in the triple junction. These will not effect the energy of the system, which relies on interfacial quantities only, however they can be controlled by adding in higher order terms as a penalty to the potential, for example, one could use*

$$w(\varphi_\varepsilon) = 9 \sum_{i<j} b_{i,j} (\varphi_\varepsilon^{(i)})^2 (\varphi_\varepsilon^{(j)})^2 \Big(1 + \sum_{k \neq i,j} \varphi_\varepsilon^{(k)}\Big) + \sum_{i<j<k} b_{i,j,k} (\varphi_\varepsilon^{(i)})^2 (\varphi_\varepsilon^{(j)})^2 (\varphi_\varepsilon^{(k)})^2 + \sum_{i<j<k<l} b_{i,j,k,l} (\varphi_\varepsilon^{(i)})^2 (\varphi_\varepsilon^{(j)})^2 (\varphi_\varepsilon^{(k)})^2 (\varphi_\varepsilon^{(l)})^2,$$

for $b_{i,j,k,l} > 0$ sufficiently large.

Note that we have

$$\gamma_{i,j}(\nu) = b_{i,j} s_{i,j}(\nu).$$

With inclusion of surfactants, one can define $b_{i,j} = b_{i,j}(c^{(i,j)})$, then define

$$a(c^{(\cdot,\cdot)}, \varphi_\varepsilon, \nabla\varphi_\varepsilon) \coloneqq \sum_{\substack{i,j=1,\dots,M \\ i<j}} \gamma_{i,j}(c_\varepsilon^{(i,j)}) \underbrace{|\varphi_\varepsilon^{(i)} \nabla\varphi_\varepsilon^{(j)} - \varphi_\varepsilon^{(j)} \nabla\varphi_\varepsilon^{(i)}|^2}_{=: a_{i,j}(\varphi_\varepsilon^{(i)}, \varphi_\varepsilon^{(j)}, \nabla\varphi_\varepsilon^{(i)}, \nabla\varphi_\varepsilon^{(j)})}, \tag{2.186}$$

$$w(c, \varphi_\varepsilon) \coloneqq \sum_{\substack{i,j=1,\dots,M \\ i<j}} \gamma_{i,j}(c_\varepsilon^{(i,j)}) \underbrace{(w_{i,j}(\varphi_\varepsilon^{(i)}, \varphi_\varepsilon^{(j)}) + \tilde{w}_{i,j}(\varphi_\varepsilon))}_{=: \overline{w}_{i,j}(\varphi_\varepsilon)},$$

$$f(c, \varphi_\varepsilon) \coloneqq \sum_{i=1,\dots,M} \xi_i(\varphi_\varepsilon^{(i)}) G_i(c_\varepsilon^{(i)}). \tag{2.187}$$

In particular w and a satisfy the conditions required to form an admissable multiwell potential and admissable gradient term.

Choice of Boyer, Lapuerta and Minjeaud

During subsequent implementation in Chapter 4 we frequently make use of a particular choice of a, w for an $M = 3$ phase Cahn-Hilliard system. This is a construction that

satisfies the admissibility criteria of Section 2.2.8, and can be identified with the model investigated in [21, 23] with further choice of the mobility matrix (2.159). We take a and w to be:

$$w(q_\varepsilon, \varphi_\varepsilon) = \sum_{i<j} \tilde{\sigma}_{i,j} \overline{w}_{i,j}(\varphi_\varepsilon), \qquad a(q_\varepsilon, \varphi_\varepsilon, \nabla\varphi_\varepsilon) = \sum_{i<j} \tilde{\sigma}_{i,j} a_{i,j}(\varphi_\varepsilon, \nabla\varphi_\varepsilon), \tag{2.188}$$

with the following choice for the multiwell potential,

$$\begin{aligned}\overline{w}_{i,j}(\varphi_\varepsilon) =& 12\Big((\varphi_\varepsilon^{(i)})^2(\varphi_\varepsilon^{(j)})^2 + \sum_{k\neq i,j} \big(\varphi_\varepsilon^{(j)}\varphi_\varepsilon^{(k)}(\varphi_\varepsilon^{(i)})^2 + \varphi_\varepsilon^{(i)}\varphi_\varepsilon^{(k)}(\varphi_\varepsilon^{(j)})^2 - \varphi_\varepsilon^{(i)}\varphi_\varepsilon^{(j)}(\varphi_\varepsilon^{(k)})^2 \\ &+ \frac{1}{3}\Lambda(\varphi_\varepsilon^{(i)})^2(\varphi_\varepsilon^{(j)})^2(\varphi_\varepsilon^{(k)})^2\big)\Big).\end{aligned} \tag{2.189}$$

We take the constant $\Lambda \geq 0$. This regularisation term is of sixth order and helps to prevent the leaking of third phase contributions between two other phases outside of the triple junction regions. Note that this is a specific form of (2.187). We choose the gradient term as:

$$a_{i,j}(\nabla\varphi_\varepsilon) = \frac{3}{8}(|\nabla\varphi_\varepsilon^{(i)}|^2 + |\nabla\varphi_\varepsilon^{(j)}|^2 - \sum_{k\neq i,j} |\nabla\varphi_\varepsilon^{(k)}|^2), \tag{2.190}$$

which is a different construction to (2.186). For the operator $\mathcal{L}$ in the setting of Section 2.2.7 we choose a q_ε dependent matrix defined as follows:

$$\mathcal{L}^{(k,l)}(q_\varepsilon) = \begin{cases} -\frac{M_c \bar{S}(q_\varepsilon)}{3S_k(q_\varepsilon)S_l(q_\varepsilon)}, & \text{for } l \neq k, \\ \sum_{i\neq l} \frac{M_c \bar{S}(q_\varepsilon)}{3S_i(q_\varepsilon)S_l(q_\varepsilon)}, & \text{for } k = l. \end{cases} \tag{2.191}$$

Where the functions $S_k(q_\varepsilon) = \tilde{\sigma}_{i,k}(q_\varepsilon) + \tilde{\sigma}_{j,k}(q_\varepsilon) - \tilde{\sigma}_{i,j}(q_\varepsilon)$, where $S_k(q_\varepsilon) = -S^{(i,j,k)}(q_\varepsilon)$ from (2.37) their harmonic average is given by $\bar{S} = \sum_{i=1}^{3} \frac{3}{S_i(q_\varepsilon)}$, and finally we take a constant mobility parameter M_c. It can be shown that these choices lead to the following Cahn-Hilliard system for all $i = 1, 2, 3$

$$\partial_t \varphi_\varepsilon^{(i)} = \nabla \cdot \Big(\frac{M_c}{S_i(q_\varepsilon)} \nabla \mu_\varepsilon^{(i)}\Big), \tag{2.192}$$

$$\mu_\varepsilon^{(i)} = -\frac{3}{4}\varepsilon S_i(q_\varepsilon)\Delta\varphi_\varepsilon^{(i)} + \frac{4\bar{S}}{\varepsilon}\mathcal{D}_i F(\varphi_\varepsilon), \tag{2.193}$$

where,

$$\mathcal{D}_i F(\varphi_\varepsilon) = \sum_{j\neq i} \frac{1}{S_j(q_\varepsilon)} \Big(F(\varphi_\varepsilon)_{,\varphi_\varepsilon^{(i)}} - F(\varphi_\varepsilon)_{,\varphi_\varepsilon^{(j)}}\Big).$$

2.2.9 A note regarding asymptotic analysis

The recovery of the sharp interface model (2.58) – (2.36) (with initial and boundary conditions) from the diffuse model (2.158) – (2.167) as $\varepsilon \to 0$ is completed in an asymptotic analysis (a good introduction can be found in [49]). We shall not consider it here as the focus of this thesis is on the derivation and implementation of schemes for the flows, and not the reconstruction techniques. The difficulties and details have been carried out and shall be presented in a forthcoming paper [42] that generalises the work of [54] to $M \geq 3$.

Chapter 3

Numerical Schemes

3.1 Fractional-theta scheme for Cahn-Hilliard Navier-Stokes problem

In this chapter we derive the numerical scheme for the diffuse interface model of Section 2.2. In particular we focus on the time discretisation for the following two phase Cahn-Hilliard Navier-Stokes system.

Problem 3.1.1. Find $\{\boldsymbol{v}_\varepsilon(\boldsymbol{x},t), p_\varepsilon(\boldsymbol{x},t), \mu_\varepsilon(\boldsymbol{x},t), \varphi_\varepsilon(\boldsymbol{x},t)\}$, such that:

$$\begin{aligned}
\partial_t \varphi_\varepsilon + \boldsymbol{v}_\varepsilon \cdot \nabla \varphi_\varepsilon &= \Delta \mu_\varepsilon, && \text{in } \Omega \times (0,T),\\
\mu_\varepsilon + \varepsilon \Delta \varphi_\varepsilon - \frac{1}{\varepsilon} F'(\varphi_\varepsilon) &= 0, && \text{in } \Omega \times (0,T),\\
\partial_t \boldsymbol{v}_\varepsilon - \eta \Delta \boldsymbol{v}_\varepsilon + \boldsymbol{v}_\varepsilon \cdot \nabla \boldsymbol{v}_\varepsilon + \nabla p_\varepsilon &= \boldsymbol{f} + \mu_\varepsilon \nabla \varphi_\varepsilon, && \text{in } \Omega \times (0,T),\\
\nabla \cdot \boldsymbol{v}_\varepsilon &= 0, && \text{in } \Omega \times (0,T),\\
\boldsymbol{v} &= \mathbf{g}, && \text{on } \partial\Omega \times [0,T],\\
\nabla \varphi_\varepsilon \cdot \boldsymbol{\nu}_\Omega &= 0, && \text{on } \partial\Omega \times [0,T],\\
\nabla \mu_\varepsilon \cdot \boldsymbol{\nu}_\Omega &= 0, && \text{on } \partial\Omega \times [0,T],
\end{aligned}$$

where $F(\varphi_\varepsilon)$ is a smooth double well potential with minima at 0 and 1, and $\boldsymbol{f} : \Omega \times [0,T] \to \mathbb{R}^d$ is a body force. This is complete with initial conditions,

$$\boldsymbol{v}_\varepsilon(\boldsymbol{x},t) = \boldsymbol{v}_{\varepsilon 0}(\boldsymbol{x}),\ \varphi_\varepsilon(\boldsymbol{x},0) = \varphi_{\varepsilon 0}(\boldsymbol{x}),$$

where $\{\boldsymbol{v}_{\varepsilon 0}, p_{\varepsilon 0}, \mu_{\varepsilon 0}, \varphi_{\varepsilon 0}\}$ are given functions. To avoid additional boundary terms for the phase fields, we take $\mathbf{g} \cdot \boldsymbol{\nu}_\Omega = 0$, that is, a tangential flow condition for the velocity. This may be extended to a zero net flow condition where $\mathbf{g}$ only satisfies $\int_{\partial\Omega} \mathbf{g} \cdot \boldsymbol{\nu}_\Omega = 0$.

There is substantial literature for time discretisation schemes of this coupled problem, some examples include [53, 95, 91] (further introduction is given in Section 1.2.2). The offered schemes are often based on exploitating the thermodynamic framework of the continuous problem in Section 2.2 for the discrete in time problem. To acheive this, intelligent discretisation of the Cahn-Hilliard system is required, but often is coupled to a simple first order in time (or multistep for formally second order [53]) scheme for Navier-Stokes. By preserving a discrete energy inequality (reflecting the continuous setting) one obtains natural unconditional stability for the scheme, however this comes at the cost of a first order scheme.

The idea of this chapter is to present a second order accurate in time scheme, which is motivated from a Navier-Stokes solver through a more involved operator splitting technique than seen in aforementioned literature. The fractional-theta scheme [26, 60] is well known for its robustness properties compared to other second order accurate methods such as Crank-Nicholson based schemes, we provide some validation of why this is true with an example in Remark 3.1.2. A comparison to some other schemes for Navier-Stokes has been carried out by Turek [134].

We first present the scheme we have chosen in an abstract form. Then we shall formulate the full discretisation scheme, derived from a weak formulation of Problem 3.1.1. In Section 3.2.3 construct an energy inequality for the coupled scheme for matched densities, relying upon dependence between the spatial and time discretisation parameters. These restrictions are identical to the Navier-Stokes fractional-theta scheme [81]. We consider the extension to multiple phases in Section 3.3. In Section 3.4 we will construct a scheme for a flow with different densities in each fluid, and demonstrate that this is indeed second order accurate in time. We also consider and extension for the inclusion of surfactants in Section 3.5, which we shall use in our implementation. We leave the presentation of numerical findings for the scheme until Chapter 4.

3.1.1 The abstract scheme

Consider a Hilbert space H, with an initial value problem over the time interval $[0, T]$:

$$\frac{\mathrm{d}u}{\mathrm{d}t} + \mathcal{F}(u) = 0, \qquad u(0) = u_0, \tag{3.1}$$

with $\mathcal{F}\colon H \to H$ an operator, u_0 given initial value. We take $\mathcal{F}_1$ and $\mathcal{F}_2$ operators so that we may nontrivially decompose $\mathcal{F} = \mathcal{F}_1 + \mathcal{F}_2$. We say nontrivial to mean that the choices of $\mathcal{F}_i$ should increase the solvability of the following subproblems:

$$\frac{\mathrm{d}u}{\mathrm{d}t} + \mathcal{F}_i(u) = f, \qquad \text{for } i = 1, 2, \tag{3.2}$$

where f is a given forcing function. The following scheme was first presented in [26] motivated by work in [124]. First we set up the time discretisation, take $\theta \in (0, \frac{1}{2})$, let $\tilde{\theta} = 1 - \theta$, and denote the timestep size by Δt. We use the notation $f^k = f(t^k)$ and $t^k = k\Delta t$. Let $T = N\Delta t$, then for any $n \in \{0, \dots, N-1\}$ we split the interval $[n\Delta t, (n+1)\Delta t]$ into three sub intervals and solve the following time discrete problems:

1. For $[n\Delta t, (n+\theta)\Delta t]$, solve the substep $t^n \to t^{n+\theta}$,

$$\frac{u^{n+\theta} - u^n}{\theta \Delta t} + \mathcal{F}_1(u^{n+\theta}) = -\mathcal{F}_2(u^n). \tag{3.3}$$

2. For $[(n+\theta)\Delta t, (n+\tilde{\theta})\Delta t]$, solve the substep $t^{n+\theta} \to t^{n+\tilde{\theta}}$,

$$\frac{u^{n+\tilde{\theta}} - u^{n+\theta}}{(\tilde{\theta} - \theta)\Delta t} + \mathcal{F}_2(u^{n+\tilde{\theta}}) = -\mathcal{F}_1(u^{n+\theta}). \tag{3.4}$$

3. For $[(n+\tilde{\theta})\Delta t, (n+1)\Delta t]$, solve the substep $t^{n+\tilde{\theta}} \to t^{n+1}$,

$$\frac{u^{n+1} - u^{n+\tilde{\theta}}}{\theta \Delta t} + \mathcal{F}_1(u^{n+1}) = -\mathcal{F}_2(u^{n+\tilde{\theta}}). \tag{3.5}$$

The form of each of these steps is that of (3.2) with operator $\mathcal{F}_i$ and forcing function $\mathcal{F}_j(u^*)$, $j \neq i$ with t^* the previous time substep.

Remark 3.1.2. *Consider the splitting $\mathcal{F}_1 = \alpha A$ and $\mathcal{F}_2 = \beta A$ for a time independent positive definite symmetric matrix A and nonegative constants $\alpha + \beta = 1$. We will briefly state some analysis from [26, 60] (methods in [94]) for the scheme* (3.2) *with this choice, with the aim of determining suitable parameter ranges for α and β. The system operators for Step 1-3 are given by*

1. $u^{n+\theta} = G_1^\theta u^n$ *where* $G_1^\theta = (I + \alpha\theta\Delta t A)^{-1}(I - \beta\theta\Delta t A)$,
2. $u^{n+\tilde{\theta}} = G_2^{\tilde{\theta}-\theta} u^{n+\theta}$ *where* $G_2^{\tilde{\theta}-\theta} = (I + \beta(\tilde{\theta} - \theta)\Delta t A)^{-1}(I - \alpha(\tilde{\theta} - \theta)\Delta t A)$,
3. $u^{n+1} = G_3^\theta u^{n+\tilde{\theta}}$ *where* $G_3^\theta = G_1^\theta$.

This scheme can be represented by the mulitplicative identity

$$u^{n+1} = G_1^\theta G_2^{\tilde{\theta}-\theta} G_1^\theta u^n.$$

Let $\lambda_1 < \lambda_2 < \dots$ be the eigenvalues of A and $u_1, u_2, \dots$ be a corresponding basis of

orthonormal eigenvectors. Choosing $u_i^0 = u_i$ we have

$$u_i^{n+1} = R(\lambda_i)u_i^n = \frac{(1-\beta\theta\Delta t\lambda_i)^2(1-\alpha(\tilde{\theta}-\theta)\Delta t\lambda_i)}{(1+\alpha\theta\Delta t\lambda_i)^2(1+\beta(\tilde{\theta}-\theta)\Delta t\lambda_i)}u_i^n.$$

The above rational function $R(x) \to \frac{\beta}{\alpha}$ as $x \to \infty$, so we require $\alpha > \beta$ for stiff A-stability. Further inspection reveals that the stronger property of unconditional stability requires $|R(x)| \leq 1,\ \forall x \in \mathbb{R}_+$ and this is satisfied when also $\theta \in [\frac{1}{4}, \frac{1}{2}),\ 0 < \alpha < \beta < 1$.

The accuracy of the scheme is found by comparison of

$$R(x) = 1 - x + \frac{1}{2}(1 + (\beta^2 - \alpha^2)(2\theta^2 - 4\theta + 1))x^2 + \mathcal{O}(x^3),$$

with the solution of the linear eigenvalue problem: $e^{-x} = 1 - x + \frac{1}{2}x^2 + \mathcal{O}(x^3)$. Second order accuracy is obtained where $(\beta^2 - \alpha^2)(2\theta^2 - 4\theta + 1) = 0$, hence either

$$\theta \in \left(0, \frac{1}{2}\right),\ \ \alpha = \beta = \frac{1}{2}, \qquad \textit{or} \qquad \theta = 1 - \frac{\sqrt{2}}{2},\ \ \alpha = 2 - \sqrt{2}\ \ \beta = \sqrt{2} - 1.$$

If $\alpha = \beta = \frac{1}{2}$, a Crank-Nicholson type scheme, one obtains unconditionally stability for all $\theta \in (0, \frac{1}{2})$ but this has problems with damping stiff systems with large values of $\frac{\lambda_i}{\lambda_1}$. The latter case, a θ type scheme, with particular choice of θ that ensures that the substeps of the scheme all have the same matrix, also has good asymptotic properties as it is "stiff A-stable" ([26] shows these hold in the range $\theta \in [0.0873\ldots, \frac{1}{3}]$).

The most significant area of application for this particular splting scheme is for the Navier-Stokes equations. Presented in [26], a detailed analysis of the second order accuracy is performed in [97] and stability and convergence analysis is carried out by [81]. The splitting is applied to the momentum balance equation, separating the incompressibility constraint from the convection nonlinearity. Stated in a strong form, the system operator $\mathcal{F} = -\eta\Delta\boldsymbol{v} + \boldsymbol{v}\cdot\nabla\boldsymbol{v} + \nabla p - \boldsymbol{f}$, is split into:

$$\mathcal{F}_1 = -\alpha\eta\Delta\boldsymbol{v} + \nabla p - \boldsymbol{f}, \qquad \mathcal{F}_2 = -\beta\eta\Delta\boldsymbol{v} + \boldsymbol{v}\cdot\nabla\boldsymbol{v}, \qquad (0 \leq)\,\alpha + \beta = 1.$$

This results in the solving in each full timestep

1. A Stokes type problem (3.3) accounting for the incompressibility constraint and fluid pressure.

2. A Burgers type problem (3.4) accounting for the convection nonlinearity.

3. A Stokes type problem (3.5), to enforce divergence free velocity at the end of the full

timestep.

The steps can be seen in the as part of the fully coupled scheme in Section 3.1.2, so we shall not detail them individually here.

3.1.2 Formulation of the coupled scheme

We focus our analysis on the scheme for time discretisation of the Problem 3.1.1. We seek to discretise in space using a finite element method in Section 3.2.1, therefore it is convenient to first write down the weak formulation in the continuous setting. Let Ω be a bounded domain in $\mathbb{R}^d$ for $d = 2, 3$. For ease of notation in the equations, we encorporate boundary conditions into the space, for any $t > 0$:

$$(H^1_g(\Omega))^d = \Big\{ \mathbf{w}(\cdot, t) \in (W^{1,2}(\Omega))^d \;\Big|\; \mathbf{w}(\cdot, t) = \mathbf{g}(\cdot, t) \text{ on } \partial\Omega \Big\}. \tag{3.6}$$

We now express the weak formulation of the Problem 3.1.1:

Problem 3.1.3. Given initial data $\{\boldsymbol{v}_{\varepsilon 0}, \varphi_{\varepsilon 0}, \} \in (H^1_g(\Omega))^d \times H^1(\Omega)$ and functions $\boldsymbol{f} \in (L^2(\Omega))^d$, $\mathbf{g} \in (H^1(\Omega))^d$ find $\boldsymbol{v}_\varepsilon(\cdot, t) \in (H^1_g(\Omega))^d, p_\varepsilon(\cdot, t) \in L^2(\Omega)/\mathbb{R}$ and $\varphi_\varepsilon(\cdot, t),\ \mu_\varepsilon(\cdot, t) \in H^1(\Omega)$ such that, for all $t \in [0, T]$

$$\begin{aligned}
\int_\Omega \zeta(\partial_t \varphi_\varepsilon + \boldsymbol{v}_\varepsilon \cdot \nabla \varphi_\varepsilon) &= -\int_\Omega \nabla \mu_\varepsilon \cdot \nabla \zeta, && \forall\, \zeta \in H^1(\Omega), \\
\int_\Omega \varepsilon \nabla \varphi_\varepsilon \cdot \nabla \zeta + \frac{1}{\varepsilon} F'(\varphi_\varepsilon)\zeta &= \int_\Omega \mu_\varepsilon \zeta, && \forall\, \zeta \in H^1(\Omega), \\
\int_\Omega \boldsymbol{\zeta}(\partial_t \boldsymbol{v}_\varepsilon + \boldsymbol{v}_\varepsilon \cdot \nabla \boldsymbol{v}_\varepsilon) + \eta \nabla \boldsymbol{v}_\varepsilon \cdot \nabla \boldsymbol{\zeta} - p_\varepsilon \nabla \cdot \boldsymbol{\zeta} &= \int_\Omega \boldsymbol{\zeta} \boldsymbol{f} + \boldsymbol{\zeta} \mu_\varepsilon \nabla \varphi_\varepsilon, && \forall\, \boldsymbol{\zeta} \in (H^1(\Omega))^d, \\
\int_\Omega \zeta \nabla \cdot \boldsymbol{v}_\varepsilon &= 0, && \forall\, \zeta \in L^2(\Omega).
\end{aligned}$$

Now we construct a scheme for the time discretisation of Problem 3.1.3. We gain insight into how a coupled approach may work by looking at the methods in [36]. This arises naturally from using a vector of functions in the framework presented in Section 3.1.1, with one component block for the fluid system, and the other component block for the Cahn-Hilliard system. First considering the formulation of Problem 3.1.1 we define for

$\alpha, \gamma \in [0,1]$ the following operator splitting,

$$\text{Fluid operator: } \begin{cases} \mathcal{F}_1(\boldsymbol{v}_\varepsilon, p_\varepsilon) & = -\alpha\eta\Delta\boldsymbol{v}_\varepsilon + \nabla p_\varepsilon - \boldsymbol{f}, \\ \mathcal{F}_2(\boldsymbol{v}_\varepsilon, \varphi_\varepsilon, \mu_\varepsilon) & = -(1-\alpha)\eta\Delta\boldsymbol{v}_\varepsilon + \boldsymbol{v}_\varepsilon \cdot \nabla\boldsymbol{v}_\varepsilon - \mu_\varepsilon\nabla\varphi_\varepsilon. \end{cases}$$

$$\text{Phase field operator: } \begin{cases} \mathcal{G}_1(\varphi_\varepsilon, \mu_\varepsilon, \boldsymbol{v}_\varepsilon) & = -\gamma\Delta\mu_\varepsilon + \boldsymbol{v}_\varepsilon \cdot \nabla\varphi_\varepsilon, \\ \mathcal{G}_2(\mu_\varepsilon) & = -(1-\gamma)\Delta\mu_\varepsilon. \end{cases}$$

To convey the structure of the coupling within the scheme we state the abstract formulation of the problem *to be understood in a weak sense*. This description of the scheme demonstrates how the splitting works more clearly than seeing the weak formulation directly.

Step 1(a): Find $(\boldsymbol{v}_\varepsilon^{n+\theta}, p_\varepsilon^{n+\theta}) \in (H_g^1(\Omega))^d \times L^2(\Omega)$, such that

$$\begin{aligned} \frac{\boldsymbol{v}_\varepsilon^{n+\theta} - \boldsymbol{v}_\varepsilon^n}{\theta\Delta t} + \mathcal{F}_1(\boldsymbol{v}_\varepsilon^{n+\theta}, p_\varepsilon^{n+\theta}) &= -\mathcal{F}_2(\boldsymbol{v}_\varepsilon^n, \varphi_\varepsilon^n, \mu_\varepsilon^n), \\ \nabla \cdot \boldsymbol{v}_\varepsilon^{n+\theta} &= 0. \end{aligned} \tag{3.7}$$

Step 1(b): Find $(\varphi_\varepsilon^{n+\theta}, \mu_\varepsilon^{n+\theta}) \in H^1(\Omega) \times H^1(\Omega)$, such that

$$\frac{\varphi_\varepsilon^{n+\theta} - \varphi_\varepsilon^n}{\theta\Delta t} + \mathcal{G}_1(\varphi_\varepsilon^{n+\theta}, \mu_\varepsilon^{n+\theta}, \boldsymbol{v}_\varepsilon^{n+\theta}) = -\mathcal{G}_2(\mu_\varepsilon^n). \tag{3.8}$$

Step 2(a): Set $\tilde{\theta} = 1 - \theta$. Find $(\varphi_\varepsilon^{n+\tilde{\theta}}, \mu_\varepsilon^{n+\tilde{\theta}}) \in H^1(\Omega) \times H^1(\Omega)$, such that

$$\frac{\varphi_\varepsilon^{n+\tilde{\theta}} - \varphi_\varepsilon^{n+\theta}}{(\tilde{\theta}-\theta)\Delta t} + \mathcal{G}_2(\mu_\varepsilon^{n+\tilde{\theta}}) = -\mathcal{G}_1(\varphi_\varepsilon^{n+\theta}, \mu_\varepsilon^{n+\theta}, \boldsymbol{v}_\varepsilon^{n+\theta}). \tag{3.9}$$

Step 2(b): Find $(\boldsymbol{v}_\varepsilon^{n+\tilde{\theta}}) \in (H_g^1(\Omega))^d \times L^2(\Omega)$, such that

$$\frac{\boldsymbol{v}_\varepsilon^{n+\tilde{\theta}} - \boldsymbol{v}_\varepsilon^{n+\theta}}{(\tilde{\theta}-\theta)\Delta t} + \mathcal{F}_2(\boldsymbol{v}_\varepsilon^{n+\tilde{\theta}}, p_\varepsilon^{n+\tilde{\theta}}, \varphi_\varepsilon^{n+\tilde{\theta}}, \mu_\varepsilon^{n+\tilde{\theta}}) = -\mathcal{F}_1(\boldsymbol{v}_\varepsilon^{n+\theta}, p_\varepsilon^{n+\theta}). \tag{3.10}$$

Step 3(a): Find $(\boldsymbol{v}_\varepsilon^{n+1}, p_\varepsilon^{n+1}) \in (H_g^1(\Omega))^d \times L^2(\Omega)$, such that

$$\begin{aligned} \frac{\boldsymbol{v}_\varepsilon^{n+1} - \boldsymbol{v}_\varepsilon^{n+\tilde{\theta}}}{\theta\Delta t} + \mathcal{F}_1(\boldsymbol{v}_\varepsilon^{n+1}, p_\varepsilon^{n+1}) &= -\mathcal{F}_2(\boldsymbol{v}_\varepsilon^{n+\tilde{\theta}}, \varphi_\varepsilon^{n+\tilde{\theta}}, \mu_\varepsilon^{n+\tilde{\theta}}), \\ \nabla \cdot \boldsymbol{v}_\varepsilon^{n+1} &= 0. \end{aligned} \tag{3.11}$$

Step 3(b): Find $(\varphi_\varepsilon^{n+1}, \mu_\varepsilon^{n+1}) \in H^1(\Omega) \times H^1(\Omega)$, such that

$$\frac{\varphi_\varepsilon^{n+1} - \varphi_\varepsilon^{n+\tilde{\theta}}}{\theta \Delta t} + \mathcal{G}_1(\varphi_\varepsilon^{n+1}, \mu_\varepsilon^{n+1}, \boldsymbol{v}_\varepsilon^{n+1}) = -\mathcal{G}_2(\mu_\varepsilon^{n+\tilde{\theta}}). \tag{3.12}$$

As indicated by the labelling of the different steps, the choices of operators $\mathcal{F}_i, \mathcal{G}_i$ lead to a natural decomposition of the three-step scheme into six steps. The later analysis will still require treating the scheme as a three-step method, however this natural decoupling greatly improves solvability and simplicity of the scheme. Indeed, the six steps are linear equations, with two exceptions: the convection term in the Burgers type equation (3.10), and the choice of time discretisation of the Cahn-Hilliard potential F' in Problem 3.1.3 (discussed in Section 3.2.3).

As stability for this scheme relies upon the spatial discretisation, we will proceed directly into the fully discrete problem.

3.2 Stability analysis for the matched density CHNS scheme

For simplicity of notation we shall neglect all ε subscripts for variables dependent on the phase field variable φ_ε and treat them as independent quanitities.

3.2.1 Fully discrete formulation

Ideally, the stability of a time discretisation scheme can be considered 'unconditional'. In this case one may perform an analysis of the discretisation in time without requiring any dependency on the spatial discretisation, and often first order schemes will yield this property [95, 53, 119]. However, even for the Navier Stokes problem alone, this scheme will not yield such a stability result due to the nonlinear treatment of the convection operator required for second order accuracy [81]. We will setup the spatial discretisation for the fully coupled problem, and investigate whether the stability constraint assumed in [81] is sufficient for stability. Two such results for a convection diffusion equation [35] and a viscoelastic flow [36] have been shown.

The spatial discretisation is taken as a mixed finite element formulation whose spaces are defined below. The notation H_h^1, L_h^2 denotes (conformal) finite element ap-

proximations of the spaces H^1, L^2:

$$\Pi_h(\Omega) = (L_h^2(\Omega))/\mathbb{R}, \tag{3.13}$$

$$X_h(\Omega) = \{\mathbf{w}_h \in (H_h^1(\Omega))^d \mid \mathbf{w}_h = \mathbf{g} \text{ on } \partial\Omega\}, \tag{3.14}$$

$$X_{0h}(\Omega) = \{\mathbf{w}_h \in (H_h^1(\Omega))^d \mid \mathbf{w}_h = \mathbf{0} \text{ on } \partial\Omega\}, \tag{3.15}$$

$$V_h(\Omega) = \{\mathbf{w}_h \in X_h \mid (\nabla \cdot \mathbf{w}_h, q_h) = 0,\ \forall q_h \in \Pi_h(\Omega)\}. \tag{3.16}$$

The finite element spaces related to the saddle point problem in the Navier Stokes solver must satisfy an 'inf-sup' or Ladyzhenskaya-Babuška-Brezzi condition [59], there exists $\zeta \in \mathbb{R}$ such that:

$$\inf_{q_h \in \Pi_h(\Omega)} \sup_{\mathbf{w}_h \in X_h} \left(\frac{(q_h, \nabla_h \cdot \mathbf{w}_h)}{|q_h||\nabla \mathbf{w}_h|} \right) \geq \zeta > 0, \tag{3.17}$$

and with a uniform bound of the spatial grid size h over any triangulation $\mathcal{T}_h$ of Ω:

$$\frac{\max_{T \in \mathcal{T}_h} h(T)}{\min_{\bar{T} \in \mathcal{T}_h} h(\bar{T})} \leq C. \tag{3.18}$$

Examples of such spaces are given by P^2-P^1Taylor-Hood elements or MINI elements [9]. Over the finite element spaces, denote the natural discrete norm on L_h^2 as $|\cdot|$ that is, over $L_h^2(\Omega_h)$ and $(L_h^2(\Omega_h))^d$ respectively:

$$|w_h| = \Big(\int_{\Omega_h} (w_h)^2 \, \mathrm{d}x \Big)^{\frac{1}{2}}, \qquad |\mathbf{w}_h| = \Big(\int_{\Omega_h} \mathbf{w}_h \cdot \mathbf{w}_h \, \mathrm{d}x \Big)^{\frac{1}{2}} \tag{3.19}$$

and these satisfy a Poincaré and reverse Poincaré inequality:

$$C_1 |\cdot| \leq |\nabla \cdot| \leq C_2 h^{-1} |\cdot|. \tag{3.20}$$

In the following we assume C_1, C_2 are 1 for simplicity. We denote the corresponding L^2 inner products over Ω_h as $(\cdot, \cdot)$ for simplicity. We have to introduce two trilinear operators, for $\mathbf{u}, \mathbf{v}, \mathbf{w} \in (H^1(\Omega_h))^d$, $v, w \in H^1(\Omega_h)$

$$b(\mathbf{u}, \mathbf{v}, \mathbf{w}) \coloneqq \int_{\Omega_h} \mathbf{u} \cdot \nabla \mathbf{v} \cdot \mathbf{w} = \int_{\Omega_h} \mathbf{u}_i \partial_i \mathbf{v}_j \mathbf{w}_j, \qquad \hat{b}(\mathbf{u}, v, w) \coloneqq \int_{\Omega_h} w \mathbf{u} \cdot \nabla v,$$

where one sums over recurring indices. For the convective term (as in [130] and [131]), we use the skew symmetric form of the trilinear operator b and the spatial discretisation we denote as follows.

$$b_h(\mathbf{u}_h, \mathbf{v}_h, \mathbf{w}_h) = \frac{1}{2}\big(b(\mathbf{u}_h, \mathbf{v}_h, \mathbf{w}_h) - b(\mathbf{u}_h, \mathbf{w}_h, \mathbf{v}_h)\big) \ \forall \mathbf{u}_h, \mathbf{v}_h, \mathbf{w}_h \in H_h^1((\Omega_h))^d \tag{3.21}$$

which is still trilinear, continuous and satisfies

$$b_h(\mathbf{u}_h, \mathbf{v}_h, \mathbf{v}_h) = 0 \ \ \forall \mathbf{u}_h, \mathbf{v}_h \in (H_h^1(\Omega_h))^d. \tag{3.22}$$

The discrete form satisfies the following bound,

$$b_h(\mathbf{u}_h, \mathbf{v}_h, \mathbf{w}_h) \leq S(h)|\mathbf{u}_h||\nabla \mathbf{v}_h||\mathbf{w}_h| \quad \forall \mathbf{u}_h, \mathbf{v}_h, \mathbf{w}_h \in (H_h^1(\Omega))^d \tag{3.23}$$

where $S(h) = C_S h^{-1}$ in two dimensions and $S(h) = C_S h^{-\frac{3}{2}}$ in three dimensions for conforming finite elements, C_S independent of the spatial grid size h. Details on the bound can be found in Appendix 6.3.

Remark 3.2.1. *It is possible to formulate this analysis with nonconforming finite elements, and one cost of this approach appears as an additional exponent $S(h) = C_S h^{-1-\delta}$ in 2D. We will proceed with conforming elements.*

The advective operators representing the coupling terms for CHNS are of a similar form to that of the convective terms. We represent their spatial discretisation as the operator $\hat{b}(\mathbf{u}_h, v_h, w_h)$ for the coupling terms defined as:

$$\hat{b}(\mathbf{u_h}, v_h, w_h) = ((\mathbf{u}_h \cdot \nabla)v_h, w_h)_{L^2(\Omega_h)}, \quad \forall \mathbf{u}_h \in (H_h^1(\Omega_h))^d \ \ v_h, w_h \in H_h^1(\Omega_h). \tag{3.24}$$

This operator can be bounded as follows:

$$\hat{b}(\mathbf{u}_h, v_h, w_h) \leq T(h)|\mathbf{u}_h||\nabla v_h||\nabla w_h| \quad \forall \mathbf{u}_h \in (H_h^1(\Omega_h))^d, \ v_h, w_h \in H_h^1(\Omega_h), \tag{3.25}$$

where $T(h) = C_T h^{-\xi}$ for any $\xi > 0$ in two dimensions and $T(h) = C_T h^{-\frac{1}{2}}$ in three dimensions for conforming finite elements and C_T independent of the spatial grid size h. Details on the bound can be found in Appendix 6.3.

3.2.2 Stability inequalities

In the continuous time and space setting we have shown in Section 2.2.3 that the global system satisfies an energy dissipation estimate. This estimate holds true for two phases and in the case of no surfactant presence. If the numerical approximation can demonstrate similar properties of its corresponding discrete energy, then we obtain numerical stability. To construct such a dissipation type inequality, we first find estimates for the substeps of the scheme (3.7) - (3.12) using the finite element formulation described in Section 3.2.1. These are gathered in Section 3.2.3 to construct the energy estimate. Before proceeding, we list

the most basic (in)equalities which we use the most frequently:

Young's inequality	$ab \le \frac{a^2}{2\delta} + \frac{\delta b^2}{2},$	$\forall a, b, \in \mathbb{R},\ \delta > 0.$
Rewriting products	$(f,g) = \frac{1}{2}(\lvert f\rvert^2 + \lvert g\rvert^2 - \lvert f-g\rvert^2),$	$\forall f, g \in L^2(\Omega),$
	$(f,g) = -\frac{1}{2}(\lvert f\rvert^2 + \lvert g\rvert^2 - \lvert f+g\rvert^2),$	$\forall f, g \in L^2(\Omega).$
Cauchy Schwarz	$(f,g) \le \lvert f\rvert\lvert g\rvert,$	$\forall f, g \in L^2(\Omega).$

Step 1(a)

Given $\varphi_{\varepsilon h}^n, \mu_{\varepsilon h}^n$ in H_h^1, $\boldsymbol{v}_h^n \in X_h$ find $\boldsymbol{v}_h^{n+\theta} \in V_h$, such that for all $\mathbf{w}_h \in X_h$:

$$\begin{aligned}&\Big(\frac{\boldsymbol{v}_{\varepsilon h}^{n+\theta} - \boldsymbol{v}_{\varepsilon h}^n}{\theta\Delta t}, \mathbf{w}_h\Big) + \alpha\eta(\nabla \boldsymbol{v}_{\varepsilon h}^{n+\theta}, \nabla \mathbf{w}_h) - (\boldsymbol{f}_h^{n+\theta}, \mathbf{w}_h)\\ &= -(1-\alpha)\eta(\nabla \boldsymbol{v}_{\varepsilon h}^n, \nabla \mathbf{w}_h) - b_h(\boldsymbol{v}_{\varepsilon h}^n, \boldsymbol{v}_{\varepsilon h}^n, \mathbf{w}_h) + \hat{b}(\mathbf{w}_h, \varphi_{\varepsilon h}^n, \mu_{\varepsilon h}^n).\end{aligned} \tag{3.26}$$

Test (3.26) with $\mathbf{w}_h = \boldsymbol{v}_{\varepsilon h}^{n+\theta} \in V_h \subset X_h$,

$$\begin{aligned}&\frac{1}{\theta\Delta t}|\boldsymbol{v}_{\varepsilon h}^{n+\theta}|^2 + \alpha\eta|\nabla \boldsymbol{v}_{\varepsilon h}^{n+\theta}|^2\\ &= \frac{1}{\theta\Delta t}(\boldsymbol{v}_{\varepsilon h}^n, \boldsymbol{v}_{\varepsilon h}^{n+\theta}) - (1-\alpha)\eta(\nabla \boldsymbol{v}_{\varepsilon h}^n, \nabla \boldsymbol{v}_{\varepsilon h}^{n+\theta}) - b_h(\boldsymbol{v}_{\varepsilon h}^n, \boldsymbol{v}_{\varepsilon h}^n, \boldsymbol{v}_{\varepsilon h}^{n+\theta})\\ &\quad + \hat{b}(\boldsymbol{v}_{\varepsilon h}^{n+\theta}, \varphi_{\varepsilon h}^n, \mu_{\varepsilon h}^n) + (\boldsymbol{f}_h^{n+\theta}, \boldsymbol{v}_{\varepsilon h}^{n+\theta}).\end{aligned} \tag{3.27}$$

Rewriting products, and applying Young's inequality and (3.20),

$$\begin{aligned}&\frac{1}{2}|\boldsymbol{v}_{\varepsilon h}^{n+\theta}|^2 + \frac{1}{2}|\boldsymbol{v}_{\varepsilon h}^{n+\theta} - \boldsymbol{v}_{\varepsilon h}^n|^2 + \frac{1+\alpha}{2}\eta\theta\Delta t|\nabla \boldsymbol{v}_{\varepsilon h}^{n+\theta}|^2 + \frac{1-\alpha}{2}\eta\theta\Delta t|\nabla \boldsymbol{v}_{\varepsilon h}^n|^2\\ &\le \frac{1}{2}|\boldsymbol{v}_{\varepsilon h}^n|^2 + \frac{1-\alpha}{2}\eta\theta\Delta t|\nabla \boldsymbol{v}_{\varepsilon h}^{n+\theta} - \nabla \boldsymbol{v}_{\varepsilon h}^n|^2 - \theta\Delta t b_h(\boldsymbol{v}_{\varepsilon h}^n, \boldsymbol{v}_{\varepsilon h}^n, \boldsymbol{v}_{\varepsilon h}^{n+\theta})\\ &\quad + \theta\Delta t\hat{b}(\boldsymbol{v}_{\varepsilon h}^{n+\theta}, \varphi_{\varepsilon h}^n, \mu_{\varepsilon h}^n) + \frac{\theta\Delta t}{\eta}|\boldsymbol{f}_h^{n+\theta}|^2 + \frac{1}{4}\eta\theta\Delta t|\nabla \boldsymbol{v}_{\varepsilon h}^{n+\theta}|^2.\end{aligned} \tag{3.28}$$

From (3.22), it holds that $b_h(\boldsymbol{v}_{\varepsilon h}^n, \boldsymbol{v}_{\varepsilon h}^n, \boldsymbol{v}_{\varepsilon h}^{n+\theta}) = b_h(\boldsymbol{v}_{\varepsilon h}^n, \boldsymbol{v}_{\varepsilon h}^n, \boldsymbol{v}_{\varepsilon h}^{n+\theta} - \boldsymbol{v}_{\varepsilon h}^n)$. Then (3.20) and (3.23) yield,

$$\begin{aligned}&\frac{1}{2}|\boldsymbol{v}_{\varepsilon h}^{n+\theta}|^2 + \Big(\frac{1}{2} - \frac{1-\alpha}{2h^2}\eta\theta\Delta t\Big)|\boldsymbol{v}_{\varepsilon h}^{n+\theta} - \boldsymbol{v}_{\varepsilon h}^n|^2 + \frac{1+2\alpha}{4}\eta\theta\Delta t|\nabla \boldsymbol{v}_{\varepsilon h}^{n+\theta}|^2\\ &+ \frac{1-\alpha}{2}\eta\theta\Delta t|\nabla \boldsymbol{v}_{\varepsilon h}^n|^2\\ &\le \frac{1}{2}|\boldsymbol{v}_{\varepsilon h}^n|^2 + \frac{\theta\Delta t}{\eta}|\boldsymbol{f}_h^{n+\theta}|^2 + S(h)\theta\Delta t|\boldsymbol{v}_{\varepsilon h}^n||\nabla \boldsymbol{v}_{\varepsilon h}^n||\boldsymbol{v}_{\varepsilon h}^{n+\theta} - \boldsymbol{v}_{\varepsilon h}^n|\\ &\quad + \theta\Delta t\hat{b}(\boldsymbol{v}_{\varepsilon h}^{n+\theta}, \varphi_{\varepsilon h}^n, \mu_{\varepsilon h}^n),\end{aligned} \tag{3.29}$$

and applying Young's inequality:

$$\begin{aligned}
&\frac{1}{2}|\boldsymbol{v}_{\varepsilon h}^{n+\theta}|^2 + \Big(\frac{1}{4} - \frac{1-\alpha}{2h^2}\eta\theta\Delta t\Big)|\boldsymbol{v}_{\varepsilon h}^{n+\theta} - \boldsymbol{v}_{\varepsilon h}^{n}|^2 + \frac{1+2\alpha}{2}\eta\theta\Delta t|\nabla\boldsymbol{v}_{\varepsilon h}^{n+\theta}|^2 \\
&+ \frac{1-\alpha}{2}\eta\theta\Delta t|\nabla\boldsymbol{v}_{\varepsilon h}^{n}|^2 \\
&\leq \frac{1}{2}|\boldsymbol{v}_{\varepsilon h}^{n}|^2 + 2(S(h)\theta\Delta t)^2|\boldsymbol{v}_{\varepsilon h}^{n}|^2|\nabla\boldsymbol{v}_{\varepsilon h}^{n}|^2 + \theta\Delta t\hat{b}(\boldsymbol{v}_{\varepsilon h}^{n+\theta}, \varphi_{\varepsilon h}^{n}, \mu_{\varepsilon h}^{n}) + \frac{\theta\Delta t}{\eta}|\boldsymbol{f}_h^{n+\theta}|^2.
\end{aligned}$$

We finally bound the coupling term using (3.25) and Young's inequality ($\omega > 0$):

$$\begin{aligned}
&\theta\Delta t\hat{b}(\boldsymbol{v}_{\varepsilon h}^{n+\theta}, \varphi_{\varepsilon h}^{n}, \mu_{\varepsilon h}^{n}) \\
&= \theta\Delta t(\hat{b}(\boldsymbol{v}_{\varepsilon h}^{n+\theta} - \boldsymbol{v}_{\varepsilon h}^{n}, \varphi_{\varepsilon h}^{n}, \mu_{\varepsilon h}^{n}) + \hat{b}(\boldsymbol{v}_{\varepsilon h}^{n}, \varphi_{\varepsilon h}^{n}, \mu_{\varepsilon h}^{n})) \\
&\leq \frac{1}{8}|\boldsymbol{v}_{\varepsilon h}^{n+\theta} - \boldsymbol{v}_{\varepsilon h}^{n}|^2 + \frac{2(T(h)\theta\Delta t)^2}{\varepsilon}\varepsilon|\nabla\varphi_{\varepsilon h}^{n}|^2|\nabla\mu_{\varepsilon h}^{n}|^2 \\
&\quad + \frac{T(h)^2\theta\Delta t}{\omega\varepsilon}\varepsilon|\nabla\varphi_{\varepsilon h}^{n}|^2|\boldsymbol{v}_{\varepsilon h}^{n}|^2 + \omega\theta\Delta t|\nabla\mu_{\varepsilon h}^{n}|^2.
\end{aligned} \tag{3.30}$$

We have now arrived at the stability inequality for the first substep of the scheme:

$$\begin{aligned}
&\frac{1}{2}|\boldsymbol{v}_{\varepsilon h}^{n+\theta}|^2 + \Big(\frac{1}{8} - \frac{1-\alpha}{2h^2}\eta\theta\Delta t\Big)|\boldsymbol{v}_{\varepsilon h}^{n+\theta} - \boldsymbol{v}_{\varepsilon h}^{n}|^2 + \frac{1+2\alpha}{2}\eta\theta\Delta t|\nabla\boldsymbol{v}_{\varepsilon h}^{n+\theta}|^2 \\
&+ \frac{1-\alpha}{2}\eta\theta\Delta t|\nabla\boldsymbol{v}_{\varepsilon h}^{n}|^2 \\
&\leq \frac{1}{2}|\boldsymbol{v}_{\varepsilon h}^{n}|^2 + 2(S(h)\theta\Delta t)^2|\boldsymbol{v}_{\varepsilon h}^{n}|^2|\nabla\boldsymbol{v}_{\varepsilon h}^{n}|^2 + \frac{\theta\Delta t}{\eta}|\boldsymbol{f}_h^{n+\theta}|^2 \\
&\quad + \frac{2(T(h)\theta\Delta t)^2}{\varepsilon}\varepsilon|\nabla\varphi_{\varepsilon h}^{n}|^2|\nabla\mu_{\varepsilon h}^{n}|^2 + \frac{T(h)^2\theta\Delta t}{\omega\varepsilon}\varepsilon|\nabla\varphi_{\varepsilon h}^{n}|^2|\boldsymbol{v}_{\varepsilon h}^{n}|^2 + \omega\theta\Delta t|\nabla\mu_{\varepsilon h}^{n}|^2.
\end{aligned} \tag{3.31}$$

Remark 3.2.2. *Under the assumption that $\alpha \leq 1$ and $(1-\alpha)\eta\theta\Delta t \leq \frac{1}{4}h^2$, inequality* (3.31) *can be viewed as being of the form*

$$\frac{1}{2}|\boldsymbol{v}_{\varepsilon h}^{n+\theta}|^2 - \frac{1}{2}|\boldsymbol{v}_{\varepsilon h}^{n}|^2 + \{\textit{positive terms}\} \leq \{\textit{remainder terms}\} + \{\textit{force terms}\}. \tag{3.32}$$

The remainder terms are given by squared L^2 norms of computed solutions at $n\Delta t$ and will be shown later in full detail. The force terms are given by the squared L^2 norm of the body force. This perspective will be useful in the upcoming Section 3.2.3.

Step 1(b) Given $\varphi_{\varepsilon h}^{n}, \mu_{\varepsilon h}^{n}$ in H_h^1, $\boldsymbol{v}_{\varepsilon h}^{n}, \boldsymbol{v}_{\varepsilon h}^{n+\theta} \in V_h$ find $\varphi_{\varepsilon h}^{n+\theta}, \mu_{\varepsilon h}^{n+\theta} \in H_h^1$, such that

$\forall \psi_h, \zeta_h \in H_h^1$:

$$\Big(\frac{\varphi_{\varepsilon h}^{n+\theta} - \varphi_{\varepsilon h}^{n}}{\theta \Delta t}, \psi_h\Big) + \hat{b}(\boldsymbol{v}_{\varepsilon h}^{n+\theta}, \varphi_{\varepsilon h}^{n+\theta}, \psi_h) + \gamma(\nabla \mu_{\varepsilon h}^{n+\theta}, \nabla \psi_h) = -(1-\gamma)(\nabla \mu_{\varepsilon h}^{n}, \nabla \psi_h), \tag{3.33}$$

$$\varepsilon(\nabla \varphi_{\varepsilon h}^{n+\theta}, \nabla \zeta_h) + \frac{1}{\varepsilon}(F_\theta(\varphi_{\varepsilon h}^{n}, \varphi_{\varepsilon h}^{n+\theta}), \zeta_h) = (\mu_{\varepsilon h}^{n+\theta}, \zeta_h). \tag{3.34}$$

We denote the time discrete approximation of the Cahn-Hilliard potential derivative $F'(\varphi_{\varepsilon h})$ in each timestep by $F_\theta(\varphi_{\varepsilon h}^{n+k})$ or $F_{(\tilde{\theta}-\theta)}(\varphi_{\varepsilon h}^{n+k})$ for $k \in \{0, \theta, \tilde{\theta}, 1\}$ and subscripts θ or $(\tilde{\theta} - \theta)$ matching the size of the current time substep. We discuss the accuracy of these discretisations in Section 3.2.3, but for now one may assume that they either satisfy a dissipation inequality or approximate F' to a high enough degree to have a negligible error in calculation of the discrete system energy.

Test (3.33) with $\psi_h = \mu_{\varepsilon h}^{n+\theta}$ and (3.34) with $\zeta_h = \varphi_{\varepsilon h}^{n+\theta} - \varphi_{\varepsilon h}^{n}$, and perform a substitution for $(\varphi_{\varepsilon h}^{n+\theta} - \varphi_{\varepsilon h}^{n}, \mu_{\varepsilon h}^{n+\theta})$:

$$\begin{aligned}
&\varepsilon(\nabla \varphi_{\varepsilon h}^{n+\theta}, \nabla \varphi_{\varepsilon h}^{n+\theta} - \nabla \varphi_{\varepsilon h}^{n}) + \frac{1}{\varepsilon}(F_\theta(\varphi_{\varepsilon h}^{n}, \varphi_{\varepsilon h}^{n+\theta}), \varphi_{\varepsilon h}^{n+\theta} - \varphi_{\varepsilon h}^{n}) + \gamma\theta\Delta t|\nabla \mu_{\varepsilon h}^{n+\theta}|^2 \\
&= -(1-\gamma)\theta\Delta t(\nabla \mu_{\varepsilon h}^{n}, \nabla \mu_{\varepsilon h}^{n+\theta}) - \theta\Delta t\hat{b}(\boldsymbol{v}_{\varepsilon h}^{n+\theta}, \varphi_{\varepsilon h}^{n+\theta}, \mu_{\varepsilon h}^{n+\theta}).
\end{aligned} \tag{3.35}$$

Using Young's inequality and rewriting the inner products, we obtain:

$$\begin{aligned}
&\frac{\varepsilon}{2}(|\nabla \varphi_{\varepsilon h}^{n+\theta}|^2 - |\nabla \varphi_{\varepsilon h}^{n}|^2) + \frac{1}{\varepsilon}(F_\theta(\varphi_{\varepsilon h}^{n}, \varphi_{\varepsilon h}^{n+\theta}), \varphi_{\varepsilon h}^{n+\theta} - \varphi_{\varepsilon h}^{n}) + \frac{\varepsilon}{2}|\nabla \varphi_{\varepsilon h}^{n+\theta} - \nabla \varphi_{\varepsilon h}^{n}|^2 \\
&+ \frac{3\gamma - 1}{2}\theta\Delta t|\nabla \mu_{\varepsilon h}^{n+\theta}|^2 \\
&\leq \frac{1-\gamma}{2}\theta\Delta t|\nabla \mu_{\varepsilon h}^{n}|^2 - \theta\Delta t\hat{b}(\boldsymbol{v}_{\varepsilon h}^{n+\theta}, \varphi_{\varepsilon h}^{n+\theta}, \mu_{\varepsilon h}^{n+\theta}).
\end{aligned} \tag{3.36}$$

Apply (3.25) as in (3.30), but with a difference in $\varphi_{\varepsilon h}$. Then apply Young's inequality (assuming ω to be small),

$$\begin{aligned}
&\frac{\varepsilon}{2}(|\nabla \varphi_{\varepsilon h}^{n+\theta}|^2 - |\nabla \varphi_{\varepsilon h}^{n}|^2) + \frac{1}{\varepsilon}(F_\theta(\varphi_{\varepsilon h}^{n}, \varphi_{\varepsilon h}^{n+\theta}), \varphi_{\varepsilon h}^{n+\theta} - \varphi_{\varepsilon h}^{n}) + \frac{\varepsilon}{2}|\nabla \varphi_{\varepsilon h}^{n+\theta} - \nabla \varphi_{\varepsilon h}^{n}|^2 \\
&+ \frac{3\gamma - 1}{2}\theta\Delta t|\nabla \mu_{\varepsilon h}^{n+\theta}|^2 \\
&\leq T(h)\theta\Delta t|\boldsymbol{v}_{\varepsilon h}^{n+\theta}|(|\nabla \varphi_{\varepsilon h}^{n+\theta} - \nabla \varphi_{\varepsilon h}^{n}| + |\nabla \varphi_{\varepsilon h}^{n}|)|\nabla \mu_{\varepsilon h}^{n+\theta}| + \frac{1-\gamma}{2}\theta\Delta t|\nabla \mu_{\varepsilon h}^{n}|^2 \\
&\leq \frac{T(h)^2\theta\Delta t}{2\omega\varepsilon}|\boldsymbol{v}_{\varepsilon h}^{n+\theta}|^2\varepsilon|\nabla \varphi_{\varepsilon}^{n}|^2 + \frac{\omega}{2}\theta\Delta t|\nabla \mu_{\varepsilon h}^{n+\theta}|^2 + \frac{\varepsilon}{4}|\nabla \varphi_{\varepsilon h}^{n+\theta} - \nabla \varphi_{\varepsilon h}^{n}|^2 \\
&\quad + \frac{(T(h)\theta\Delta t)^2}{\varepsilon}|\boldsymbol{v}_{\varepsilon h}^{n+\theta}|^2|\nabla \mu_{\varepsilon h}^{n+\theta}|^2 + \frac{1-\gamma}{2}\theta\Delta t|\nabla \mu_{\varepsilon h}^{n}|^2.
\end{aligned} \tag{3.37}$$

Remark 3.2.3. *We may write* (3.37) *in a form akin to Remark 3.2.2. Assume* $\gamma \geq \frac{1}{3}$*, and we have a suitable discretisation* F_θ *- described in more detail in Section 3.2.3. Then, we may rewrite* (3.37) *as:*

$$\frac{\varepsilon}{2}(|\nabla\varphi_{\varepsilon h}^{n+\theta}|^2 - |\nabla\varphi_{\varepsilon h}^{n}|^2) + (F(\varphi_{\varepsilon h}^{n+\theta}) - F(\varphi_{\varepsilon h}^{n}), 1) + \{\textit{positive terms}\} \leq \{\textit{remainder}\}.$$

Once again this is important in the full energy inequality in Section 3.2.3 and the stability assumptions within.

We now summarise the inequalities obtained from Step 1, by adding (3.31) and (3.37) as follows:

(1) Stokes-Cahn-Hilliard Inequality

Under the assumption that $\alpha \leq 1$, $\frac{1+\omega}{3} \leq \gamma \leq 1+\omega$ and $(1-\alpha)\eta\theta\Delta t \leq \frac{1}{4}h^2$, and with suitable choice of discretisation $F_\theta(\varphi_{\varepsilon h}^n, \varphi_{\varepsilon h}^{n+\theta})$ we have shown:

$$\begin{aligned}
&\frac{1}{2}(|\boldsymbol{v}_{\varepsilon h}^{n+\theta}|^2 - |\boldsymbol{v}_{\varepsilon h}^{n}|^2) + \Big(\frac{1}{8} - \frac{1-\alpha}{2h^2}\eta\theta\Delta t\Big)|\boldsymbol{v}_{\varepsilon h}^{n+\theta} - \boldsymbol{v}_{\varepsilon h}^{n}|^2 + \frac{1+2\alpha}{2}\eta\theta\Delta t|\nabla\boldsymbol{v}_{\varepsilon h}^{n+\theta}|^2 \\
&+ \frac{1-\alpha}{2}\eta\theta\Delta t|\nabla\boldsymbol{v}_{\varepsilon h}^{n}|^2 \\
&+ \frac{\varepsilon}{2}(|\nabla\varphi_{\varepsilon h}^{n+\theta}|^2 - |\nabla\varphi_{\varepsilon h}^{n}|^2) + \frac{1}{\varepsilon}(F_\theta(\varphi_{\varepsilon h}^{n}, \varphi_{\varepsilon h}^{n+\theta}), \varphi_{\varepsilon h}^{n+\theta} - \varphi_{\varepsilon h}^{n}) + \frac{\varepsilon}{4}|\nabla\varphi_{\varepsilon h}^{n+\theta} - \nabla\varphi_{\varepsilon h}^{n}|^2 \\
&+ \frac{3\gamma - 1 - \omega}{2}\theta\Delta t|\nabla\mu_{\varepsilon h}^{n+\theta}|^2 \\
&\leq\ 2(S(h)\theta\Delta t)^2|\boldsymbol{v}_{\varepsilon h}^{n}|^2|\nabla\boldsymbol{v}_{\varepsilon h}^{n}|^2 + \frac{1-\gamma+\omega}{2}\theta\Delta t|\nabla\mu_{\varepsilon h}^{n}|^2 \\
&\quad + \frac{2(T(h)\theta\Delta t)^2}{\varepsilon}\varepsilon|\nabla\varphi_{\varepsilon h}^{n}|^2|\nabla\mu_{\varepsilon h}^{n}|^2 + \frac{T(h)^2\theta\Delta t}{\omega\varepsilon}\varepsilon|\nabla\varphi_{\varepsilon h}^{n}|^2|\boldsymbol{v}_{\varepsilon h}^{n}|^2 \\
&+ \frac{T(h)^2\theta\Delta t}{2\omega\varepsilon}|\boldsymbol{v}_{\varepsilon h}^{n+\theta}|^2\varepsilon|\nabla\varphi_{\varepsilon}^{n}|^2 + \frac{(T(h)\theta\Delta t)^2}{\varepsilon}|\boldsymbol{v}_{\varepsilon h}^{n+\theta}|^2|\nabla\mu_{\varepsilon h}^{n+\theta}|^2 + \frac{\theta\Delta t}{\eta}|\boldsymbol{f}_h^{n+\theta}|^2. \quad (3.38)
\end{aligned}$$

We now proceed to the second substep in the time discretisation.

Step 2(a)

Given $\varphi_{\varepsilon h}^{n+\theta}, \mu_{\varepsilon h}^{n+\theta} \in H_h^1$, $\boldsymbol{v}_{\varepsilon h}^{n+\theta} \in V_h$ find $\varphi_{\varepsilon h}^{n+\tilde{\theta}}, \mu_{\varepsilon h}^{n+\tilde{\theta}} \in H_h^1$, such that $\forall \psi_h, \zeta_h \in H_h^1$:

$$\Big(\frac{\varphi_{\varepsilon h}^{n+\tilde{\theta}} - \varphi_{\varepsilon h}^{n+\theta}}{(\tilde{\theta}-\theta)\Delta t}, \psi_h\Big) + (1-\gamma)(\nabla\mu_{\varepsilon h}^{n+\tilde{\theta}}, \nabla\psi_h) = -\gamma(\nabla\mu_{\varepsilon h}^{n+\theta}, \nabla\psi_h) - \hat{b}(\boldsymbol{v}_{\varepsilon h}^{n+\theta}, \varphi_{\varepsilon h}^{n+\theta}, \psi_h), \quad (3.39)$$

$$\varepsilon(\nabla\varphi_{\varepsilon h}^{n+\tilde{\theta}}, \nabla\zeta_h) + \frac{1}{\varepsilon}(F_{(\tilde{\theta}-\theta)}(\varphi_{\varepsilon h}^{n+\theta}, \varphi_{\varepsilon h}^{n+\tilde{\theta}}), \zeta_h) = (\mu_{\varepsilon h}^{n+\tilde{\theta}}, \zeta_h). \quad (3.40)$$

As with obtaining (3.35) from (3.33)-(3.34), we test (3.39) with $\psi_h = \mu_{\varepsilon h}^{n+\tilde{\theta}}$ and test (3.40) with $\zeta_h = \varphi_{\varepsilon h}^{n+\tilde{\theta}} - \varphi_{\varepsilon h}^{n+\theta}$. Perform a substitution for $(\varphi_{\varepsilon h}^{n+\tilde{\theta}} - \varphi_{\varepsilon h}^{n+\theta}, \mu_{\varepsilon h}^{n+\tilde{\theta}})$:

$$\begin{aligned}
&\varepsilon(\nabla\varphi_{\varepsilon h}^{n+\tilde{\theta}}, \nabla\varphi_{\varepsilon h}^{n+\tilde{\theta}} - \nabla\varphi_{\varepsilon h}^{n+\theta}) + \frac{1}{\varepsilon}(F_{(\tilde{\theta}-\theta)}(\varphi_{\varepsilon h}^{n+\theta}, \varphi_{\varepsilon h}^{n+\tilde{\theta}}), \varphi_{\varepsilon h}^{n+\tilde{\theta}} - \varphi_{\varepsilon h}^{n+\theta}) \\
&+ (1-\gamma)(\tilde{\theta}-\theta)\Delta t|\nabla\mu_{\varepsilon h}^{n+\tilde{\theta}}|^2 \\
&= -\gamma(\tilde{\theta}-\theta)\Delta t(\nabla\mu_{\varepsilon h}^{n+\theta}, \nabla\mu_{\varepsilon h}^{n+\tilde{\theta}}) - (\tilde{\theta}-\theta)\Delta t\hat{b}(\boldsymbol{v}_{\varepsilon h}^{n+\theta}, \varphi_{\varepsilon h}^{n+\theta}, \mu_{\varepsilon h}^{n+\tilde{\theta}}),
\end{aligned} \tag{3.41}$$

then from Young's inequality and writing inner products as squared norms,

$$\begin{aligned}
&\frac{\varepsilon}{2}(|\nabla\varphi_{\varepsilon h}^{n+\tilde{\theta}}|^2 - |\nabla\varphi_{\varepsilon h}^{n+\theta}|^2) + \frac{1}{\varepsilon}(F_{(\tilde{\theta}-\theta)}(\varphi_{\varepsilon h}^{n+\theta}, \varphi_{\varepsilon h}^{n+\tilde{\theta}}), \varphi_{\varepsilon h}^{n+\tilde{\theta}} - \varphi_{\varepsilon h}^{n+\theta}) \\
&+ \frac{\varepsilon}{2}|\nabla\varphi_{\varepsilon h}^{n+\tilde{\theta}} - \nabla\varphi_{\varepsilon h}^{n+\theta}|^2 + \frac{2-3\gamma}{2}(\tilde{\theta}-\theta)\Delta t|\nabla\mu_{\varepsilon h}^{n+\tilde{\theta}}|^2 \\
&\leq \frac{\gamma}{2}(\tilde{\theta}-\theta)\Delta t|\nabla\mu_{\varepsilon h}^{n+\theta}|^2 - (\tilde{\theta}-\theta)\Delta t\hat{b}(\boldsymbol{v}_{\varepsilon h}^{n+\theta}, \varphi_{\varepsilon h}^{n+\theta}, \mu_{\varepsilon h}^{n+\tilde{\theta}}).
\end{aligned} \tag{3.42}$$

We bound $\hat{b}(\cdot,\cdot,\cdot)$ using (3.25) and Young's inequality for $\omega > 0$:

$$\begin{aligned}
&\frac{\varepsilon}{2}(|\nabla\varphi_{\varepsilon h}^{n+\tilde{\theta}}|^2 - |\nabla\varphi_{\varepsilon h}^{n+\theta}|^2) + \frac{1}{\varepsilon}(F_{(\tilde{\theta}-\theta)}(\varphi_{\varepsilon h}^{n+\theta}, \varphi_{\varepsilon h}^{n+\tilde{\theta}}), \varphi_{\varepsilon h}^{n+\tilde{\theta}} - \varphi_{\varepsilon h}^{n+\theta}) \\
&+ \frac{\varepsilon}{2}|\nabla\varphi_{\varepsilon h}^{n+\tilde{\theta}} - \nabla\varphi_{\varepsilon h}^{n+\theta}|^2 + \frac{(2-3\gamma)}{2}(\tilde{\theta}-\theta)\Delta t|\nabla\mu_{\varepsilon h}^{n+\tilde{\theta}}|^2 \\
&\leq T(h)(\tilde{\theta}-\theta)\Delta t|\boldsymbol{v}_{\varepsilon h}^{n+\theta}||\nabla\varphi_{\varepsilon h}^{n+\theta}||\nabla\mu_{\varepsilon h}^{n+\tilde{\theta}}| + \frac{\gamma}{2}(\tilde{\theta}-\theta)\Delta t|\nabla\mu_{\varepsilon h}^{n+\theta}|^2 \\
&\leq \frac{T(h)^2(\tilde{\theta}-\theta)\Delta t}{2\omega}|\boldsymbol{v}_{\varepsilon h}^{n+\theta}|^2|\nabla\varphi_{\varepsilon h}^{n+\theta}|^2 + \frac{\omega}{2}(\tilde{\theta}-\theta)\Delta t|\nabla\mu_{\varepsilon h}^{n+\tilde{\theta}}|^2 \\
&\quad + \frac{\gamma}{2}(\tilde{\theta}-\theta)\Delta t|\nabla\mu_{\varepsilon h}^{n+\theta}|^2.
\end{aligned} \tag{3.43}$$

We obtain the inequality

$$\begin{aligned}
&\frac{\varepsilon}{2}(|\nabla\varphi_{\varepsilon h}^{n+\tilde{\theta}}|^2 - |\nabla\varphi_{\varepsilon h}^{n+\theta}|^2) + \frac{1}{\varepsilon}(F_{(\tilde{\theta}-\theta)}(\varphi_{\varepsilon h}^{n+\theta}, \varphi_{\varepsilon h}^{n+\tilde{\theta}}), \varphi_{\varepsilon h}^{n+\tilde{\theta}} - \varphi_{\varepsilon h}^{n+\theta}) \\
&+ \frac{\varepsilon}{2}|\nabla\varphi_{\varepsilon h}^{n+\tilde{\theta}} - \nabla\varphi_{\varepsilon h}^{n+\theta}|^2 + \frac{(2-3\gamma-\omega)}{2}(\tilde{\theta}-\theta)\Delta t|\nabla\mu_{\varepsilon h}^{n+\tilde{\theta}}|^2 \\
&\leq \frac{T(h)^2(\tilde{\theta}-\theta)\Delta t}{2\omega}|\boldsymbol{v}_{\varepsilon h}^{n+\theta}|^2|\nabla\varphi_{\varepsilon h}^{n+\theta}|^2 + \frac{\gamma}{2}(\tilde{\theta}-\theta)\Delta t|\nabla\mu_{\varepsilon h}^{n+\theta}|^2.
\end{aligned} \tag{3.44}$$

We have now arrived at the stability inequality for Step 2(a).

Remark 3.2.4. *For positivity of the left hand side of* (3.44)*, we require that* $\gamma \leq \frac{2-\omega}{3}$.

Step 2(b)

Given $\varphi_{\varepsilon h}^{n+\tilde{\theta}}, \mu_{\varepsilon h}^{n+\tilde{\theta}}$ in H_h^1, $\boldsymbol{v}_{\varepsilon h}^{n+\theta} \in V_h$ find $\boldsymbol{v}_{\varepsilon h}^{n+\tilde{\theta}} \in X_h$, such that $\forall \mathbf{w_h} \in X_h$:

$$\begin{aligned}
&\Big(\frac{\boldsymbol{v}_{\varepsilon h}^{n+\tilde{\theta}} - \boldsymbol{v}_{\varepsilon h}^{n+\theta}}{(\tilde{\theta}-\theta)\Delta t}, \mathbf{w}_h\Big) + (1-\alpha)\eta(\nabla \boldsymbol{v}_{\varepsilon h}^{n+\tilde{\theta}}, \nabla \mathbf{w}_h) + b_h(\boldsymbol{v}_{\varepsilon h}^{n+\tilde{\theta}}, \boldsymbol{v}_{\varepsilon h}^{n+\tilde{\theta}}, \mathbf{w}_h) \\
&- \hat{b}(\mathbf{w}_h, \varphi_{\varepsilon h}^{n+\tilde{\theta}}, \mu_{\varepsilon h}^{n+\tilde{\theta}}) \\
&= -\alpha\eta(\nabla \boldsymbol{v}_{\varepsilon h}^{n+\theta}, \nabla \mathbf{w}_h) + (p_{\varepsilon h}^{n+\theta}, \nabla \cdot \mathbf{w}_h) + (\boldsymbol{f}^{n+\theta}, \mathbf{w}_h),
\end{aligned} \tag{3.45}$$

where we take the discretised fluid pressure $p_{\varepsilon h}^{n+\theta} \in \Pi_h$ defined by the following weak formulation:

$$\begin{aligned}
(p_{\varepsilon h}^{n+\theta}, \nabla \cdot \mathbf{w}_h) = &\Big(\frac{\boldsymbol{v}_{\varepsilon h}^{n+\theta} - \boldsymbol{v}_{\varepsilon h}^{n}}{\theta \Delta t}, \mathbf{w}_h\Big) + \alpha\eta(\nabla \boldsymbol{v}_{\varepsilon h}^{n+\theta}, \nabla \mathbf{w}_h) + (1-\alpha)\eta(\nabla \boldsymbol{v}_{\varepsilon h}^{n}, \nabla \mathbf{w}_h) \\
&+ b_h(\boldsymbol{v}_{\varepsilon h}^{n}, \boldsymbol{v}_{\varepsilon h}^{n}, \mathbf{w}_h) - \hat{b}(\mathbf{w}_h, \varphi_{\varepsilon h}^{n}, \mu_{\varepsilon h}^{n}) - (\boldsymbol{f}^{n+\theta}, \mathbf{w}_h).
\end{aligned} \tag{3.46}$$

Test (3.45) with $\mathbf{w}_h = \boldsymbol{v}_{\varepsilon h}^{n+\tilde{\theta}} \in X_h$

$$\begin{aligned}
&\Big(\frac{\boldsymbol{v}_{\varepsilon h}^{n+\tilde{\theta}} - \boldsymbol{v}_{\varepsilon h}^{n+\theta}}{(\tilde{\theta}-\theta)\Delta t}, \boldsymbol{v}_{\varepsilon h}^{n+\tilde{\theta}}\Big) + (1-\alpha)\eta|\nabla \boldsymbol{v}_{\varepsilon h}^{n+\tilde{\theta}}|^2 + b_h(\boldsymbol{v}_{\varepsilon h}^{n+\tilde{\theta}}, \boldsymbol{v}_{\varepsilon h}^{n+\tilde{\theta}}, \boldsymbol{v}_{\varepsilon h}^{n+\tilde{\theta}}) \\
&- \hat{b}(\boldsymbol{v}_{\varepsilon h}^{n+\tilde{\theta}}, \varphi_{\varepsilon h}^{n+\tilde{\theta}}, \mu_{\varepsilon h}^{n+\tilde{\theta}}) \\
&= -\alpha\eta(\nabla \boldsymbol{v}_{\varepsilon h}^{n+\theta}, \nabla \boldsymbol{v}_{\varepsilon h}^{n+\tilde{\theta}}) + (p_{\varepsilon h}^{n+\theta}, \nabla \cdot \boldsymbol{v}_{\varepsilon h}^{n+\tilde{\theta}}) + (\boldsymbol{f}^{n+\theta}, \boldsymbol{v}_{\varepsilon h}^{n+\tilde{\theta}}),
\end{aligned} \tag{3.47}$$

and by definition $b_h(\boldsymbol{v}_{\varepsilon h}^{n+\tilde{\theta}}, \boldsymbol{v}_{\varepsilon h}^{n+\tilde{\theta}}, \boldsymbol{v}_{\varepsilon h}^{n+\tilde{\theta}}) = 0$. Rewrite inner products as squared norms, then

$$\begin{aligned}
&\frac{1}{2}|\boldsymbol{v}_{\varepsilon h}^{n+\tilde{\theta}}|^2 + \frac{1}{2}|\boldsymbol{v}_{\varepsilon h}^{n+\tilde{\theta}} - \boldsymbol{v}_{\varepsilon h}^{n+\theta}|^2 + \frac{2-\alpha}{2}\eta(\tilde{\theta}-\theta)\Delta t|\nabla \boldsymbol{v}_{\varepsilon h}^{n+\tilde{\theta}}|^2 + \frac{\alpha}{2}\eta(\tilde{\theta}-\theta)\Delta t|\nabla \boldsymbol{v}_{\varepsilon h}^{n+\theta}|^2 \\
&= \frac{1}{2}|\boldsymbol{v}_{\varepsilon h}^{n+\theta}|^2 + \frac{\alpha}{2}\eta(\tilde{\theta}-\theta)\Delta t|\nabla \boldsymbol{v}_{\varepsilon h}^{n+\tilde{\theta}} - \nabla \boldsymbol{v}_{\varepsilon h}^{n+\theta}|^2 + (\tilde{\theta}-\theta)\Delta t(p_{\varepsilon h}^{n+\theta}, \nabla \cdot \boldsymbol{v}_{\varepsilon h}^{n+\tilde{\theta}}) \\
&\quad + (\tilde{\theta}-\theta)\Delta t\hat{b}(\boldsymbol{v}_{\varepsilon h}^{n+\tilde{\theta}}, \varphi_{\varepsilon h}^{n+\tilde{\theta}}, \mu_{\varepsilon h}^{n+\tilde{\theta}}) + (\tilde{\theta}-\theta)\Delta t(\boldsymbol{f}^{n+\theta}, \boldsymbol{v}_{\varepsilon h}^{n+\tilde{\theta}}).
\end{aligned} \tag{3.48}$$

Due to incompressibility of the velocity $\boldsymbol{v}_{\varepsilon h}^{n+\theta}$,

$$(p_{\varepsilon h}^{n+\theta}, \nabla \cdot \boldsymbol{v}_{\varepsilon h}^{n+\tilde{\theta}}) = (p_{\varepsilon h}^{n+\theta}, \nabla \cdot (\boldsymbol{v}_{\varepsilon h}^{n+\tilde{\theta}} - \boldsymbol{v}_{\varepsilon h}^{n+\theta})).$$

We then evaluate the pressure term from (3.48) using the definition (3.46):

$$
\begin{aligned}
&(p_{\varepsilon h}^{n+\theta}, \nabla \cdot \boldsymbol{v}_{\varepsilon h}^{n+\tilde{\theta}}) \\
&= \Big(\frac{\boldsymbol{v}_{\varepsilon h}^{n+\theta} - \boldsymbol{v}_{\varepsilon h}^{n}}{\theta \Delta t}, \boldsymbol{v}_{\varepsilon h}^{n+\tilde{\theta}} - \boldsymbol{v}_{\varepsilon h}^{n+\theta}\Big) + \alpha\eta(\nabla \boldsymbol{v}_{\varepsilon h}^{n+\theta}, \nabla(\boldsymbol{v}_{\varepsilon h}^{n+\tilde{\theta}} - \boldsymbol{v}_{\varepsilon h}^{n+\theta})) \\
&\quad + (1-\alpha)\eta(\nabla \boldsymbol{v}_{\varepsilon h}^{n}, \nabla(\boldsymbol{v}_{\varepsilon h}^{n+\tilde{\theta}} - \boldsymbol{v}_{\varepsilon h}^{n+\theta})) + b_h(\boldsymbol{v}_{\varepsilon h}^{n}, \boldsymbol{v}_{\varepsilon h}^{n}, \boldsymbol{v}_{\varepsilon h}^{n+\tilde{\theta}} - \boldsymbol{v}_{\varepsilon h}^{n+\theta}) \\
&\quad - \hat{b}(\boldsymbol{v}_{\varepsilon h}^{n+\tilde{\theta}} - \boldsymbol{v}_{\varepsilon h}^{n+\theta}, \varphi_{\varepsilon h}^{n}, \mu_{\varepsilon h}^{n}) - (\boldsymbol{f}^{n+\theta}, \boldsymbol{v}_{\varepsilon h}^{n+\tilde{\theta}} - \boldsymbol{v}_{\varepsilon h}^{n+\theta}).
\end{aligned}
$$

Rewriting products and using Cauchy Schwarz

$$
\begin{aligned}
&(p_{\varepsilon h}^{n+\theta}, \nabla \cdot \boldsymbol{v}_{\varepsilon h}^{n+\tilde{\theta}}) \\
&\leq \frac{1}{\theta \Delta t}|\boldsymbol{v}_{\varepsilon h}^{n+\theta} - \boldsymbol{v}_{\varepsilon h}^{n}||\boldsymbol{v}_{\varepsilon h}^{n+\tilde{\theta}} - \boldsymbol{v}_{\varepsilon h}^{n+\theta}| \\
&\quad - \frac{\alpha\eta}{2}(|\nabla \boldsymbol{v}_{\varepsilon h}^{n+\theta}|^2 + |\nabla \boldsymbol{v}_{\varepsilon h}^{n+\tilde{\theta}} - \nabla \boldsymbol{v}_{\varepsilon h}^{n+\theta}|^2 - |\nabla \boldsymbol{v}_{\varepsilon h}^{n+\tilde{\theta}}|^2) \\
&+ (1-\alpha)\eta|\nabla \boldsymbol{v}_{\varepsilon h}^{n}||\nabla \boldsymbol{v}_{\varepsilon h}^{n+\tilde{\theta}} - \nabla \boldsymbol{v}_{\varepsilon h}^{n+\theta}| - (\boldsymbol{f}^{n+\theta}, \boldsymbol{v}_{\varepsilon h}^{n+\tilde{\theta}} - \boldsymbol{v}_{\varepsilon h}^{n+\theta}) \\
&\quad + b_h(\boldsymbol{v}_{\varepsilon h}^{n}, \boldsymbol{v}_{\varepsilon h}^{n}, \boldsymbol{v}_{\varepsilon h}^{n+\tilde{\theta}} - \boldsymbol{v}_{\varepsilon h}^{n+\theta}) - \hat{b}(\boldsymbol{v}_{\varepsilon h}^{n+\tilde{\theta}} - \boldsymbol{v}_{\varepsilon h}^{n+\theta}, \varphi_{\varepsilon h}^{n}, \mu_{\varepsilon h}^{n}).
\end{aligned} \tag{3.49}
$$

We substitute (3.49) into (3.48):

$$
\begin{aligned}
&\frac{1}{2}|\boldsymbol{v}_{\varepsilon h}^{n+\tilde{\theta}}|^2 + \frac{1}{2}|\boldsymbol{v}_{\varepsilon h}^{n+\tilde{\theta}} - \boldsymbol{v}_{\varepsilon h}^{n+\theta}|^2 + (1-\alpha)\eta(\tilde{\theta}-\theta)\Delta t|\nabla \boldsymbol{v}_{\varepsilon h}^{n+\tilde{\theta}}|^2 + \alpha\eta(\tilde{\theta}-\theta)\Delta t|\nabla \boldsymbol{v}_{\varepsilon h}^{n+\theta}|^2 \\
&\leq \frac{1}{2}|\boldsymbol{v}_{\varepsilon h}^{n+\theta}|^2 + \frac{\tilde{\theta}-\theta}{\theta}|\boldsymbol{v}_{\varepsilon h}^{n+\theta} - \boldsymbol{v}_{\varepsilon h}^{n}||\boldsymbol{v}_{\varepsilon h}^{n+\tilde{\theta}} - \boldsymbol{v}_{\varepsilon h}^{n+\theta}| + (\tilde{\theta}-\theta)\Delta t b_h(\boldsymbol{v}_{\varepsilon h}^{n}, \boldsymbol{v}_{\varepsilon h}^{n}, \boldsymbol{v}_{\varepsilon h}^{n+\tilde{\theta}} - \boldsymbol{v}_{\varepsilon h}^{n+\theta}) \\
&\quad + (1-\alpha)\eta(\tilde{\theta}-\theta)\Delta t|\nabla \boldsymbol{v}_{\varepsilon h}^{n}||\nabla \boldsymbol{v}_{\varepsilon h}^{n+\tilde{\theta}} - \nabla \boldsymbol{v}_{\varepsilon h}^{n+\theta}| - (\tilde{\theta}-\theta)\Delta t\hat{b}(\boldsymbol{v}_{\varepsilon h}^{n+\tilde{\theta}} - \boldsymbol{v}_{\varepsilon h}^{n+\theta}, \varphi_{\varepsilon h}^{n}, \mu_{\varepsilon h}^{n}) \\
&\quad + (\tilde{\theta}-\theta)\Delta t\hat{b}(\boldsymbol{v}_{\varepsilon h}^{n+\tilde{\theta}}, \varphi_{\varepsilon h}^{n+\tilde{\theta}}, \mu_{\varepsilon h}^{n+\tilde{\theta}}) + (\tilde{\theta}-\theta)\Delta t(\boldsymbol{f}^{n+\theta}, \boldsymbol{v}_{\varepsilon h}^{n+\theta}).
\end{aligned} \tag{3.50}
$$

Using weighted Young's inequality with $\delta > 0$ with (3.20):

$$
\begin{aligned}
&\frac{1}{2}|\boldsymbol{v}_{\varepsilon h}^{n+\tilde{\theta}}|^2 + \frac{1}{2}(1-2\delta)|\boldsymbol{v}_{\varepsilon h}^{n+\tilde{\theta}} - \boldsymbol{v}_{\varepsilon h}^{n+\theta}|^2 + (1-\alpha)\eta(\tilde{\theta}-\theta)\Delta t|\nabla \boldsymbol{v}_{\varepsilon h}^{n+\tilde{\theta}}|^2 \\
&+ \alpha\eta(\tilde{\theta}-\theta)\Delta t|\nabla \boldsymbol{v}_{\varepsilon h}^{n+\theta}|^2 \\
&\leq \frac{1}{2}|\boldsymbol{v}_{\varepsilon h}^{n+\theta}|^2 + \frac{(\tilde{\theta}-\theta)^2}{2\delta\theta^2}|\boldsymbol{v}_{\varepsilon h}^{n+\theta} - \boldsymbol{v}_{\varepsilon h}^{n}|^2 + (\tilde{\theta}-\theta)\Delta t b_h(\boldsymbol{v}_{\varepsilon h}^{n}, \boldsymbol{v}_{\varepsilon h}^{n}, \boldsymbol{v}_{\varepsilon h}^{n+\tilde{\theta}} - \boldsymbol{v}_{\varepsilon h}^{n+\theta}) \\
&\quad + \frac{((1-\alpha)\eta(\tilde{\theta}-\theta)\Delta t)^2}{2\delta h^2}|\nabla \boldsymbol{v}_{\varepsilon h}^{n}|^2 - (\tilde{\theta}-\theta)\Delta t\hat{b}(\boldsymbol{v}_{\varepsilon h}^{n+\tilde{\theta}} - \boldsymbol{v}_{\varepsilon h}^{n+\theta}, \varphi_{\varepsilon h}^{n}, \mu_{\varepsilon h}^{n}) \\
&\quad + (\tilde{\theta}-\theta)\Delta t\hat{b}(\boldsymbol{v}_{\varepsilon h}^{n+\tilde{\theta}}, \varphi_{\varepsilon h}^{n+\tilde{\theta}}, \mu_{\varepsilon h}^{n+\tilde{\theta}}) + (\tilde{\theta}-\theta)\Delta t(\frac{1}{2\alpha\eta}|\boldsymbol{f}_h^{n+\theta}|^2 + \frac{\alpha\eta}{2}|\nabla \boldsymbol{v}|^2).
\end{aligned} \tag{3.51}
$$

Apply (3.23) to the convection term, then use Young's inequality (weighted by $\delta > 0$):

$$\begin{aligned}
&\frac{1}{2}|\boldsymbol{v}_{\varepsilon h}^{n+\tilde{\theta}}|^2 + \frac{1}{2}(1-3\delta)|\boldsymbol{v}_{\varepsilon h}^{n+\tilde{\theta}} - \boldsymbol{v}_{\varepsilon h}^{n+\theta}|^2 + (1-\alpha)\eta(\tilde{\theta}-\theta)\Delta t|\nabla \boldsymbol{v}_{\varepsilon h}^{n+\tilde{\theta}}|^2 \\
&+ \frac{\alpha}{2}\eta(\tilde{\theta}-\theta)\Delta t|\nabla \boldsymbol{v}_{\varepsilon h}^{n+\theta}|^2 \\
&\leq \frac{1}{2}|\boldsymbol{v}_{\varepsilon h}^{n+\theta}|^2 + \frac{(\tilde{\theta}-\theta)^2}{2\delta\theta^2}|\boldsymbol{v}_{\varepsilon h}^{n+\theta} - \boldsymbol{v}_{\varepsilon h}^{n}|^2 + \frac{((1-\alpha)\eta(\tilde{\theta}-\theta)\Delta t)^2}{2\delta h^2}|\nabla \boldsymbol{v}_{\varepsilon h}^{n}|^2 \\
&\quad + \frac{(S(h)(\tilde{\theta}-\theta)\Delta t)^2}{2\delta}|\boldsymbol{v}_{\varepsilon h}^{n}|^2|\nabla \boldsymbol{v}_{\varepsilon h}^{n}|^2 - (\tilde{\theta}-\theta)\Delta t\hat{b}(\boldsymbol{v}_{\varepsilon h}^{n+\tilde{\theta}} - \boldsymbol{v}_{\varepsilon h}^{n+\theta}, \varphi_{\varepsilon h}^{n}, \mu_{\varepsilon h}^{n}) \\
&\quad + (\tilde{\theta}-\theta)\Delta t\hat{b}(\boldsymbol{v}_{\varepsilon h}^{n+\tilde{\theta}}, \varphi_{\varepsilon h}^{n+\tilde{\theta}}, \mu_{\varepsilon h}^{n+\tilde{\theta}}) + \frac{(\tilde{\theta}-\theta)\Delta t}{2\alpha\eta}|\boldsymbol{f}_h^{n+\theta}|^2. \qquad (3.52)
\end{aligned}$$

We now bound the velocity difference $|\boldsymbol{v}_{\varepsilon h}^{n+\theta} - \boldsymbol{v}_{\varepsilon h}^{n}|^2$ by first observing that by incompressibility:

$$(p_{\varepsilon h}^{n+\theta}, \nabla \cdot (\boldsymbol{v}_{\varepsilon h}^{n+\theta} - \boldsymbol{v}_{\varepsilon h}^{n})) = 0.$$

Then, using (3.46), we can see that:

$$\begin{aligned}
&|\boldsymbol{v}_{\varepsilon h}^{n+\theta} - \boldsymbol{v}_{\varepsilon h}^{n}|^2 + \alpha\eta\theta\Delta t(\nabla \boldsymbol{v}_{\varepsilon h}^{n+\theta}, \nabla \boldsymbol{v}_{\varepsilon h}^{n+\theta} - \nabla \boldsymbol{v}_{\varepsilon h}^{n}) \\
&+ (1-\alpha)\eta\theta\Delta t(\nabla \boldsymbol{v}_{\varepsilon h}^{n}, \nabla \boldsymbol{v}_{\varepsilon h}^{n+\theta} - \nabla \boldsymbol{v}_{\varepsilon h}^{n}) \\
&= -\theta\Delta t b_h(\boldsymbol{v}_{\varepsilon h}^{n}, \boldsymbol{v}_{\varepsilon h}^{n}, \boldsymbol{v}_{\varepsilon h}^{n+\theta} - \boldsymbol{v}_{\varepsilon h}^{n}) + \theta\Delta t\hat{b}(\boldsymbol{v}_{\varepsilon h}^{n+\theta} - \boldsymbol{v}_{\varepsilon h}^{n}, \varphi_{\varepsilon h}^{n}, \mu_{\varepsilon h}^{n}) \\
&\quad + \theta\Delta t(\boldsymbol{f}^{n+\theta}, \boldsymbol{v}_{\varepsilon h}^{n+\theta} - \boldsymbol{v}_{\varepsilon h}^{n}),
\end{aligned}$$

and rewriting both inner products, we obtain an inequality

$$\begin{aligned}
&|\boldsymbol{v}_{\varepsilon h}^{n+\theta} - \boldsymbol{v}_{\varepsilon h}^{n}|^2 + (2\alpha-1)\eta\theta\Delta t|\nabla \boldsymbol{v}_{\varepsilon h}^{n+\theta} - \nabla \boldsymbol{v}_{\varepsilon h}^{n}|^2 + \eta\theta\Delta t|\nabla \boldsymbol{v}_{\varepsilon h}^{n+\theta}|^2 \\
&\leq \eta\theta\Delta t|\nabla \boldsymbol{v}_{\varepsilon h}^{n}|^2 + (S(h)\theta\Delta t)^2|\boldsymbol{v}_{\varepsilon h}^{n}|^2|\nabla \boldsymbol{v}_{\varepsilon h}^{n}|^2 + 2\theta\Delta t\hat{b}(\boldsymbol{v}_{\varepsilon h}^{n+\theta} - \boldsymbol{v}_{\varepsilon h}^{n}, \varphi_{\varepsilon h}^{n}, \mu_{\varepsilon h}^{n}) \\
&\quad + \frac{\theta\Delta t}{\eta}|\boldsymbol{f}^{n+\theta}|^2. \qquad (3.53)
\end{aligned}$$

Substitute (3.53) into (3.52),

$$
\begin{aligned}
&\frac{1}{2}|\boldsymbol{v}_{\varepsilon h}^{n+\tilde{\theta}}|^2+\frac{1}{2}(1-3\delta)|\boldsymbol{v}_{\varepsilon h}^{n+\tilde{\theta}}-\boldsymbol{v}_{\varepsilon h}^{n+\theta}|^2+(1-\alpha)\eta(\tilde{\theta}-\theta)\Delta t|\nabla\boldsymbol{v}_{\varepsilon h}^{n+\tilde{\theta}}|^2\\
&+\Big(\frac{\alpha}{2}(\tilde{\theta}-\theta)+\frac{(\tilde{\theta}-\theta)^2}{2\delta\theta^2}\Big)\Delta t|\nabla\boldsymbol{v}_{\varepsilon h}^{n+\theta}|^2+\frac{(2\alpha-1)(\tilde{\theta}-\theta)^2}{2\delta\theta^2}\eta\theta\Delta t|\nabla\boldsymbol{v}_{\varepsilon h}^{n+\theta}-\nabla\boldsymbol{v}_{\varepsilon h}^{n}|^2\\
&\le\frac{1}{2}|\boldsymbol{v}_{\varepsilon h}^{n+\theta}|^2+\frac{(\tilde{\theta}-\theta)^2}{2\delta\theta^2}\eta\theta\Delta t|\nabla\boldsymbol{v}_{\varepsilon h}^{n}|^2+2\frac{(S(h)(\tilde{\theta}-\theta)\Delta t)^2}{2\delta}|\boldsymbol{v}_{\varepsilon h}^{n}|^2|\nabla\boldsymbol{v}_{\varepsilon h}^{n}|^2\\
&\quad+\frac{((1-\alpha)\eta(\tilde{\theta}-\theta)\Delta t)^2}{2\delta h^2}|\nabla\boldsymbol{v}_{\varepsilon h}^{n}|^2+\Big(\frac{(\tilde{\theta}-\theta)}{\delta\theta}+\frac{1}{\alpha}\Big)\frac{(\tilde{\theta}-\theta)\Delta t}{2\eta}|\boldsymbol{f}_h^{n+\theta}|^2\\
&\quad+\frac{(\tilde{\theta}-\theta)^2}{\delta\theta}\Delta t\hat{b}(\boldsymbol{v}_{\varepsilon h}^{n+\theta}-\boldsymbol{v}_{\varepsilon h}^{n},\varphi_{\varepsilon h}^{n},\mu_{\varepsilon h}^{n})-(\tilde{\theta}-\theta)\Delta t\hat{b}(\boldsymbol{v}_{\varepsilon h}^{n+\tilde{\theta}}-\boldsymbol{v}_{\varepsilon h}^{n+\theta},\varphi_{\varepsilon h}^{n},\mu_{\varepsilon h}^{n})\\
&\quad+(\tilde{\theta}-\theta)\Delta t\hat{b}(\boldsymbol{v}_{\varepsilon h}^{n+\tilde{\theta}},\varphi_{\varepsilon h}^{n+\tilde{\theta}},\mu_{\varepsilon h}^{n+\tilde{\theta}}).
\end{aligned}
\tag{3.54}
$$

We use (3.25) and Young's inequality for $\omega>0$, to bound all coupling terms:

$$
\begin{aligned}
&\frac{(\tilde{\theta}-\theta)^2}{\delta\theta}\Delta t\hat{b}(\boldsymbol{v}_{\varepsilon h}^{n+\theta}-\boldsymbol{v}_{\varepsilon h}^{n},\varphi_{\varepsilon h}^{n},\mu_{\varepsilon h}^{n})-(\tilde{\theta}-\theta)\Delta t\hat{b}(\boldsymbol{v}_{\varepsilon h}^{n+\tilde{\theta}}-\boldsymbol{v}_{\varepsilon h}^{n+\theta},\varphi_{\varepsilon h}^{n},\mu_{\varepsilon h}^{n})\\
&+(\tilde{\theta}-\theta)\Delta t\hat{b}(\boldsymbol{v}_{\varepsilon h}^{n+\tilde{\theta}},\varphi_{\varepsilon h}^{n+\tilde{\theta}},\mu_{\varepsilon h}^{n+\tilde{\theta}})\\
&\le\Big(\frac{(\tilde{\theta}-\theta)^2}{\delta\theta}\Delta tT(h)|\boldsymbol{v}_{\varepsilon h}^{n+\theta}-\boldsymbol{v}_{\varepsilon h}^{n}|+(\tilde{\theta}-\theta)\Delta tT(h)|\boldsymbol{v}_{\varepsilon h}^{n+\tilde{\theta}}-\boldsymbol{v}_{\varepsilon h}^{n+\theta}|\Big)|\nabla\varphi_{\varepsilon h}^{n}||\nabla\mu_{\varepsilon h}^{n}|\\
&\quad+(\tilde{\theta}-\theta)\Delta tT(h)(|\boldsymbol{v}_{\varepsilon h}^{n+\tilde{\theta}}-\boldsymbol{v}_{\varepsilon h}^{n+\theta}|+|\boldsymbol{v}_{\varepsilon h}^{n+\theta}|)|\nabla\varphi_{\varepsilon h}^{n+\tilde{\theta}}||\nabla\mu_{\varepsilon h}^{n+\tilde{\theta}}|\\
&\le\frac{\delta}{2}|\boldsymbol{v}_{\varepsilon h}^{n+\theta}-\boldsymbol{v}_{\varepsilon h}^{n}|^2+\frac{\delta}{2}|\boldsymbol{v}_{\varepsilon h}^{n+\tilde{\theta}}-\boldsymbol{v}_{\varepsilon h}^{n+\theta}|^2\\
&\quad+\frac{(T(h)(\tilde{\theta}-\theta)\Delta t)^2}{\varepsilon}\Big(\frac{(\tilde{\theta}-\theta)^2}{2\delta(\delta\theta)^2}+1\Big)\varepsilon|\nabla\varphi_{\varepsilon h}^{n}|^2|\nabla\mu_{\varepsilon h}^{n}|^2\\
&\quad+\frac{(T(h)(\tilde{\theta}-\theta)\Delta t)^2}{\varepsilon}\varepsilon|\nabla\varphi_{\varepsilon h}^{n+\tilde{\theta}}|^2|\nabla\mu_{\varepsilon h}^{n+\tilde{\theta}}|^2+\frac{T(h)^2(\tilde{\theta}-\theta)\Delta t}{\varepsilon\omega}\varepsilon|\boldsymbol{v}_{\varepsilon h}^{n+\theta}|^2|\nabla\varphi_{\varepsilon h}^{n+\tilde{\theta}}|^2\\
&\quad+\omega(\tilde{\theta}-\theta)\Delta t|\nabla\mu_{\varepsilon h}^{n+\tilde{\theta}}|^2.
\end{aligned}
\tag{3.55}
$$

We arive at the following inequality:

$$
\begin{aligned}
&\frac{1}{2}|\boldsymbol{v}_{\varepsilon h}^{n+\tilde{\theta}}|^2+\frac{1}{2}(1-4\delta)|\boldsymbol{v}_{\varepsilon h}^{n+\tilde{\theta}}-\boldsymbol{v}_{\varepsilon h}^{n+\theta}|^2+(1-\alpha)\eta(\tilde{\theta}-\theta)\Delta t|\nabla\boldsymbol{v}_{\varepsilon h}^{n+\tilde{\theta}}|^2\\
&+\Big(\frac{\alpha}{2}(\tilde{\theta}-\theta)+\frac{(\tilde{\theta}-\theta)^2}{2\delta\theta^2}\Big)\Delta t|\nabla\boldsymbol{v}_{\varepsilon h}^{n+\theta}|^2+\frac{(2\alpha-1)(\tilde{\theta}-\theta)^2}{2\delta\theta^2}\eta\theta\Delta t|\nabla\boldsymbol{v}_{\varepsilon h}^{n+\theta}-\nabla\boldsymbol{v}_{\varepsilon h}^{n}|^2\\
&\leq\frac{1}{2}|\boldsymbol{v}_{\varepsilon h}^{n+\theta}|^2+\frac{(\tilde{\theta}-\theta)^2}{2\delta\theta^2}\eta\theta\Delta t|\nabla\boldsymbol{v}_{\varepsilon h}^{n}|^2+2\frac{(S(h)(\tilde{\theta}-\theta)\Delta t)^2}{2\delta}|\boldsymbol{v}_{\varepsilon h}^{n}|^2|\nabla\boldsymbol{v}_{\varepsilon h}^{n}|^2\\
&\quad+\frac{((1-\alpha)\eta(\tilde{\theta}-\theta)\Delta t)^2}{2\delta h^2}|\nabla\boldsymbol{v}_{\varepsilon h}^{n}|^2+\Big(\frac{(\tilde{\theta}-\theta)}{\delta\theta}+\frac{1}{\alpha}\Big)\frac{(\tilde{\theta}-\theta)\Delta t}{2\eta}|\boldsymbol{f}_h^{n+\theta}|^2\\
&\quad+\frac{\delta}{2}|\boldsymbol{v}_{\varepsilon h}^{n+\theta}-\boldsymbol{v}_{\varepsilon h}^{n}|^2+\frac{(T(h)(\tilde{\theta}-\theta)\Delta t)^2}{\varepsilon}\Big(\frac{(\tilde{\theta}-\theta)^2}{2\delta(\delta\theta)^2}+1\Big)\varepsilon|\nabla\varphi_{\varepsilon h}^{n}|^2|\nabla\mu_{\varepsilon h}^{n}|^2\\
&\quad+\frac{(T(h)(\tilde{\theta}-\theta)\Delta t)^2}{\varepsilon}\varepsilon|\nabla\varphi_{\varepsilon h}^{n+\tilde{\theta}}|^2|\nabla\mu_{\varepsilon h}^{n+\tilde{\theta}}|^2+\frac{T(h)^2(\tilde{\theta}-\theta)\Delta t}{\varepsilon\omega}\varepsilon|\boldsymbol{v}_{\varepsilon h}^{n+\theta}|^2|\nabla\varphi_{\varepsilon h}^{n+\tilde{\theta}}|^2\\
&\quad+\omega(\tilde{\theta}-\theta)\Delta t|\nabla\mu_{\varepsilon h}^{n+\tilde{\theta}}|^2.
\end{aligned}
\tag{3.56}
$$

Remark 3.2.5. *For positivity of the terms of* (3.56)*, we require the constraint that* $0<\delta\leq\frac{1}{4}$ *and that* $\alpha\geq\frac{1}{2}$.

Then we summarise step 2 by adding (3.44) and (3.56).

(2) Cahn-Hilliard-Burgers inequality

Under the assumption that $\gamma\leq\frac{2-3\omega}{3}$, $\alpha\geq\frac{1}{2}$, $0<\delta\leq\frac{1}{4}$, and with suitable discretisation of $F_{(\tilde{\theta}-\theta)}(\varphi_{\varepsilon h}^{n+\tilde{\theta}},\varphi_{\varepsilon h}^{n+\theta})$, we have shown:

$$
\begin{aligned}
&\frac{1}{2}(|\boldsymbol{v}_{\varepsilon h}^{n+\tilde{\theta}}|^2-|\boldsymbol{v}_{\varepsilon h}^{n+\theta}|^2)+\frac{1}{2}(1-4\delta)|\boldsymbol{v}_{\varepsilon h}^{n+\tilde{\theta}}-\boldsymbol{v}_{\varepsilon h}^{n+\theta}|^2+(1-\alpha)\eta(\tilde{\theta}-\theta)\Delta t|\nabla\boldsymbol{v}_{\varepsilon h}^{n+\tilde{\theta}}|^2\\
&+\Big(\frac{\alpha}{2}(\tilde{\theta}-\theta)+\frac{(\tilde{\theta}-\theta)^2}{2\delta\theta^2}\Big)\Delta t|\nabla\boldsymbol{v}_{\varepsilon h}^{n+\theta}|^2+\frac{(2\alpha-1)(\tilde{\theta}-\theta)^2}{2\delta\theta^2}\eta\theta\Delta t|\nabla\boldsymbol{v}_{\varepsilon h}^{n+\theta}-\nabla\boldsymbol{v}_{\varepsilon h}^{n}|^2\\
&+\frac{\varepsilon}{2}(|\nabla\varphi_{\varepsilon h}^{n+\tilde{\theta}}|^2-|\nabla\varphi_{\varepsilon h}^{n+\theta}|^2)+\frac{1}{\varepsilon}(F_{(\tilde{\theta}-\theta)}(\varphi_{\varepsilon h}^{n+\theta},\varphi_{\varepsilon h}^{n+\tilde{\theta}}),\varphi_{\varepsilon h}^{n+\tilde{\theta}}-\varphi_{\varepsilon h}^{n+\theta})\\
&+\frac{\varepsilon}{2}|\nabla\varphi_{\varepsilon h}^{n+\tilde{\theta}}-\nabla\varphi_{\varepsilon h}^{n+\theta}|^2+\frac{(2-3\gamma-3\omega)}{2}(\tilde{\theta}-\theta)\Delta t|\nabla\mu_{\varepsilon h}^{n+\tilde{\theta}}|^2\\
&\leq\frac{(\tilde{\theta}-\theta)^2}{2\delta\theta^2}\eta\theta\Delta t|\nabla\boldsymbol{v}_{\varepsilon h}^{n}|^2+2\frac{(S(h)(\tilde{\theta}-\theta)\Delta t)^2}{2\delta}|\boldsymbol{v}_{\varepsilon h}^{n}|^2|\nabla\boldsymbol{v}_{\varepsilon h}^{n}|^2\\
&\quad+\frac{((1-\alpha)\eta(\tilde{\theta}-\theta)\Delta t)^2}{2\delta h^2}|\nabla\boldsymbol{v}_{\varepsilon h}^{n}|^2+\Big(\frac{(\tilde{\theta}-\theta)}{\delta\theta}+\frac{1}{\alpha}\Big)\frac{(\tilde{\theta}-\theta)\Delta t}{2\eta}|\boldsymbol{f}_h^{n+\theta}|^2\\
&\quad+\frac{\delta}{2}|\boldsymbol{v}_{\varepsilon h}^{n+\theta}-\boldsymbol{v}_{\varepsilon h}^{n}|^2+\frac{(T(h)(\tilde{\theta}-\theta)\Delta t)^2}{\varepsilon}\Big(\frac{(\tilde{\theta}-\theta)^2}{2\delta(\delta\theta)^2}+1\Big)\varepsilon|\nabla\varphi_{\varepsilon h}^{n}|^2|\nabla\mu_{\varepsilon h}^{n}|^2\\
&\quad+\frac{(T(h)(\tilde{\theta}-\theta)\Delta t)^2}{\varepsilon}\varepsilon|\nabla\varphi_{\varepsilon h}^{n+\tilde{\theta}}|^2|\nabla\mu_{\varepsilon h}^{n+\tilde{\theta}}|^2+\frac{T(h)^2(\tilde{\theta}-\theta)\Delta t}{\varepsilon\omega}\varepsilon|\boldsymbol{v}_{\varepsilon h}^{n+\theta}|^2|\nabla\varphi_{\varepsilon h}^{n+\tilde{\theta}}|^2\\
&\quad+\frac{T(h)^2(\tilde{\theta}-\theta)\Delta t}{2\omega}|\boldsymbol{v}_{\varepsilon h}^{n+\theta}|^2|\nabla\varphi_{\varepsilon h}^{n+\theta}|^2+\frac{\gamma}{2}(\tilde{\theta}-\theta)\Delta t|\nabla\mu_{\varepsilon h}^{n+\theta}|^2.
\end{aligned}
\tag{3.57}
$$

Step 3(a)-3(b)

The calculations involved in Step 3(a) begin identically to those in Step 1(a). We shall begin where they differ, after an inequality mimicking (3.29) has been reached:

$$\begin{aligned}
&\frac{1}{2}|\boldsymbol{v}_{\varepsilon h}^{n+1}|^2 + \Big(\frac{1}{2} - \frac{(1-\alpha)}{2h^2}\eta\theta\Delta t\Big)|\boldsymbol{v}_{\varepsilon h}^{n+1} - \boldsymbol{v}_{\varepsilon h}^{n+\tilde{\theta}}|^2 + \frac{1+2\alpha}{4}\eta\theta\Delta t|\nabla\boldsymbol{v}_{\varepsilon h}^{n+1}|^2 \\
&+ \frac{(1-\alpha)}{2}\eta\theta\Delta t|\nabla\boldsymbol{v}_{\varepsilon h}^{n+\tilde{\theta}}|^2 \\
&\leq \frac{1}{2}|\boldsymbol{v}_{\varepsilon h}^{n+\tilde{\theta}}|^2 - \theta\Delta t b_h(\boldsymbol{v}_{\varepsilon h}^{n+\tilde{\theta}}, \boldsymbol{v}_{\varepsilon h}^{n+\tilde{\theta}}, \boldsymbol{v}_{\varepsilon h}^{n+1}) + \theta\Delta t\hat{b}(\boldsymbol{v}_{\varepsilon h}^{n+1}, \varphi_{\varepsilon h}^{n+\tilde{\theta}}, \mu_{\varepsilon h}^{n+\tilde{\theta}}) + \frac{\theta\Delta t}{\eta}|\boldsymbol{f}_h^{n+1}|^2.
\end{aligned} \tag{3.58}$$

We do not bound the the convection operator $b_h(\boldsymbol{v}_{\varepsilon h}^{n+\tilde{\theta}}, \boldsymbol{v}_{\varepsilon h}^{n+\tilde{\theta}}, \boldsymbol{v}_{\varepsilon h}^{n+1})$ directly, instead we use the Burgers' equation and the pressure equation to rewrite this object. To this end, we note from (3.22) that $b_h(\boldsymbol{v}_{\varepsilon h}^{n+\tilde{\theta}}, \boldsymbol{v}_{\varepsilon h}^{n+\tilde{\theta}}, \boldsymbol{v}_{\varepsilon h}^{n+1}) = b_h(\boldsymbol{v}_{\varepsilon h}^{n+\tilde{\theta}}, \boldsymbol{v}_{\varepsilon h}^{n+\tilde{\theta}}, \boldsymbol{v}_{\varepsilon h}^{n+1} - \boldsymbol{v}_{\varepsilon h}^{n+\tilde{\theta}})$. Testing (3.45) with $\boldsymbol{v}_{\varepsilon h}^{n+1} - \boldsymbol{v}_{\varepsilon h}^{n+\tilde{\theta}}$ and rearranging gives:

$$\begin{aligned}
&b_h(\boldsymbol{v}_{\varepsilon h}^{n+\tilde{\theta}}, \boldsymbol{v}_{\varepsilon h}^{n+\tilde{\theta}}, \boldsymbol{v}_{\varepsilon h}^{n+1}) \\
&= -\Big(\frac{\boldsymbol{v}_{\varepsilon h}^{n+\tilde{\theta}} - \boldsymbol{v}_{\varepsilon h}^{n+\theta}}{(\tilde{\theta}-\theta)\Delta t}, \boldsymbol{v}_{\varepsilon h}^{n+1} - \boldsymbol{v}_{\varepsilon h}^{n+\tilde{\theta}}\Big) - (1-\alpha)\eta(\nabla\boldsymbol{v}_{\varepsilon h}^{n+\tilde{\theta}}, \nabla\boldsymbol{v}_{\varepsilon h}^{n+1} - \nabla\boldsymbol{v}_{\varepsilon h}^{n+\tilde{\theta}}) \\
&\quad - \alpha\eta(\nabla\boldsymbol{v}_{\varepsilon h}^{n+\theta}, \nabla\boldsymbol{v}_{\varepsilon h}^{n+1} - \nabla\boldsymbol{v}_{\varepsilon h}^{n+\tilde{\theta}}) + \hat{b}(\boldsymbol{v}_{\varepsilon h}^{n+1} - \boldsymbol{v}_{\varepsilon h}^{n+\tilde{\theta}}, \varphi_{\varepsilon h}^{n+\tilde{\theta}}, \mu_{\varepsilon h}^{n+\tilde{\theta}}) \\
&\quad + (p_{\varepsilon h}^{n+\theta}, \nabla\cdot(\boldsymbol{v}_{\varepsilon h}^{n+1} - \nabla\boldsymbol{v}_{\varepsilon h}^{n+\tilde{\theta}}) + (\boldsymbol{f}^{n+\theta}, \boldsymbol{v}_{\varepsilon h}^{n+1} - \boldsymbol{v}_{\varepsilon h}^{n+\tilde{\theta}}).
\end{aligned} \tag{3.59}$$

We substitute the for the pressure by testing equation (3.46) with $\boldsymbol{v}_{\varepsilon h}^{n+1} - \boldsymbol{v}_{\varepsilon h}^{n+\tilde{\theta}}$:

$$\begin{aligned}
&- \theta\Delta t b_h(\boldsymbol{v}_{\varepsilon h}^{n+\tilde{\theta}}, \boldsymbol{v}_{\varepsilon h}^{n+\tilde{\theta}}, \boldsymbol{v}_{\varepsilon h}^{n+1}) \\
&= \frac{\theta}{(\tilde{\theta}-\theta)}(\boldsymbol{v}_{\varepsilon h}^{n+\tilde{\theta}} - \boldsymbol{v}_{\varepsilon h}^{n+\theta}, \boldsymbol{v}_{\varepsilon h}^{n+1} - \boldsymbol{v}_{\varepsilon h}^{n+\tilde{\theta}}) - (\boldsymbol{v}_{\varepsilon h}^{n+\theta} - \boldsymbol{v}_{\varepsilon h}^{n}, \boldsymbol{v}_{\varepsilon h}^{n+1} - \boldsymbol{v}_{\varepsilon h}^{n+\tilde{\theta}}) \\
&\quad + (1-\alpha)\eta\theta\Delta t(\nabla\boldsymbol{v}_{\varepsilon h}^{n+\tilde{\theta}} - \nabla\boldsymbol{v}_{\varepsilon h}^{n}, \nabla\boldsymbol{v}_{\varepsilon h}^{n+1} - \nabla\boldsymbol{v}_{\varepsilon h}^{n+\tilde{\theta}}) \\
&\quad + \theta\Delta t b_h(\boldsymbol{v}_{\varepsilon h}^{n}, \boldsymbol{v}_{\varepsilon h}^{n}, \boldsymbol{v}_{\varepsilon h}^{n+1} - \boldsymbol{v}_{\varepsilon h}^{n+\tilde{\theta}}) - \theta\Delta t\hat{b}(\boldsymbol{v}_{\varepsilon h}^{n+1} - \boldsymbol{v}_{\varepsilon h}^{n+\tilde{\theta}}, \varphi_{\varepsilon h}^{n+\tilde{\theta}}, \mu_{\varepsilon h}^{n+\tilde{\theta}}) \\
&\quad + \theta\Delta t\hat{b}(\boldsymbol{v}_{\varepsilon h}^{n+1} - \boldsymbol{v}_{\varepsilon h}^{n+\tilde{\theta}}, \varphi_{\varepsilon h}^{n}, \mu_{\varepsilon h}^{n}),
\end{aligned} \tag{3.60}$$

and bound the expressions as before. Substituting this expression into (3.58), we arrive at

$$
\begin{aligned}
&\frac{1}{2}|\boldsymbol{v}_{\varepsilon h}^{n+1}|^2+\Big(\frac{1}{2}-\frac{(1-\alpha)}{2h^2}\eta\theta\Delta t\Big)|\boldsymbol{v}_{\varepsilon h}^{n+1}-\boldsymbol{v}_{\varepsilon h}^{n+\tilde\theta}|^2+\frac{1+2\alpha}{4}\eta\theta\Delta t|\nabla\boldsymbol{v}_{\varepsilon h}^{n+1}|^2\\
&+\frac{(1-\alpha)}{2}\eta\theta\Delta t|\nabla\boldsymbol{v}_{\varepsilon h}^{n+\tilde\theta}|^2\\
&\leq\frac{1}{2}|\boldsymbol{v}_{\varepsilon h}^{n+\tilde\theta}|^2+T(h)\theta\Delta t\big(|\boldsymbol{v}_{\varepsilon h}^{n+1}-\boldsymbol{v}_{\varepsilon h}^{n+\tilde\theta}|+|\boldsymbol{v}_{\varepsilon h}^{n+\tilde\theta}|\big)|\nabla\varphi_{\varepsilon h}^{n+\tilde\theta}||\nabla\mu_{\varepsilon h}^{n+\tilde\theta}|+\frac{\theta\Delta t}{\eta}|\boldsymbol{f}_h^{n+1}|^2\\
&\quad+\frac{\theta}{(\tilde\theta-\theta)}|\boldsymbol{v}_{\varepsilon h}^{n+\tilde\theta}-\boldsymbol{v}_{\varepsilon h}^{n+\theta}||\boldsymbol{v}_{\varepsilon h}^{n+1}-\boldsymbol{v}_{\varepsilon h}^{n+\tilde\theta}|+|\boldsymbol{v}_{\varepsilon h}^{n+\theta}-\boldsymbol{v}_{\varepsilon h}^{n}||\boldsymbol{v}_{\varepsilon h}^{n+1}-\boldsymbol{v}_{\varepsilon h}^{n+\tilde\theta}|\\
&\quad+(1-\alpha)\eta\theta\Delta t(|\nabla\boldsymbol{v}_{\varepsilon h}^{n+\tilde\theta}||\nabla\boldsymbol{v}_{\varepsilon h}^{n+1}-\nabla\boldsymbol{v}_{\varepsilon h}^{n+\tilde\theta}|+|\nabla\boldsymbol{v}_{\varepsilon h}^{n}||\nabla\boldsymbol{v}_{\varepsilon h}^{n+1}-\nabla\boldsymbol{v}_{\varepsilon h}^{n+\tilde\theta}|)\\
&\quad+S(h)\theta\Delta t|\boldsymbol{v}_{\varepsilon h}^{n}||\nabla\boldsymbol{v}_{\varepsilon h}^{n}||\boldsymbol{v}_{\varepsilon h}^{n+1}-\boldsymbol{v}_{\varepsilon h}^{n+\tilde\theta}|\\
&\quad+\theta\Delta t\hat b(\boldsymbol{v}_{\varepsilon h}^{n+\tilde\theta},\varphi_{\varepsilon h}^{n+\tilde\theta},\mu_{\varepsilon h}^{n+\tilde\theta})+\theta\Delta t\hat b(\boldsymbol{v}_{\varepsilon h}^{n+1}-\boldsymbol{v}_{\varepsilon h}^{n+\tilde\theta},\varphi_{\varepsilon h}^{n},\mu_{\varepsilon h}^{n})\\
&\leq\frac{2\theta^2}{(\tilde\theta-\theta)^2}|\boldsymbol{v}_{\varepsilon h}^{n+\tilde\theta}-\boldsymbol{v}_{\varepsilon h}^{n+\theta}|^2+\frac{1}{4}|\boldsymbol{v}_{\varepsilon h}^{n+1}-\boldsymbol{v}_{\varepsilon h}^{n+\tilde\theta}|^2+2|\boldsymbol{v}_{\varepsilon h}^{n+\theta}-\boldsymbol{v}_{\varepsilon h}^{n}|^2\\
&\quad+\frac{4((1-\alpha)\eta\theta\Delta t)^2}{h^2}|\nabla\boldsymbol{v}_{\varepsilon h}^{n+\tilde\theta}|^2+\frac{4((1-\alpha)\eta\theta\Delta t)^2}{h^2}|\nabla\boldsymbol{v}_{\varepsilon h}^{n}|^2+\frac{1}{8}|\boldsymbol{v}_{\varepsilon h}^{n+1}-\boldsymbol{v}_{\varepsilon h}^{n+\tilde\theta}|^2\\
&\quad+4(S(h)\theta\Delta t)^2|\boldsymbol{v}_{\varepsilon h}^{n}|^2|\nabla\boldsymbol{v}_{\varepsilon h}^{n}|^2+\frac{1}{16}|\boldsymbol{v}_{\varepsilon h}^{n+1}-\boldsymbol{v}_{\varepsilon h}^{n+\tilde\theta}|^2\\
&\quad+\theta\Delta t\hat b(\boldsymbol{v}_{\varepsilon h}^{n+\tilde\theta},\varphi_{\varepsilon h}^{n+\tilde\theta},\mu_{\varepsilon h}^{n+\tilde\theta})+\theta\Delta t\hat b(\boldsymbol{v}_{\varepsilon h}^{n+1}-\boldsymbol{v}_{\varepsilon h}^{n+\tilde\theta},\varphi_{\varepsilon h}^{n},\mu_{\varepsilon h}^{n}).
\end{aligned}
\tag{3.61}
$$

To deal with the difference terms $|\boldsymbol{v}_{\varepsilon h}^{n+\tilde\theta}-\boldsymbol{v}_{\varepsilon h}^{n+\theta}|^2$ and $|\boldsymbol{v}_{\varepsilon h}^{n+\theta}-\boldsymbol{v}_{\varepsilon h}^{n}|^2$ we use the inequalities (3.56) and (3.53) respectively:

$$
\begin{aligned}
&\frac{1}{2}|\boldsymbol{v}_{\varepsilon h}^{n+1}|^2+\Big(\frac{1}{32}-\frac{(1-\alpha)}{2h^2}\eta\theta\Delta t\Big)|\boldsymbol{v}_{\varepsilon h}^{n+1}-\boldsymbol{v}_{\varepsilon h}^{n+\tilde\theta}|^2+\frac{1+2\alpha}{2}\eta\theta\Delta t|\nabla\boldsymbol{v}_{\varepsilon h}^{n+1}|^2\\
&+\Big(1-\frac{4(1-\alpha)}{h^2}\eta\theta\Delta t\Big)\frac{(1-\alpha)}{2}\eta\theta\Delta t|\nabla\boldsymbol{v}_{\varepsilon h}^{n+\tilde\theta}|^2\\
&\leq\frac{1}{2}|\boldsymbol{v}_{\varepsilon h}^{n+\tilde\theta}|^2+6(S(h)\theta\Delta t)^2|\boldsymbol{v}_{\varepsilon h}^{n}|^2|\nabla\boldsymbol{v}_{\varepsilon h}^{n}|^2+\theta\Delta t\hat b(\boldsymbol{v}_{\varepsilon h}^{n+\tilde\theta},\varphi_{\varepsilon h}^{n+\tilde\theta},\mu_{\varepsilon h}^{n+\tilde\theta})\\
&\quad+\Big(2\eta\theta\Delta t+\frac{4((1-\alpha)\eta\theta\Delta t)^2}{h^2}\Big)|\nabla\boldsymbol{v}_{\varepsilon h}^{n}|^2+\frac{2\theta\Delta t}{\eta}|\boldsymbol{f}_h^{n+1}|^2\\
&\quad+\theta\Delta t\hat b(\boldsymbol{v}_{\varepsilon h}^{n+1}-\boldsymbol{v}_{\varepsilon h}^{n+\tilde\theta},\varphi_{\varepsilon h}^{n},\mu_{\varepsilon h}^{n})+4\theta\Delta t\hat b(\boldsymbol{v}_{\varepsilon h}^{n+\theta}-\boldsymbol{v}_{\varepsilon h}^{n},\varphi_{\varepsilon h}^{n},\mu_{\varepsilon h}^{n}).
\end{aligned}
\tag{3.62}
$$

Using (3.25) and Young's inequality as seen in previous steps, with $\omega > 0$, we have:

$$\begin{aligned}
&\theta\Delta t\hat{b}(\boldsymbol{v}_{\varepsilon h}^{n+\tilde{\theta}}, \varphi_{\varepsilon h}^{n+\tilde{\theta}}, \mu_{\varepsilon h}^{n+\tilde{\theta}}) + \theta\Delta t\hat{b}(\boldsymbol{v}_{\varepsilon h}^{n+1} - \boldsymbol{v}_{\varepsilon h}^{n+\tilde{\theta}}, \varphi_{\varepsilon h}^{n}, \mu_{\varepsilon h}^{n}) + 4\theta\Delta t\hat{b}(\boldsymbol{v}_{\varepsilon h}^{n+\theta} - \boldsymbol{v}_{\varepsilon h}^{n}, \varphi_{\varepsilon h}^{n}, \mu_{\varepsilon h}^{n}) \\
&\leq T(h)\theta\Delta t|\boldsymbol{v}_{\varepsilon h}^{n+\tilde{\theta}}||\varphi_{\varepsilon h}^{n+\tilde{\theta}}||\mu_{\varepsilon h}^{n+\tilde{\theta}}| + T(h)\theta\Delta t(|\boldsymbol{v}_{\varepsilon h}^{n+1} - \boldsymbol{v}_{\varepsilon h}^{n+\tilde{\theta}}| + 4|\boldsymbol{v}_{\varepsilon h}^{n+\theta} - \boldsymbol{v}_{\varepsilon h}^{n}|)|\varphi_{\varepsilon h}^{n}||\mu_{\varepsilon h}^{n}| \\
&\leq \frac{T(h)^2\theta\Delta t}{\omega\varepsilon}\varepsilon|\boldsymbol{v}_{\varepsilon h}^{n+\tilde{\theta}}|^2|\varphi_{\varepsilon h}^{n+\tilde{\theta}}|^2 + \omega\theta\Delta t|\mu_{\varepsilon h}^{n+\tilde{\theta}}|^2 + \frac{\delta}{2}|\boldsymbol{v}_{\varepsilon h}^{n+1} - \boldsymbol{v}_{\varepsilon h}^{n+\tilde{\theta}}|^2 + \frac{\delta}{2}|\boldsymbol{v}_{\varepsilon h}^{n+\theta} - \boldsymbol{v}_{\varepsilon h}^{n}|^2 \\
&\quad + \frac{5(T(h)\theta\Delta t)^2}{\delta\varepsilon}\varepsilon|\varphi_{\varepsilon h}^{n}|^2|\mu_{\varepsilon h}^{n}|^2,
\end{aligned}$$

and so we arrive at an inequality analogous to (3.31):

$$\begin{aligned}
&\frac{1}{2}|\boldsymbol{v}_{\varepsilon h}^{n+1}|^2 + \Big(\frac{1}{32} - \frac{\delta}{2} - \frac{(1-\alpha)}{2h^2}\eta\theta\Delta t\Big)|\boldsymbol{v}_{\varepsilon h}^{n+1} - \boldsymbol{v}_{\varepsilon h}^{n+\tilde{\theta}}|^2 + \frac{1+2\alpha}{2}\eta\theta\Delta t|\nabla\boldsymbol{v}_{\varepsilon h}^{n+1}|^2 \\
&+ \Big(1 - \frac{4(1-\alpha)}{h^2}\eta\theta\Delta t\Big)\frac{(1-\alpha)}{2}\eta\theta\Delta t|\nabla\boldsymbol{v}_{\varepsilon h}^{n+\tilde{\theta}}|^2 \\
&\leq \frac{1}{2}|\boldsymbol{v}_{\varepsilon h}^{n+\tilde{\theta}}|^2 + 6(S(h)\theta\Delta t)^2|\boldsymbol{v}_{\varepsilon h}^{n}|^2|\nabla\boldsymbol{v}_{\varepsilon h}^{n}|^2 + \frac{\delta}{2}|\boldsymbol{v}_{\varepsilon h}^{n+\theta} - \boldsymbol{v}_{\varepsilon h}^{n}|^2 \\
&\quad + \Big(2\eta\theta\Delta t + \frac{4((1-\alpha)\eta\theta\Delta t)^2}{h^2}\Big)|\nabla\boldsymbol{v}_{\varepsilon h}^{n}|^2 + \frac{2\theta\Delta t}{\eta}|\boldsymbol{f}_h^{n+1}|^2 \\
&\quad + \frac{T(h)^2\theta\Delta t}{\omega\varepsilon}\varepsilon|\boldsymbol{v}_{\varepsilon h}^{n+\tilde{\theta}}|^2|\varphi_{\varepsilon h}^{n+\tilde{\theta}}|^2 + \omega\theta\Delta t|\mu_{\varepsilon h}^{n+\tilde{\theta}}|^2 + \frac{5(T(h)\theta\Delta t)^2}{\delta\varepsilon}\varepsilon|\varphi_{\varepsilon h}^{n}|^2|\mu_{\varepsilon h}^{n}|^2, \quad (3.63)
\end{aligned}$$

and, as the analysis for Step 1(b) may be repeated for Step 3(b), the final inequality analogous to (3.37) reads:

$$\begin{aligned}
&\frac{\varepsilon}{2}(|\nabla\varphi_{\varepsilon h}^{n+1}|^2 - |\nabla\varphi_{\varepsilon h}^{n+\tilde{\theta}}|^2) + \frac{1}{\varepsilon}(F_\theta(\varphi_{\varepsilon h}^{n+\tilde{\theta}}, \varphi_{\varepsilon h}^{n+1}), \varphi_{\varepsilon h}^{n+1} - \varphi_{\varepsilon h}^{n+\tilde{\theta}}) \\
&+ \frac{\varepsilon}{4}|\nabla\varphi_{\varepsilon h}^{n+1} - \nabla\varphi_{\varepsilon h}^{n+\tilde{\theta}}|^2 + \frac{3\gamma - 1 - \omega}{2}\theta\Delta t|\nabla\mu_{\varepsilon h}^{n+1}|^2 \\
&\leq \frac{1-\gamma}{2}\theta\Delta t|\nabla\mu_{\varepsilon h}^{n+\tilde{\theta}}|^2 + \frac{T(h)^2\theta\Delta t}{2\omega\varepsilon}|\boldsymbol{v}_{\varepsilon h}^{n+1}|^2\varepsilon|\nabla\varphi_{\varepsilon}^{n+\tilde{\theta}}|^2 \\
&\quad + \frac{(T(h)\theta\Delta t)^2}{\varepsilon}|\boldsymbol{v}_{\varepsilon h}^{n+1}|^2|\nabla\mu_{\varepsilon h}^{n+1}|^2. \quad (3.64)
\end{aligned}$$

We summarise the final substep stability inequality by adding (3.63) and (3.64) together:

(3) Stokes-Cahn-Hilliard inequality

Under the assumption that $\alpha \leq 1$, $\gamma \geq \frac{1+\omega}{3}$ and $(1-\alpha)\eta\theta\Delta t \leq \frac{1}{16}h^2$, and a

suitable choice of discretisation $F_\theta(\varphi_{\varepsilon h}^{n+\tilde{\theta}}, \varphi_{\varepsilon h}^{n+1})$ we have shown:

$$
\begin{aligned}
&\frac{1}{2}(|\boldsymbol{v}_{\varepsilon h}^{n+1}|^2 - |\boldsymbol{v}_{\varepsilon h}^{n+\tilde{\theta}}|^2) + \Big(\frac{1}{32} - \frac{\delta}{2} - \frac{(1-\alpha)}{2h^2}\eta\theta\Delta t\Big)|\boldsymbol{v}_{\varepsilon h}^{n+1} - \boldsymbol{v}_{\varepsilon h}^{n+\tilde{\theta}}|^2 \\
&+ \frac{1+2\alpha}{2}\eta\theta\Delta t|\nabla \boldsymbol{v}_{\varepsilon h}^{n+1}|^2 + \Big(1 - \frac{4(1-\alpha)}{h^2}\eta\theta\Delta t\Big)\frac{(1-\alpha)}{2}\eta\theta\Delta t|\nabla \boldsymbol{v}_{\varepsilon h}^{n+\tilde{\theta}}|^2 \\
&+ \frac{\varepsilon}{2}(|\nabla\varphi_{\varepsilon h}^{n+1}|^2 - |\nabla\varphi_{\varepsilon h}^{n+\tilde{\theta}}|^2) + \frac{1}{\varepsilon}(F_\theta(\varphi_{\varepsilon h}^{n+\tilde{\theta}}, \varphi_{\varepsilon h}^{n+1}), \varphi_{\varepsilon h}^{n+1} - \varphi_{\varepsilon h}^{n+\tilde{\theta}}) \\
&+ \frac{\varepsilon}{4}|\nabla\varphi_{\varepsilon h}^{n+1} - \nabla\varphi_{\varepsilon h}^{n+\tilde{\theta}}|^2 + \frac{3\gamma - 1 - \omega}{2}\theta\Delta t|\nabla\mu_{\varepsilon h}^{n+1}|^2 \\
&\leq 6(S(h)\theta\Delta t)^2|\boldsymbol{v}_{\varepsilon h}^{n}|^2|\nabla \boldsymbol{v}_{\varepsilon h}^{n}|^2 + \frac{\delta}{2}|\boldsymbol{v}_{\varepsilon h}^{n+\theta} - \boldsymbol{v}_{\varepsilon h}^{n}|^2 \\
&\quad + \Big(2\eta\theta\Delta t + \frac{4((1-\alpha)\eta\theta\Delta t)^2}{h^2}\Big)|\nabla \boldsymbol{v}_{\varepsilon h}^{n}|^2 + \frac{2\theta\Delta t}{\eta}|\boldsymbol{f}_h^{n+1}|^2 \\
&\quad + \frac{T(h)^2\theta\Delta t}{\omega\varepsilon}\varepsilon|\boldsymbol{v}_{\varepsilon h}^{n+\tilde{\theta}}|^2|\varphi_{\varepsilon h}^{n+\tilde{\theta}}|^2 + \omega\theta\Delta t|\mu_{\varepsilon h}^{n+\tilde{\theta}}|^2 + \frac{5(T(h)\theta\Delta t)^2}{\delta\varepsilon}\varepsilon|\varphi_{\varepsilon h}^{n}|^2|\mu_{\varepsilon h}^{n}|^2 \\
&\quad + \frac{1-\gamma}{2}\theta\Delta t|\nabla\mu_{\varepsilon h}^{n+\tilde{\theta}}|^2 + \frac{T(h)^2\theta\Delta t}{2\omega\varepsilon}|\boldsymbol{v}_{\varepsilon h}^{n+1}|^2\varepsilon|\nabla\varphi_{\varepsilon}^{n+\tilde{\theta}}|^2 \\
&\quad + \frac{(T(h)\theta\Delta t)^2}{\varepsilon}|\boldsymbol{v}_{\varepsilon h}^{n+1}|^2|\nabla\mu_{\varepsilon h}^{n+1}|^2. \qquad (3.65)
\end{aligned}
$$

The inequality (3.65) combined with (3.57) and (3.38) complete the stability inequalities for the whole timestep.

3.2.3 A discrete energy inequality

We now have 3 inequalities (3.38), (3.57) and (3.65), which cover one full timestep of our theta scheme. To combine them we sum these inequalities together. This leads to an expression similar to (3.32) discussed in Remark 3.2.2. This will yield the following form for the left hand side of the fully discrete energy dissipation inequality

$$
\begin{aligned}
&\{\text{Difference in kinetic energy}\} + \{\text{Difference in CH gradient part}\} \\
&+ \{\text{Difference in CH potential part}\} + \{\text{Dissipative terms}\}\,. \qquad (3.66)
\end{aligned}
$$

In full detail, given $\boldsymbol{v}_{\varepsilon h}^n, \varphi_{\varepsilon h}^n, \mu_{\varepsilon h}^n$, we perform the summation to obtain the left hand side of the energy inequality:

$$
\begin{aligned}
&\frac{1}{2}(|\boldsymbol{v}_{\varepsilon h}^{n+1}|^2 - |\boldsymbol{v}_{\varepsilon h}^{n+\tilde{\theta}}|^2) + \frac{1}{2}(|\boldsymbol{v}_{\varepsilon h}^{n+\tilde{\theta}}|^2 - |\boldsymbol{v}_{\varepsilon h}^{n+\theta}|^2) + \frac{1}{2}(|\boldsymbol{v}_{\varepsilon h}^{n+\theta}|^2 - |\boldsymbol{v}_{\varepsilon h}^{n}|^2) \\
&+ \frac{\varepsilon}{2}(|\nabla\varphi_{\varepsilon h}^{n+1}|^2 - |\nabla\varphi_{\varepsilon h}^{n+\tilde{\theta}}|^2) + \frac{\varepsilon}{2}(|\nabla\varphi_{\varepsilon h}^{n+\tilde{\theta}}|^2 - |\nabla\varphi_{\varepsilon h}^{n+\theta}|^2) + \frac{\varepsilon}{2}(|\nabla\varphi_{\varepsilon h}^{n+\theta}|^2 - |\nabla\varphi_{\varepsilon h}^{n}|^2) \\
&+ \frac{1}{\varepsilon}(F_\theta(\varphi_{\varepsilon h}^{n+\tilde{\theta}}, \varphi_{\varepsilon h}^{n+1}), \varphi_{\varepsilon h}^{n+1} - \varphi_{\varepsilon h}^{n+\tilde{\theta}}) + \frac{1}{\varepsilon}(F_{(\tilde{\theta}-\theta)}(\varphi_{\varepsilon h}^{n+\theta}, \varphi_{\varepsilon h}^{n+\tilde{\theta}}), \varphi_{\varepsilon h}^{n+\tilde{\theta}} - \varphi_{\varepsilon h}^{n+\theta}) \\
&+ \frac{1}{\varepsilon}(F_\theta(\varphi_{\varepsilon h}^{n}, \varphi_{\varepsilon h}^{n+\theta}), \varphi_{\varepsilon h}^{n+\theta} - \varphi_{\varepsilon h}^{n}) \\
&+ \Big(\frac{1}{32} - \frac{\delta}{2} - \frac{(1-\alpha)}{2h^2}\eta\theta\Delta t\Big)|\boldsymbol{v}_{\varepsilon h}^{n+1} - \boldsymbol{v}_{\varepsilon h}^{n+\tilde{\theta}}|^2 + \frac{1}{2}(1-4\delta)|\boldsymbol{v}_{\varepsilon h}^{n+\tilde{\theta}} - \boldsymbol{v}_{\varepsilon h}^{n+\theta}|^2 \\
&+ \Big(\frac{1}{8} - \delta - \Big(\frac{(1-\alpha)}{2h^2} + \frac{(\tilde{\theta}-\theta)^2}{2\delta\theta^2h^2}\Big)\eta\theta\Delta t\Big)|\boldsymbol{v}_{\varepsilon h}^{n+\theta} - \boldsymbol{v}_{\varepsilon h}^{n}|^2 \\
&+ \frac{1+2\alpha}{2}\eta\theta\Delta t|\nabla\boldsymbol{v}_{\varepsilon h}^{n+1}|^2 + (1-\alpha)\Big(\frac{\theta}{2} + (\tilde{\theta}-\theta) - \frac{4\theta^2(1-\alpha)\eta\Delta t}{h^2}\Big)\eta\Delta t|\nabla\boldsymbol{v}_{\varepsilon h}^{n+\tilde{\theta}}|^2 \\
&+ \Big(\frac{\alpha}{2}\tilde{\theta} + \frac{\theta}{2} + \frac{(2\alpha-1)(\tilde{\theta}-\theta)^2}{2\delta\theta^2}\Big)\eta\Delta t|\nabla\boldsymbol{v}_{\varepsilon h}^{n+\theta}|^2 + \frac{(1-\alpha)}{2}\eta\theta\Delta t|\nabla\boldsymbol{v}_{\varepsilon h}^{n}|^2 \\
&+ \frac{\varepsilon}{4}|\nabla\varphi_{\varepsilon h}^{n+1} - \nabla\varphi_{\varepsilon h}^{n+\tilde{\theta}}|^2 + \frac{\varepsilon}{2}|\nabla\varphi_{\varepsilon h}^{n+\tilde{\theta}} - \nabla\varphi_{\varepsilon h}^{n+\theta}|^2 + \frac{\varepsilon}{2}|\nabla\varphi_{\varepsilon h}^{n+\theta} - \nabla\varphi_{\varepsilon h}^{n}|^2 \\
&+ \frac{3\gamma-1-\omega}{2}\theta\Delta t|\nabla\mu_{\varepsilon h}^{n+1}|^2 + \Big(\frac{2-3\gamma-3\omega}{2}(\tilde{\theta}-\theta) - \omega\theta\Big)\Delta t|\nabla\mu_{\varepsilon h}^{n+\tilde{\theta}}|^2 \\
&+ \Big(\frac{3\gamma-1-\omega}{2}\theta - \frac{\gamma}{2}(\tilde{\theta}-\theta)\Big)\Delta t|\nabla\mu_{\varepsilon h}^{n+\theta}|^2 - \frac{1-\gamma+\omega}{2}\theta\Delta t|\nabla\mu_{\varepsilon h}^{n}|^2 \\
&= \Big(\frac{1}{2}|\boldsymbol{v}_{\varepsilon h}^{n+1}|^2 + \frac{\varepsilon}{2}|\nabla\varphi_{\varepsilon h}^{n+1}|^2 + \frac{1}{\varepsilon}\int_\Omega F(\varphi_{\varepsilon h}^{n+1})\,\mathrm{d}x\Big) \\
&- \Big(\frac{1}{2}|\boldsymbol{v}_{\varepsilon h}^{n}|^2 + \frac{\varepsilon}{2}|\nabla\varphi_{\varepsilon h}^{n}|^2 + \frac{1}{\varepsilon}\int_\Omega F(\varphi_{\varepsilon h}^{n})\,\mathrm{d}x\Big) \\
&- \frac{1}{\varepsilon}\int_\Omega (F(\varphi_{\varepsilon h}^{n+1}) - F(\varphi_{\varepsilon h}^{n})) - \Big(F_\theta(\varphi_{\varepsilon h}^{n+\tilde{\theta}}, \varphi_{\varepsilon h}^{n+1})(\varphi_{\varepsilon h}^{n+1} - \varphi_{\varepsilon h}^{n+\tilde{\theta}}) \\
&\qquad + F_{(\tilde{\theta}-\theta)}(\varphi_{\varepsilon h}^{n+\theta}, \varphi_{\varepsilon h}^{n+\tilde{\theta}})(\varphi_{\varepsilon h}^{n+\tilde{\theta}} - \varphi_{\varepsilon h}^{n+\theta}) + F_\theta(\varphi_{\varepsilon h}^{n}, \varphi_{\varepsilon h}^{n+\theta})(\varphi_{\varepsilon h}^{n+\theta} - \varphi_{\varepsilon h}^{n})\Big)\,\mathrm{d}x \\
&+ (H_{Diss})_n^{n+1} \\
&= E_\varepsilon(\varphi_{\varepsilon h}^{n+1}, \mu_{\varepsilon h}^{n+1}, \boldsymbol{v}_{\varepsilon h}^{n+1}) - E_\varepsilon(\varphi_{\varepsilon h}^{n}, \mu_{\varepsilon h}^{n}, \boldsymbol{v}_{\varepsilon h}^{n}) + (H_{cons})_n^{n+1} + (H_{Diss})_n^{n+1}. \qquad (3.67)
\end{aligned}
$$

Where $(H_{cons})_n^{n+1}$ is the consistency error from the approximation of F' by $F_\theta, F_{(\tilde{\theta}-\theta)}$ and $(H_{Diss})_n^{n+1}$ are dissipative terms. We now look at these terms in greater detail

Form of $(H_{Diss})_n^{n+1}$

We wish to state the conditions on the parameters required for $(H_{Diss})_n^{n+1}$ to be nonnegative. In almost all terms this seen clearly due to the parameter choices and inspection of (3.67). However, the terms of the form $|\nabla\mu_{\varepsilon h}^{n+k}|^2$, appear to have a mismatch of a

positive $k=1$ term and negative $k=0$. More precisely we have:

$$\frac{3\gamma-1-\omega}{2}\theta\Delta t|\nabla\mu_{\varepsilon h}^{n+1}|^2-\frac{1-\gamma+\omega}{2}\theta\Delta t|\nabla\mu_{\varepsilon h}^{n}|^2.$$

This seemingly unmatched term, can be always made positive when we consider the sum $\sum_n(H_{Diss})_n^{n+1}$, and one looks at successive timesteps. In particular, the comparison of the n-term at time $n=K$ and the $(n+1)$-term at time $n=(K-1)$ reads:

$$\frac{3\gamma-1-\omega}{2}\theta\Delta t|\nabla\mu_{\varepsilon h}^{K}|^2-\frac{1-\gamma+\omega}{2}\theta\Delta t|\nabla\mu_{\varepsilon h}^{K}|^2.$$

Choosing $\gamma\geq\frac{1+\omega}{2}$ causes the difference to remain nonnegative in the summation (see subsequent sections). We now deal with all other contributions of (3.67).

From the conditions gathered throughout Section 3.2.2, we see that $(H_{Diss})_n^{n+1}$ is nonnegative when the parameters $\alpha\in(\frac{1}{2},1)$, $\gamma\in(\frac{1}{2}+\omega,\frac{2}{3}-\omega)$ for $0<\omega\ll 1$, $\delta\in(0,\frac{1}{16})$ and $\theta\in(0,\frac{1}{2})$ and also when the following essential stability constraint on Δt is satisfied [81]:

$$\Delta t\approx Ch^{1+\frac{d}{2}}. \tag{3.68}$$

Note, this also gives the quantities $S(h)\Delta t=\mathcal{O}(h)$. For $d=2$ we obtain $T(h)^2\Delta t=\mathcal{O}(h^{2-2\xi})$, for any $\xi>0$ and for $d=3$ we obtain $T(h)^2\Delta t=\mathcal{O}(h^{\frac{3}{2}})$.

Form of $(H_{cons})_n^{n+1}$

The consistency term here (by adding and subtracting $F(\varphi_{\varepsilon h}^{n+\tilde{\theta}}), F(\varphi_{\varepsilon h}^{n+\theta})$) can be written as:

$$\begin{aligned}
&\int_\Omega(F(\varphi_{\varepsilon h}^{n+1})-F(\varphi_{\varepsilon h}^{n+\tilde{\theta}}))-F_\theta(\varphi_{\varepsilon h}^{n+\tilde{\theta}},\varphi_{\varepsilon h}^{n+1})(\varphi_{\varepsilon h}^{n+1}-\varphi_{\varepsilon h}^{n+\tilde{\theta}})\\
&+\int_\Omega(F(\varphi_{\varepsilon h}^{n+\tilde{\theta}})-F(\varphi_{\varepsilon h}^{n+\theta}))-F_{(\tilde{\theta}-\theta)}(\varphi_{\varepsilon h}^{n+\theta},\varphi_{\varepsilon h}^{n+\tilde{\theta}})(\varphi_{\varepsilon h}^{n+\tilde{\theta}}-\varphi_{\varepsilon h}^{n+\theta})\\
&+\int_\Omega(F(\varphi_{\varepsilon h}^{n+\theta})-F(\varphi_{\varepsilon h}^{n}))-F_\theta(\varphi_{\varepsilon h}^{n},\varphi_{\varepsilon h}^{n+\theta})(\varphi_{\varepsilon h}^{n+\theta}-\varphi_{\varepsilon h}^{n}).
\end{aligned}$$

There are several available approximations for F in this case which we can take for any accuracy, many more examples are given in [133]:

- Convex $(+)$ Concave $(-)$ splitting $f_*(a,b)=F'_+(b)+F'_-(a)$ - First order accurate, no consistency error.
- Midpoint approximation $f_*(a,b)=\frac{F(b)-F(a)}{b-a}$ - severe timestep restriction, no consistency error.

- Taylor expansion $f_*(a,b) = F'(a) + \frac{1}{2}F''(a)(b-a) + \frac{1}{3!}F'''(a)(b-a)^2$ - Second order accurate.

We consider hereafter that our discretisation is of a sufficient order to bound the consistency terms $(H_{cons})_n^{n+1}$, so they may be treated as negligible.

Form of the energy inequality

We have concluded the discussion for the terms on the left hand side of the energy inequality. We investigate the entire energy inequality, therefore we now consider the sum of the inequalities (3.38), (3.57) and (3.65) seeking an expression as follows for the full inequality:

$$E_\varepsilon(\varphi_{\varepsilon h}^{n+1}, \mu_{\varepsilon h}^{n+1}, \boldsymbol{v}_{\varepsilon h}^{n+1}) + (H_{Diss})_n^{n+1} \\ \leq E_\varepsilon(\varphi_{\varepsilon h}^{n}, \mu_{\varepsilon h}^{n}, \boldsymbol{v}_{\varepsilon h}^{n}) + H_{Rem}(|\boldsymbol{v}_{\varepsilon h}^n|, |\nabla\varphi_{\varepsilon h}^n|) + \frac{\theta\Delta t}{\alpha\eta}|f_h^{n+1}|^2, \quad (3.69)$$

where H_{Rem}, are the non dissipative terms and f_h^* are the given body forces. If this inequality holds for $n = 0, \ldots, K$ for some time $K \in \mathbb{N}$, then summing (3.69) over n we may write down an energy inequality. Given the conditions on parameters γ, α, θ (in particular (3.68)),

$$E_\varepsilon(\varphi_{\varepsilon h}^{K+1}, \mu_{\varepsilon h}^{K+1}, \boldsymbol{v}_{\varepsilon h}^{K+1}) + \sum_{n=0}^{K}(H_{Diss})_n^{n+1} \\ \leq E_\varepsilon(\varphi_{\varepsilon h}^{0}, \mu_{\varepsilon h}^{0}, \boldsymbol{v}_{\varepsilon h}^{0}) + \sum_{n=0}^{K} H_{Rem}(|\boldsymbol{v}_{\varepsilon h}^n|^2, |\nabla\varphi_{\varepsilon h}^n|^2) + \sum_{n=0}^{K}\frac{\theta\Delta t}{\alpha}|f_h^{n+1}|^2. \quad (3.70)$$

The aim from this analysis would to be to show that if $|\nabla\varphi_{\varepsilon h}^n|^2$ and $|\boldsymbol{v}_{\varepsilon h}^n|^2$ are bounded by a constant C, then at time $(n+1)\Delta t$

$$H_{Rem}(|\boldsymbol{v}_{\varepsilon h}^n|^2, |\nabla\varphi_{\varepsilon h}^n|^2) \leq C(1 + g_n(h,\varepsilon)\Delta t),$$

for some nonnegative valued function g_n. Showing this for each step, would enable us to make use of a discrete form of a Gronwall estimate, found in [70]: If,

$$E_\varepsilon(\varphi_{\varepsilon h}^{K+1}, \mu_{\varepsilon h}^{K+1}, \boldsymbol{v}_{\varepsilon h}^{K+1}) + \Delta t\sum_{n=0}^{K}(H_{Diss})_n^{n+1} \\ \leq E_\varepsilon(\varphi_{\varepsilon h}^{0}, \mu_{\varepsilon h}^{0}, \boldsymbol{v}_{\varepsilon h}^{0}) + \sum_{n=0}^{K} H_{Rem} + \Delta t\sum_{n=0}^{K} C|f_h^{n+1}|^2, \quad (3.71)$$

then,

$$E_\varepsilon(\varphi_{\varepsilon h}^{K+1}, \mu_{\varepsilon h}^{K+1}, \boldsymbol{v}_{\varepsilon h}^{K+1}) + \Delta t \sum_{n=0}^{K} (H_{Diss})_n^{n+1}$$
$$\leq E_\varepsilon(\varphi_{\varepsilon h}^0, \mu_{\varepsilon h}^0, \boldsymbol{v}_{\varepsilon h}^0) + \exp\Big(\Delta t \sum_{n=0}^{K} g_n(h,\varepsilon)\Big) \cdot \Big\{\Delta t \sum_{n=0}^{K+1} C|f_h^{n+1}|^2\Big\}. \quad (3.72)$$

For a stability result one would require the form of $g_n(h,\varepsilon) \leq C\frac{h^a}{\varepsilon^b}$, ideally with $a \geq b$. Unfortunately, the result of this $g_n(h,\varepsilon)$ we obtain is insufficient for a stability result of the required form, however we shall detail the exact result obtained and comment on the shortcomings.

Form of H_{Rem}

We assume for this section that the following inductive assumption holds:

$$|\boldsymbol{v}_{\varepsilon h}^n|^2 \leq C_n, \qquad \varepsilon|\nabla\varphi_{\varepsilon h}^n|^2 \leq D_n \quad (3.73)$$

for some constants C_n, D_n. We sum the right hand sides of the inequalities (3.38), (3.57), and (3.65), ignoring terms which have been previously been absorbed in the dissipation

term $(H_{Diss})_n^{n+1}$, or from the Navier-Stokes body force terms:

$$
\begin{aligned}
&\Bigg\{(S(h)\theta\Delta t)^2|\boldsymbol{v}_{\varepsilon h}^n|^2|\nabla\boldsymbol{v}_{\varepsilon h}^n|^2+\frac{2(T(h)\theta\Delta t)^2}{\varepsilon}\varepsilon|\nabla\varphi_{\varepsilon h}^n|^2|\nabla\mu_{\varepsilon h}^n|^2\\
&\quad+\frac{T(h)^2\theta\Delta t}{\omega\varepsilon}\varepsilon|\nabla\varphi_{\varepsilon h}^n|^2|\boldsymbol{v}_{\varepsilon h}^n|^2+\frac{T(h)^2\theta\Delta t}{2\omega\varepsilon}|\boldsymbol{v}_{\varepsilon h}^{n+\theta}|^2\varepsilon|\nabla\varphi_{\varepsilon}^n|^2\\
&\quad+\frac{(T(h)\theta\Delta t)^2}{\varepsilon}|\boldsymbol{v}_{\varepsilon h}^{n+\theta}|^2|\nabla\mu_{\varepsilon h}^{n+\theta}|^2\Bigg\}\\
&+\Bigg\{2\frac{(S(h)(\tilde\theta-\theta)\Delta t)^2}{2\delta}|\boldsymbol{v}_{\varepsilon h}^n|^2|\nabla\boldsymbol{v}_{\varepsilon h}^n|^2+\frac{(T(h)(\tilde\theta-\theta)\Delta t)^2}{\varepsilon}\varepsilon|\nabla\varphi_{\varepsilon h}^{n+\tilde\theta}|^2|\nabla\mu_{\varepsilon h}^{n+\tilde\theta}|^2\\
&\quad+\frac{(T(h)(\tilde\theta-\theta)\Delta t)^2}{\varepsilon}\Big(\frac{(\tilde\theta-\theta)^2}{2\delta(\delta\theta)^2}+1\Big)\varepsilon|\nabla\varphi_{\varepsilon h}^n|^2|\nabla\mu_{\varepsilon h}^n|^2\\
&\quad+\frac{T(h)^2(\tilde\theta-\theta)\Delta t}{2\omega\varepsilon}\varepsilon|\boldsymbol{v}_{\varepsilon h}^{n+\theta}|^2|\nabla\varphi_{\varepsilon h}^{n+\theta}|^2+\frac{T(h)^2(\tilde\theta-\theta)\Delta t}{\varepsilon\omega}\varepsilon|\boldsymbol{v}_{\varepsilon h}^{n+\theta}|^2|\nabla\varphi_{\varepsilon h}^{n+\tilde\theta}|^2\Bigg\}\\
&+\Bigg\{6(S(h)\theta\Delta t)^2|\boldsymbol{v}_{\varepsilon h}^n|^2|\nabla\boldsymbol{v}_{\varepsilon h}^n|^2+\frac{T(h)^2\theta\Delta t}{\omega\varepsilon}\varepsilon|\boldsymbol{v}_{\varepsilon h}^{n+\tilde\theta}|^2|\varphi_{\varepsilon h}^{n+\tilde\theta}|^2\\
&\quad+\frac{5(T(h)\theta\Delta t)^2}{\delta\varepsilon}\varepsilon|\varphi_{\varepsilon h}^n|^2|\mu_{\varepsilon h}^n|^2\\
&\quad+\frac{T(h)^2\theta\Delta t}{2\omega\varepsilon}|\boldsymbol{v}_{\varepsilon h}^{n+1}|^2\varepsilon|\nabla\varphi_{\varepsilon}^{n+\tilde\theta}|^2+\frac{(T(h)\theta\Delta t)^2}{\varepsilon}|\boldsymbol{v}_{\varepsilon h}^{n+1}|^2|\nabla\mu_{\varepsilon h}^{n+1}|^2\Bigg\}.
\end{aligned}
$$

We shall consider H_{Rem} by looking only at terms with order strictly less than $\mathcal{O}(\Delta t)$. These contributions, are those which cause the Gronwall estimate to grow at a worse rate than required for stability. Thus we use the stability assumption (3.68), and recall the definition of $S(h)$ and $T(h)$ from (3.23) and (3.25) to get:

$$
\begin{aligned}
&\Bigg\{\frac{T(h)^2\theta\Delta t}{\omega\varepsilon}\varepsilon|\nabla\varphi_{\varepsilon h}^n|^2|\boldsymbol{v}_{\varepsilon h}^n|^2+\frac{T(h)^2\theta\Delta t}{2\omega\varepsilon}|\boldsymbol{v}_{\varepsilon h}^{n+\theta}|^2\varepsilon|\nabla\varphi_{\varepsilon}^n|^2\Bigg\}\\
&+\Bigg\{\frac{T(h)^2(\tilde\theta-\theta)\Delta t}{2\varepsilon\omega}\varepsilon|\boldsymbol{v}_{\varepsilon h}^{n+\theta}|^2|\nabla\varphi_{\varepsilon h}^{n+\theta}|^2+\frac{T(h)^2(\tilde\theta-\theta)\Delta t}{\varepsilon\omega}\varepsilon|\boldsymbol{v}_{\varepsilon h}^{n+\theta}|^2|\nabla\varphi_{\varepsilon h}^{n+\tilde\theta}|^2\Bigg\}\\
&+\Bigg\{\frac{T(h)^2\theta\Delta t}{\omega\varepsilon}\varepsilon|\boldsymbol{v}_{\varepsilon h}^{n+\tilde\theta}|^2|\varphi_{\varepsilon h}^{n+\tilde\theta}|^2+\frac{T(h)^2\theta\Delta t}{2\omega\varepsilon}|\boldsymbol{v}_{\varepsilon h}^{n+1}|^2\varepsilon|\nabla\varphi_{\varepsilon}^{n+\tilde\theta}|^2\Bigg\}+\mathcal{O}(\Delta t).
\end{aligned}
\tag{3.74}
$$

To bound the functions $|\boldsymbol{v}_{\varepsilon h}^{n+k}|^2$, $k=\theta,\tilde\theta,1$ and $|\nabla\varphi_{\varepsilon h}^{n+l}|^2$, $l=\theta,\tilde\theta$ as functions of $|\boldsymbol{v}_{\varepsilon h}^n|^2$ and $|\nabla\varphi_{\varepsilon h}^n|^2$, we use the inequalities of Section 3.2.2. We begin with the first substep, and

use inequalities (3.31), (3.37), and the assumption (3.73) to define:

$$\begin{aligned} C_{n+\theta} = |\boldsymbol{v}_{\varepsilon h}^{n+\theta}|^2 &\leq |\boldsymbol{v}_{\varepsilon h}^{n}|^2 + \frac{T(h)^2\theta\Delta t}{\omega\varepsilon}\varepsilon|\nabla\varphi_{\varepsilon h}^{n}|^2|\boldsymbol{v}_{\varepsilon h}^{n}|^2 + \mathcal{O}(\Delta t) \\ &\leq C_n + \frac{T(h)^2\theta\Delta t}{\omega\varepsilon}C_nD_n, \\ D_{n+\theta} = \varepsilon|\nabla\varphi_{\varepsilon h}^{n+\theta}|^2 &\leq \varepsilon|\nabla\varphi_{\varepsilon h}^{n+\theta}|^2 + \frac{T(h)^2\theta\Delta t}{\varepsilon\omega}\varepsilon|\nabla\varphi_{\varepsilon h}^{n}|^2|\boldsymbol{v}_{\varepsilon h}^{n+\theta}|^2 + \mathcal{O}(\Delta t) \\ &\leq D_n + \frac{T(h)^2\theta\Delta t}{\varepsilon\omega}C_{n+\theta}D_n + \mathcal{O}(\Delta t). \end{aligned} \tag{3.75}$$

In a similar fashion we may define the constants using (3.44), (3.56), along with (3.75):

$$\begin{aligned} D_{n+\tilde{\theta}} &\leq D_{n+\theta} + \frac{T(h)^2(\tilde{\theta}-\theta)\Delta t}{\omega}C_{n+\theta}D_{n+\theta} + \mathcal{O}(\Delta t), \\ C_{n+\tilde{\theta}} &\leq C_{n+\theta} + \frac{T(h)^2(\tilde{\theta}-\theta)\Delta t}{\varepsilon\omega}C_{n+\theta}D_{n+\tilde{\theta}} + \mathcal{O}(\Delta t), \end{aligned} \tag{3.76}$$

and, from (3.63), (3.64), along with (3.76):

$$\begin{aligned} C_{n+1} &\leq C_{n+\tilde{\theta}} + \frac{T(h)^2\theta\Delta t}{\varepsilon\omega}C_{n+\tilde{\theta}}D_{n+\tilde{\theta}} + \mathcal{O}(\Delta t), \\ D_{n+1} &\leq D_{n+\tilde{\theta}} + \frac{T(h)^2\theta\Delta t}{\omega\varepsilon}C_{n+1}D_{n+\tilde{\theta}} + \mathcal{O}(\Delta t). \end{aligned} \tag{3.77}$$

In this way, we can now estimate $|\varphi_{\varepsilon h}^{n+1}|^2$ and $|\boldsymbol{v}_{\varepsilon h}^{n+1}|^2$ in terms of $|\varphi_{\varepsilon h}^{n}|^2$ and$|\boldsymbol{v}_{\varepsilon h}^{n}|^2$. One can see how through (3.77), (3.76) and (3.75), the expression $C_{n+1} + D_{n+1} \leq P(C_n + D_n)$ leads to a choice of sixth order polynomial P in $C_n + D_n$, to zeroth order in Δt. The coefficients of this polynomial can be bounded above by:

$$\begin{aligned} C_{n+1} + D_{n+1} \leq P(C_n + D_n) \leq (C_n + D_n)\left(1 + \sum_{i=1}^{5} A_i\Big(\frac{T(h)^2\Delta t}{\varepsilon}(C_n + D_n)\Big)^i\right) \\ + \mathcal{O}(\Delta t) \end{aligned}$$

for positive constants A_i. Let $C_n + D_n \leq C$, using the stability assumption (3.68) note that in two dimensions, for $0 < \xi \ll 1$

$$\frac{T(h)^2\Delta t}{\varepsilon} \leq C\frac{h^{2-2\xi}}{\varepsilon},$$

and in three dimensions,

$$\frac{T(h)^2\Delta t}{\varepsilon} \leq C\frac{h^{\frac{3}{2}}}{\varepsilon}.$$

Thus, as these decay for small h, the polynomial P is dominated by the first terms:

$$P(C_n + D_n) \leq (C_n + D_n)(1 + \bar{A}\frac{T(h)^2\theta\Delta t}{\varepsilon}(C_n + D_n)\Big) + \mathcal{O}(\Delta t)$$

for constant $\bar{A}$. We now define

$$g_n(h,\varepsilon) = \bar{A}\frac{T(h)^2}{\varepsilon}, \qquad \text{where} \qquad H_{Rem}(|\nabla\varphi_{\varepsilon h}|^2, |\boldsymbol{v}_{\varepsilon h}|^2) \leq C(1 + g_n(h,\varepsilon)\Delta t).$$

We finally observe that our Gronwall estimate (3.72) will be of the following form. Let $T = (K+1)\Delta t$. In two dimensions,

$$E_\varepsilon(\varphi_{\varepsilon h}^{K+1}, \mu_{\varepsilon h}^{K+1}, \boldsymbol{v}_{\varepsilon h}^{K+1}) + \Delta t\sum_{n=0}^{K}(H_{Diss})_n^{n+1} \\ \leq E_\varepsilon(\varphi_{\varepsilon h}^0, \mu_{\varepsilon h}^0, \boldsymbol{v}_{\varepsilon h}^0) + \exp\left(\bar{A}\frac{h^{-2\xi}}{\varepsilon}\right)\cdot\Big\{\Delta t\sum_{n=0}^{K+1} C|f_h^{n+1}|^2\Big\}, \quad (3.78)$$

and in three dimensions,

$$E_\varepsilon(\varphi_{\varepsilon h}^{K+1}, \mu_{\varepsilon h}^{K+1}, \boldsymbol{v}_{\varepsilon h}^{K+1}) + \Delta t\sum_{n=0}^{K}(H_{Diss})_n^{n+1} \\ \leq E_\varepsilon(\varphi_{\varepsilon h}^0, \mu_{\varepsilon h}^0, \boldsymbol{v}_{\varepsilon h}^0) + \exp\left(\bar{A}\frac{h^{-1}}{\varepsilon}\right)\cdot\Big\{\Delta t\sum_{n=0}^{K+1} C|f_h^{n+1}|^2\Big\}. \quad (3.79)$$

Thus refinement of numerical parameters will lead to blow up. The key idea to be taken from this section is that one may formulate the problem in terms of a discrete energy inequality. This energy (under the parameter choices of Section 3.2.3) is well behaved except for the coupling terms which link the Cahn-Hilliard and Navier-Stokes. We have simply bounded these terms individually here, but this is insufficient for Gronwall type estimates. However there is promise if one could consider differences of these terms. Unfortunately we were unable to write these in the required form (due to the fourth order nature of the Cahn-Hilliard equation). In the following remarks, we reflect on the shortcomings of this analysis and point out the origins of the suboptimality of the estimate.

Remark 3.2.6. *It is important to see that the result from the Gronwall inequality is not improved by taking a stronger stability condition than* (3.68)*. This is because the* Δt *appearing in* (3.72) *is compensated by summing over the total number of timesteps. Also in other fields it has been noted that the factor* $\frac{1}{\varepsilon}$ *appears naturally in Gronwall estimates, though there is work to create first order schemes which depend only polynomially (rather*

than expontially) on $\frac{1}{\varepsilon}$, see [48].

Remark 3.2.7. *We can identify precisely where the problem in the analysis presents itself. The error is due to the $\hat{b}(\cdot,\cdot,\cdot)$ terms which couple the Cahn-Hilliard and Navier-Stokes problems together. The treatment of the individual terms separately in each step leads to the above result. If one instead considers treating them in the pairs* (3.7) + (3.8)*,* (3.9) + (3.10) *and* (3.11) + (3.12)*, or even summing over all steps, then one may expect differences to appear. However the differences are difficult to work with due to the fourth order nature of the Cahn-Hilliard equation. There could also be scope for this theory to work for Navier-Stokes coupled to a second order equation (perhaps an Allen-Cahn type equation), but this is not considered here.*

Remark 3.2.8. *One may rewrite the coupling terms, and retain second order accuracy and solvability by exploiting the updates of $\varphi_{\varepsilon h}$ during the timestepping. For example, in* (3.8) *one may take the term $\hat{b}(\boldsymbol{v}_{\varepsilon h}^{n+\theta}, \varphi_{\varepsilon h}^{n}, \mu_{\varepsilon h}^{n+\theta})$ as opposed to $\hat{b}(\boldsymbol{v}_{\varepsilon h}^{n+\theta}, \varphi_{\varepsilon h}^{n+\theta}, \mu_{\varepsilon h}^{n+\theta})$. This retains accuracy so long as in* (3.9) *the term $\hat{b}(\boldsymbol{v}_{\varepsilon h}^{n+\tilde{\theta}}, \varphi_{\varepsilon h}^{n+\tilde{\theta}}, \mu_{\varepsilon h}^{n+\tilde{\theta}})$, and in* (3.12) *the term $\hat{b}(\boldsymbol{v}_{\varepsilon h}^{n+1}, \varphi_{\varepsilon h}^{n+\tilde{\theta}}, \mu_{\varepsilon h}^{n+1})$ are also inserted.*

This was investigated as the differences between terms within a step become more comparable as only one variable changes value over each timestep. However the resulting estimates also lead to difficulties due to terms arising being incomparable with the dissipation terms.

3.3 Extension to more than two phases

In order to deal with multiple phases we consider here, the following problem in (strong) form. We denote as in Chapter 2, the notation $\varphi_\varepsilon = (\varphi_\varepsilon^{(1)}, \dots, \varphi_\varepsilon^{(M)})$ and $\mu_\varepsilon = (\mu_\varepsilon^{(1)}, \dots, \mu_\varepsilon^{(M)})$ for the multi phase field variables.

Problem 3.3.1. Let $(2 \leq) M \in \mathbb{N}$, find $\{\boldsymbol{v}_\varepsilon(\boldsymbol{x},t), p_\varepsilon(\boldsymbol{x},t), \mu_\varepsilon^{(k)}(\boldsymbol{x},t), \varphi_\varepsilon^{(k)}(\boldsymbol{x},t)\}$ for all

$k = 1, \dots, M$, such that:

$$
\begin{aligned}
\partial_t \varphi_\varepsilon^{(k)} + \boldsymbol{v}_\varepsilon \cdot \nabla \varphi_\varepsilon^{(k)} &= \nabla \cdot \Big(\sum_{l=1}^{M} \mathcal{L}^{k,l} \nabla \mu_\varepsilon^{(l)} \Big), && \text{in } \Omega \times (0,T), \\
\mu_\varepsilon^{(k)} + \varepsilon \Delta \varphi_\varepsilon^{(k)} - \frac{1}{\varepsilon} \sum_{i<j} \partial_{\varphi_\varepsilon^{(k)}} \overline{w}_{i,j}(\varphi_\varepsilon) &= 0, && \text{in } \Omega \times (0,T), \\
\partial_t \boldsymbol{v}_\varepsilon - \eta \Delta \boldsymbol{v}_\varepsilon + \boldsymbol{v}_\varepsilon \cdot \nabla \boldsymbol{v}_\varepsilon + \nabla p_\varepsilon &= \boldsymbol{f} + \sum_{k=1}^{M} \mu_\varepsilon^{(k)} \nabla \varphi_\varepsilon^{(k)}, && \text{in } \Omega \times (0,T), \\
\nabla \cdot \boldsymbol{v}_\varepsilon &= 0, && \text{in } \Omega \times (0,T), \\
\boldsymbol{v}_\varepsilon &= \mathbf{g}, && \text{on } \partial\Omega \times [0,T], \\
\nabla \varphi_\varepsilon^{(k)} \cdot \boldsymbol{\nu}_\Omega &= 0, && \text{on } \partial\Omega \times [0,T], \\
\nabla \mu_\varepsilon^{(k)} \cdot \boldsymbol{\nu}_\Omega &= 0, && \text{on } \partial\Omega \times [0,T].
\end{aligned}
$$

We additionally denote $F(\varphi_\varepsilon) = \sum_{i<j} \overline{w}_{i,j}(\varphi_\varepsilon)$ to be the multiwell potential, and take a positive definite constant mobility matrix $\mathcal{L}^{(\cdot,\cdot)}$ (see Section 2.2.8 for choices of these functions).

The operator splitting we choose for Problem 3.3.1 is as follows. Define for $\alpha, \gamma \in [0,1]$

$$
\begin{cases}
\mathcal{F}_1(\boldsymbol{v}_\varepsilon, p_\varepsilon) & = -\alpha \Delta \boldsymbol{v}_\varepsilon + \nabla p_\varepsilon - \boldsymbol{f}, \\
\mathcal{F}_2(\boldsymbol{v}_\varepsilon, \varphi_\varepsilon, \mu_\varepsilon) & = -(1-\alpha) \Delta \boldsymbol{v}_\varepsilon + \boldsymbol{v}_\varepsilon \cdot \nabla \boldsymbol{v}_\varepsilon - \sum_{k=1}^{M} \mu_\varepsilon^{(k)} \nabla \varphi_\varepsilon^{(k)}.
\end{cases}
$$

$$
\begin{cases}
\mathcal{G}_1(\varphi_\varepsilon, \mu_\varepsilon, \boldsymbol{v}_\varepsilon) & = -\gamma \sum_{k=1}^{M} \nabla \cdot (\sum_{l=1}^{M} \mathcal{L}^{(k,l)} \nabla \mu_\varepsilon^{(k)}) + \boldsymbol{v}_\varepsilon \cdot \sum_{k=1}^{M} \nabla \varphi_\varepsilon^{(k)}, \\
\mathcal{G}_2(\mu_\varepsilon) & = -(1-\gamma) \sum_{k=1}^{M} \nabla \cdot (\sum_{l=1}^{M} \mathcal{L}^{(k,l)} \nabla \mu_\varepsilon^{(l)}).
\end{cases}
$$

The structure of the problem follows as in scheme (3.7) - (3.12). To demonstrate the similarity between the scheme for multi-phase flow and for 2 phase we shall write down the weak fully discrete formulation for the Cahn-Hilliard system in the first step.

For Step 1(b), the analogy of (3.33)-(3.34) is as follows. For $k = 1, \dots, M$, given $\varphi_h^{(k),n}, \mu_h^{(k),n}$ in H_h^1, $\boldsymbol{v}_{\varepsilon h}^n, \boldsymbol{v}_{\varepsilon h}^{n+\theta} \in V_h$, find $\varphi_h^{(k),n+\theta}, \mu_h^{(k),n+\theta} \in H_h^1$, such that $\forall \psi, \zeta \in H_h^1(\Omega_h)$,

$$\Big(\frac{\varphi_h^{(k),n+\theta}-\varphi_h^{(k),n}}{\theta\Delta t},\psi\Big)+\hat{b}(\boldsymbol{v}_{\varepsilon h}^{n+\theta},\varphi_h^{(k),n+\theta},\psi)+\gamma\sum_{l=1}^{M}\mathcal{L}^{(k,l)}(\nabla\mu_h^{(l),n+\theta},\nabla\psi)$$
$$=-(1-\gamma)\sum_{l=1}^{M}\mathcal{L}^{(k,l)}(\nabla\mu_h^{(l),n},\nabla\psi),$$
$$(\mu_h^{(l),n+\theta},\zeta)=\varepsilon(\nabla\varphi_h^{(l),n+\theta},\nabla\zeta)+\frac{1}{\varepsilon}(F_{l(\theta)}(\varphi_{\varepsilon h}^{n},\varphi_{\varepsilon h}^{n+\theta}),\zeta)$$

where $F_{l(\theta)}(\varphi_{\varepsilon h}^{n},\varphi_{\varepsilon h}^{n+\theta})$ is a discrete approximation in time of the derivative $\partial_{\varphi_{\varepsilon h}^{(l)}}F(\varphi_{\varepsilon h})$. For each equation indexed by k, we test with $\psi=\mu_h^{(k),n+\theta}$ and $\zeta=\varphi_h^{(k),n+\theta}-\varphi_h^{(k),n}$. Summing the M equations gives:

$$\varepsilon\sum_{k=1}^{M}(\nabla\varphi_h^{(k),n+\theta},\nabla\varphi_h^{(k),n+\theta}-\nabla\varphi_h^{(k),n})+\overbrace{\frac{1}{\varepsilon}\sum_{k=1}^{M}(F_{k(\theta)}(\varphi_{\varepsilon h}^{n},\varphi_{\varepsilon h}^{n+\theta}),\varphi_h^{(k),n+\theta}-\varphi_h^{(k),n})}^{(*)}$$
$$+\gamma\theta\Delta t\sum_{k,l=1}^{M}\mathcal{L}^{(k,l)}(\nabla\mu_h^{(l),n+\theta},\nabla\mu_h^{(k),n+\theta})$$
$$=-(1-\gamma)\theta\Delta t\sum_{k,l=1}^{M}\mathcal{L}^{(k,l)}(\nabla\mu_h^{(l),n+\theta},\nabla\mu_h^{(k),n+\theta})-\theta\Delta t\sum_{k=1}^{M}\hat{b}(\boldsymbol{v}_{\varepsilon h}^{n+\theta},\varphi_h^{(k),n+\theta},\mu_h^{(k),n+\theta}).$$

For a simple generalisation to multiple phases such as this, with a constant positive definite symmetric mobility matrix $\mathcal{L}^{(\cdot,\cdot)}$, there is not an increase in complexity of the system from two phases. The analysis follows identically to that of the two phase case, if one can show that the derivative of the multiwell potential F can be approximated by the term $(*)$ in a consistent way. This form however is a natural generalisation of the cases studied in [133] for the two phase potential.

3.4 Fractional-theta scheme for variable density CHNS problem

The extension to a variable density is a significant step regarding the analysis and simulation. This is due to delicate interplay between two seemingly opposed balance laws of the system, the conservation of mass for the fluid:

$$\partial_t\rho^{(i)}+\nabla\cdot(\rho^{(i)}\boldsymbol{v}^{(i)})=0\ \text{ in }\Omega^{(i)},\tag{3.80}$$

and the incompressibility of the fluid:

$$\nabla \cdot \boldsymbol{v}^{(i)} = 0 \text{ in } \Omega^{(i)}. \tag{3.81}$$

For the matched density $\rho^{(i)}(\boldsymbol{x}, t) \equiv C, \ \forall i = 1, \dots, M$ hence (3.80) and (3.81) are equivalent, thus enforcing (3.81) allows them to hold true. For the variable density $\rho_\varepsilon^{(i)}(\boldsymbol{x}, t)$, The system becomes heavily coupled if we solve for both conservations (3.80) and (3.81) strongly. Instead we enforce one constraint in the strong sense and the other in a weak sense.

To this end, we reflect the modelling in Section 2.2.1, which we summarise here briefly for convenience. We choose to enforce the divergence free constraint strongly; we take a solenoidal velocity (3.81) in the scheme. We then postulate a *volume averaged velocity* (2.107) for the motion of the fluid mixture, this then does not lead to mass conservation (3.80) for the total mass density (2.112), but instead (2.113):

$$\partial_t^{\bullet(\boldsymbol{v}_\varepsilon)} \rho + \rho \nabla \cdot \boldsymbol{v}_\varepsilon = -\nabla \cdot \overline{\boldsymbol{j}}_\varepsilon \quad \text{with } \overline{\boldsymbol{j}}_\varepsilon = \sum_{i=1}^{M} \overline{\rho}^{(i)} \boldsymbol{j}_{\varphi_\varepsilon^{(i)}}.$$

We take an admissible choice $\boldsymbol{j}_{\varphi_\varepsilon^{(k)}} = \sum_{l=1}^{M} \mathcal{L}^{(k,l)} \nabla \mu_\varepsilon^{(l)}$. We do not preseve the conservation of total mass of fluid in the diffuse model strongly, however the error is described by an explicit mass flux in divergence form. Thus the total mass density is completely determined by φ_ε, in fact recall, we take the linear interpolation $\rho(\varphi_\varepsilon) \coloneqq \sum_{i=1}^{M} \varphi_\varepsilon^{(i)} \overline{\rho}^{(i)}$. If we account for the extra flux $\overline{\boldsymbol{j}}_\varepsilon$ we may weakly conserve the density. It is encorporated into the momentum equation for the Navier-Stokes as in [1], by inserting an additional mass transport term of $\nabla \cdot (\boldsymbol{v}_\varepsilon \otimes \overline{\boldsymbol{j}}_\varepsilon)$.

3.4.1 Weak formulation and discretisation

Our weak formulation for the variable density Cahn-Hilliard Navier-Stokes is thus:

Problem 3.4.1. Given initial data $\{\boldsymbol{v}_{\varepsilon 0}, \varphi_{\varepsilon 0}\} \in (H_g^1(\Omega))^d \times H^1(\Omega)$ and $\boldsymbol{f} \in (L^2(\Omega))^d$, $\mathbf{g} \in (H^1(\Omega))^d$ find $\boldsymbol{v}_\varepsilon(\cdot, t) \in (H_g^1(\Omega))^d$, $p(\cdot, t) \in L^2(\Omega)/\mathbb{R}$ and $\varphi_\varepsilon(\cdot, t), \ \mu_\varepsilon(\cdot, t) \in H^1(\Omega)$

such that, for all $t \in [0,T]$

$$\begin{aligned}
\int_\Omega \zeta(\partial_t \varphi_\varepsilon + \boldsymbol{v}_\varepsilon \cdot \nabla \varphi_\varepsilon) &= -\int_\Omega \nabla \mu_\varepsilon \cdot \nabla \zeta, && \forall\, \zeta \in H^1(\Omega),\\
\int_\Omega \varepsilon \nabla \varphi_\varepsilon \cdot \nabla \zeta + \frac{1}{\varepsilon} F'(\varphi_\varepsilon)\zeta &= \int_\Omega \mu_\varepsilon \zeta, && \forall\, \zeta \in H^1(\Omega),\\
\int_\Omega \boldsymbol{\zeta}\rho \partial_t \boldsymbol{v}_\varepsilon + \boldsymbol{\zeta}(\rho \boldsymbol{v}_\varepsilon + \overline{\boldsymbol{j}}_\varepsilon)\cdot\nabla)\boldsymbol{v}_\varepsilon & \\
+ \int_\Omega \eta \nabla \boldsymbol{v}_\varepsilon \cdot \nabla \boldsymbol{\zeta} - p_\varepsilon \nabla \cdot \boldsymbol{\zeta} &= \int_\Omega \boldsymbol{\zeta} \boldsymbol{f} + \boldsymbol{\zeta}\mu_\varepsilon \nabla \varphi_\varepsilon, && \forall\, \boldsymbol{\zeta} \in (H^1(\Omega))^d,\\
\int_\Omega \zeta \nabla \cdot \boldsymbol{v}_\varepsilon &= 0, && \forall\, \zeta \in L^2(\Omega). \qquad (3.82)
\end{aligned}$$

Remark 3.4.2. *The form of incompressible Navier-Stokes in Problem 3.4.1 is based on a nonconservative strong formulation:*

$$\begin{aligned}
\rho \partial_t(\boldsymbol{v}_\varepsilon) + ((\rho \boldsymbol{v}_\varepsilon + \overline{\boldsymbol{j}}_\varepsilon)\cdot\nabla)\boldsymbol{v}_\varepsilon - \Delta \boldsymbol{v}_\varepsilon + \nabla p_\varepsilon &= \boldsymbol{f} + \mu_\varepsilon \nabla \varphi_\varepsilon,\\
\nabla \cdot \boldsymbol{v}_\varepsilon &= 0.
\end{aligned}$$

One could instead work directly from the more conservative form,

$$\begin{aligned}
\partial_t(\rho \boldsymbol{v}_\varepsilon) + \nabla \cdot ((\rho \boldsymbol{v}_\varepsilon + \overline{\boldsymbol{j}}_\varepsilon) \otimes \boldsymbol{v}_\varepsilon) - \Delta \boldsymbol{v}_\varepsilon + \nabla p_\varepsilon &= \boldsymbol{f} + \mu_\varepsilon \nabla \varphi_\varepsilon,\\
\nabla \cdot \boldsymbol{v}_\varepsilon &= 0.
\end{aligned}$$

however this will lead to a highly coupled system when coupled to the Cahn-Hillard equation. This is due to the fact that the density (a function $\rho = \rho(\varphi_\varepsilon)$) appears in the time derivative of the Navier-Stokes problem.

To overcome these difficulties, authors in [66] have used yet another formulation of Navier-Stokes, and ideas have been adopted in multi-phase flow in [95] where energy estimates for the scheme are exploited to obtain an unconditionally stable first order scheme. The chosen form is

$$\sqrt{\rho}\partial_t(\sqrt{\rho}\boldsymbol{v}_\varepsilon) + (\rho \boldsymbol{v}_\varepsilon \cdot \nabla)\boldsymbol{v}_\varepsilon + \frac{\boldsymbol{v}_\varepsilon}{2}\nabla \cdot (\rho \boldsymbol{v}_\varepsilon) - \Delta \boldsymbol{v}_\varepsilon + \nabla p_\varepsilon = \boldsymbol{f} + \mu_\varepsilon \nabla \varphi_\varepsilon,$$

where additional terms arise from the following energy equality

$$\frac{d}{dt}\int_\Omega \frac{1}{2}\rho |\boldsymbol{v}_\varepsilon|^2 = \int_\Omega \left[\sqrt{\rho}\partial_t(\sqrt{\rho}\boldsymbol{v}_\varepsilon) + (\rho \boldsymbol{v}_\varepsilon \cdot \nabla)\boldsymbol{v}_\varepsilon + \frac{\boldsymbol{v}_\varepsilon}{2}\nabla \cdot (\rho \boldsymbol{v}_\varepsilon)\right] \cdot \boldsymbol{v}_\varepsilon.$$

This is used in the Gauge-Uzawa type schemes of [100]. It is unclear how one may obtain higher accuracy from this scheme as this formulation introduces more nonlinearity into the

problem.

Mimicking the form of Section 3.1.2, we now write down our scheme for Problem 3.4.1. First define the operators for $\alpha, \gamma \in [0,1]$

$$\begin{cases} \mathcal{F}_1(\boldsymbol{v}_\varepsilon, p_\varepsilon) & = -\alpha\Delta\boldsymbol{v}_\varepsilon + \nabla p_\varepsilon - \boldsymbol{f}, \\ \mathcal{F}_2(\boldsymbol{v}_\varepsilon, \rho, \varphi_\varepsilon, \mu_\varepsilon) & = -(1-\alpha)\Delta\boldsymbol{v}_\varepsilon + ((\rho\boldsymbol{v}_\varepsilon + \overline{\boldsymbol{j}}_\varepsilon)\cdot\nabla)\boldsymbol{v}_\varepsilon - \mu_\varepsilon\nabla\varphi_\varepsilon. \end{cases} \tag{3.83}$$

$$\begin{cases} \mathcal{G}_1(\varphi_\varepsilon, \mu_\varepsilon, \boldsymbol{v}_\varepsilon) & = -\gamma\Delta\mu_\varepsilon + \boldsymbol{v}_\varepsilon\cdot\nabla\varphi_\varepsilon, \\ \mathcal{G}_2(\mu_\varepsilon) & = -(1-\gamma)\Delta\mu_\varepsilon. \end{cases} \tag{3.84}$$

The Cahn-Hilliard system is formed identically to (3.8), (3.9) and (3.12). The variable density Navier-Stokes has a different semi discrete abstract formulation in the place of (3.7), (3.10) and (3.11) respectively. The equations, in their place are given below and hold in a weak sense:

Step 1(a): Find $(\boldsymbol{v}_\varepsilon^{n+\theta}, p_\varepsilon^{n+\theta}) \in (H_g^1(\Omega))^d \times L^2(\Omega)$

$$\begin{aligned} \rho^n\frac{\boldsymbol{v}_\varepsilon^{n+\theta} - \boldsymbol{v}_\varepsilon^n}{\theta\Delta t} + \mathcal{F}_1(\boldsymbol{v}_\varepsilon^{n+\theta}, p_\varepsilon^{n+\theta}) &= -\mathcal{F}_2(\boldsymbol{v}_\varepsilon^n, \varphi_\varepsilon^n, \mu_\varepsilon^n), \\ \nabla\cdot\boldsymbol{v}_\varepsilon^{n+\theta} &= 0. \end{aligned} \tag{3.85}$$

Step 2(b): Find $(\boldsymbol{v}_\varepsilon^{n+\tilde{\theta}}) \in (H_g^1(\Omega))^d \times L^2(\Omega)$

$$\rho^{n+\tilde{\theta}}\frac{\boldsymbol{v}_\varepsilon^{n+\tilde{\theta}} - \boldsymbol{v}_\varepsilon^{n+\theta}}{(\tilde{\theta}-\theta)\Delta t} + \mathcal{F}_2(\boldsymbol{v}_\varepsilon^{n+\tilde{\theta}}, \varphi_\varepsilon^{n+\tilde{\theta}}, \mu_\varepsilon^{n+\tilde{\theta}}) = -\mathcal{F}_1(\boldsymbol{v}_\varepsilon^{n+\theta}, p_\varepsilon^{n+\theta}). \tag{3.86}$$

Step 3(a): Find $(\boldsymbol{v}_\varepsilon^{n+1}, p_\varepsilon^{n+1}) \in (H_g^1(\Omega))^d \times L^2(\Omega)$

$$\begin{aligned} \rho^{n+\tilde{\theta}}\frac{\boldsymbol{v}_\varepsilon^{n+1} - \boldsymbol{v}_\varepsilon^{n+\tilde{\theta}}}{\theta\Delta t} + \mathcal{F}_1(\boldsymbol{v}_\varepsilon^{n+1}, p_\varepsilon^{n+1}) &= -\mathcal{F}_2(\boldsymbol{v}_\varepsilon^{n+\tilde{\theta}}, \varphi_\varepsilon^{n+\tilde{\theta}}, \mu_\varepsilon^{n+\tilde{\theta}}), \\ \nabla\cdot\boldsymbol{v}_\varepsilon^{n+1} &= 0. \end{aligned} \tag{3.87}$$

This is not in the framework for the scheme we have previously investigated, as the density ρ^{n+*} cannot be absorbed into $\mathcal{F}_1$ and $\mathcal{F}_2$ by dividing through. This then requires us to show that the scheme is still of second order. It is however solvable and is still naturally coupled into the 6 linear stages. The nonlinearities that feature are as in the fixed density case stated in Section 3.1.2.

Remark 3.4.3. *As ρ^{n+*} no longer features in the time derivative of the fluid solvers, we anticipate that this may have an effect on the stability of the system. This will need to be*

considered in future investigation, but here we are only concerned with the consistency for variable density scheme.

3.4.2 Consistency analysis for the variable density scheme

We investigate the accuracy of the variable density scheme, by using the linear combinations in [36]. These allow us to compare unit step lengths and Taylor expansion comparisons with exact solutions to investigate the truncation error. Consider the following linear combination in variational form of the steps above over the time interval $[n\Delta t, (n+1)\Delta t]$:

$$\begin{aligned}&\Big\{\text{Step 1(a)+Step 1(b)}\Big\}\times\theta + \Big\{\text{Step 2(a)+Step 2(b)}\Big\}\times(\tilde{\theta}-\theta) + \Big\{\text{Step 3(a)+Step 3(b)}\Big\}\times\theta\\ &\quad\Longleftrightarrow \Big\{\text{(3.85)+(3.8)}\Big\}\times\theta + \Big\{\text{(3.9)+(3.86)}\Big\}\times(\tilde{\theta}-\theta) + \Big\{\text{(3.87)+(3.12)}\Big\}\times\theta.\end{aligned} \tag{3.88}$$

Compare these with the solution $(\boldsymbol{v}_\varepsilon, p_\varepsilon, \varphi_\varepsilon, \mu_\varepsilon)$ of the continuous problem evaluated at the midpoint of the interval $t^{n+\frac{1}{2}} = (n+\frac{1}{2})\Delta t$, by using Taylor expansions of the above about $t^{n+\frac{1}{2}}$. The midpoint is a sensible choice of evaluation for optimal low order term cancellation between the two schemes, and this is a typical choice for implicit-explicit schemes.

We first present the Taylor expansions for functions around the different substeps of the interval $[n\Delta t, (n+1)\Delta t]$ for convenience. We use the notation

$$g_t^{n+\frac{1}{2}} = \frac{\mathrm{d}g}{\mathrm{d}t}(t)\Big|_{t=t^{n+\frac{1}{2}}}, \qquad \text{and} \qquad g_{tt}^{n+\frac{1}{2}} = \frac{\mathrm{d}^2 g}{\mathrm{d}t^2}(t)\Big|_{t=t^{n+\frac{1}{2}}}$$

to represent the derivative of the solution function evaluated at the midpoint of the interval.

$$\begin{aligned}
g^n &= g^{n+\frac{1}{2}} - \frac{\Delta t}{2} g_t^{n+\frac{1}{2}} + \frac{(\Delta t)^2}{8} g_{tt}^{n+\frac{1}{2}} + \mathcal{O}((\Delta t)^3),\\
g^{n+\theta} &= g^{n+\frac{1}{2}} - \Big(\frac{1}{2}-\theta\Big)\Delta t g_t^{n+\frac{1}{2}} + \frac{1}{2}\Big(\frac{1}{2}-\theta\Big)^2 (\Delta t)^2 g_{tt}^{n+\frac{1}{2}} + \mathcal{O}((\Delta t)^3),\\
g^{n+\tilde{\theta}} &= g^{n+\frac{1}{2}} + \Big(\tilde{\theta}-\frac{1}{2}\Big)\Delta t g_t^{n+\frac{1}{2}} + \frac{1}{2}\Big(\tilde{\theta}-\frac{1}{2}\Big)^2 (\Delta t)^2 g_{tt}^{n+\frac{1}{2}} + \mathcal{O}((\Delta t)^3),\\
g^{n+1} &= g^{n+\frac{1}{2}} + \frac{\Delta t}{2} g_t^{n+\frac{1}{2}} + \frac{(\Delta t)^2}{8} g_{tt}^{n+\frac{1}{2}} + \mathcal{O}((\Delta t)^3).
\end{aligned}$$

The interests in the following analysis is for second order accuracy, therefore we truncate expansions after order $(\Delta t)^2$. We shall now deal with the linear combination terms. Firstly we deal with terms involving a time derivative.

Time derivative terms

We collect the terms with time derivatives from the linear combination (3.88), with test functions $\boldsymbol{\zeta} \in (H^1(\Omega))^d$ and $\zeta \in H^1(\Omega)$.

$$\Big(\frac{\rho^n \boldsymbol{v}^{n+\theta} - \rho^n \boldsymbol{v}^n}{\Delta t} + \frac{\rho^{n+\tilde{\theta}} \boldsymbol{v}^{n+1} - \rho^{n+\tilde{\theta}} \boldsymbol{v}^{n+\theta}}{\Delta t} - \rho^{n+\frac{1}{2}} \boldsymbol{v}_t^{n+\frac{1}{2}}, \boldsymbol{\zeta}\Big) + \Big(\frac{\varphi^{n+1} - \varphi^n}{\Delta t} - \varphi_t^{n+\frac{1}{2}}, \zeta\Big). \tag{3.89}$$

Evaluation of these terms individually with their Taylor expansions yields,

$$\begin{aligned}
\frac{\rho^n(\boldsymbol{v}^{n+\theta} - \boldsymbol{v}^n)}{\Delta t} &= \frac{1}{\Delta t}\Big(\rho^{n+\frac{1}{2}} - \frac{\Delta t}{2}\rho_t^{n+\frac{1}{2}} + \frac{(\Delta t)^2}{8}\rho_{tt}^{n+\frac{1}{2}}\Big) \\
&\qquad \cdot \Big((\boldsymbol{v}^{n+\frac{1}{2}} - (\frac{1}{2} - \theta)\Delta t \boldsymbol{v}_t^{n+\frac{1}{2}} + \frac{(\frac{1}{2} - \theta)^2(\Delta t)^2}{2}\boldsymbol{v}_{tt}^{n+\frac{1}{2}}) \\
&\qquad\quad - (\boldsymbol{v}^{n+\frac{1}{2}} - \frac{\Delta t}{2}\boldsymbol{v}_t^{n+\frac{1}{2}} + \frac{(\Delta t)^2}{8}\boldsymbol{v}_{tt}^{n+\frac{1}{2}})\Big) + \mathcal{O}(\Delta t^2) \\
&= \theta \rho^{n+\frac{1}{2}} \boldsymbol{v}_t^{n+\frac{1}{2}} - \frac{\theta \Delta t}{2}\rho_t^{n+\frac{1}{2}} \boldsymbol{v}_t^{n+\frac{1}{2}} \\
&\quad + \Big(\frac{(\frac{1}{2} - \theta)^2}{2} - \frac{1}{8}\Big)\Delta t \rho^{n+\frac{1}{2}} \boldsymbol{v}_{tt}^{n+\frac{1}{2}} + \mathcal{O}(\Delta t^2), \\
\frac{\rho^{n+\tilde{\theta}}(\boldsymbol{v}^{n+1} - \boldsymbol{v}^{n+\theta})}{\Delta t} &= \frac{1}{\Delta t}(\rho^{n+\frac{1}{2}} + (\tilde{\theta} - \frac{1}{2})\Delta t \rho_t^{n+\frac{1}{2}} + \frac{(\tilde{\theta} - \frac{1}{2})^2(\Delta t)^2}{2}\rho_{tt}^{n+\frac{1}{2}}) \\
&\qquad \cdot \Big((\boldsymbol{v}^{n+\frac{1}{2}} + \frac{\Delta t}{2}\boldsymbol{v}_t^{n+\frac{1}{2}} + \frac{(\Delta t)^2}{8}\boldsymbol{v}_{tt}^{n+\frac{1}{2}}) \\
&\qquad\quad - (\boldsymbol{v}^{n+\frac{1}{2}} - (\frac{1}{2} - \theta)\Delta t \boldsymbol{v}_t^{n+\frac{1}{2}} + \frac{(\frac{1}{2} - \theta)^2(\Delta t)^2}{2}\boldsymbol{v}_{tt}^{n+\frac{1}{2}})\Big) \\
&\qquad\quad + \mathcal{O}(\Delta t^2) \\
&= (1 - \theta)\rho^{n+\frac{1}{2}} \boldsymbol{v}_t^{n+\frac{1}{2}} - (\tilde{\theta} - \frac{1}{2})(1 - \theta)\Delta t \rho_t^{n+\frac{1}{2}} \boldsymbol{v}_t^{n+\frac{1}{2}} \\
&\quad + \Big(\frac{1}{8} - \frac{(\frac{1}{2} - \theta)^2}{2}\Big)\Delta t \rho^{n+\frac{1}{2}} \boldsymbol{v}_{tt}^{n+\frac{1}{2}} + \mathcal{O}(\Delta t^2).
\end{aligned}$$

Therefore, the first argument in (3.89) to second order is given by,

$$(\theta + (1 - \theta) - 1)\rho^{n+\frac{1}{2}} \boldsymbol{v}_t^{n+\frac{1}{2}} + (-\frac{\theta}{2} + (\tilde{\theta} - \frac{1}{2})(1 - \theta))\Delta t \rho_t^{n+\frac{1}{2}} \boldsymbol{v}_t^{n+\frac{1}{2}} + \mathcal{O}(\Delta t^2). \tag{3.90}$$

We notice that,

$$\theta \coloneqq 1 - \frac{\sqrt{2}}{2} \implies (3.90) = \mathcal{O}(\Delta t^2).$$

Considering the second term in (3.89) and we see it is clearly $\mathcal{O}(\Delta t^2)$ without dependence on the value of θ.

Spatial derivative terms

We repeat the above analysis, by taking spatial terms arising in the linear combination (3.88) and compare them with the operators acting on the exact solution evaluated at the midpoint of the interval. The resulting consistency error is given here:

$$
\begin{aligned}
&\Big(\theta(\mathcal{F}_1^{n+1}+\mathcal{F}_2^{n+\tilde{\theta}},\boldsymbol{\zeta})+(\tilde{\theta}-\theta)(\mathcal{F}_2^{n+\tilde{\theta}}+\mathcal{F}_1^{n+\theta},\boldsymbol{\zeta})+\theta(\mathcal{F}_1^{n+\theta}+\mathcal{F}_2^{n},\boldsymbol{\zeta})\\
&+\theta(\mathcal{G}_1^{n+1}+\mathcal{G}_2^{n+\tilde{\theta}},\zeta)+(\tilde{\theta}-\theta)(\mathcal{G}_2^{n+\tilde{\theta}}+\mathcal{G}_1^{n+\theta},\zeta)+\theta(\mathcal{G}_1^{n+\theta}+\mathcal{G}_2^{n},\zeta)\Big)\\
&-(\mathcal{F}^{n+\frac{1}{2}},\boldsymbol{\zeta})-(\mathcal{G}^{n+\frac{1}{2}},\zeta)\\
=\;&(\theta\mathcal{F}_1^{n+1}+\tilde{\theta}(\mathcal{F}_2^{n+\tilde{\theta}}+\mathcal{F}_1^{n+\theta})+\theta\mathcal{F}_2^{n}-(\mathcal{F}_1^{n+\frac{1}{2}}+\mathcal{F}_2^{n+\frac{1}{2}}),\boldsymbol{\zeta}) && (3.91)\\
&+(\theta\mathcal{G}_1^{n+1}+\tilde{\theta}(\mathcal{G}_2^{n+\tilde{\theta}}+\mathcal{G}_1^{n+\theta})+\theta\mathcal{G}_2^{n}-(\mathcal{G}_1^{n+\frac{1}{2}}+\mathcal{G}_2^{n+\frac{1}{2}}),\zeta) && (3.92)\\
=\;&(\theta\alpha\eta\nabla\boldsymbol{v}^{n+1}+\tilde{\theta}\alpha\eta\nabla\boldsymbol{v}^{n+\theta}-\alpha\eta\nabla\boldsymbol{v}^{n+\frac{1}{2}},\nabla\boldsymbol{\zeta}) && (3.93)\\
&+(\theta p^{n+1}+\tilde{\theta}p^{n+\theta}-p^{n+\frac{1}{2}},\nabla\cdot\boldsymbol{\zeta}) && (3.94)\\
&-(\theta f^{n+1}+\tilde{\theta}f^{n+\theta}-f^{n+\frac{1}{2}},\boldsymbol{\zeta}) && (3.95)\\
&+(\tilde{\theta}(1-\alpha)\eta\nabla\boldsymbol{v}^{n+\tilde{\theta}}+\theta(1-\alpha)\eta\nabla\boldsymbol{v}^{n}-(1-\alpha)\eta\nabla\boldsymbol{v}^{n+\frac{1}{2}},\nabla\boldsymbol{\zeta}) && (3.96)\\
&+\tilde{\theta}b(\rho^{n+\tilde{\theta}}\boldsymbol{v}^{n+\tilde{\theta}}+\overline{\boldsymbol{j}}^{n+\tilde{\theta}},\boldsymbol{v}^{n+\tilde{\theta}},\boldsymbol{\zeta})+\theta b(\rho^{n}\boldsymbol{v}^{n}+\overline{\boldsymbol{j}}^{n},\boldsymbol{v}^{n},\boldsymbol{\zeta})\\
&-b(\rho^{n+\frac{1}{2}}\boldsymbol{v}^{n+\frac{1}{2}}+\overline{\boldsymbol{j}}^{n+\frac{1}{2}},\boldsymbol{v}^{n+\frac{1}{2}},\boldsymbol{\zeta}) && (3.97)\\
&+\tilde{\theta}\hat{b}(\boldsymbol{\zeta},\varphi^{n+\tilde{\theta}},\mu^{n+\tilde{\theta}})+\theta\hat{b}(\boldsymbol{\zeta},\varphi^{n},\mu^{n})-\hat{b}(\boldsymbol{\zeta},\varphi^{n+\frac{1}{2}},\mu^{n+\frac{1}{2}}) && (3.98)\\
&+(\theta\gamma\nabla\mu^{n+1}+\tilde{\theta}\gamma\nabla\mu^{n+\theta}-\gamma\nabla\mu^{n+\frac{1}{2}},\nabla\zeta) && (3.99)\\
&+\theta b(\boldsymbol{v}^{n+1},\varphi^{n+1},\zeta)+\tilde{\theta}b(\boldsymbol{v}^{n+\theta},\varphi^{n+\theta},\zeta)-b(\boldsymbol{v}^{n+\frac{1}{2}},\varphi^{n+\frac{1}{2}},\zeta) && (3.100)\\
&+(\tilde{\theta}(1-\gamma)\nabla\mu^{n+\tilde{\theta}}+\theta(1-\gamma)\nabla\mu^{n}-(1-\gamma)\nabla\mu^{n+\frac{1}{2}},\nabla\zeta). && (3.101)
\end{aligned}
$$

We have written out (3.91) in a convenient grouping given by equations (3.93) – (3.98), (respectively (3.92) by the equations (3.99) – (3.100)). We will not consider every term given in the above expression, but candidate examples for the two types of difference.

First we consider the expression (3.93) + (3.96), note this is also a candidate for

terms (3.99) + (3.101). Expand terms about the midpoint of the interval:

$$
\begin{aligned}
&\alpha\eta(\theta\nabla\boldsymbol{v}^{n+1}+\tilde{\theta}\nabla\boldsymbol{v}^{n+\theta}-\nabla\boldsymbol{v}^{n+\frac{1}{2}})+(1-\alpha)\eta(\tilde{\theta}\nabla\boldsymbol{v}^{n+\tilde{\theta}}+\theta\nabla\boldsymbol{v}^{n}-\nabla\boldsymbol{v}^{n+\frac{1}{2}})\\
&=\alpha\eta\Big(\theta\nabla\Big(\boldsymbol{v}^{n+\frac{1}{2}}+\frac{\Delta t}{2}\boldsymbol{v}_t^{n+\frac{1}{2}}+\frac{(\Delta t)^2}{8}\boldsymbol{v}_{tt}^{n+\frac{1}{2}}\Big)+\tilde{\theta}\nabla\Big(\boldsymbol{v}^{n+\frac{1}{2}}-\Big(\frac{1}{2}-\theta\Big)\Delta t\boldsymbol{v}_t^{n+\frac{1}{2}}\\
&\qquad+\frac{1}{2}\Big(\frac{1}{2}-\theta\Big)^2(\Delta t)^2\boldsymbol{v}_{tt}^{n+\frac{1}{2}}\Big)-\nabla\boldsymbol{v}^{n+\frac{1}{2}}\Big)\\
&\quad+(1-\alpha)\eta\Big(\tilde{\theta}\Big(\boldsymbol{v}^{n+\frac{1}{2}}+\Big(\tilde{\theta}-\frac{1}{2}\Big)\Delta t\boldsymbol{v}_t^{n+\frac{1}{2}}+\frac{1}{2}\Big(\tilde{\theta}-\frac{1}{2}\Big)^2(\Delta t)^2\boldsymbol{v}_{tt}^{n+\frac{1}{2}}\Big)\\
&\qquad\qquad+\theta\Big(\boldsymbol{v}^{n+\frac{1}{2}}-\frac{\Delta t}{2}\boldsymbol{v}_t^{n+\frac{1}{2}}+\frac{(\Delta t)^2}{8}\boldsymbol{v}_{tt}^{n+\frac{1}{2}}\Big)-\nabla\boldsymbol{v}^{n+\frac{1}{2}}\Big)+\mathcal{O}(\Delta t^3)\\
&=\alpha\eta\Big(\Big(\frac{\theta}{2}-\tilde{\theta}\Big(\frac{1}{2}-\theta\Big)\Big)\Delta t\nabla\boldsymbol{v}_t^{n+\frac{1}{2}}+\frac{1}{2}\Big(\frac{\theta}{4}+\tilde{\theta}\Big(\frac{1}{2}-\theta\Big)^2\Big)(\Delta t)^2\nabla\boldsymbol{v}_{tt}^{n+\frac{1}{2}}\Big)\\
&\quad+(1-\alpha)\eta\Big(\tilde{\theta}\Big(\tilde{\theta}-\frac{1}{2}\Big)-\frac{\theta}{2}\Big)\Delta t\nabla\boldsymbol{v}_t^{n+\frac{1}{2}}+\frac{1}{2}\Big(\tilde{\theta}\Big(\theta-\frac{1}{2}\Big)^2+\frac{\theta}{4}\Big)(\Delta t)^2\nabla\boldsymbol{v}_{tt}^{n+\frac{1}{2}}\Big)\\
&\quad+\mathcal{O}(\Delta t^3),
\end{aligned}
$$

recalling that $\tilde{\theta}=1-\theta$ and so $(\frac{1}{2}-\theta)=(\tilde{\theta}-\frac{1}{2})$. We consider the form for the quadratic expressions in θ:

$$\frac{\theta}{2}-(1-\theta)\Big(\frac{1}{2}-\theta\Big)=2\theta^2-4\theta+1.$$

If $\theta=1-\frac{\sqrt{2}}{2}$, then $2\theta^2-4\theta+1=0$, and this is the only root in $(0,\frac{1}{2})$. With this choice of θ, we find that terms (3.93)+(3.96) yield a (second order) power series:

$$\Big(\frac{\eta}{2}\Big(\tilde{\theta}\Big(\theta-\frac{1}{2}\Big)^2+\frac{\theta}{4}\Big)\nabla\boldsymbol{v}_{tt}^{n+\frac{1}{2}},\boldsymbol{\zeta}\Big)(\Delta t)^2+\mathcal{O}(\Delta t^3).$$

We now consider the following (3.97), which is also a prototype for the terms (3.98) and

(3.100). Expand terms about the midpoint of the interval.

$$
\begin{aligned}
&\tilde{\theta}(\rho^{n+\tilde{\theta}}\boldsymbol{v}^{n+\tilde{\theta}}+\overline{\boldsymbol{j}}^{n+\tilde{\theta}})\cdot\nabla\boldsymbol{v}^{n+\tilde{\theta}}+\theta(\rho^{n}\boldsymbol{v}^{n}+\overline{\boldsymbol{j}}^{n})\cdot\nabla\boldsymbol{v}^{n}-(\rho^{n+\frac{1}{2}}\boldsymbol{v}^{n+\frac{1}{2}}+\overline{\boldsymbol{j}}^{n+\frac{1}{2}})\cdot\nabla\boldsymbol{v}^{n+\frac{1}{2}}\\
&=\tilde{\theta}\Big(\Big(\rho^{n+\frac{1}{2}}+\Big(\tilde{\theta}-\frac{1}{2}\Big)\Delta t\rho_t^{n+\frac{1}{2}}+\frac{1}{2}\Big(\tilde{\theta}-\frac{1}{2}\Big)^2(\Delta t)^2\rho_{tt}^{n+\frac{1}{2}}\Big)\\
&\qquad\cdot\Big(\boldsymbol{v}^{n+\frac{1}{2}}+\Big(\tilde{\theta}-\frac{1}{2}\Big)\Delta t\boldsymbol{v}_t^{n+\frac{1}{2}}+\frac{1}{2}\Big(\tilde{\theta}-\frac{1}{2}\Big)^2(\Delta t)^2\boldsymbol{v}_{tt}^{n+\frac{1}{2}}\Big)\\
&\qquad+\Big(\overline{\boldsymbol{j}}^{n+\frac{1}{2}}+\Big(\tilde{\theta}-\frac{1}{2}\Big)\Delta t\overline{\boldsymbol{j}}_t^{n+\frac{1}{2}}+\frac{1}{2}\Big(\tilde{\theta}-\frac{1}{2}\Big)^2(\Delta t)^2\overline{\boldsymbol{j}}_{tt}^{n+\frac{1}{2}}\Big)\Big)\\
&\qquad\cdot\nabla\Big(\boldsymbol{v}^{n+\frac{1}{2}}+\Big(\tilde{\theta}-\frac{1}{2}\Big)\Delta t\boldsymbol{v}_t^{n+\frac{1}{2}}+\frac{1}{2}\Big(\tilde{\theta}-\frac{1}{2}\Big)^2(\Delta t)^2\boldsymbol{v}_{tt}^{n+\frac{1}{2}}\Big)\Big)\\
&\quad+\theta\Big(\Big(\rho^{n+\frac{1}{2}}-\frac{\Delta t}{2}\rho_t^{n+\frac{1}{2}}+\frac{(\Delta t)^2}{8}\rho_{tt}^{n+\frac{1}{2}}\Big)\Big(\boldsymbol{v}^{n+\frac{1}{2}}-\frac{\Delta t}{2}\boldsymbol{v}_t^{n+\frac{1}{2}}+\frac{(\Delta t)^2}{8}\boldsymbol{v}_{tt}^{n+\frac{1}{2}}\Big)\\
&\qquad+\Big(\overline{\boldsymbol{j}}^{n+\frac{1}{2}}-\frac{\Delta t}{2}\overline{\boldsymbol{j}}_t^{n+\frac{1}{2}}+\frac{(\Delta t)^2}{8}\overline{\boldsymbol{j}}_{tt}^{n+\frac{1}{2}}\Big)\Big)\cdot\nabla\Big(\boldsymbol{v}^{n+\frac{1}{2}}-\frac{\Delta t}{2}\boldsymbol{v}_t^{n+\frac{1}{2}}+\frac{(\Delta t)^2}{8}\boldsymbol{v}_{tt}^{n+\frac{1}{2}}\Big)\\
&\quad-(\rho^{n+\frac{1}{2}}\boldsymbol{v}^{n+\frac{1}{2}}+\overline{\boldsymbol{j}}^{n+\frac{1}{2}})\cdot\nabla\boldsymbol{v}^{n+\frac{1}{2}}+\mathcal{O}(\Delta t^3)\\
&=\Delta t\Big(\tilde{\theta}\Big(\tilde{\theta}-\frac{1}{2}\Big)-\frac{\theta}{2}\Big)\Big((\rho_t^{n+\frac{1}{2}}\boldsymbol{v}^{n+\frac{1}{2}}+\rho^{n+\frac{1}{2}}\boldsymbol{v}_t^{n+\frac{1}{2}}+\overline{\boldsymbol{j}}_t^{n+\frac{1}{2}})\cdot\nabla\boldsymbol{v}^{n+\frac{1}{2}}\\
&\qquad\qquad+(\rho^{n+\frac{1}{2}}\boldsymbol{v}^{n+\frac{1}{2}}+\overline{\boldsymbol{j}})\cdot\nabla\boldsymbol{v}_t^{n+\frac{1}{2}}\Big)\\
&\quad+(\Delta t)^2\Big(\tilde{\theta}\Big(\tilde{\theta}-\frac{1}{2}\Big)^2+\frac{\theta}{4}\Big)\Big((\rho_t^{n+\frac{1}{2}}\boldsymbol{v}_t^{n+\frac{1}{2}}+\frac{1}{2}\rho_{tt}^{n+\frac{1}{2}}\boldsymbol{v}^{n+\frac{1}{2}}+\frac{1}{2}\rho^{n+\frac{1}{2}}\boldsymbol{v}_{tt}^{n+\frac{1}{2}})\cdot\nabla\boldsymbol{v}^{n+\frac{1}{2}}\\
&\qquad\qquad+(\rho_t^{n+\frac{1}{2}}\boldsymbol{v}^{n+\frac{1}{2}}+\rho^{n+\frac{1}{2}}\boldsymbol{v}_t^{n+\frac{1}{2}}+\overline{\boldsymbol{j}}_t^{n+\frac{1}{2}})\cdot\nabla\boldsymbol{v}_t^{n+\frac{1}{2}})\\
&\qquad\qquad+\frac{1}{2}(\rho^{n+\frac{1}{2}}\boldsymbol{v}^{n+\frac{1}{2}}+\overline{\boldsymbol{j}}^{n+\frac{1}{2}})\cdot\nabla\boldsymbol{v}_{tt}^{n+\frac{1}{2}}\Big)+\mathcal{O}(\Delta t^3).
\end{aligned}
$$

If $\theta=1-\frac{\sqrt{2}}{2}$, then $\tilde{\theta}\Big(\tilde{\theta}-\frac{1}{2}\Big)-\frac{\theta}{2}=0$, and we get the following second order power series from (3.97):

$$
\begin{aligned}
&\Big(\Big(\tilde{\theta}\Big(\tilde{\theta}-\frac{1}{2}\Big)^2+\frac{\theta}{4}\Big)\Big((\rho_t^{n+\frac{1}{2}}\boldsymbol{v}_t^{n+\frac{1}{2}}+\frac{1}{2}\rho_{tt}^{n+\frac{1}{2}}\boldsymbol{v}^{n+\frac{1}{2}}+\frac{1}{2}\rho^{n+\frac{1}{2}}\boldsymbol{v}_{tt}^{n+\frac{1}{2}})\cdot\nabla\boldsymbol{v}^{n+\frac{1}{2}}\\
&\qquad\qquad+(\rho_t^{n+\frac{1}{2}}\boldsymbol{v}^{n+\frac{1}{2}}+\rho^{n+\frac{1}{2}}\boldsymbol{v}_t^{n+\frac{1}{2}}+\overline{\boldsymbol{j}}_t^{n+\frac{1}{2}})\cdot\nabla\boldsymbol{v}_t^{n+\frac{1}{2}})\\
&\qquad\qquad+\frac{1}{2}(\rho^{n+\frac{1}{2}}\boldsymbol{v}^{n+\frac{1}{2}}+\overline{\boldsymbol{j}}^{n+\frac{1}{2}})\cdot\nabla\boldsymbol{v}_{tt}^{n+\frac{1}{2}}\Big),\boldsymbol{\zeta}\Big)(\Delta t)^2+\mathcal{O}((\Delta t)^3).
\end{aligned}
$$

Other terms are either of an identical form to these prototype calculations, or they are simpler than those considered and so can be treated similarly as the terms already considered. We conclude with the following:

Theorem 3.4.4. The numerical scheme for the Problem 3.4.1 with steps 1a, 2b, 3a defined by (3.85), (3.86), (3.87) and steps 1b, 2a, 3b defined by (3.8), (3.9), (3.12), and operator

splitting given by (3.83), (3.84) is of second order accuracy with respect to the timestep, if

$$\theta = 1 - \frac{\sqrt{2}}{2}.$$

3.5 Extension for inclusion of surfactants

In Chapter 4 we implement the full model for multi-phase flow with surfactant derived in 2.1.9. The precise setup of these simulations will be described in Section 4.3.3 and Section 4.4 where they are used. Here we shall detail how the surfactants are encorporated into the numerical scheme in the case of the quadratic isotherm seen in Section 2.1.11, which we use in implementation. This can be extended for other isotherm choices however the quadratic isotherm allows us to deal with linear equations.

We see that the scheme allows for the insertion of the surfactant flow equation in a way that does not disrupt the second order accuracy of the scheme. By inserting the definition of the isotherm into the governing equations (2.177)-(2.178) for the surfactant in the M phase diffuse interface model, we obtain:

$$\partial_t^{\bullet(\boldsymbol{v}_\varepsilon)}\Big(\Big(\sum_i^M \frac{\xi_i}{\beta_i} + \sum_{i<j}^M \frac{\delta_{i,j}}{\beta_{i,j}}\Big) q_\varepsilon\Big) = \nabla \cdot \Big(\Big(\sum_i^M \xi_i M_c^{(i)} + \sum_{i<j}^M \delta_{i,j} M_c^{(i,j)}\Big)\nabla q_\varepsilon\Big), \quad (3.102)$$

for positive constants $\beta_i, \beta_{i,j}$. For brevity, we define

$$\Xi_\beta(\varphi_\varepsilon) = \sum_i^M \frac{\xi_i(\varphi_\varepsilon^{(i)})}{\beta_i} + \sum_{i<j}^M \frac{\delta_{i,j}(\varphi_\varepsilon, \nabla\varphi_\varepsilon)}{\beta_{i,j}},$$
$$\Xi_c(\varphi_\varepsilon) = \sum_i^M \xi_i(\varphi_\varepsilon^{(i)}) M_c^{(i)} + \sum_{i<j}^M \delta_{i,j}(\varphi_\varepsilon, \nabla\varphi_\varepsilon) M_c^{(i,j)}.$$

We integrate (3.102) against a test function and then, extending from Problem 3.4.1 for $M = 2$ phases, we state the following weak problem:

Problem 3.5.1. Given initial data $\{\boldsymbol{v}_{\varepsilon 0}, \varphi_{\varepsilon 0}, q_{\varepsilon 0}\} \in (H_g^1(\Omega))^d \times H^1(\Omega) \times H^1(\Omega)$ and $\boldsymbol{f} \in (L^2(\Omega))^d$, $\mathbf{g_1} \in (H^1(\Omega))^d$ and $g_2 \in H^1(\Omega)$, find $\boldsymbol{v}_\varepsilon(\cdot, t) \in (H_{g_1}^1(\Omega))^d$, $p(\cdot, t) \in L^2(\Omega)/\mathbb{R}$

and $\varphi_\varepsilon(\cdot,t),\ \mu_\varepsilon(\cdot,t) \in H^1(\Omega)$ and $q \in H^1_{g_2}(\Omega)$ such that, for all $t \in [0,T]$

$$\begin{aligned}
\int_\Omega \zeta(\partial_t \varphi_\varepsilon + \boldsymbol{v}_\varepsilon \cdot \nabla \varphi_\varepsilon) &= -\int_\Omega \nabla \mu_\varepsilon \cdot \nabla \zeta, && \forall\, \zeta \in H^1(\Omega),\\
\int_\Omega \varepsilon \nabla \varphi_\varepsilon \cdot \nabla \zeta + \frac{1}{\varepsilon} F'(\varphi_\varepsilon)\zeta &= \int_\Omega \mu_\varepsilon \zeta, && \forall\, \zeta \in H^1(\Omega),\\
\int_\Omega \zeta(\partial_t(\Xi_\beta q_\varepsilon) + \boldsymbol{v}_\varepsilon \cdot \nabla(\Xi_\beta q_\varepsilon)) &= \int \Xi_c \nabla q_\varepsilon \cdot \nabla \zeta, && \forall \zeta \in H^1(\Omega),\\
\int_\Omega \boldsymbol{\zeta}\rho\partial_t \boldsymbol{v}_\varepsilon + \boldsymbol{\zeta}(\rho \boldsymbol{v}_\varepsilon + \overline{\boldsymbol{j}}_\varepsilon)\cdot\nabla)\boldsymbol{v}_\varepsilon & \\
+ \int_\Omega \eta \nabla \boldsymbol{v}_\varepsilon \cdot \nabla \boldsymbol{\zeta} - p_\varepsilon \nabla \cdot \boldsymbol{\zeta} &= \int_\Omega \boldsymbol{\zeta}\boldsymbol{f} + \boldsymbol{\zeta}\mu_\varepsilon \nabla \varphi_\varepsilon, && \forall\, \boldsymbol{\zeta} \in (H^1(\Omega))^d,\\
\int_\Omega \zeta \nabla \cdot \boldsymbol{v}_\varepsilon &= 0, && \forall\, \zeta \in L^2(\Omega). \qquad (3.103)
\end{aligned}$$

To discretise this problem in time we wish to follow similar extensions to the fractional-theta scheme framework as seen in Section 3.4.1. We use the strong form notation to write the problem in terms of abstract operators. We take the operators $\mathcal{F}_1, \mathcal{F}_2$ from (3.83) for the fluid equations and operators $\mathcal{G}_1, \mathcal{G}_2$ from (3.84) for the phase field equations. For simplicity we assume that the mobilities in the Cahn-Hilliard equations are constant. We additionally construct the operators $\mathcal{H}_1, \mathcal{H}_1$ as follows for the surfactant equations, for $\omega \in [0,1]$

$$\begin{cases} \mathcal{H}_1(q_\varepsilon, \Xi_\beta, \Xi_c, \boldsymbol{v}_\varepsilon) &= \omega \nabla \cdot (\Xi_c \nabla q_\varepsilon) + \boldsymbol{v}_\varepsilon \cdot \nabla(\Xi_\beta \nabla q_\varepsilon), \\ \mathcal{H}_2(q_\varepsilon, \Xi_c) &= -(1-\omega)\nabla \cdot (\Xi_c \nabla q_\varepsilon). \end{cases} \qquad (3.104)$$

We then extend the system detailed in 3.4.1 in the following manner.

- **Step 1**
  - **(a)** We solve the variable density Stokes problem (3.85).
  - **(b)** We solve the surfactant equation (3.105).
  - **(c)** We solve the Cahn-Hilliard problem (3.8).
- **Step 2**
  - **(a)** We solve the Cahn-Hilliard problem (3.9).
  - **(b)** We solve the surfactant equation (3.106).
  - **(c)** we solve the variable density Stokes problem (3.86).
- **Step 3**
  - **(a)** We solve the variable density Stokes problem (3.87).

– **(b)** We solve the surfactant equation (3.107).

– **(c)** We solve the Cahn-Hilliard problem (3.12).

We use the shortening $\Xi_*^n = \Xi_*(\varphi_\varepsilon^n)$ and write the surfactant equations with respect to the operators $\mathcal{H}_1$ and $\mathcal{H}_2$ as follows:
Step 1(b): Find $q_\varepsilon^{n+\theta} \in H^1_{g_2}(\Omega)$

$$\Xi_\beta^n \frac{q_\varepsilon^{n+\theta} - q_\varepsilon^n}{\theta \Delta t} + \mathcal{H}_1(q_\varepsilon^{n+\theta}, \Xi_\beta^n, \Xi_c^n, \boldsymbol{v}_\varepsilon^{n+\theta}) = -\mathcal{H}_2(q_\varepsilon^n, \Xi_c^n). \tag{3.105}$$

Step 2(b): Find $q_\varepsilon^{n+\tilde{\theta}} \in H^1_{g_2}(\Omega)$

$$\Xi_\beta^{n+\tilde{\theta}} \frac{q_\varepsilon^{n+\tilde{\theta}} - q_\varepsilon^{n+\theta}}{(\tilde{\theta} - \theta)\Delta t} + \mathcal{H}_2(q_\varepsilon^{n+\tilde{\theta}}, \Xi_c^{n+\tilde{\theta}}) = -\mathcal{H}_1(q_\varepsilon^{n+\theta}, \Xi_\beta^{n+\tilde{\theta}}, \Xi_c^{n+\tilde{\theta}}, \boldsymbol{v}_\varepsilon^{n+\theta}). \tag{3.106}$$

Step 3(b): Find $q_\varepsilon^{n+\tilde{\theta}} \in H^1_{g_2}(\Omega)$

$$\Xi_\beta^{n+\tilde{\theta}} \frac{q_\varepsilon^{n+1} - q_\varepsilon^{n+\tilde{\theta}}}{\theta \Delta t} + \mathcal{H}_1(q_\varepsilon^{n+1}, \Xi_\beta^{n+\tilde{\theta}}, \Xi_c^{n+\tilde{\theta}}, \boldsymbol{v}_\varepsilon^{n+1}) = -\mathcal{H}_2(q_\varepsilon^{n+\tilde{\theta}}, \Xi_c^{n+\tilde{\theta}}). \tag{3.107}$$

The scheme is solvable, and none of the steps are strongly coupled. The linearity is no worse than that of the variable density Cahn-Hilliard Navier-Stokes scheme. We still retain the same ordering of the equations as before, so the velocities which are used by the surfactant and Cahn-Hilliard equations are always divergence free. This allows us to perform integration by parts on the transport terms. In practice we solve the equations by substituting the transport term in implementation with using the following identity:

$$\int_\Omega \boldsymbol{v}_\varepsilon \cdot \nabla(\Xi_\beta q_\varepsilon)\zeta = -\int_\Omega \Xi_\beta q_\varepsilon \boldsymbol{v}_\varepsilon \cdot \nabla \zeta,$$

we have also used the boundary condition $\boldsymbol{v}_\varepsilon \cdot \nu_\Omega = 0$. This is more convenient in practice as in discretisation we take $\varphi_\varepsilon^{(k)} \in H^1(\Omega_h)$, and so do not wish to compute second derivatives of φ_ε.

In fact this scheme retains the second order accuracy. This can be seen by taking the linear combination (3.88) for the current scheme. In the notation of Section 3.4.2, we compare with the midpoint of the interval we arrive at the expression:

$$(3.89) + \Big(\Xi_\beta^n \frac{q^{n+\theta} - q^n}{\Delta t} + \Xi_\beta^{n+\tilde{\theta}} \frac{q^{n+1} - q^{n+\theta}}{\Delta t} - \Xi_\beta^{n+\frac{1}{2}} q_t^{n+\frac{1}{2}}, \zeta\Big).$$

This uses an identical discretisation as taken with $\partial_t(\rho \boldsymbol{v}_\varepsilon)$ and can be dealt with as shown in the calculation directly following the statement of expression (3.89). The other terms are

as follows

$$
\begin{aligned}
&\theta(\mathcal{H}_1^{n+1} + \mathcal{H}_2^{n+\tilde{\theta}}, \zeta) + (\tilde{\theta} - \theta)(\mathcal{H}_2^{n+\tilde{\theta}} + \mathcal{H}_1^{n+\theta}, \zeta) + \theta(\mathcal{H}_1^{n+\theta} + \mathcal{H}_2^{n}, \zeta) \\
&- (\mathcal{H}^{n+\frac{1}{2}}, \zeta) \\
&= \omega(\theta \Xi_c^{n+\tilde{\theta}} \nabla q^{n+1} + (\tilde{\theta} - \theta)\Xi_c^{n+\tilde{\theta}} \nabla q^{n+\theta} + \theta \Xi_c^{n} \nabla q^{n+\theta} - \Xi_c^{n+\frac{1}{2}} \nabla q^{n+\frac{1}{2}}, \nabla \zeta) \\
&\quad + (1-\omega)(\tilde{\theta} \Xi_c^{n+\tilde{\theta}} \nabla q^{n+\tilde{\theta}} + \theta \Xi_c^{n} \nabla q^{n} - \Xi_c^{n+\frac{1}{2}} \nabla q^{n+\frac{1}{2}}, \nabla \zeta) \\
&\quad - \big((\theta \Xi_\beta^{n+\tilde{\theta}} (\boldsymbol{v} \cdot \nabla q)^{n+1} + (\tilde{\theta} - \theta)\Xi_\beta^{n+\tilde{\theta}} (\boldsymbol{v} \cdot \nabla q)^{n+\theta} + \theta \Xi_\beta^{n} (\boldsymbol{v} \cdot \nabla q)^{n+\theta}, \nabla \zeta) \\
&\qquad - \Xi_\beta^{n+\frac{1}{2}} (\boldsymbol{v} \cdot \nabla q)^{n+\frac{1}{2}}, \nabla \zeta) \big).
\end{aligned}
$$

We can show that each set of grouped terms is $\mathcal{O}((\Delta t)^2)$ using the techniques of Section 3.4.2 if condition $\theta = 1 - \frac{\sqrt{2}}{2}$ holds. Therefore, we have shown:

Proposition 3.5.1. The numerical scheme for the Problem 3.5.1 with steps 1a, 2c, 3a defined by (3.85), (3.86), (3.87), steps 1c, 2a, 3c defined by (3.8), (3.9), (3.12), and steps 1b, 2b, 3b defined by (3.105), (3.106), (3.107), the operator splitting given by (3.83), (3.84), (3.104) is of second order accuracy with respect to the timestep, if

$$\theta = 1 - \frac{\sqrt{2}}{2}.$$

Chapter 4

Numerical Results

4.1 Preliminaries

This chapter is comprised of several self contained sections, each detailing the motivation, setup, presentation and discussion of a particular computational test series. These simulations are used both to validate results that have been discussed earlier in the thesis, and to demonstrate the performance and flexibility of the code package that has been written.

There are two types of convergence of interest, one with respect to scheme parameters Δt and h, and one with respect to the modelling parameter ε. More precisely, the numerical scheme should display numerical convergence to the diffuse interface model when temporal and spatial grids are reduced, this will demonstrate the results proved in Chapter 3. We should also obtain the convergence to the sharp interface model as $\varepsilon \to 0$, this will computationally verify the theoretical results of Section 2.2. We are interested in the rate at which solutions converge with respect to these parameters and account for this by calculating experimental orders of convergence (EOCs).

Let x_{true} be a solution to the problem of interest and let x_{η_i} be calculated solutions to an approximating problem dependent on a finite parameter sequence $(\eta_i)_{i=0}^N$ satisfying $\eta_i = \frac{\eta_{i-1}}{k_i}$ for $i = 1, \dots, N$, and k_i reduction parameter. The estimated order of convergence in the norm $\|\cdot\|_*$ with respect to η_i is given for $i = 1, \dots, N$:

$$*\text{-EOC}(\eta_i) = \log_{k_i}\left(\frac{\|x_{\eta_{i-1}} - x_{\text{true}}\|_*}{\|x_{\eta_i} - x_{\text{true}}\|_*}\right). \tag{4.1}$$

The meaning of the value of (4.1) can be seen clearly when one takes $f(\eta) \coloneqq \|x_\eta - x_{\text{true}}\|_*$ and considers the ansatz $f(\eta) \approx C\eta^p$ for C independent of η. Evaluating (4.1) under this assumption leads to $*\text{-EOC}(\eta_i) = p$, and so in this case it would yield exactly the order of convergence.

The choice of norm will be made depending on the test we are considering. One choice is for the norm $*$ in (4.1) to be l^p. We use this norm when we will be comparing different scalar functions which are evaluated along a 1D interval as in Section 4.3.1 for the surfactant potential q. For a finite data sample $y = (y_i)_{i=1}^N = (f(x_i))_{i=1}^N$,

$$\|y\|_{l^\infty} = \max_{i=1,\dots,N}(y_i), \qquad \|y\|_{l^p} = \Big(\sum_{i=1}^N y_i^p\Big)^{\frac{1}{p}}. \tag{4.2}$$

Another choice of norm $*$ for comparison of the full discrete solutions, is the discrete L_h^2 norm for vector valued functions (recall (3.19)). For the comparing the phase field solutions, we will consider the following norm, which acts as a way of summarising the norms for each of the individual component fields. Consider a function $\mathbf{f}\colon \Omega \to \mathbb{R}^M$ with decomposition $\mathbf{f} = (\mathbf{f}_i)_{i=1}^M$ for $\mathbf{f}_i \in H^1(\Omega)$ a $\Omega \subset \mathbb{R}^d$, then we use the following shorthand:

$$\|\mathbf{f}\|_{\hat{L}_h^{2,M}} = \sum_{i=1}^M \|\mathbf{f}_i\|_{L^2(\Omega)}, \qquad \text{and} \qquad \|\nabla \mathbf{f}\|_{\hat{L}_h^{2,d\times M}} = \sum_{i=1}^M \|\nabla \mathbf{f}_i\|_{L^2(\Omega,\mathbb{R}^d)}. \tag{4.3}$$

We emphasise the difference here from considering the norms which are used for the velocities. The norm for velocities was defined in Section 3.2.1 and treat the velocity as a quantity of interest, and not as a collection of components. For a function $\mathbf{w}\colon \Omega \to \mathbb{R}^d$:

$$|\mathbf{w}| = \|\mathbf{w}\|_{L^2(\Omega,\mathbb{R}^d)} \qquad \text{and} \qquad |\nabla \mathbf{w}| = \|\nabla \mathbf{w}\|_{L^2(\Omega,\mathbb{R}^{d\times d})}. \tag{4.4}$$

The norms are equivalent as they are only finite dimensional, however the separate treatment of the phase fields and velocity can be seen throughout in the way the equations are constructed. The velocity equations are constructed for the velocity vector field, whereas the phase field equations have been set up for the individual components. Having different choices do not affect the rates of convergence, but are the most natural quantities to consider.

For $\varepsilon \to 0$ convergence studies of diffuse interface approximations, we choose the discretised solution of the sharp interface problem to be a true solution x_{true} of the discrete problem. For numerical convergence studies we typically take a very fine resolution respect to the parameter of interest and consider this to be a reference solution for the discrete problem x_h^{ref}.

In Section 4.2 we first present the consistency result for the scheme, showing that in practice we acheive second order accuracy in time, we also comment on the stability of the scheme in practice. In Section 4.3.1 we shall establish the convergence of solutions of the diffuse interface model to the sharp interface model, with particular consideration to

surfactant effects. Finally, in Section 4.4, we demonstrate the flexibility of the scheme to a more complex problem, a 3D simulation of a three phase flow with different densities, viscosities and in the presence of surfactant.

4.2 Second order accuracy in time of the fractional-theta scheme

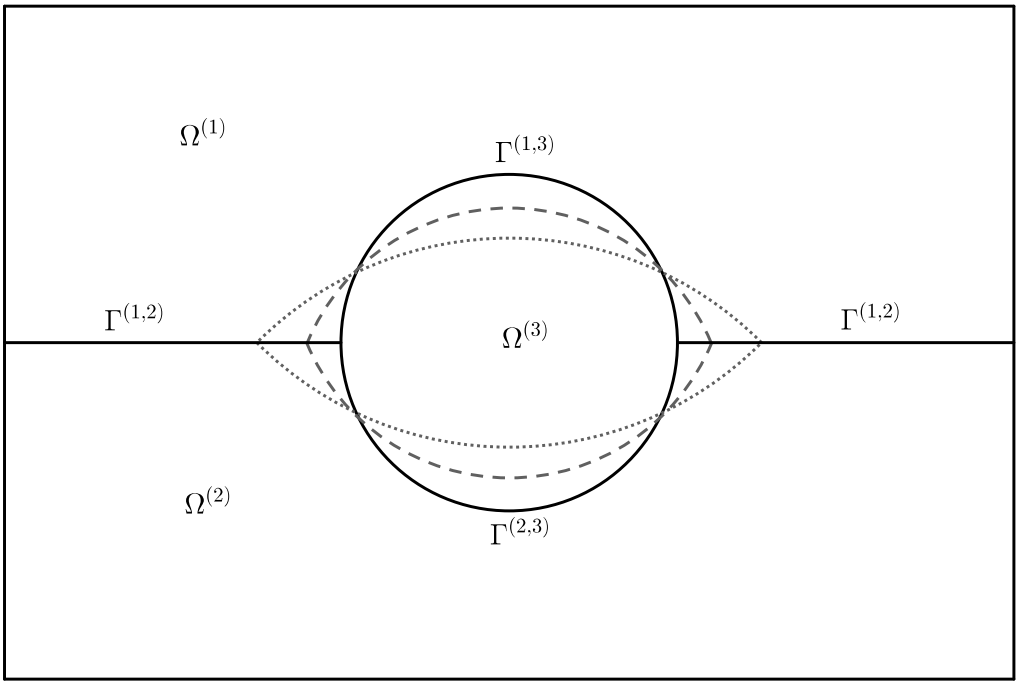

Figure 4.1: *Inital conditions for a lens represented by solid lines.* $\Omega^{(3)}$ *is trapped between two fluids* $\Omega^{(2)}$ *and* $\Omega^{(3)}$*. The dashed and dotted lines represent snapshots of the of the relaxation we expect at some time* $t_1 > 0$ *and* $t_2 > t_1$ *respectively in the absence of external forces.*

We demonstrate the second order accuracy of our numerical scheme for multi-phase flow (see Chapter 3) by creating a phase field model of an oscillating droplet and refining the numerical time stepping for fixed spatial parameters fixed. For each choice of timestep $(\Delta t)_i$ we ran the simulation upto a fixed time $T = N_i(\Delta t)_i$ to obtain computed velocities $\boldsymbol{v}_{\varepsilon h}^{N_i}$ at this time. We then compared computed solutions with a reference solution computed on a very fine resolution time scale.

The sharp interface problem we wish to approximate is initialised by the domain as shown in solid lines in Figure 4.1. There, two fluid layers represented by $\Omega^{(1)}$ and $\Omega^{(2)}$ trap a third phase $\Omega^{(3)}$ initially in the shape of a disc. More precisely, the domain is given by $\Omega = [-3, 3] \times [-2, 2]$, and time $t \in [0, T]$ and initially, $\Gamma^{(1,2)}(\boldsymbol{z}, 0)$ is given by

$\boldsymbol{z} \in \big((-3,-r) \cup (r,3)\big) \times \{0\}$, and $\Gamma^{(1,3)}(\boldsymbol{z},0)$, (resp. $\Gamma^{(2,3)}(\boldsymbol{z},0)$) given by the upper (resp. lower) open semicircle of radius r and centred at the origin. $T^{(1,2,3)}(\boldsymbol{z},0)$ are at $(\pm r,0)$. In this test we have taken $r = \sqrt{\frac{5}{\pi}}$ (This was chosen as it gives an easy check for volume conservation for the phases).

The viscosities of each subregion are fixed in time, $\eta^{(i)} = 0.01$ for all $i = 1,2,3$. The fluid densities are different in each region, and given by $\overline{\rho}^{(1)} = 1.0$, $\overline{\rho}^{(2)} = 2.0$ and $\overline{\rho}^{(3)} = 1.5$. The choice of these values allowed for significant movement of the interfaces during the course of the simulation. As we are investigating the time discretisation, this will should give clearer results of the effects on the system dynamics.

The initial velocity is given by $\boldsymbol{v}(\boldsymbol{z},0) = \mathbf{0}$, $\forall \boldsymbol{z} \in \Omega$, and the boundary condition $\boldsymbol{v}(\boldsymbol{z},t) = \mathbf{0}, \forall (\boldsymbol{z},t) \in \partial\Omega \times [0,T]$, to observe the effects of density more clearly, we introduce gravity via the forcing $\boldsymbol{f} = -9.8\overline{\rho}^{(i)}\mathbf{e}_2$ where $\mathbf{e}_2$ is the standard basis vector $(0,1) \in \mathbb{R}^2$. We furthermore assume there are no surfactants present, and fix the surface tension, $\sigma_{i,j} = 1$, for $(i,j) = (1,2),\ (1,3),\ (2,3)$. It should be emphasised that these choices of parameters were not physically motivated.

The multi-phase flow equations we wish to solve are given by (2.82)-(2.90), where, in the absence of surfactant, equations (2.84), (2.87) and (2.89) disappear. The parameters chosen are enough to define the model in this case.

To create an approximating diffuse interface model, we initialise as follows. Firstly, to localize the inconsistencies about the triple junctions only, we initialize the phase field using the profile of an exact solution for the two-phase Cahn-Hilliard equation to represent the initial hypersurfaces $\Gamma^{(i,j)}(\boldsymbol{z},0)$. Let $\varepsilon = 0.2$ then, for $z = (x,y) \in \Omega$:

$$\varphi_\varepsilon^{(1)}(x,y,t=0) = \begin{cases} \frac{1}{2}(1+\tanh(\frac{2y}{\varepsilon})), & \text{for} \quad x \in [-3,-r) \cup (r,3], \\ \frac{1}{2}(1+\tanh(\frac{2(r-1)}{\varepsilon})), & \text{for} \quad (x,y) \in [-r,r] \times (0,2], \\ 0, & \text{otherwise.} \end{cases}$$

$$\varphi_\varepsilon^{(2)}(x,y,t=0) = \begin{cases} \frac{1}{2}(1+\tanh(\frac{-2y}{\varepsilon})), & \text{for} \quad x \in [-3,-r) \cup (r,3], \\ \frac{1}{2}(1+\tanh(\frac{2(r-1)}{\varepsilon})), & \text{for} \quad (x,y) \in [-r,r] \times [-2,0], \\ 0, & \text{otherwise.} \end{cases}$$

along with $\varphi_\varepsilon^{(3)} = 1 - \varphi_\varepsilon^{(1)} - \varphi_\varepsilon^{(2)}$ to conserve (2.103). Take initial velocity $\boldsymbol{v}_\varepsilon(\boldsymbol{z},0) = \mathbf{0}$. In practice we solve a problem to relax the triple junctions due to inconsistency of the initial conditions, and after this is complete we will begin the test series there.

We solve the system (2.174) – (2.178) for the phase field, and in the absence of surfactant, this reduces to solving (2.174) – (2.176) with constant surface tension $\tilde{\sigma}_{i,j} = 1$. We take the choice of Boyer, Lapuerta and Minjeaud for the Cahn-Hilliard potential

found in Section 2.2.8 with a constant mobility parameter $M_c = 0.002$ and regularisation parameter $\Lambda = 5$ and subsitute these choices into equations (2.174) – (2.176). For the Navier-Stokes we solve the system (2.179) – (2.180) using the rewritten force term (2.168). We take $\eta(\varphi_\varepsilon) = 1$ and take a linear interpolation for $\rho(\varphi_\varepsilon)$ as in Section 2.2.1. We also take a zero velocity boundary condition for $\boldsymbol{v}_\varepsilon$ as in the sharp interface model for $\boldsymbol{v}$.

We discretise the diffuse interface model by using the timestepping scheme for variable density flow in Section 3.4.1, for three phases. This requires solving the equations (3.85), (3.8), (3.9), (3.86), (3.87), (3.12) for each timestep. For this time discretisation scheme we choose the optimal choice of $\theta = 1 - \frac{\sqrt{2}}{2}$ (discussed in Section 3.1.1), and we choose the parameters $\alpha = 2 - \sqrt{2}$ and $1 - \alpha = \sqrt{2} - 1$ implicit-explicit splitting for dissipation in the Navier-Stokes and an identical choice for γ and $1 - \gamma$ for the Cahn-Hilliard equations. For the spatial discretisation parameters, we choose a fixed uniform spatial grid of size 300×200, which equates to h to be smaller than $\frac{\varepsilon}{12}$.

The simuation will run as follows. We solve our discrete system first with step size $\Delta t = 0.001$ until a time $T_0 = 0.05$, this is sufficient to relax the triple junction from the inconsistency of the initial conditions. We then begin the timestep series. For each subsequent run i we choose a timestep $(\Delta t)_i$, and solve steps of the scheme until an end time $T = T_0 + N_i(\Delta t)_i$, where we shall have computed an approximate solution $\boldsymbol{v}_{\varepsilon h}^{N_i}$ to the velocity $\boldsymbol{v}_\varepsilon(\cdot, T)$. At time T we compare the L^2 difference $\|\boldsymbol{v}_{\varepsilon h}^{N_i} - \boldsymbol{v}_{\varepsilon h}^{ref}\|_{L^2(\Omega_h, \mathbb{R}^d)}$ with a reference solution $\boldsymbol{v}_{\varepsilon h}^{ref}$. Here we choose $T - T_0 = 1.05$, and the reference $\boldsymbol{v}_{\varepsilon h}^{ref}$ is computed by running the simulation with $\Delta t = 0.001$ and $N = 1000$, it is important that we have chosen $\Delta t \ll (\Delta t)_i$.

Snapshots of the progression of the simulation run for the reference solution at times $t = T_0$, $t = T_0 + 0.5$ and $t = T$ are given in the Figures 4.2, 4.3 and 4.4 respectively. On the bottom right of each figure $\varphi_\varepsilon^{(3)}$ is plotted, with the $\varphi_\varepsilon^{(i)} = 0.5$ level sets for the other phases. The top right of each figure shows the computed pressure gradient due to gravity and the dynamics of the system. The left hand diagram shows the vector field of the fluid flow.

We display the results of the test series for the choices of N_i in Table 4.1, and Table 4.2. We also display the actual error in the total energy caculated from the test series, displayed in Figures 4.5 and 4.6.

The purpose of this test series was to demonstrate that the choice of scheme for the discrete system (with a variable density) was of second order accuracy with regards to the parameter Δt. We have proved this in Section 3.4.2 theoretically, and this was of particular importance as the introduction of the variable density into the scheme, was outside of the traditional framework for the operator splitting and so required proof. In Table 4.1 we see that the scheme achieves an order of convergence of in excess of 2 for the velocity $\boldsymbol{v}_{\varepsilon h}$ in

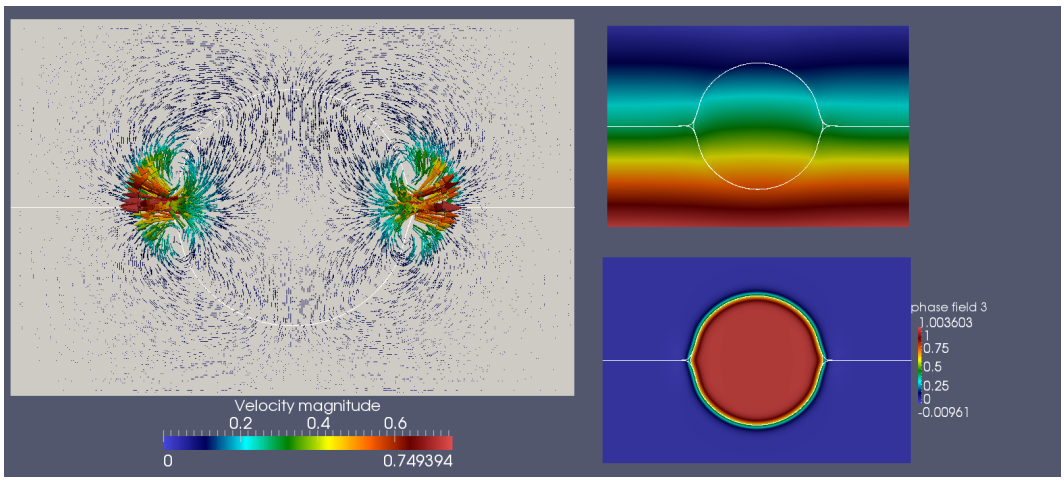

Figure 4.2: *Figure displaying the state of the system at time $t = T_0$. The bottom right displays $\varphi_\varepsilon^{(3)}$ field, with $\varphi_\varepsilon^{(i)} = 0.5$ level sets in white (appearing in all diagrams). The top right shows pressure field. The left shows the velocity vector field where the size and colour of the arrows represent the magnitude of the velocity field.*

the discrete L^2 norm when calculating an extended range of timesteps. We also observe this reduces to below 2 when the errors due to the timestepping are reduced. This is perhaps due to unknown numerical error, or errors due to the approximation in the EOC formula and may require further investigation. This error could be reduced by running on a finer mesh, or perhaps running simulations with exact solutions available, or using a much finer mesh reference solution (but this becomes restrictive due to resources as we are required to use a fine and uniform spatial mesh).

One can see the actual size of energy errors in Figure 4.6 at this time. For $\nabla \boldsymbol{v}_{\varepsilon h}$ we see similar behaviour, where the orders of convergence are in excess of 1 until the point already commented on. We have not performed any analysis to determine the correct rate of convergence for the velocity gradient. In Table 4.2 we observe idential behaviour for $\varphi_{\varepsilon h}$ and $\nabla \varphi_{\varepsilon h}$, but these reach peak orders of 4.57 and 4.97 respectively before reduction due to aforementioned error.

In Figure 4.5 we observe the actual error to the total discrete energy (2.170) (note this is decreasing when the problem is posed without the presence of gravity), a magnification in Figure 4.6 displays the convergence more clearly. The difference in actual values of the energy in l^∞ is very good, within a maximum error of %0.4 from the reference solution to $\Delta t = 0.0625$ and the error to the solution $\Delta t = 0.02083$ is just %0.002.

The tests conducted were to give validation to the consistency results of Section 3.4.2, however during testing We were able to observe some of the features of stability, which imply it is significantly better than the theory of Section 3.2. In the case of variable

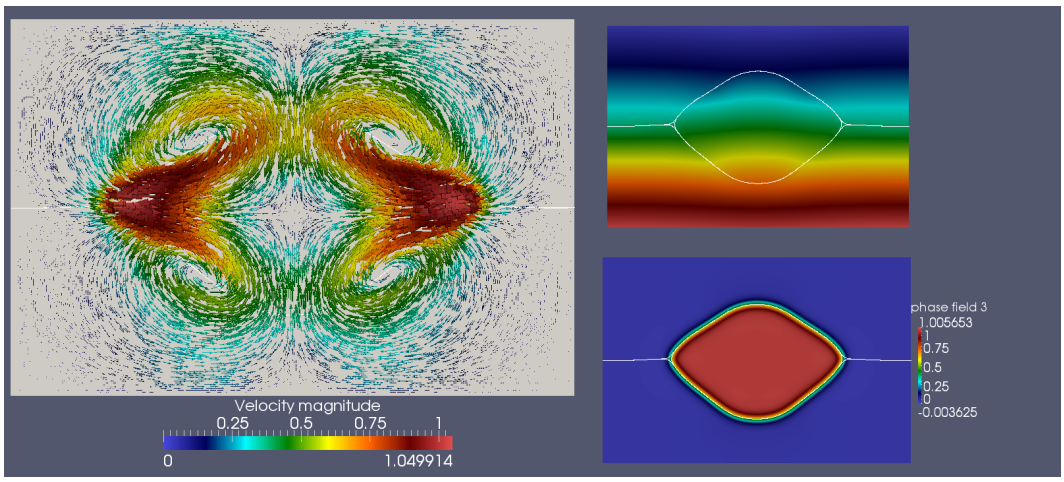

Figure 4.3: *Figure displaying the state of the system at time $t = T_0 + 0.5$. The bottom right displays $\varphi_\varepsilon^{(3)}$ field, with $\varphi_\varepsilon^{(i)} = 0.5$ level sets in white (appearing in all diagrams). The top right shows pressure field. The left shows the velocity vector field where the size and colour of the arrows represent the magnitude of the velocity field.*

density (and without the presence of gravity), the discrete energy would always decrease over time. Also the stability relation (3.68) in two dimensions was, in practice, a more relaxed condition, and discrete energy decay persisted with test runs of $\Delta t \approx Ch$ for different mesh sizes.

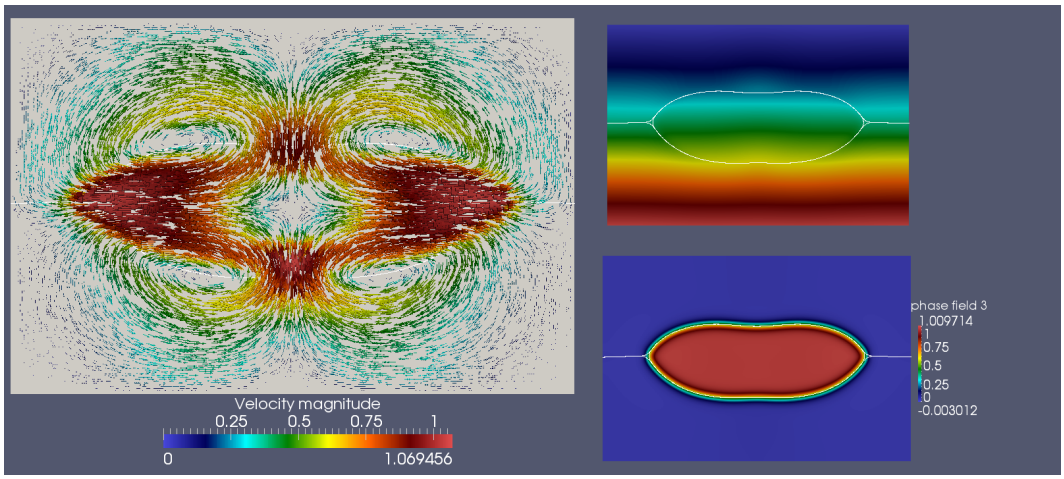

Figure 4.4: *Figure displaying the state of the system at time $t = T_0 + 1$. The bottom right displays $\varphi_\varepsilon^{(3)}$ field, with $\varphi_\varepsilon^{(i)} = 0.5$ level sets in white (appearing in all diagrams). The top right shows pressure field. The left shows the velocity vector field where the size and colour of the arrows represent the magnitude of the velocity field.*

N_i	$\lvert \boldsymbol{v}_{\varepsilon h}^{N_i} - \boldsymbol{v}_{\varepsilon h}^{ref} \rvert$	L_h^2-EOC(N_i)	$\lvert \nabla \boldsymbol{v}_{\varepsilon h}^{N_i} - \nabla \boldsymbol{v}_{\varepsilon h}^{ref} \rvert$	$(L_h^2)^d$-EOC(N_i)
16	0.110741	5.34141	2.68818	7.55768
20	0.0336258	1.74474	0.497787	1.4903
24	0.0244637	1.90179	0.37935	1.22721
28	0.0182475	2.23624	0.313966	1.04965
32	0.0134369	2.53646	0.272905	0.77727
36	0.0100409	2.29003	0.24903	0.57897
40	0.00788835	1.89885	0.234293	0.449098
44	0.00658245	1.53922	0.224476	0.384404
48	0.00575735	–	0.217092	–

Table 4.1: *The table displays the results of the timestepping test series where timestep size is given by $(\Delta t)_i = \frac{1}{N_i}$. We present differences between the computed solution (and their gradients) for run i and the computed reference solution (with $\Delta t = 0.001, N = 1000$). The definition of the norms are given in* (4.4) *and EOC in* (4.1)*. We provide estimated orders of convergence between subsequence steps.*

N_i	$\|\varphi_{\varepsilon h}^{N_i} - \varphi_{\varepsilon h}^{ref}\|_{\hat{L}_h^{2,3}}$	$\hat{L}_h^{2,3}$-EOC(N_i)	$\|\nabla\varphi_{\varepsilon h}^{N_i} - \nabla\varphi_{\varepsilon h}^{ref}\|_{\hat{L}_h^{2,2\times 3}}$	$\hat{L}_h^{2,2\times 3}$-EOC(N_i)
16	0.189574	3.32117	1.80561	3.34943
20	0.0903491	3.50728	0.855128	3.45206
24	0.0476665	4.10728	0.455714	3.98944
28	0.0253072	4.76252	0.246384	4.52721
32	0.0133985	4.95185	0.134608	4.57555
36	0.0074775	3.70869	0.0785272	3.48656
40	0.0050589	1.68757	0.0543856	1.90868
44	0.00430728	0.37857	0.0453397	0.834122
48	0.00416771	–	0.04216561	–

Table 4.2: *The table displays the results of the timestepping test series where timestep size is given by* $(\Delta t)_i = \frac{1}{N_i}$. *We present differences between the computed solution (and their gradients) for run* i *and the computed reference solution (with* $\Delta t = 0.001,\ N = 1000$*). The definition of the norms are given in* (4.3) *and EOC in* (4.1)*. We provide estimated orders of convergence between subsequence steps.*

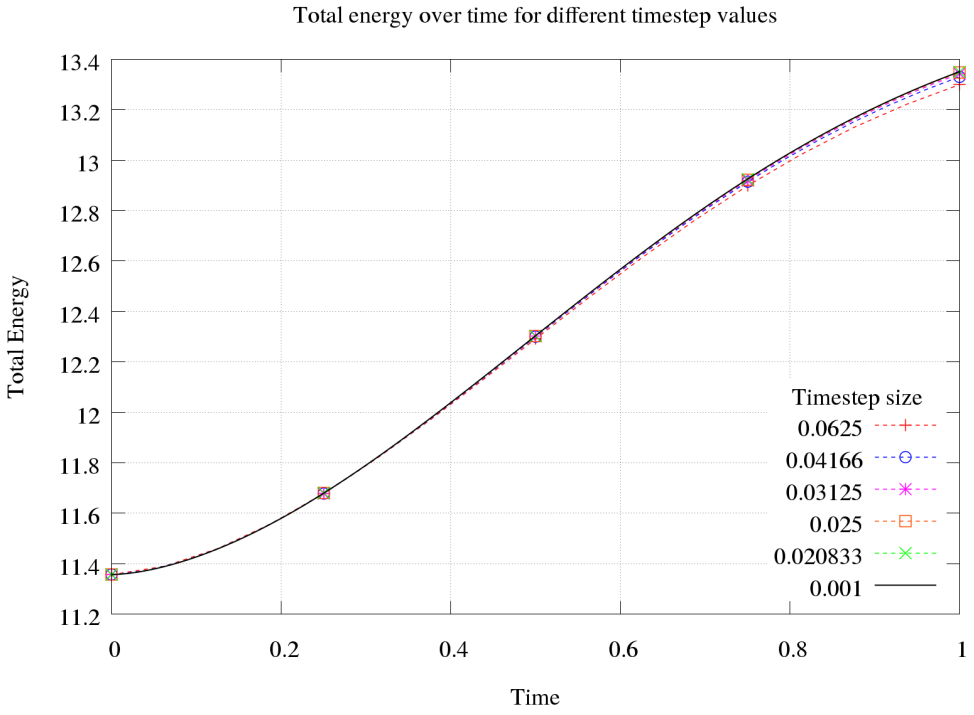

Figure 4.5: *The figure displays the total discrete energy value E_ε^n, that is, the discretisation of* (2.170) *(see Section 3.2.3 for two phase matched density case). For clarity we have not displayed every solution in the test series, but have captured the full range of accuracies, and the reference solution is given by the solid black line.*

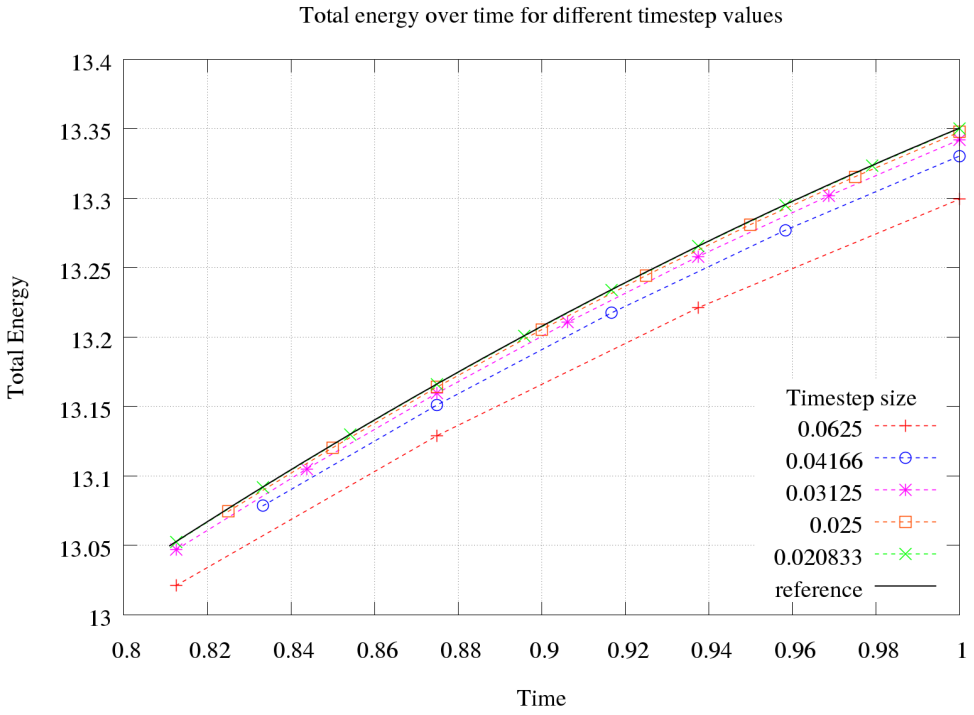

Figure 4.6: *A magnified section of Figure 4.5 displaying the right hand edge where the EOCs in Tables 4.1 and 4.2 were calculated. In this figure, the symbols are placed at every evaluation of the time stepping scheme*

4.3 Convergence of DIM to SIM

4.3.1 Surfactant equation through a triple junction

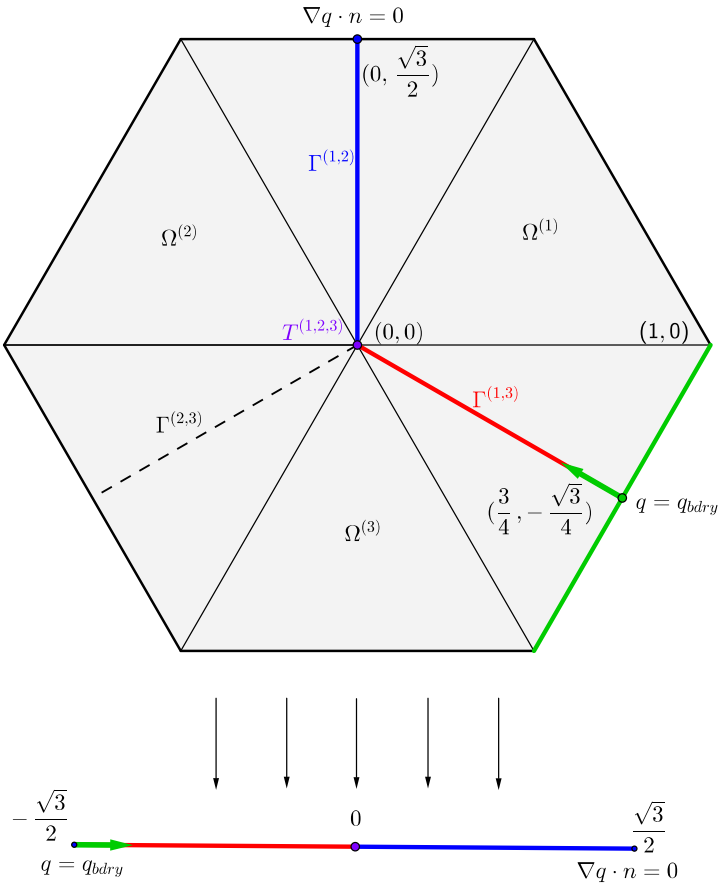

Figure 4.7: *Setup for the ε-convergence test for the surfactant equation as considered in Section 4.3.1.*

We demonstrate the convergence of the diffuse surfactant equation (2.177)-(2.178) to the sharp interface setting (2.87) without being subjected to a multi-phase flow. We display the configuration for this test in Figure 4.7. The domain is a regular hexagon of side length 1. It is comprised of 3 subregions $\Omega^{(i)}$, $i = 1, 2, 3$ separated by fixed straight interfaces $\Gamma^{(i,j)}$, $(i, j) = (1, 2), (1, 3), (2, 3)$, which meet at a triple junction $T^{(1,2,3)}$ at the origin.

The sharp interface equation for the surfactant equation (2.87) in the absence of fluid flow is a surface heat type equation. Here we consider the case where $c^{(2,3)}(q) = 0$ (the dashed line in Figure 4.7), and $c^{(i)}(q) = 0$, $\forall i = 1, 2, 3$. The interfaces $\Gamma^{(1,2)}$, $\Gamma^{(1,3)}$ are straight lines of length $L = \frac{\sqrt{3}}{2}$, and we transform the equations for $c^{(1,2)}(q)$ and $c^{(1,3)}(q)$

onto the interval $[-L, L]$. This is shown in Figure 4.7; the interval $[-L, 0)$ is the transformation of $\Gamma^{(1,3)}$, $(0, L]$ is the transformation of $\Gamma^{(1,2)}$ and the triple junction $T^{(i,j,k)}$ is mapped to 0. We assume a linear relationship in (2.70), that is, we use the quadratic isotherm (2.99)-(2.101). For $(i, j) = (1, 2), (1, 3)$, take $c^{(i,j)}(q) = \frac{q}{\beta_{i,j}}$ for constants $\beta_{i,j} > 0$ and moreover assume the mobilities $M_c^{(i)}, M_c^{(i,j)} > 0$ are constants.

The surfactant is initially absent $q(s, 0) = 0,\ \forall s \in [-L, L]$. It will be supplied from $s = -L$ by imposing a Dirichlet condition corresponding to $q(-L, t) = q_{\text{bdry}}$. At the other boundary $s = L$ we take a homogeneous Neumann boundary condition. In the long run, the solution will approximate $q = q_{\text{bdry}}$ so we stop the test early at a final time $T = 0.01$ to ensure gradients still have a significant influence on behaviour.

Application of the above transformation, conditions and assumptions to the equations (2.89) and (2.87), results in the following problem:

$$\begin{aligned}
\partial_t c^{(1,3)}(q(s,t)) - M_c^{(1,3)} \partial_{ss} q(s,t) &= 0, && \forall (s,t) \in [-L, 0] \times (0, T], \\
\partial_t c^{(1,2)}(q(s,t)) - M_c^{(1,2)} \partial_{ss} q(s,t) &= 0, && \forall (s,t) \in (0, L] \times (0, T], \\
q(-L,t) = q_{\text{bdry}}, \quad \partial_s q(L,t) &= 0, && \forall t \in (0, T], \\
[M_c^{(\cdot,\cdot)} q']_-^+(0,t) = 0, \quad [q]_-^+(0,t) &= 0, && \forall t \in (0, T], \\
q(s,0) &= 0, && \forall s \in [-L, L].
\end{aligned} \tag{4.5}$$

For the numerical scheme parameters, we perform a 1D linear finite differences method. In brief, we use a standard second order difference for $\partial_s s$, and backward Euler difference for ∂_s. To enforce the jump condition at 0 and the homogeneous Neumann boundary condition at L we use one-sided first order differences. (4.5) is solved in MATLAB 2016b, with a grid of $N = 4000$ points and a timestep $\Delta t = 2.5 \times 10^{-6}$. This is sampled uniformly across the domain at the final time at 400 points for comparison with the diffuse modelling solution. These parameters ensure a sufficient accuracy for comparison with the diffuse interface model.

To approximate the solution of the diffuse interface model, the test is built in two stages. The first stage involves the relaxation of the phase field to form the triple junction with a given ε value. To be more precise we define the initial conditions on Ω for the phase field as,

$$\varphi_\varepsilon^{(1)}(x, y, t = 0) = \begin{cases} \frac{1}{2}(1 + \tanh(\frac{2x}{\varepsilon})), & \text{for} \quad y \geq 0, \\ \frac{1}{2}(1 + \tanh(\frac{2}{\varepsilon}(y + \frac{\sqrt{3}}{3}x))), & \text{for} \quad \{x \geq -\varepsilon\} \cap \{y < 0\}, \\ 0, & \text{otherwise.} \end{cases}$$

$$\varphi_\varepsilon^{(2)}(x,y,t=0) = \begin{cases} \frac{1}{2}(1+\tanh(\frac{-2x}{\varepsilon})), & \text{for} \quad y \geq 0, \\ \frac{1}{2}(1+\tanh(\frac{2}{\varepsilon}(y-\frac{\sqrt{3}}{3}x))), & \text{for} \quad \{x \leq \varepsilon\} \cap \{y < 0\}, \\ 0, & \text{otherwise.} \end{cases}$$

along with $\varphi_\varepsilon^{(3)} = 1 - \varphi_\varepsilon^{(1)} - \varphi_\varepsilon^{(2)}$. The Cahn-Hilliard system (2.174) - (2.180) is solved in the absence of fluids or surfactant until it reaches a stationary state. That is, we fix $\boldsymbol{v}_\varepsilon = 0$ and $q_\varepsilon = 0$, and choose the functions $\mathcal{L}^{i,j}, a_{i,j}, \overline{w}_{i,j}$ as in Section 2.2.8 and set $\tilde{\sigma}_{i,j} = 1$. The second stage involves fixing the final computed phase field solutions, and then substituting them into equations (2.177)-(2.178). These are then solved with conditions which imitate the setting of the sharp interface model test. We set $\xi_i = 0$ and $\delta_{2,3} = 0$, and the surfactant is supplied at the boundary $\partial\Omega_{\text{in}} := \left\{(r, \frac{\sqrt{3}}{2}(r-1)) \middle| r \in (0,1)\right\}$, using a Dirichlet condition q_{bdry}. All other boundaries carry a homogeneous Neumann boundary condition. We replace the distributions $\delta_{1,2}, \delta_{1,3}$ with a regularisation (4.6). This is because the distributions $\delta_{i,j}$ decay exponentially outside of the interfacial regions, which may cause numerical complications due to the problem being almost degenerate in the bulk:

$$\tilde{\delta_{i,j}}(\varphi_\varepsilon, \nabla\varphi_\varepsilon) = \begin{cases} \delta_{i,j}(\varphi_\varepsilon, \nabla\varphi_\varepsilon), & \text{if } |\delta_{i,j}(\varphi_\varepsilon, \nabla\varphi_\varepsilon)| > C\varepsilon^2, \\ C\varepsilon^2, & \text{otherwise.} \end{cases} \tag{4.6}$$

We found $C = 0.001$ was sufficient to be comparable to discretisation errors, for all values of ε. A similar technique of regularisation in the case of degeneracy in the bulk has been studied by [114]. The problem tackled was to mimic zero diffusion off of a surface into the embedding domain, and required a regularisation to the phase field. The authors chose to add a function $0 < \delta(\varepsilon) \ll \varepsilon$ to the two phase potential and showed this did not affect convergence properties $\varepsilon \to 0$ through asymptotic analysis.

We choose discretisation parameters to ensure accuracy is sufficient to observe the ε-convergence. We use an adaptive spatial grid paramter h, and refine the grid by using a strategy to bisect any element where $|\nabla\varphi_\varepsilon^{(\cdot)}| > \frac{C_a}{\varepsilon}$, taking $C_a = 0.004$, $h_{\text{min}} \approx \frac{\varepsilon}{5}$, and the maximum number of adaption levels as 4. This h_{min} yields approximately 10 elements across the interface. We choose the time step $\Delta t = 2.5 \times 10^{-6}$. At the final time $t = T$, we sample q_ε uniformly at $N = 400$ points along the straight lines representing $\Gamma^{(1,3)}$ and $\Gamma^{(1,2)}$.

We perform two test series for demonstration of the ε-convergence test. For the first, we choose the model parameters $\beta_{12} = \beta_{13} = 1$ and set mobilities $M_c^{(1,2)} = M_c^{(1,3)} = 100$. The profiles of the surfactant potential q_ε at time T, for different values of ε, and the sharp interface model solution are displayed in Figure 4.8. A closer view of the right hand boundary is displayed in Figure 4.9. We also display information in Table 4.3 using

the notation defined in (4.1) - (4.2). The maximum error occurs at points furthest from the source boundary condition, so the difference in value between q and q_ε at $s = L$ will yield the ε - error in the discrete L^∞ norm stated above.

ε	$q_\varepsilon(L)$	$\|\text{ref} - q_\varepsilon\|_{l^\infty}$	l^∞-EOC(ε)	$\|\text{ref} - q_\varepsilon\|_{l^2}$	l^2-EOC(ε)
0.08	0.219128	0.003256	0.888345	0.002375	0.868456
0.04	0.217631	0.001759	0.845374	0.001301	0.809466
0.02	0.216851	0.000979	0.795614	0.000742	0.732636
0.01	0.216436	0.000564	–	0.000447	–
ref	0.215872	–	–	–	–

Table 4.3: *The table displays the results of the first test series. The value of the surfactant potential q_ε is taken at the point $\left(0, \frac{\sqrt{3}}{2}\right)$ at different sizes of ϵ. 'ref' is the solution of the sharp interface problem* (4.5) *at the point $s = L$. The notation is defined in* (4.1)-(4.2).

We observe in Figure 4.8 that we have excellent agreement across all ranges of ε to the sharp interface model. Qualitative information for q_ε is preserved in the diffuse approximation, in particular the gradient of q_ε either side of the triple junction is equal. This condition is strongly enforced in the finite difference scheme for the sharp model, and weakly by the finite element scheme for the diffuse model. Quantitative analysis can be seen more clearly in Figure 4.9 and Table 4.3. We observed that there is convergence of q_ε as ε is reduced and we determine an estimated convergence order towards the sharp interface model solution is approximately 0.8 in both l^2 and l^∞ norms. For the largest value $\varepsilon = 0.08$ we obtain an accuracy of 1.51% in l^∞, and at the finest width of $\varepsilon = 0.01$ we obtain an error of 0.26% to the sharp interface solution.

For the second test series, we choose the model parameters $\beta_{12} = 4,\ \beta_{13} = 1$ and set mobilities $M_c^{(1,2)} = 25,\ M_c^{(1,3)} = 100$. This will produce a jump of $\partial_s q$ at $s = 0$. The profiles of the surfactant potential q_ε at time T for different values of ε and the sharp interface model solution are displayed in Figure 4.10. A closer view of the triple junction region is displayed in Figure 4.11. We display information regarding errors and EOCs in Table 4.3.

ε	$q_\varepsilon(L)$	$\|\text{ref} - q_\varepsilon\|_{l^\infty}$	l^∞-EOC(ε)	$\|\text{ref} - q_\varepsilon\|_{l^2}$	l^2-EOC(ε)
0.08	0.127939	0.005887	0.910448	0.005596	0.865238
0.04	0.125184	0.003132	0.927244	0.003072	0.882334
0.02	0.123699	0.001617	0.919096	0.001667	0.852642
0.01	0.122923	0.000871	–	0.000923	–
ref	0.122052	–	–	–	–

Table 4.4: *The table displays the results of the second test series. The value of the surfactant potential q_ε is taken at the point $\left(0, \frac{\sqrt{3}}{2}\right)$ at different sizes of ϵ. 'ref' is the solution of the sharp interface problem* (4.5) *at the point $s = L$. The notation is defined in* (4.1)-(4.2).

We observe good agreement of the solution across all ε values (4.82% in l^∞ for $\varepsilon = 0.08$ and 0.71% at $\varepsilon = 0.01$). The accuracy is lower than in the first test series, but the estimated order of convergence is still similar, at around 0.9 in l^∞ and 0.85 in l^2. Figure 4.11 demonstrates the greatest source of inaccuracy of the model, arising from the jump at $s = 0$ in the gradient $\partial_s q$. Thus ε must be small if one requires an accurate description of the flow near this region.

We have obtained a sublinear convergence for our scheme, this may due to the asymptotic scaling behaviour of the triple junction. Investigations in [55] have shown that these regions have the scaling regime of a triangle with sidelengths proportional to ε^ω where $\omega \in (0, 1)$. This behaviour could be causing the sublinear convergence but will require further investigation.

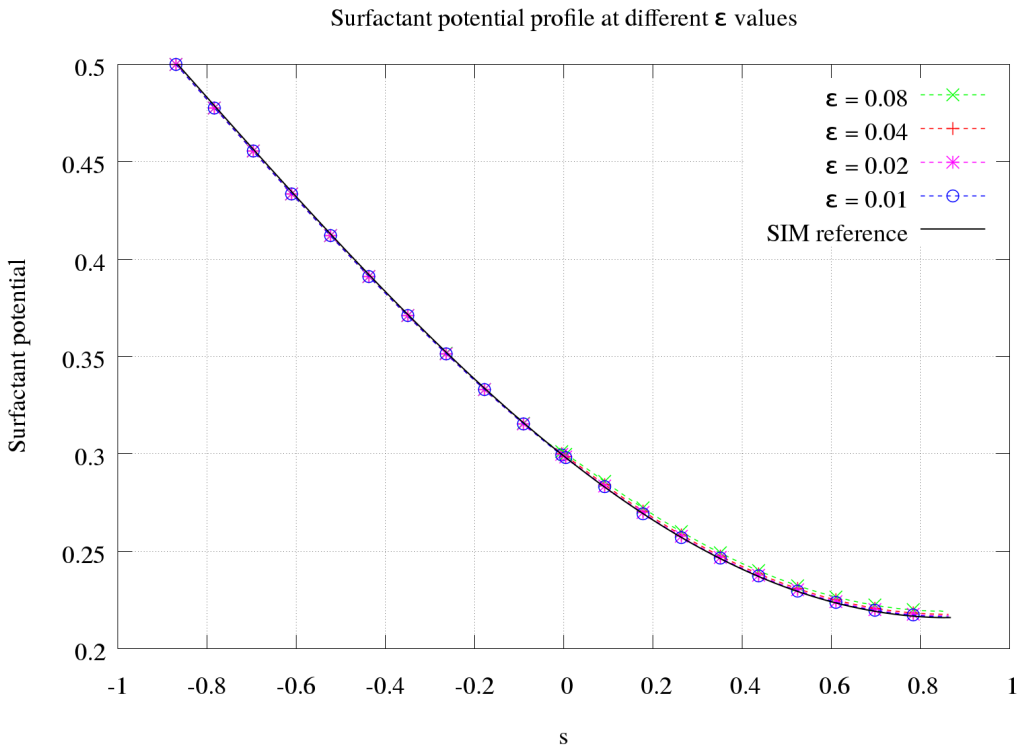

Figure 4.8: *The profile of the computed potential q_ε at at different ε values and compared to the solution of the sharp interface problem* (4.5). *Values were taken at time $t = 0.01$, and the diffuse approximation was sampled along the path displayed in Figure 4.7 and transformed to be displayed over the interval $\big(-L, L\big)$.*

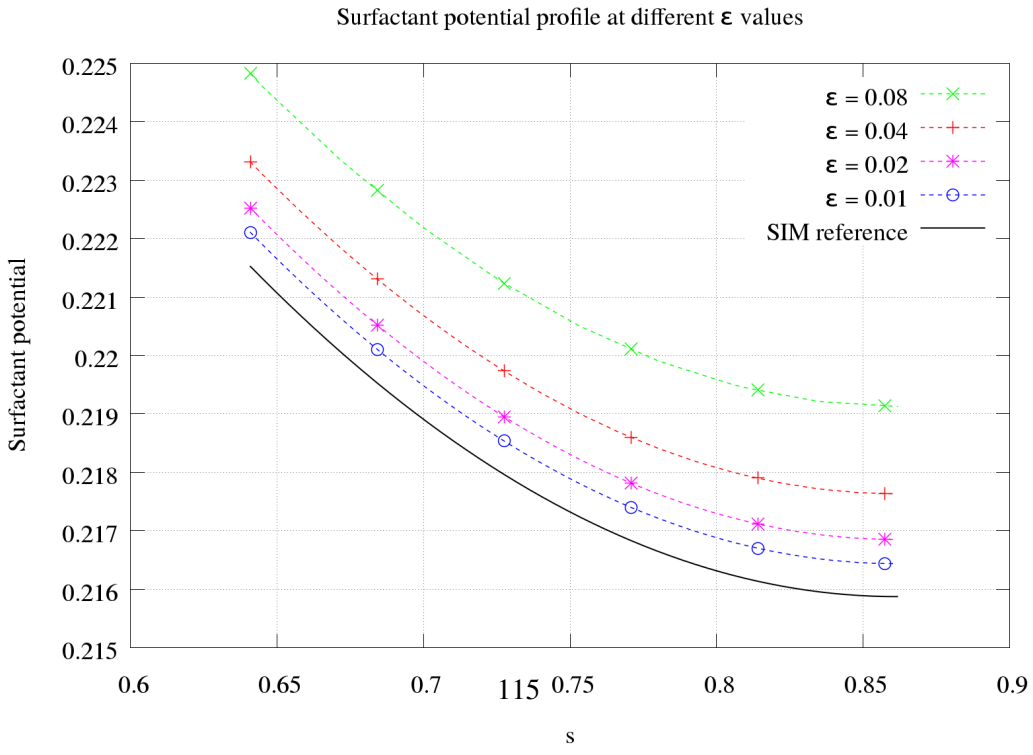

Figure 4.9: *A magnified section of Figure 4.8 displaying the right hand end of the profile of computed potentials. We display the solutions over the interval $(\frac{L}{2}, L)$.*

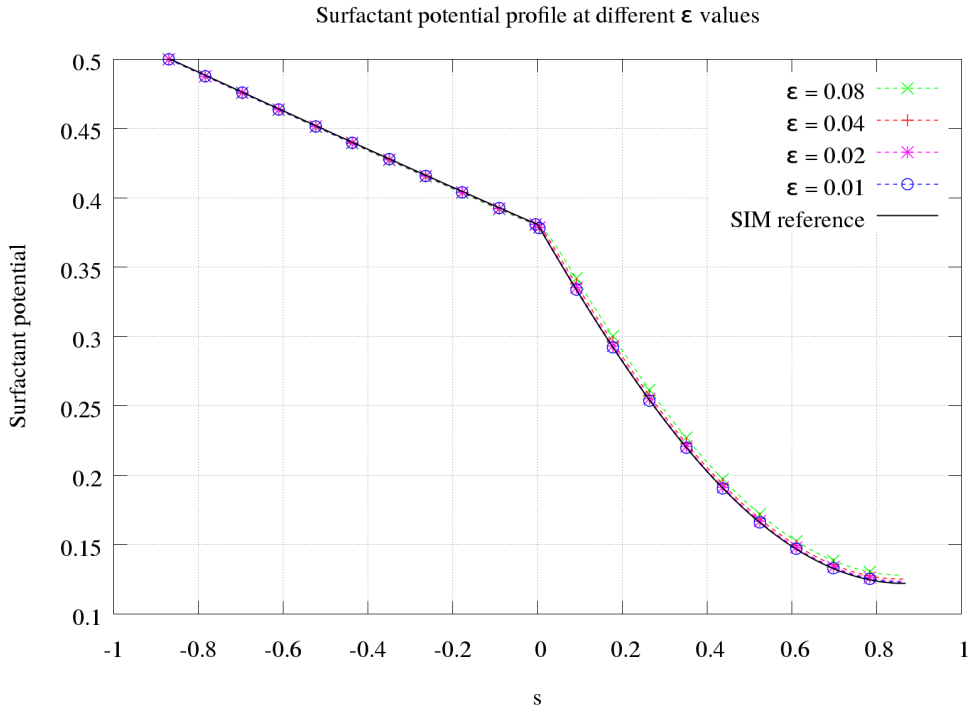

Figure 4.10: *The profile of the q_ε at different ε values and compared to the solution of the sharp interface problem* (4.5). *Values were taken at time* $t = 0.01$, *the diffuse approximation was sampled along a path as in Figure 4.7 and projected onto the interval* $\left(-\frac{\sqrt{3}}{2}, \frac{\sqrt{3}}{2}\right)$. *The triple junction is centred at* 0.

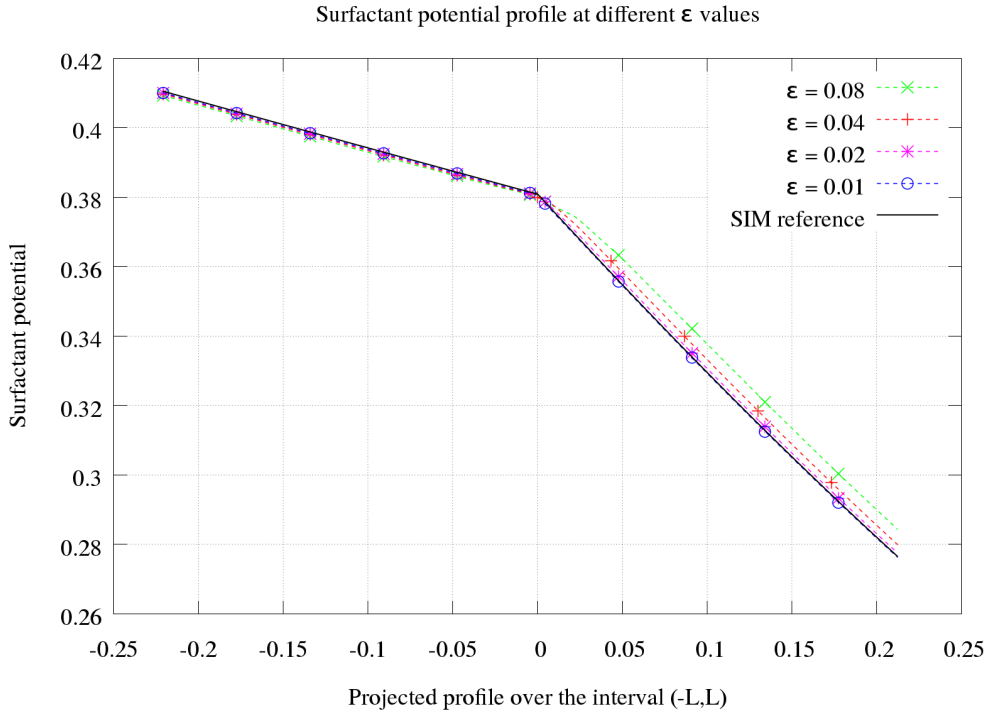

Figure 4.11: *A section of Figure 4.10 displaying the profile of the computed potential q_ε at at different ε values and compared to the solution of the sharp interface problem* (4.5). *We display the path only from* $\left(-\frac{\sqrt{3}}{8}, \frac{\sqrt{3}}{8}\right)$ *to observe the approximation of the triple junction.*

4.3.2 Angles at a triple junction

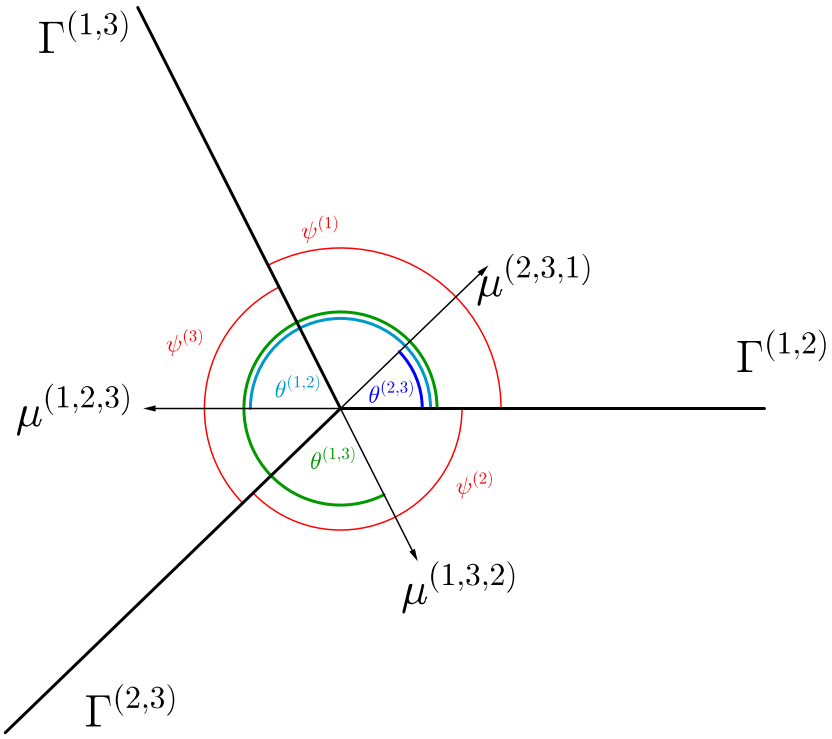

Figure 4.12: *Diagram of a triple junction between three hypersurfaces* $\Gamma^{(i,j)}$ *and their conormals* $\boldsymbol{\mu}^{(i,j,k)}$. *The angles* $\theta^{(i,j)}$ *represent the angles described by the Neumann triangle relation of the surface tensions* $\sigma_{i,j}$, *and the angles* $\psi^{(k)}$ *are the angles between the corresponding branches* $\Gamma^{(j,k)}, \Gamma^{(k,i)}$.

For this test, we wish to demonstrate the recovery of angles about a triple junction in the absence of flow, these are predicted by the force balance (2.36). We once again consider a three phase lens setting as described in Figure 4.1, and as the junctions only touch the boundary at only one of the branches, this allows for good isolation of boundary effects on the junction angles.

The domain is rectangular $\Omega = [-1.75, 1.75] \times [-2, 2]$. A similar setting is constructed in Section 4.2, and so we refer to this for initialisation of the geometrical features, with the parameter choice $r = \sqrt{\frac{3}{\pi}}$ for the radius the initial disc centred at the origin representing $\Omega^{(3)}$.

We assume for the surfactants that we are within the instantaneous adsorption regime, that is, we will consider the model summarised in Section 2.1.10. In the absence of the fluid flow the equations (2.82), (2.83), (2.85), (2.88) disappear and we consider the the model in this case. We choose the quadratic isotherm of Section 2.1.11, and we choose the parame-

ters to acheive desired angles, we will go into detail about how these choices were made.

It may be useful to consult Figure 4.12, which displays the triple junction complete with all angles. Recall the balance (2.36) with instantaneous adsorption leads to:

$$\sigma_{1,2}\boldsymbol{\mu}^{(1,2,3)} + \sigma_{1,3}\boldsymbol{\mu}^{(1,3,2)} + \sigma_{2,3}\boldsymbol{\mu}^{(2,3,1)} = 0.$$

With regards to Figure 4.12, centre the triple junction at the origin and orient it such that the $\Gamma^{(1,2)}$ interface is the positive x axis. Define $\theta^{(i,j)}$ to be the angle anticlockwise from the positive x axis to $\boldsymbol{\mu}^{(i,j,k)}$ for distinct $i, j, k = 1, 2, 3$. Then the following holds,

$$\begin{cases} \sigma_{1,2}\cos(\theta^{(1,2)}) + \sigma_{1,3}\cos(\theta^{(1,3)}) + \sigma_{2,3}\cos(\theta^{(2,3)}) &= 0, \\ \sigma_{1,2}\sin(\theta^{(1,2)}) + \sigma_{1,3}\sin(\theta^{(1,3)}) + \sigma_{2,3}\sin(\theta^{(2,3)}) &= 0. \end{cases} \tag{4.7}$$

For clarity, we transform $\theta^{(i,j)}$ to more meaningful angles. Let $\psi^{(k)}$ be the angle between hypersurfaces $\Gamma^{(j,k)}$ and $\Gamma^{(k,i)}$, for distinct $i, j, k = 1, 2, 3$. Then:

$$\theta^{(1,2)} = \pi, \qquad \theta^{(1,3)} = \pi + \psi^{(1)}, \qquad \theta^{(2,3)} = \pi - \psi^{(2)}, \qquad \psi^{(1)} + \psi^{(2)} = 2\pi - \psi^{(3)}.$$

For our simulation we set our target angles $\psi^{(1)} = \frac{\pi}{2}$, $\psi^{(2)} = \frac{2\pi}{3}$, $\psi^{(3)} = \frac{5\pi}{6}$ at the junctions between the interfaces. Therefore, we have targets $\theta^{(1,2)} = \pi$, $\theta^{(1,3)} = \frac{3\pi}{2}$, $\theta^{(2,3)} = \frac{\pi}{3}$. From equations (4.7), (in the absence of fluids) we may only solve $\sigma_{i,j}$ upto a ratio. We set $\sigma_{1,2} = 1$, and solve for $\sigma_{1,3}$, $\sigma_{2,3}$:

$$\sigma_{1,3}\cos\left(\frac{3\pi}{2}\right) + \sigma_{2,3}\cos\left(\frac{\pi}{3}\right) = 1, \quad \sigma_{1,3}\sin\left(\frac{3\pi}{2}\right) + \sigma_{2,3}\sin\left(\frac{\pi}{3}\right) = 0,$$
$$\implies \sigma_{1,3} = \sqrt{3}, \quad \sigma_{2,3} = 2.$$

These are then the target equilibrium surface tensions for the interfaces between our phases. To obtain parameters we recall that the surface tension is given by (2.72), that is, $\tilde{\sigma}_{i,j}(q) = \sigma_0 - \frac{q^2}{2\beta_{i,j}}$. We take the constant $\sigma_0 = 4$ and we choose boundary conditions so that the surfactant equation reaches a steady state of $q = 0.5$ in Ω. For long times the surface tension will converge to $\tilde{\sigma}_{i,j}(0.5)$ thus we require $\tilde{\sigma}_{i,j}(0.5) = \sigma_{i,j}$, so we set the model parameters $\beta_{1,2} = \frac{1}{24}$, $\beta_{1,3} = \frac{1}{8(4-\sqrt{3})}$, $\beta_{2,3} = \frac{1}{16}$ to obtain the desired angle configuration. We also take mobilities $M_c^{(i)} = 100\ \forall i = 1, 2, 3$ and $M_c^{(i,j)} = \frac{100}{\beta_{i,j}}$.

Initially there are no surfactants present in the domain. However at a chosen time T_0, they will be introduced through Dirichlet boundary conditions. We additionally define a relaxation time T_q to ensure the boundary conditions are smoothly realised by time $T_0 + T_q$. We apply the following boundary condition for q: Let $z_L = (-1.75, y)$ and $z_R =$

$(1.75, y)\ \forall y \in [-2, 2]$ then,

$$q(z_L, t) = q(z_R, t) = \begin{cases} 0, & \text{for } t \in (0, T_0), \\ \frac{t-T_0}{2T_q}, & \text{for } t \in (T_0, T_0 + T_q), \\ 0.5, & \text{for } t \in (T_q, T). \end{cases}$$

These are symmetric about the y axis and so will not enforce asymmetric dynamics, they also give the equilibrium solution to the model as $q = 0.5$ in Ω. We have now sufficiently defined parameters for the sharp interface model to be well defined.

To create the diffuse interface approximation of this model we initialise as described in Section 4.2. This localises the inconsistencies that are present in initialisation around the triple junction by using the exact profile expected along two phase interfaces. For each ε, let $z = (x, y) \in \Omega$ then:

$$\varphi_\varepsilon^{(1)}(x, y, t = 0) = \begin{cases} \frac{1}{2}(1 + \tanh(\frac{2y}{\varepsilon})), & \text{for} \quad x \in [-1.75, -r) \cup (r, 1.75], \\ \frac{1}{2}(1 + \tanh(\frac{2(r-1)}{\varepsilon})), & \text{for} \quad (x, y) \in [-r, r] \times (0, 2], \\ 0, & \text{otherwise.} \end{cases}$$

$$\varphi_\varepsilon^{(2)}(x, y, t = 0) = \begin{cases} \frac{1}{2}(1 + \tanh(\frac{-2y}{\varepsilon})), & \text{for} \quad x \in [-1.75, -r) \cup (r, 1.75], \\ \frac{1}{2}(1 + \tanh(\frac{2(r-1)}{\varepsilon})), & \text{for} \quad (x, y) \in [-r, r] \times [-2, 0], \\ 0, & \text{otherwise.} \end{cases}$$

with $\varphi_\varepsilon^{(3)} = 1 - \varphi_\varepsilon^{(1)} - \varphi_\varepsilon^{(2)}$ to conserve (2.103).

We solve the system (2.174)-(2.178) for the phase field, and in the absence of the flow, this reduces to solving (2.174)-(2.176), and (2.177)-(2.178). We take the choice of Boyer, Lapuerta and Minjeaud for the Cahn-Hilliard potential found in Section 2.2.8 with a constant mobility parameter $M_c = 0.1$ and regularisation parameter $\Lambda = 5$ and subsitute these choices into equations (2.174)-(2.176). For the surfactant equations we use the parameters discussed in the sharp interface model and there are no additional choices to be made.

We discretise the diffuse interface model by using the timestepping scheme presented in Section 3.5 extended to multi phase Cahn-Hilliard as discussed in Section 3.3. We do not solve the for the flow. For this time discretisation scheme we choose the optimal choice of $\theta = 1 - \frac{\sqrt{2}}{2}$ (discussed in Section 3.1.1), and we choose the parameters $\gamma = 2 - \sqrt{2}$ and $1 - \gamma = \sqrt{2} - 1$ for the implicit-explicit splitting for dissipation in the Cahn-Hilliard equations, and an identical choice for ω and $1 - \omega$ for the surfactant equations.

For the spatial discretisation parameters, we wish to utilize adaptive refinement to reduce the computational demands while maintaining a high enough precision across the interfacial layers of the phase field. For ε fixed, we use an adaptive spatial grid paramter h, and refine the grid by using a strategy to bisect any element where $|\nabla\varphi_\varepsilon^{(\cdot)}| > \frac{C_a}{\varepsilon}$, taking $C_a = 0.02$, We have observed good accuracy of solutions if we retain $h_{\min} \approx \frac{\varepsilon}{4}$, and the maximum number of adaption levels as 3. This gives the number of elements across the interface as approximately 8, and the initial grid for Ω should be approximately $\frac{7}{\sqrt{2}\varepsilon}$ elements in the x-direction and $\frac{8}{\sqrt{2}\varepsilon}$ elements in the y-direction. Define the time domain, taking $T_0 = 0.04$, $T_q = 0.05$ and $T = 30$. We keep our timestep fixed for this test to keep the error consistent from initial conditions thus we take $\Delta t = 0.0025$. Now we have defined all the discretisation parameters for this test series.

In the test series we wish to observe the effect of the surfactants on the angles at the (left) triple junction. To measure the angles we linearly interpolate between the centre point of the junction $T^{(1,2,3)}$ (we take $\varphi_\varepsilon^{(1)} = \varphi_\varepsilon^{(2)} = \varphi_\varepsilon^{(3)} = \frac{1}{3}$) and the start of the branch $\Gamma^{(i,j)}$ (we take the closest point to $T^{(1,2,3)}$ where $\varphi_\varepsilon^{(i)} = \varphi_\varepsilon^{(j)} = 0.5$). In practice these features were ≈ 4 grid spaces apart across all values of ε. We then measure the angles between these lines. This is a natural method in a phase field setting, however there may be more accurate methods available to measure the angles [72].

We run the series for $\varepsilon = 0.2, 0.1333, 0.1, 0.05$. Some snapshots of the lens before and after the surfactant has been added are given by Figure 4.13 and Figure 4.14 respectively. Magnifications of the junctions at these times are also displayed in Figure 4.15 and 4.16. The angles recorded by the surfactant at time T_0 and time T are given in Table 4.5 and Table 4.6. We do not show the energy graphically, but we state the values in the second columns of Table 4.5 and 4.6 and we observe that they are convergent with respect to decreasing ε value. We also note that the energy change per timestep was in the order of 10^{-6} at the end of the simulation.

ε	$E_\varepsilon(T_0)$	$\psi^{(1)}(T_0)$	$\psi^{(2)}(T_0)$	$\psi^{(3)}(T_0)$
0.2	29.1597	122	121	125
0.1333	29.3045	122	120	118
0.1	29.4038	120	120	120
0.05	29.6846	120	120	120
ref	–	120	120	120

Table 4.5: *The table displays the measured angles (discussed for the diffuse setting in the test setup) of the test series at time $T_0 = 0.4$ in the absence of surfactant (in degrees for readability). The reference is the desired angles which were predicted by the model. We additionally provide the discrete energy calculated at this time.*

From the Figures 4.13 - 4.16 it is possible to see clear differences before and after

ε	$E_\varepsilon(T)$	$\psi^{(1)}(T)$	$\psi^{(2)}(T)$	$\psi^{(3)}(T)$
0.2	47.3503	109	126	125
0.1333	47.5829	103	126	135
0.1	47.7436	103	124	133
0.05	47.8575	96	126	141
ref	–	90	120	150

Table 4.6: *The table displays the measured angles (discussed for the diffuse setting in the test setup)of the test series at time $T = 30$ with surfactant present, (in degrees for readability). The reference is the desired angles which were predicted by the model.*

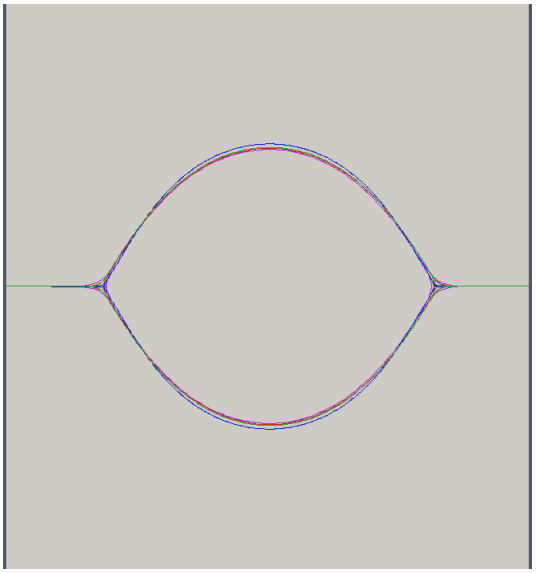

Figure 4.13: *Figure displaying the state of the system at time $t = T_0$. We see the $\varphi_\varepsilon^{(\cdot)} = 0.5$ level sets for each phase field, as well as the $\varphi_\varepsilon^{(1)} = \varphi_\varepsilon^{(2)} = \varphi_\varepsilon^{(3)} = \frac{1}{3}$ level set points. We have coloured them $\varepsilon = 0.05$ (blue), $\varepsilon = 0.1$ (green), $\varepsilon = 0.15$ (red) and $\varepsilon = 0.2$ (purple).*

the surfactant has been added. The surfactant has altered the surface tensions and the system has attempted to maintain the angle balance whilst also maintaining volume conservation and the boundary conditions for the Cahn-Hilliard system, causing the change of lens shape. We observe that all the simulations display the same effect from the surfactant however there is no observable convergence in the positions of the lens. In the quantitative results we see in Tables 4.5 and 4.6, the energies between subsequent simulations converged as $\varepsilon \to 0$ in both tests. We also see that there is some convergence of the angles, as at values $\varepsilon = 0.2$ there is poor agreement with the angles both at time T_0 and at time T where as this becomes much stronger as ε is reduced. For stronger quantitative information, the measurements of angles could be performed with different techniques, as the largest source of error is likely to be that at more diffuse junctions it is more difficult to use methods that scale with the

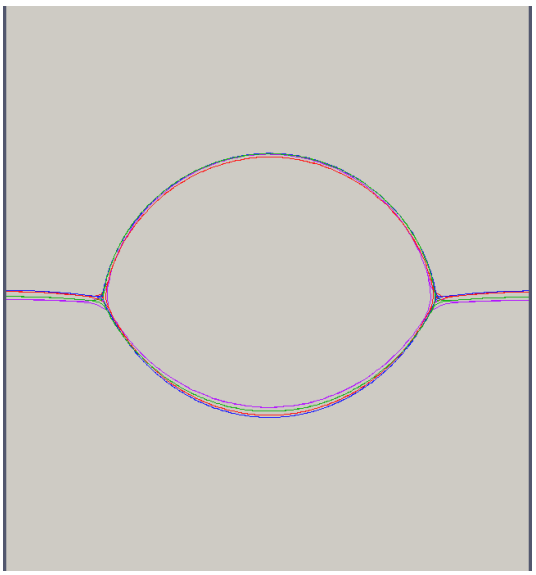

Figure 4.14: *Figure displaying the state of the system at time* $t = T$*. We see the* $\varphi_\varepsilon^{(\cdot)} = 0.5$ *level sets for each phase field, as well as the* $\varphi_\varepsilon^{(1)} = \varphi_\varepsilon^{(2)} = \varphi_\varepsilon^{(3)} = \frac{1}{3}$ *level set points. We have coloured them* $\varepsilon = 0.05$ *(blue),* $\varepsilon = 0.1$ *(green),* $\varepsilon = 0.15$ *(red) and* $\varepsilon = 0.2$ *(purple).*

size of the triple junction region. Another source of error could still be the inconsistencies within the triple junctions, and thus one could observe more clear convergence if this was perhaps further minimised.

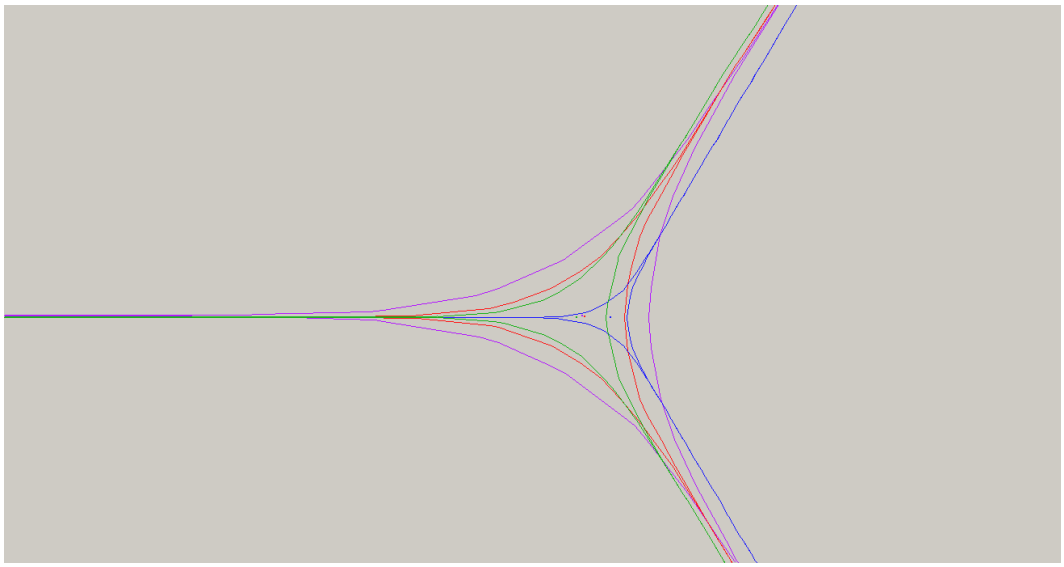

Figure 4.15: *Figure displaying the state of the system at time $t = T_0$. We see the $\varphi_\varepsilon^{(\cdot)} = 0.5$ level sets for each phase field, as well as the $\varphi_\varepsilon^{(1)} = \varphi_\varepsilon^{(2)} = \varphi_\varepsilon^{(3)} = \frac{1}{3}$ level set points. We have coloured them $\varepsilon = 0.05$ (blue), $\varepsilon = 0.1$ (green), $\varepsilon = 0.15$ (red) and $\varepsilon = 0.2$ (purple).*

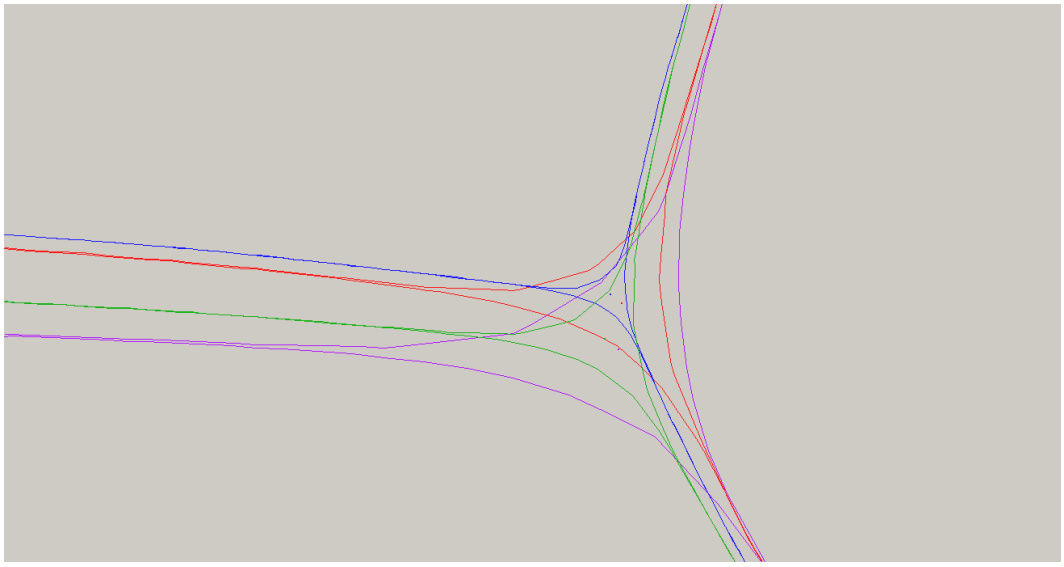

Figure 4.16: *Figure displaying the state of the system at time $t = T$. We see the $\varphi_\varepsilon^{(\cdot)} = 0.5$ level sets for each phase field, as well as the $\varphi_\varepsilon^{(1)} = \varphi_\varepsilon^{(2)} = \varphi_\varepsilon^{(3)} = \frac{1}{3}$ level set points.We have coloured them $\varepsilon = 0.05$ (blue), $\varepsilon = 0.1$ (green), $\varepsilon = 0.15$ (red) and $\varepsilon = 0.2$ (purple).*

4.3.3 Marangoni effect on a liquid lens

The goals of this simulation are twofold. We wish to demonstrate the capability of our scheme to simulate the effects of Marangoni forces upon a liquid droplet, and we wish to observe the convergence behaviour with respect to the interfacial width parameter ε. For each ε we shall relax a liquid lens then introduce surfactant into the domain forming a constant gradient. This will induce Marangoni forces along the interfaces and cause the lens to move. We stop all simulations at some time and compare the relative positions of the lenses for different epsilon values.

The sharp interface problem that is set up is similar to that which is shown in solid lines in Figure 4.1. Let $\Omega = [-2, 4] \times [-2, 2]$ and time $t \in [0, T]$, and consider it split into three time dependent subdomains separated by hypersurfaces. Initially $\Gamma^{(1,2)}(\boldsymbol{z}, 0)$ is given by $z \in \big((-2, -r) \cup (r, 4)\big) \times \{0\}$, and $\Gamma^{(1,3)}(\boldsymbol{z}, 0)$, (resp. $\Gamma^{(2,3)}(\boldsymbol{z}, 0)$) given by the upper (resp. lower) open semicircle of radius r and centred at the origin. $T^{(1,2,3)}(\boldsymbol{z}, 0)$ are at $(\pm r, 0)$. In this test we have taken $r = 1$.

The viscosities and densities of each subregion are fixed in time and matched across the different regions, take $\eta^{(i)} = 0.01$, $\overline{\rho}^{(i)} = 0.1$ for all $i = 1, 2, 3$. The initial velocity is given by $\boldsymbol{v}(\boldsymbol{z}, 0) = \mathbf{0}$, $\forall \boldsymbol{z} \in \Omega$, and take the boundary condition $\boldsymbol{v}(\boldsymbol{z}, t) = 0, \forall (\boldsymbol{z}, t) \in \partial\Omega \times [0, T]$, with no external body forces, $\boldsymbol{f} = \mathbf{0}$.

For the surfactants we make the assumption detailed in Section 2.1.9 of a local chemical equilibrium about the interfaces. We choose the quadratic isotherm of Section 2.1.11 for the study and take parameters $\sigma_0 = 1$, $\beta_i = 1$ and $\beta_{i,j} = 0.2$ for all $i = 1, 2, 3$ and $(i, j) = (1, 2), (1, 3), (2, 3)$. The surfactant mobilities we choose as $M_c^{(i)} = 10$ and $M_c^{(i,j)} = 50$.

Initially there are no surfactants present within the domain, however at a chosen time T_0 we shall introduce them, with a source at the left hand boundary and a sink along the right hand boundary. We introduce a relaxation time T_q for the flow to the boundary conditions to be more smoothly realised at $T_0 + T_q$. The boundary conditions are defined similarly to those in Section 4.3.2. More precisely, we apply the following boundary condition for q:

Let $z_L = (-2, y)$ and $z_R = (-2, y)$ $\forall y \in [-2, 2]$ then,

$$q(z_L, t) = \begin{cases} 0, & \text{for } t \in (0, T_0), \\ \frac{t - T_0}{2T_q}, & \text{for } t \in (T_0, T_0 + T_q), \\ 0.5, & \text{for } t \in (T_q, T), \end{cases} \qquad \text{and} \qquad q(z_R, t) = 0, \text{ for } t \in (0, T).$$

At the other areas of the boundary, q satisfies a Neumann condition. Also note, $q \in [0, 0.5]$ and so the isotherm relationship gives us the surface tension $\tilde{\sigma}_{i,j}(q) = \sigma_0 - \frac{1}{2}\frac{q^2}{\beta_{i,j}}$ takes val-

ues in $(0.375, 1)$. We have defined all the parameters and assumptions to satisfy solving the sharp interface problem with instantaneous adsorption, given by equations (2.82) - (2.90).

To create a diffuse interface model, we initialise as follows. We localize the inconsistencies about the triple junctions only, and so initialise the phase field similarly to Section 4.2, by using the profile of an exact solution for the two-phase Cahn-Hilliard equation to represent the initial hypersurfaces $\Gamma^{(i,j)}(\boldsymbol{z}, 0)$. We run separate test runs for different sized ε so fix this, then for $z = (x, y) \in \Omega$:

$$\varphi_\varepsilon^{(1)}(x, y, t = 0) = \begin{cases} \frac{1}{2}(1 + \tanh(\frac{2y}{\varepsilon})), & \text{for} \quad x \in [-2, -r) \cup (r, 4], \\ \frac{1}{2}(1 + \tanh(\frac{2(r-1)}{\varepsilon})), & \text{for} \quad (x, y) \in [-r, r] \times (0, 2], \\ 0, & \text{otherwise.} \end{cases}$$

$$\varphi_\varepsilon^{(2)}(x, y, t = 0) = \begin{cases} \frac{1}{2}(1 + \tanh(\frac{-2y}{\varepsilon})), & \text{for} \quad x \in [-2, -r) \cup (r, 4], \\ \frac{1}{2}(1 + \tanh(\frac{2(r-1)}{\varepsilon})), & \text{for} \quad (x, y) \in [-r, r] \times [-2, 0], \\ 0, & \text{otherwise.} \end{cases}$$

along with $\varphi_\varepsilon^{(3)} = 1 - \varphi_\varepsilon^{(1)} - \varphi_\varepsilon^{(2)}$ to conserve (2.103). Take initial velocity $\boldsymbol{v}_\varepsilon(\boldsymbol{z}, 0) = \boldsymbol{0}$. We resolve the triple junctions due to inconsistency of the initial conditions, before we allow the surfactant to enter the system.

We solve the system (2.174)-(2.176) for the phase field model. We take the choice of Boyer, Lapuerta and Minjeaud for the Cahn-Hilliard potential found in Section 2.2.8 with a constant mobility parameter $M_c = 0.005$ and regularisation parameter $\Lambda = 5$ and subsitute these choices into equations (2.174)-(2.176). For the Navier-Stokes we solve the system (2.179)-(2.180) using the rewritten force term (2.168). We take $\eta(\varphi_\varepsilon) = 0.01$ and $\rho(\varphi_\varepsilon) = 0.1$. We also take a zero velocity boundary condition for $\boldsymbol{v}_\varepsilon$ as in the sharp interface model for $\boldsymbol{v}$. We now solve the equations (2.177)-(2.178) for the surfactant, however there are no additional modelling parameters, and so we choose these as in the sharp interface description.

We discretise the diffuse interface model by using the timestepping scheme presented for fixed density Navier-Stokes (3.7) - (3.12) extended to multi phase Cahn-Hilliard as discussed in Section 3.3. We encorporate the surfactant by solving it alongside the Cahn Hilliard steps of the scheme, in this way we retain the symmetries of the scheme in order to retain the second order accuracy in time as was described in Section 3.5. For this time discretisation scheme we choose the optimal choice of $\theta = 1 - \frac{\sqrt{2}}{2}$ (discussed in Section 3.1.1), and we choose the parameters $\alpha = 2 - \sqrt{2}$ and $1 - \alpha = \sqrt{2} - 1$ for the implicit-explicit splitting for dissipation in the Navier-Stokes and an identical choice for γ and $1 - \gamma$ for the Cahn-Hilliard equations, and for ω and $1 - \omega$ for the surfactant equations.

For the spatial discretisation parameters, we wish to utilize adaptive refinement to reduce the computational demands while maintaining a high enough precision across the interfacial layers of the phase field. For ε fixed, we use an adaptive spatial grid paramter h, and refine the grid by using a strategy to bisect any element where $|\nabla\varphi_\varepsilon^{(\cdot)}| > \frac{C_a}{\varepsilon}$, taking $C_a = 0.02$, We have observed good accuracy of solutions if we retain $h_{\min} \approx \frac{\varepsilon}{5}$, and the maximum number of adaption levels as 6. This gives the number of elements across the interface as approximately 10, and the initial grid for Ω should be approximately $\frac{15}{4\varepsilon}$ elements in the x-direction and $\frac{5}{2\varepsilon}$ elements in the y-direction. Define the time domain, taking $T_0 = 2.4$, $T_q = 0.05$ and $T = 10$. Then we take the time step size also dependent on ε, that is, $\Delta t = \frac{\varepsilon}{10}$. Now we have defined all the discretisation parameters for this test series. We first display the simulation progression with $\varepsilon = 0.1$ then we will present the convergence results for various values of ε. The demonstration that the simulation can model the effects of Marangoni forces is displayed in Figure 4.17, Figure 4.18 and Figure 4.19, which capture snapshots of the $\varepsilon = 0.1$ simulation at times $t = T_0$, $t = T_0 + 0.6$ and $t = T_0 + 4$ respectively. Each displays on the left, the $\varphi_\varepsilon^{(i)} = 0.5$ level sets for $i = 1, 2, 3$ in white, the current simulation and in black, a reference solution calculated with no surfactant presence. On the right they display some velocity streamlines, these are coloured by the velocity in the x direction as this will be the dominant flow for the Marangoni effects.

The snapshots were chosen to represent the different stages of the simulation. Figure 4.17 represents the state before surfactant has been added into the system, the black and white solutions are overlayed, we see that $q = 0$ on the left figure, and on the right we note that the velocities are small, in fact the peak velocity magnitude is 0.102. Figure 4.18 is a snapshot shortly after the surfactant has been introduced to the flow, and shows the significant effects on the velocity stream lines. On the left, we see the surfactant potential has diffused into the domain, and it is now possible to differentiate between the surfactant present and non surfactant present simulations, with the white level sets further into the positive x direction compared with the black. On the right we see velocity of size 2 appearing along within the interfacial layer due to the surfactant concentration gradient. Finally Figure 4.19 shows the behaviour a long time after the surfactant has been introduced. On the left, the surfactant is near to a steady state with a constant decreasing gradient from source to sink in the x direction, which gives applies a steady Marangoni force on the droplet. It is clear that the effect this is having on the liquid lens is pushing it in a positive x direction as the white lens has moved relative to the black. The right displays a near steady x velocity too, it is pushing the droplet along the interfacial layers at a velocity of around 1.4. Until the end of the simulation this remained relatively constant.

We now move onto examining the convergence of the solutions with different values of the discretisation parameter ε. We performed the simulation for $\varepsilon = 0.2, 0.15, 0.1, 0.05$,

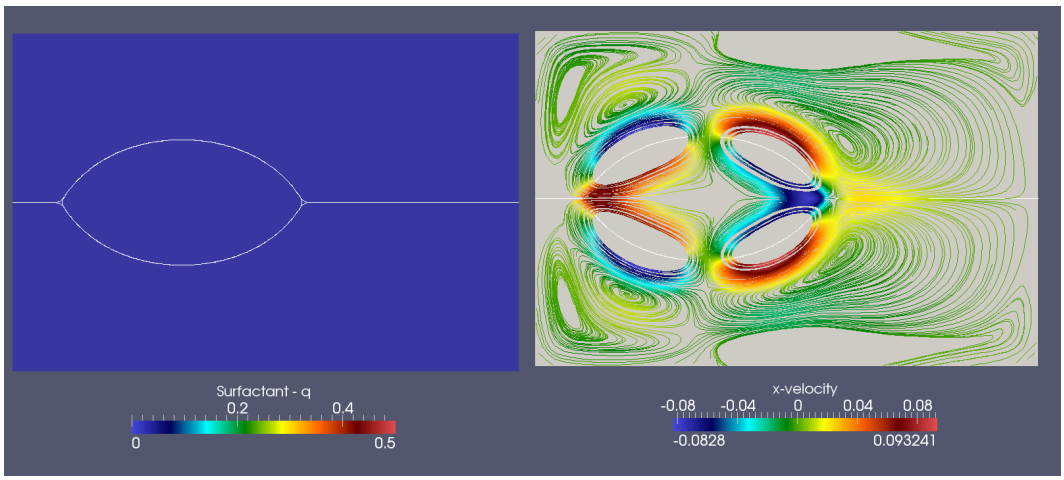

Figure 4.17: *Figure displaying the state of the system at time $t = T_0$ for $\varepsilon = 0.1$ test run. The left displays the $\varphi_\varepsilon^{(\cdot)} = 0.5$ level sets for each phase field over the background showing surfactant potential (here $q = 0$). The right displays the velocity stream lines coloured by their magnitude.*

and to evaluate this we present the differences in the coordinates of the triple junction locations of the lens upto the time T. As we are solving the diffuse problem, we may determine this by taking the intersection of the points $\varphi_\varepsilon^{(1)} = \varphi_\varepsilon^{(2)} = \varphi_\varepsilon^{(3)} = \frac{1}{3}$. Figure 4.20 displays the level sets $\varphi_\varepsilon^{(\cdot)} = 0.5$ and triple junction positions for each of the different ε values at the final time. Figure 4.21 shows the motion of the right hand junction in the x-coordinate direction until this time.

One can see in these figures that there does appear to be convergence of the solutions as epsilon is decreased. The behaviour of the larger ε solutions display less oscillations within $0 - 24$ graphical timesteps of Figure 4.21 and the effects of the surfactant introduced thereafter is more pronounced. This indicates that the interfacial forces appear to dominate inertial forces more strongly for larger ε values. This is also validated by Figure 4.22 which shows that the maximum velocity in the flow when drift occurs increases as ε decreases. A possible explanation for this ε dependence is that when the interfacial layer is large, there is a greater volume of the fluid on which the Marangoni forces take effect. Moreover, the bulk droplet volume relative to the interfacial layer volume is reduced for large interfacial thickness, and so there is a smaller region for bulk viscous forces to produce inertia to the motion. This would lead to higher dominance of interfacial forces (governed by surface tension) over the viscous forces, and so the droplet would move more quickly in the large ε regime.

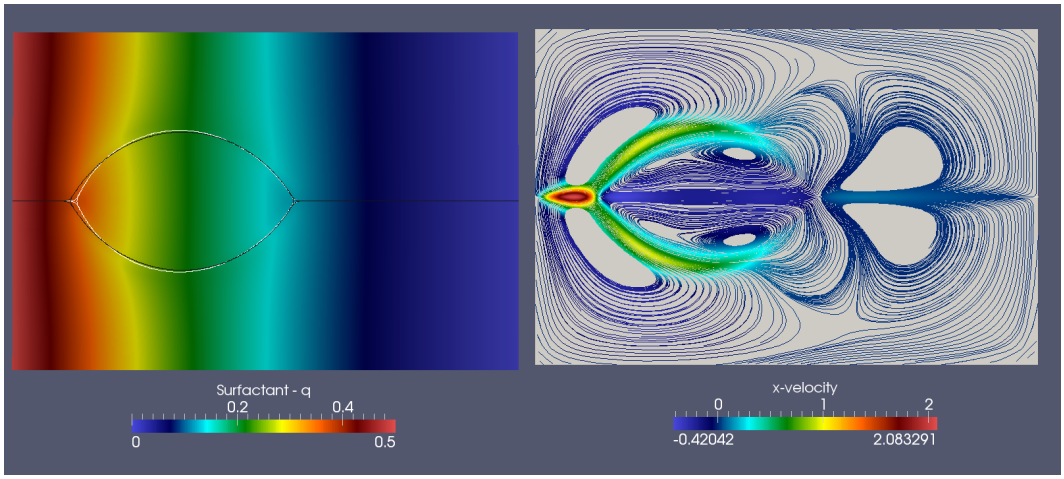

Figure 4.18: *Figure displaying the state of the system at time* $t = T_0 + 0.6$*. The left displays the* $\varphi_\varepsilon^{(\cdot)} = 0.5$ *level sets for each phase field, the black lines show a reference solution without surfactant. The white shows the effect of the background surfactant potential displayed. The right displays the velocity stream lines coloured by their magnitude.*

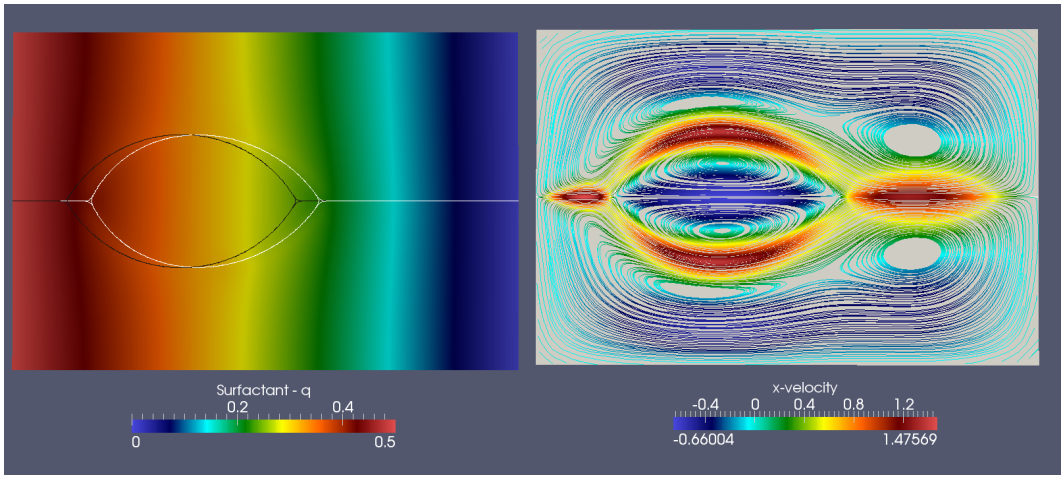

Figure 4.19: *Figure displaying the state of the system at time* $t = T$*. The left displays the* $\varphi_\varepsilon^{(\cdot)} = 0.5$ *level sets for each phase field, the black lines show a reference solution without surfactant. The white shows the effect of the background surfactant potential displayed. The right displays the velocity stream lines coloured by their magnitude.*

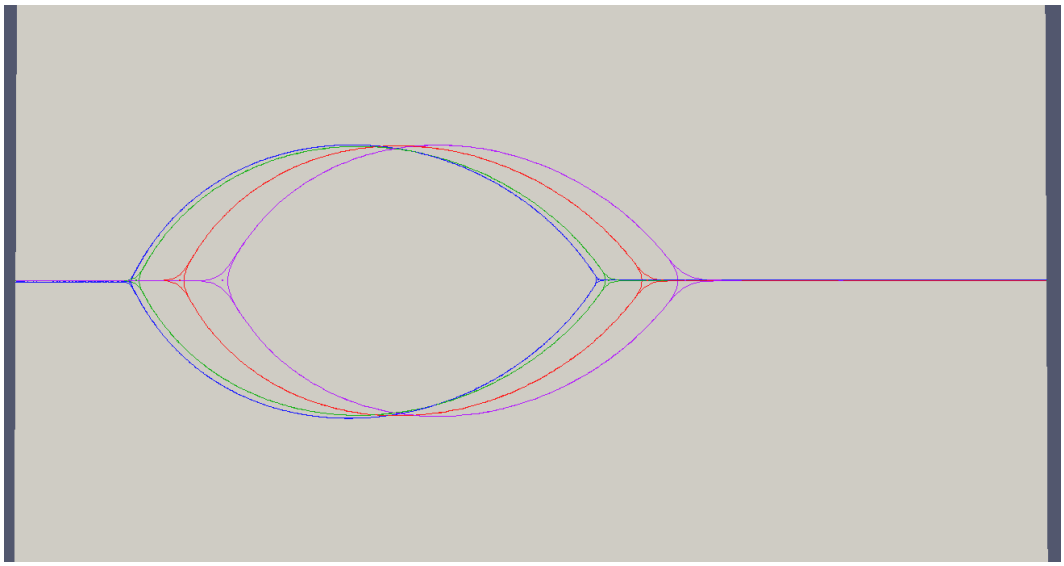

Figure 4.20: *Figure displaying the state of the test series at time $t = T$. We see the $\varphi_\varepsilon^{(\cdot)} = 0.5$ level sets for each phase field, as well as the $\varphi_\varepsilon^{(1)} = \varphi_\varepsilon^{(2)} = \varphi_\varepsilon^{(3)} = \frac{1}{3}$ level set points. From Left to Right, we have the $\varepsilon = 0.05$ (blue), $\varepsilon = 0.1$ (green), $\varepsilon = 0.15$ (red) and $\varepsilon = 0.2$ (purple).*

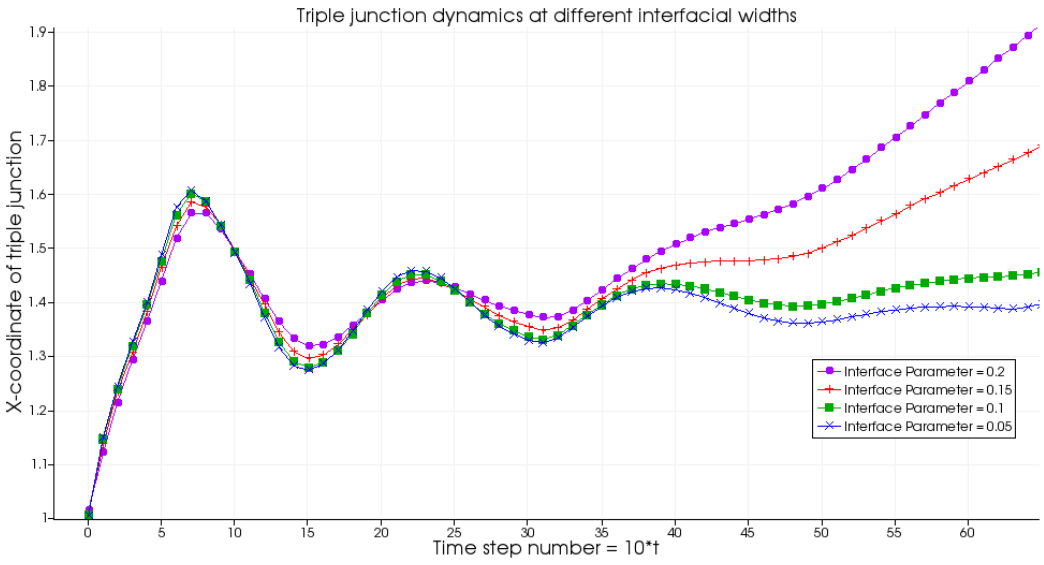

Figure 4.21: *Figure displaying the x-coordinates of the right hand triple junction of each lens over the period $t = 0$ to $t = T$ charted in ParaView. The final step is shown by Figure 4.20. The time step number of the printed solution is $\tau = 10\Delta t = 0.1$ and so the surfactant is introduced at $T_0 = 24\tau$ and final time is $T = 65\tau$. The displayed profiles are for $\varepsilon = 0.05$ (blue cross), $\varepsilon = 0.1$ (green square), $\varepsilon = 0.15$ (red plus) and $\varepsilon = 0.2$ (purple circle).*

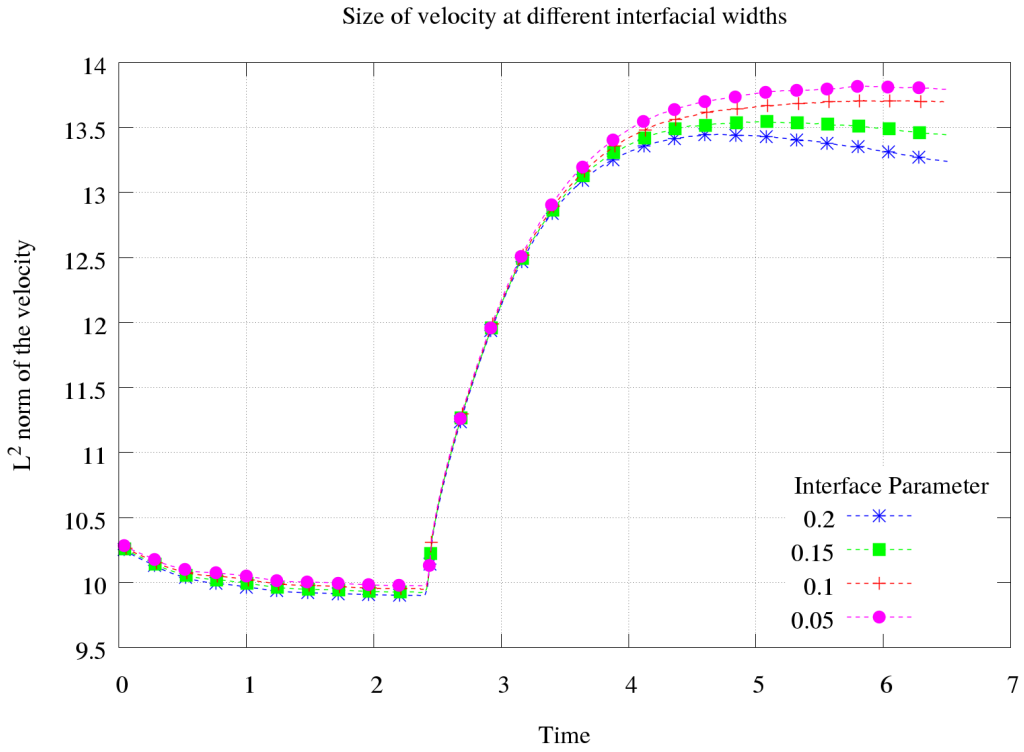

Figure 4.22: *Figure displaying the L^2 norm of the velocity over the period $t = 0$ to $t = T$. The surfactant is introduced at $t = 2.4$, and the final step is shown by Figure 4.20. The displayed profiles are for $\varepsilon = 0.05$ (blue cross), $\varepsilon = 0.1$ (green square), $\varepsilon = 0.15$ (red plus) and $\varepsilon = 0.2$ (purple circle).*

4.4 Coupled droplet with surfactant in three dimensions

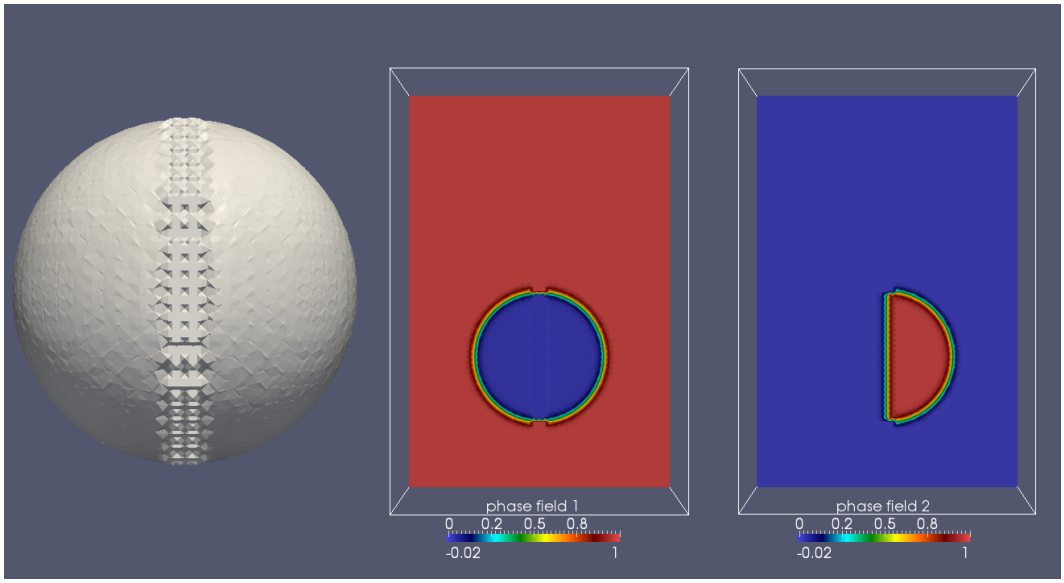

Figure 4.23: *Inital conditions for a coupled bubble represented by solid lines.* $\Omega^{(1)}$ *is an encapsulating fluid containing a coupled droplet of two fluids* $\Omega^{(2)}$ *and* $\Omega^{(3)}$*. The left demonstrates the* $\varphi_\varepsilon^{(1)} = 0.5$ *level set resolution. The middle displays a slice at* $y = 0$ *of* $\varphi_\varepsilon^{(1)}$ *and the right displays the same slice with initial values for* $\varphi_\varepsilon^{(2)}$

We wish to demonstrate the behavioural changes which may be captured by the code package in 3D. We begin with initial conditions shown in Figure 4.23, here we observe that we are simulating a coupled droplet in a surrounding fluid. $\Omega^{(2)}$ represents one droplet, $\Omega^{(3)}$ represents the other droplet, essentially at time zero these are represented by two touching hemispheres, separated by a flat surface. $\Omega^{(1)}$ represents the surrounding fluid. We prescribe different densities and viscosities to the fluids and run a simulation with and without surfactant presence. In particular we wish to observe and increase in necking (the shrinking of the interface) between the coupled droplet interface, and whether one can capture a topological change if the necking is significant enough.

The domain is given by $\Omega = [-2, 2] \times [-2, 2] \times [-2, 4]$, and the initial conditions for the sharp interface model (similarly in Figure 4.23) are given by

$$\Gamma^{(1,2)}(\mathbf{w}, 0) \cup \Gamma^{(1,3)}(\mathbf{w}, 0) = \{\mathbf{u} \in \Omega \,|\, \|\mathbf{u}\| = 1\},$$

the unit sphere, and the dividing hypersurface,

$$\Gamma^{(2,3)}(\mathbf{w}, 0) = \{\mathbf{u} \in \Omega \,|\, \|\mathbf{u}\| \leq 1\} \cap \{(x, 0, z) \,|\, x \in [-2, 2], z \in [-2, 4]\},$$

the unit disc in the second coordinate plane. The triple junction line is therefore situated at $T^{(1,2,3)}(\mathbf{w},0) = \{(x,0,z) \,|\, \|(x,z)\| = 1, x \in [-2,2], z \in [-2,4]\}$ the unit circle on the second coordinate plane.

The viscosties and densities of each subregion are taken as $\eta^{(1)} = 0.1,\ \eta^{(2)} = 0.05,\ \eta^{(3)} = 0.1$ and $\overline{\rho}^{(1)} = 0.2,\ \overline{\rho}^{(2)} = 0.25,\ \overline{\rho}^{(3)} = 0.1$. These are chosen so that the droplet represented by $\Omega^{(2)}$ wishes to rise in the surrounding fluid, and the droplet represented by $\Omega^{(3)}$ wishes to sink in the surrounding fluid. We also show that the solver can cope with different viscosities in the different phases. The initial velocity is given by $\boldsymbol{v}(\mathbf{w},0) = \mathbf{0},\ \forall \mathbf{w} \in \Omega$. We take the boundary condition $\boldsymbol{v}(\mathbf{w},t) = \mathbf{0},\ \forall (\mathbf{w},t) \in \partial\Omega \times [0,T]$, we take the body force of gravity as $\boldsymbol{f} = -9.8\overline{\rho}^{(i)}\mathbf{e}_3$ for $i = 1,2,3$ the standard basis vector in the third coordinate direction.

For the surfactants we take the instantaneous adsorption assumption, with the quadratic isotherm of Section 2.1.11, and we take parameters $\sigma_0 = 40$, $\beta_i = 1.0,\ \forall i$ and $\beta_{1,2} = \beta_{1,3} = 0.00625$, $\beta_{2,3} = 1.0$. the surfactant mobilities we take are $M_c^{(i)} = 10000$ and $M_c^{(i,j)} = \frac{10000}{\beta_{i,j}}$. As demonstrated in Section 4.3.3, it is sensible to have $q = 0$ initial surfactant, and at a time T_0 we introduce the surfactant through a dirichlet source condition smoothly, over a relaxation period T_q.

Let $\mathbf{w}_T = (x,y,4)\ \forall x,y \in [-2,2]$ then,

$$q(\mathbf{w}_T,t) = \begin{cases} 0, & \text{for } t \in (0,T_0), \\ \frac{t-T_0}{2T_q}, & \text{for } t \in (T_0,T_0+T_q), \\ 0.5, & \text{for } t \in (T_q,T). \end{cases}$$

We take Neumann boundary conditions for q at all other boundaries. Also note, as $q \in [0,0.5]$, then if q reaches the steady state $\bar{q} = 0.5$ everywhere, the isotherm predicts surface tensions of $\tilde{\sigma}_{2,3}(\bar{q}) = 39.875$ and $\tilde{\sigma}_{1,2}(\bar{q}) = \tilde{\sigma}_{1,3}(\bar{q}) = 20$. This determines all the parameters required for solving the sharp interface problem (2.82) – (2.90).

To create the phase field model we once again attempt to localise the consistency error to be about only the triple junction, to see the intial conditions for the simulation see Figure 4.23, we use the two phase solution away from the approximation of $T^{(i,j,k)}(\mathbf{w},0)$, and we do not detail the exact profiles here, as possibly more consistent approximations could be used for this discretisation. However the profiles shown in Figure 4.23 were sufficiently accurate for this simulation.

We mimic the initial conditions for the volume averaged velocity as $\boldsymbol{v}_\varepsilon(\mathbf{w},0) = \mathbf{0}$ as in the sharp interface model. We also take the initial conditions from the sharp interface problem for the surfactant.

We solve the system (2.174) – (2.180), for the diffuse interface model. We take the

choice of Boyer, Lapuerta and Minjeaud for the Cahn-Hilliard potential found in Section 2.2.8 with constant mobility $M_c = 0.005$ and regularisation parameter $\Lambda = 10$ and substitute these choices into equations (2.174) – (2.176). For the Navier-Stokes we solve the system (2.179) – (2.180) using the rewritten force term (2.168). We take $\eta(\varphi_\varepsilon)$ and $\rho(\varphi_\varepsilon)$ as the linear interpolation between the different constant values in each phase (discussed in Section 2.2.1. We also take a zero velocity boundary condition for $\boldsymbol{v}_\varepsilon$ as in the sharp interface model for $\boldsymbol{v}$. We now solve the equations (2.177) – (2.178) for the surfactant, however there are no additional modelling parameters, and so we choose these as in the sharp interface description.

We discretise the diffuse interface model by using the timestepping scheme presented for variable density Navier-Stokes with surfactant constructed in Section 3.5, extended to a three phase flow as discussed in Section 3.3. For this time discretisation scheme we choose the optimal choice of $\theta = 1 - \frac{\sqrt{2}}{2}$ (discussed in Section 3.1.1), and we choose the parameters $\alpha = 2 - \sqrt{2}$ and $1 - \alpha = \sqrt{2} - 1$ for the implicit-explicit splitting for dissipation in the Navier-Stokes and an identical choice for γ and $1 - \gamma$ for the Cahn-Hilliard equations, and for ω and $1 - \omega$ for the surfactant equations.

For the spatial discretisation parameters, we use adaptive refinement to reduce the computational demands while maintaining a high enough precision across the interfacial layers of the phase field. Fix $\varepsilon = 0.12$ then, we use an adaptive spatial grid paramter h, and refine the grid by using a strategy to bisect any element where $|\nabla\varphi_\varepsilon^{(\cdot)}| > 0.3$, this have observed good stability of solutions if we retain $h_{\min} \approx \frac{\varepsilon}{3}$, and the maximum number of adaption levels as 8 and minimum as 4. This gives the number of elements across the interface as approximately 6, and the initial grid for Ω was taken as $12, 12, 18$ in the x, y, z directions. Define the time domain, taking $T_0 = 0.01$, $T_q = 0.05$ and $T = 1.4$. We take the time step size $\Delta t = 0.0025$. Now we have defined all the discretisation parameters for this test series. The tests with and without surfactant were ran on the TNIS high performance cluster and both took approximately 5 minutes per timestep at 64 processors.

Some snapshots of the simulation can be seen in the figures produced. We first observe without the presence of surfactant, in Figure 4.24 we see that the droplet is relaxing from initial conditions, the left displays the $\varphi_\varepsilon^{(1)}$ level set coloured by the $\varphi_\varepsilon^{(3)}$ phase (to show the coupled droplets). The right hand side displays the pressure over a slice with velocity field given by the coloured glyphs. We observe that the pressure gradient is fairly minor compared with the interfacial forces. In Figure 4.25 we see much later in the simulation that the droplet begins to turn, and attempts to rise, this is due to the droplet represented by $\varphi_\varepsilon^{(3)}$ (red) is lighter than the surrounding fluid, and droplet $\varphi_\varepsilon^{(2)}$ (blue) is heavier than the surrounding fluid.

We next introduce the surfactant, our parameters allow for the dynamics to take

place quickly. Figure 4.26 displays the level sets of the surfactant flow, to show how it enters the domain. Figures 4.27, 4.28, 4.29 demonstrate three key stages of the simulation, displayed on the left the surfactant is present in the domain, on the right it is absent and the colouring is as in the previous figures. Figure 4.27 shows that with low surfactant concentration there is little difference between solution behaviour, then by the time the surfactant is almost fully saturating the domain we observe significant necking between the bubbles in Figure 4.28 this is due the decrease in surface tension along the interfacial layers representing $\Gamma^{(1,2)}$ and $\Gamma^{(1,3)}$. The parameters chosen ensure that the layer representing $\Gamma^{(2,3)}$ has a relatively comparable surface tension in the presence of surfactant and in absence. Finally we observe that our model captures a resulting topological change in Figure 4.29, where the necking has become so costly that the interface disappears between the droplets, we also observe the effects of the variable densities here are more present now the droplets are detached comparable to the coupled droplet on the right. This effect would not have been able to be captured in the sharp interface description due to the topological change.

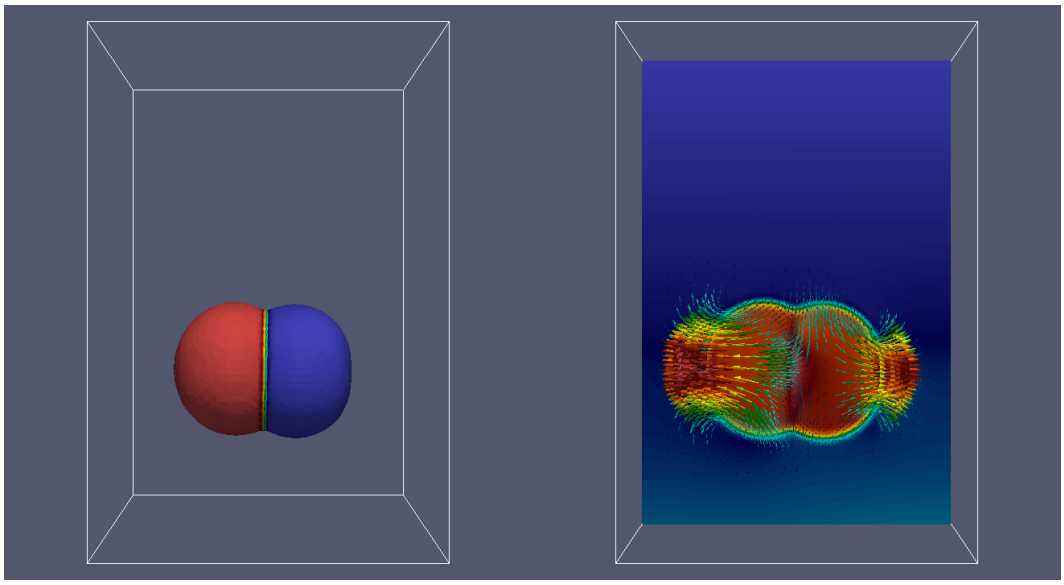

Figure 4.24: *Dynamics soon after initial conditions at* $t = 0.1$. *The left hand side displays the* $\varphi_\varepsilon^{(1)} = 0.5$ *level set coloured by the* $\varphi_\varepsilon^{(3)}$ *phase (shows the differentiation between the coupled droplets). The right hand side displays the pressure over a slice with velocity field given by the glyphs - large red arrows are higher velocity.*

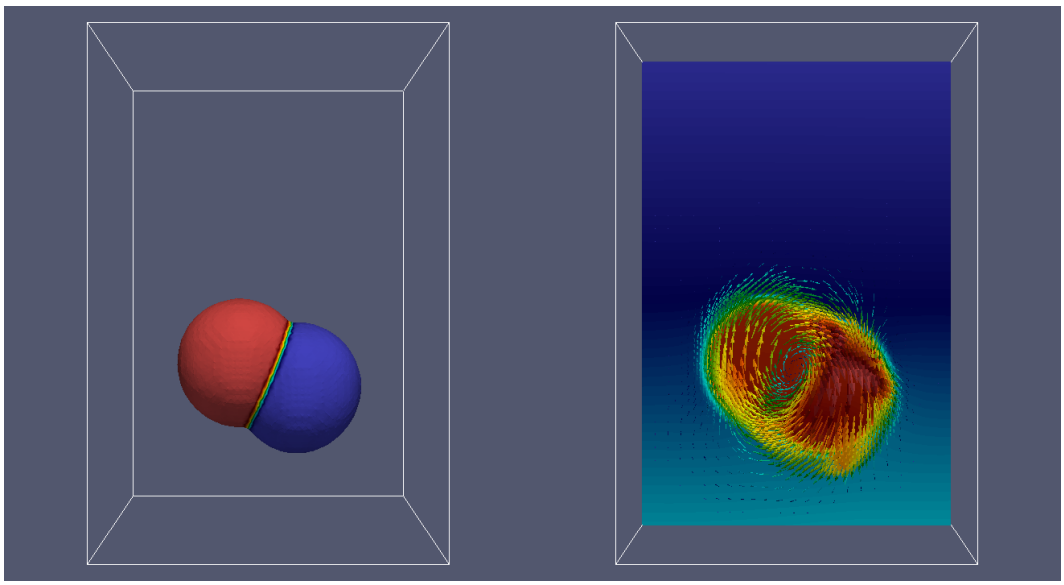

Figure 4.25: *Dynamics soon after initial conditions at* $t = 1.4$*. The left hand side displays the* $\varphi_\varepsilon^{(1)} = 0.5$ *level set coloured by the* $\varphi_\varepsilon^{(3)}$ *phase (shows the differentiation between the coupled droplets). The right hand side displays the pressure over a slice with velocity field given by the glyphs - large red arrows are higher velocity.*

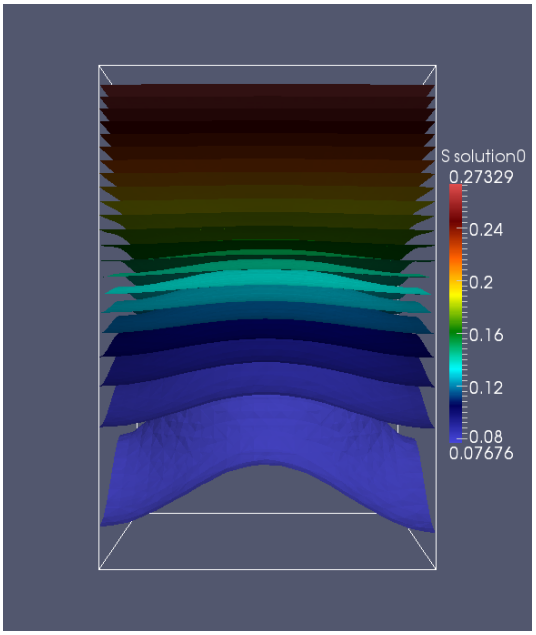

Figure 4.26: *Snapshot taken soon after initial conditions at* $t = 0.04$*. The level sets of the surfactant concentration are shown, the inflow concentration is around* 0.28 *at the top of the domain, as the snapshot is taken during the relaxation period* $(T_0, T_0 + T_q)$*.*

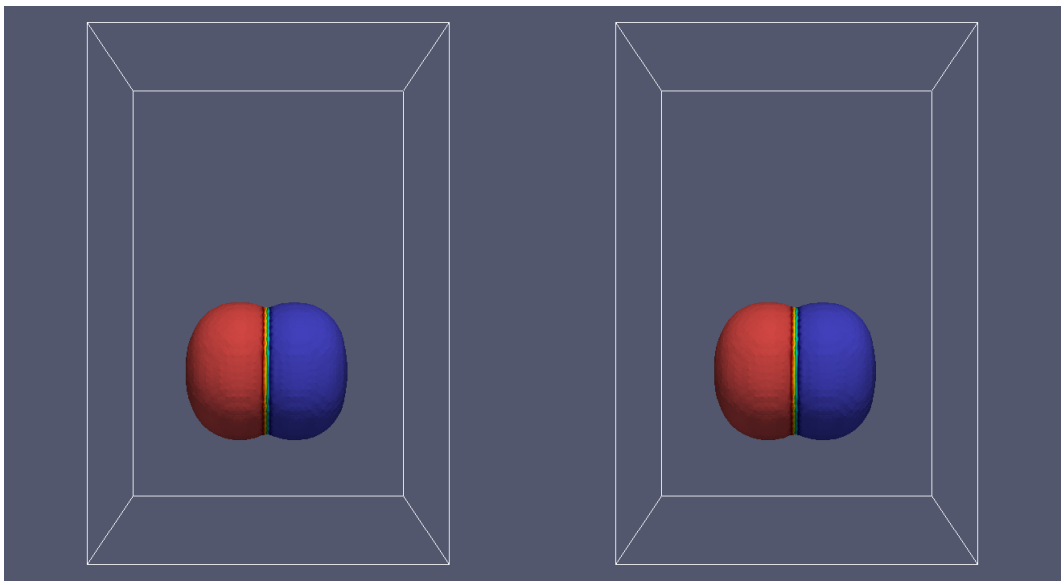

Figure 4.27: *Dynamics soon after initial conditions at* $t = 0.04$*. Displayed is the* $\varphi_\varepsilon^{(1)} = 0.5$ *level set coloured by the* $\varphi_\varepsilon^{(3)}$ *phase (shows the differentiation between the droplets). The left hand side displays the simulation with surfactant present, the right hand side displays the simulation with no surfactant present.*

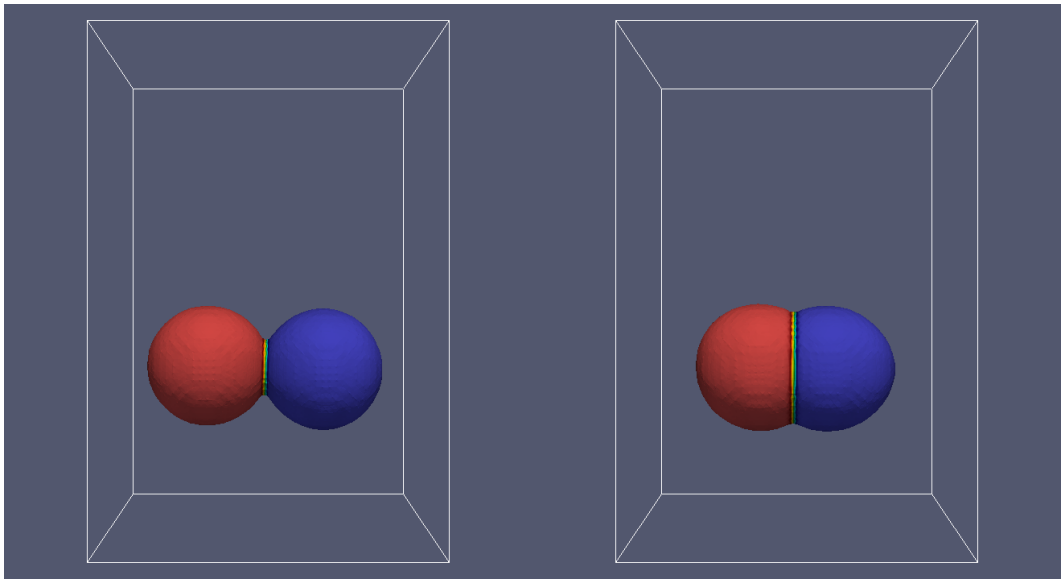

Figure 4.28: *Dynamics soon after initial conditions at* $t = 0.2$*. Displayed is the* $\varphi_\varepsilon^{(1)} = 0.5$ *level set coloured by the* $\varphi_\varepsilon^{(3)}$ *phase (shows the differentiation between the droplets). The left hand side displays the simulation with surfactant present, the right hand side displays the simulation with no surfactant present.*

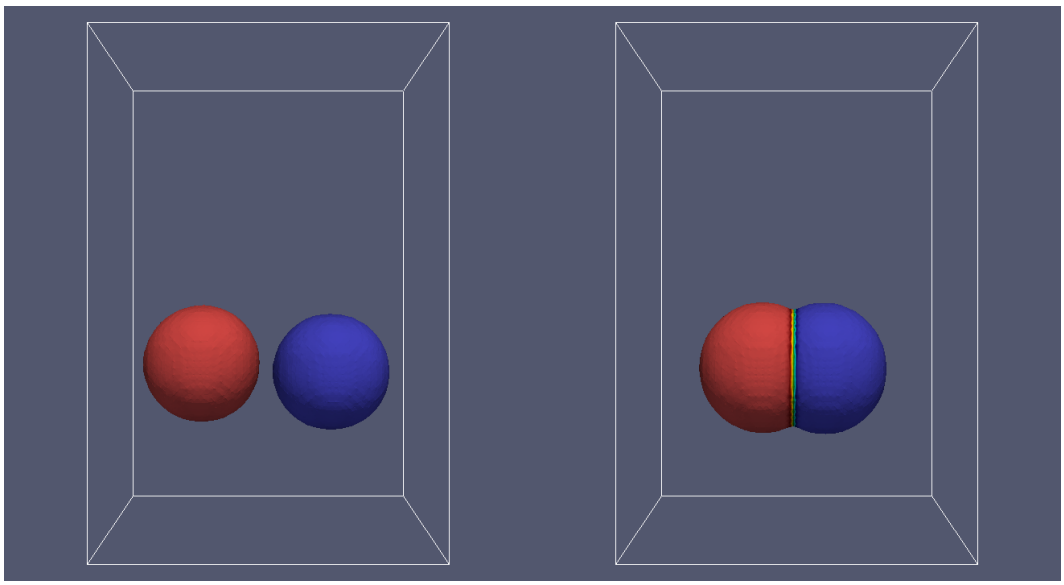

Figure 4.29: *Dynamics soon after initial conditions at* $t = 0.33$. *Displayed is the* $\varphi_\varepsilon^{(1)} = 0.5$ *level set coloured by the* $\varphi_\varepsilon^{(3)}$ *phase (shows the differentiation between the droplets). The left hand side displays the simulation with surfactant present, the right hand side displays the simulation with no surfactant present.*

Chapter 5

Conclusions

Within this thesis we made contributions to the area of mathematical modelling for a multi-phase flow with surfactant, and to the development of schemes for multi-phase flow.

With regards to the first aim, we began by setting up a problem for multi-phase flow with surfactant directly in Section 2.1. Our approach used the theoretical principles of conservation and extended the work of [54] to multiple phases. We represented moving interfaces with hypersurfaces transported by a flow and derived mass and momentum balance equations as partial differential equations over the moving domains. We closed these equations by considering a free energy formulation, and proposed constitutive assumptions on the free energies and associated fluxes that ensured the total energy of the system would be consistent with the second law of thermodynamics. The benefits of this property are discussed in [1]. For the fluid velocities, we arrived at an incompressible Navier-Stokes equation. The bulk and surface surfactant concentrations we found satisfied advection diffusion equations in the bulk domains and intefaces respectively, and were coupled by an adsorption - desorption function that was determined. The sorption process is an important consideration in the modelling of soluble surfactants and our model required relatively general properties on the form of this process. In experimental literature, for example [44], an assumption of local equilibrium is made between bulk and interfacial surfactants, leading to equilibrium relationships (isotherms [85]). With this assumption at all interfaces, we constructed a model for this case known as instantaneous sorption. This case is well suited to implementation, as it is less degenerate than the equations in the general case, as all surfactant concentrations are rewritten as functions of a continuous potential existing everywhere. For this, we additionally provided some isotherms, including one we use in simulations.

Having constructed the sharp interface model, we proceed to develop an approximating model based on phase fields in Section 2.2. The benefit of our free energy framework is observed here as we were able to repeat the the same techniques to mimic each step of

the sharp interface model development through the derivation. We first set up the phase field variables representing each domain, and used them to postulate equations for the fluid motion with a new volume averaged velocity [1]. From a distributional formulation for the surfactants, motivated by the work of [6], we proposed suitable regularisations as functions of the phase field for these equations too. The free energy of Ginzburg-Landau type was chosen [17], and we referenced some support for the minimisation problem [56] that arises using this energy, which helps for the choice of energy densities for the multi-phase problem. The constitutive assumptions for this energy allowed us to form the general sorption model which is consistent with the second law of thermodynamics. Finally, we formulated an instantaneous sorption model using the techniques of the sharp interface model derivation.

With regards to the second aim, we chose to pursue the development of a second order accurate scheme for the Navier-Stokes Cahn-Hilliard system arising in Section 2.2. The idea was to use a second order accurate scheme which has been documented for the Navier-Stokes equations [26], and then to observe whether this consistency is retained when it is extended to the coupling with a Cahn-Hilliard problem. We chose to first construct the scheme with a two phase problem and with a fixed density in all fluids using ideas from [35], and performed a stability analysis. We were able to show that coupling errors decayed in every timestep. However we conclude that the decay was insufficient for a stability estimate, due to the timestepping constraint but made significant progress towards an estimate. It is important to note that later, in Chapter 4 we observed the scheme is stable in practice, and in all simulations the energy decayed across every timestep (upto external forces). After this we considered various extensions, such as to multiple phases, inclusion of surfactants, and having different densities in the different fluid phases. For the variable density scheme, using another novel technique for inclusion of the density, we could prove that the second order accuracy is achieved. For implementation, we used multiple phases and included surfactants, we showed that in the case of instantaneous adsorption with a chosen isotherm we can retain second order accuracy as well.

We proceeded in the final chapter to verify the conclusions of the previous chapter with regards to the aims discussed. This involved significant development of a code to solve the fully discrete problems using finite element methods discussed in Chapter 3 in C++ in DUNE (Distributed Unified Numerics Environment). Use of other packages programs for this research are referenced in Chapter 1. We first discussed the second order accuracy of scheme for the Navier-Stokes coupling and found for the variable density coupling that the velocity convergence with an estimated convergence order of rate 2. We also commented on the stability, and found for this test scenario that it appeared the stability constraint (3.68) was more restrictive than appeared necessary, the exact relationship would require further

study. We also commented that the numerical energy decay (upto the action of external forces) occured in practice for all simulations.

We presented the convergence of the diffuse interface model to the sharp interface model using several test cases. This was first approached through the simulation to test the convergence for surfactant with fixed phase field and fluid equations. A triple junction was relaxed then fixed and a surfactant flow was run through it for a fixed time. The simulation was a well validated benchmark problem as we could explicitly calculate the sharp interface solution as the problem reduced to a 1D flow and compared the profile. In particular we expected this test to demonstrate the convergence (2.177) – (2.178) to (2.87) at the interface as $\varepsilon \to 0$. We showed the accuracy was good for all simulations, and converged with estimated rate of just less than 1. Next we tested the coupled phase field and surfactant equation in the absence of the fluid flow towards a steady state. This would demonstrate in particular the recovery of (2.90). We saw convergence towards desired angles, but noted drawbacks in measuring angles at large interfacial widths. In this test series we considered the fully coupled problem for surfactant Cahn-Hilliard Navier-Stokes flow. We did this to recover the dynamics of (2.75) that is, the force balance of inertial and interfacial forces at the interface that are prescribed for the sharp interface problem. We observed that in the case of larger ε value, the simulation overestimated the effects of Marangoni force at the triple junction, however it appeared to converge for small ε and reflects the care that choosing the interfacial thickness has on the behaviour of the solution. This novel simulation gives insight into the choices one must make about the size of ε in simulation.

Finally we demonstrated the flexibility and capability of the scheme. We computed a coupled droplet in three dimensions and compared the behaviour with and without surfactant presence. The results showed that we may capture significant surfactant effects which alter the behaviour of the system even in three dimensions, and also this simulation demonstrated the benefits of the diffuse model as it could capture a topological change.

Chapter 6

Appendix

6.1 Some useful identities

We state some useful identities for calculus on and with moving surfaces (for instance, see [18] and [31]).

Reynold's transport identity: For a time dependent domain $\Omega(t) \subset \mathbb{R}^d$ with exterior unit normal ν and with associated velocity field $\boldsymbol{v}$ (here note necessarily divergence free) and for a field $f(t) : \Omega(t) \to \mathbb{R}$ we have that

$$\frac{\mathrm{d}}{\mathrm{d}t} \int_{\Omega(\cdot)} f(\cdot)\Big|_t = \int_{\Omega(t)} \partial_t f(t) + \int_{\partial\Omega(t)} f(t)\, \boldsymbol{v}(t) \cdot \nu(t) = \int_{\Omega(t)} \partial_t^{\bullet(\boldsymbol{v})} f(t) + f(t)\, \nabla \cdot \boldsymbol{v}(t). \tag{6.1}$$

For a time dependent hypersurface $\Gamma(t)$ with velocity $\boldsymbol{v}$ and for a field $f(t) : \Gamma(t) \to \mathbb{R}$ we have that

$$\frac{\mathrm{d}}{\mathrm{d}t} \int_{\Gamma(\cdot)} f(\cdot)\Big|_t = \int_{\Gamma(t)} \partial_t^{\bullet(\boldsymbol{v})} f(t) + f(t) \nabla_{\Gamma(t)} \cdot \boldsymbol{v}(t). \tag{6.2}$$

Gauss-Green Formula: For an orientable hypersurface Γ with unit normal $\boldsymbol{\nu}$ and with outward unit conormal $\boldsymbol{\mu}$ on $\partial\Gamma$ and for any scalar field $f : \Gamma \to \mathbb{R}$ we have that

$$\int_\Gamma \nabla_\Gamma f = -\int_\Gamma f \boldsymbol{\kappa} + \int_{\partial\Gamma} f \boldsymbol{\mu}, \tag{6.3}$$

with the

$$\text{curvature vector } \boldsymbol{\kappa} = \nabla_\Gamma \cdot \boldsymbol{\nu}\, \nu.$$

Equivalently, for any vector field $\boldsymbol{w} : \Gamma \to \mathbb{R}^d$

$$\int_\Gamma \nabla_\Gamma \cdot \boldsymbol{w} = -\int_\Gamma \boldsymbol{w} \cdot \boldsymbol{\kappa} + \int_{\partial\Gamma} \boldsymbol{w} \cdot \boldsymbol{\mu}. \tag{6.4}$$

6.2 Non equilibrium adsorption constitutive assumptions

The flux,

$$\boldsymbol{j}_c^{(i)} \cdot \boldsymbol{\nu}^{(i,j)} = -\frac{1}{\alpha_{i,j}(c^{(i)}, c^{(i,j)})}(\gamma'_{i,j}(c^{(i,j)}) - g'_i(c^{(i)})),$$

is motivated by the energy contribution (2.24), that the following is satisfied

$$(\gamma'_{i,j}(c^{(i,j)}) - g'_i(c^{(i)}))\boldsymbol{j}_c^{(i)} \cdot \boldsymbol{\nu}^{(i,j)} \leq 0,$$

which is clearly seen. Similarly the choice of flux,

$$\boldsymbol{j}_c^{(i,j)} \cdot \boldsymbol{\mu}^{(i,j,k)} \coloneqq \beta_{j,k\leftrightarrow i,j}(\gamma'_{i,j}(c^{(i,j)}) - \gamma'_{j,k}(c^{(j,k)})) + \beta_{k,i\leftrightarrow i,j}(\gamma'_{i,j}(c^{(i,j)}) - \gamma'_{k,i}(c^{(k,i)})),$$

is motivated from the contribution (2.27), that the following is satisfied

$$-(\gamma'_{i,j}(c^{(i,j)})\boldsymbol{j}_c^{(i,j)} \cdot \boldsymbol{\mu}^{(i,j,k)} + \gamma'_{j,k}(c^{(j,k)})\boldsymbol{j}_c^{(j,k)} \cdot \boldsymbol{\mu}^{(j,k,i)} + \gamma'_{k,i}(c^{(k,i)})\boldsymbol{j}_c^{(k,i)} \cdot \boldsymbol{\mu}^{(k,i,j)}) \leq 0.$$

By using the balance of forces equation (without loss of generality we use this on the final term in the above expression), and the defined fluxes

$$\begin{aligned}
&- \Big(\gamma'_{i,j}\boldsymbol{j}_c^{(i,j)} \cdot \boldsymbol{\mu}^{(i,j,k)} + \gamma'_{j,k}\boldsymbol{j}_c^{(j,k)} \cdot \boldsymbol{\mu}^{(j,k,i)} + \gamma'_{k,i}\big(-\boldsymbol{j}_c^{(i,j)} \cdot \boldsymbol{\mu}^{(i,j,k)} - \boldsymbol{j}_c^{(j,k)} \cdot \boldsymbol{\mu}^{(j,k,i)}\big)\Big) \\
= &- \Big((\gamma'_{i,j} - \gamma'_{k,i})\boldsymbol{j}_c^{(i,j)} \cdot \boldsymbol{\mu}^{(i,j,k)} + (\gamma'_{j,k} - \gamma'_{k,i})\boldsymbol{j}_c^{(j,k)} \cdot \boldsymbol{\mu}^{(j,k,i)}\Big) \\
= &- \Big((\gamma'_{i,j} - \gamma'_{k,i})(\beta_{j,k\leftrightarrow i,j}(\gamma'_{i,j} - \gamma'_{j,k}) + \beta_{k,i\leftrightarrow i,j}(\gamma'_{i,j} - \gamma'_{k,i})) \\
&+ (\gamma'_{j,k} - \gamma'_{k,i})(\beta_{k,i\leftrightarrow j,k}(\gamma'_{j,k} - \gamma'_{k,i}) + \beta_{i,j\leftrightarrow j,k}(\gamma'_{j,k} - \gamma'_{i,j}))\Big) \\
= &- \beta_{k,i\leftrightarrow i,j}(\gamma'_{i,j} - \gamma'_{k,i})^2 - \beta_{k,i\leftrightarrow j,k}(\gamma'_{j,k} - \gamma'_{k,i})^2 - \Big(\beta_{j,k\leftrightarrow i,j}(\gamma'_{i,j} - \gamma'_{k,i})(\gamma'_{i,j} - \gamma'_{j,k}) \\
&\qquad - \beta_{i,j\leftrightarrow j,k}(\gamma'_{j,k} - \gamma'_{k,i})(\gamma'_{i,j} - \gamma'_{j,k})\Big).
\end{aligned}$$

Using the symmetry $\beta_{i,j\leftrightarrow j,k} = \beta_{j,k\leftrightarrow i,j}$ we then obtain,

$$= - \Big(\beta_{k,i\leftrightarrow i,j}(\gamma'_{i,j} - \gamma'_{k,i})^2 + \beta_{k,i\leftrightarrow j,k}(\gamma'_{j,k} - \gamma'_{k,i})^2 + \beta_{j,k\leftrightarrow i,j}(\gamma'_{i,j} - \gamma'_{j,k})^2\Big) \leq 0.$$

The other symmetries of the β's follow from the arbitrary labelling of i, j, k.

6.3 Bounds for $b(\cdot,\cdot,\cdot)$

6.3.1 Useful inequalities

We have used the following Sobolev Embeddings (summarised in [131]), L^p embeddings, and finite element reverse Poincaré inequality:

L^p Embedding: [135] If Ω is a finite domain, then for any $1 \leq p < q \leq \infty$,

$$L^q(\Omega) \subset L^p(\Omega), \qquad \text{and furthermore,} \qquad \|f\|_{L^p(\Omega)} \leq |\Omega|^{\frac{1}{r}} \|f\|_{L^q(\Omega)} \tag{6.5}$$

where $\frac{1}{r} = \frac{1}{p} - \frac{1}{q}$.

Sobolev Embedding Theorems: [131] If Ω is locally lipschitz, then for $u \in W^{m,p}(\Omega)$, $m \geq 1,\ 1 < p < \infty$ then define $r := \frac{1}{p} - \frac{m}{n}$,

- if $r = \frac{1}{q},\ |u|_{L^q(\Omega)} \leq c(m,p,n,\Omega)|u|_{W^{m,p}(\Omega)}$,
- if $r = 0,\ |u|_{L^q(\Lambda)} \leq c(m,p,n,q,\Lambda,\Omega)|u|_{W^{m,p}(\Omega)}$, $\forall 1 \leq q < \infty$ and bounded set $\Lambda \subset \bar{\Omega}$,
- if $r < 0,\ |u|_{C^0(\Lambda)} \leq c(m,p,n,\Lambda,\Omega)|u|_{W^{m,p}(\Omega)}$, for any bounded set $\Lambda \subset \bar{\Omega}$.

In particular for $m = 1, p = 2$ (i.e $r = \frac{1}{2} - \frac{1}{n}$) and without any regularity restrictions on Ω one obtains

- for $n = 2,\ |u|_{L^q(\Lambda)} \leq c(q,\Lambda,\Omega)|u|_{H^1(\Omega)}$, $\forall 1 \leq q < \infty$ and bounded set $\Lambda \subset \bar{\Omega}$,
- for $n \geq 3,\ |u|_{L^{\frac{2n}{n-2}}(\Omega)} \leq c(\Omega)|u|_{H^1(\Omega)}$.

Inverse Inequality: [25] Let $0 \leq k \leq l \in \mathbb{N}$ and $p, q \in [1,\infty)$, then $\exists\, C_{\text{inv}}$ depending on k, l, p, q and the space $\mathcal{P}(\hat{K})$ of lagrange polynomials on the reference triangle $\hat{K}$ of a triangulation in $\mathbb{R}^n$ such that,

$$\|D^l v_h\|_{L^q(K)} \leq C_{\text{inv}} h_K^{(k-\frac{n}{p})-(l-\frac{n}{q})} \|D^k v_h\|_{L^p(K)} \qquad \forall v_h \in \mathcal{P}(K).$$

Which can of course be generalised to the general triangulation if there is some uniform bound $\min_K h_K \geq h$. The main choice we see in the following arguements will be:

$$p = q = 2,\ l = 1, k = 0 \implies \|Dv_h\|_{L^2} \leq C_{\text{inv}} h^{-1} \|v_h\|_{L^2}.$$

6.3.2 Bounds for the convection operator

For the continuous setting [131] gives us some discrete bounds for $b(u, v, w)$: For $n \geq 2$ use Hölder's inequality

$$\left| \int_\Omega u_i \partial_i v_j w_j \, \mathrm{d}x \right| \leq |u_i|_{L^4(\Omega)} |\partial_i v_j|_{L^2(\Omega)} |w_j|_{L^4(\Omega)}.$$

Thus for the anti-symmetric operator $\frac{1}{2}\big(b(u, v, w) - b(u, w, v)\big)$, we obtain the bounds

$$\begin{aligned}
&\left|\frac{1}{2}\big(b(u, v, w) - b(u, w, v)\big)\right| \qquad \Big(= \frac{1}{2} \sum_{i,j=1}^{n} \left| \int_\Omega u_i \partial_i v_j w_j - u_i \partial_i w_j v_j \, \mathrm{d}x \right| \Big) \\
&\leq \frac{1}{2} \sum_{i,j=1}^{n} \Big(|u_i|_{L^4(\Omega)} |\partial_i v_j|_{L^2(\Omega)} |w_j|_{L^4(\Omega)} + |u_i|_{L^4(\Omega)} |\partial_i w_j|_{L^2(\Omega)} |v_j|_{L^4(\Omega)} \Big).
\end{aligned}$$

Then using Schwarz inequality, we obtain

$$\begin{aligned}
&\left|\frac{1}{2}\big(b(u, v, w) - b(u, w, v)\big)\right| \\
&\leq \frac{1}{2} \Big(\sum_{i=1}^{n} |u_i|^2_{L^4(\Omega)} \Big)^{\frac{1}{2}} \cdot \Big(\sum_{i,j=1}^{n} |\partial_i v_j|^2_{L^2(\Omega)} \Big)^{\frac{1}{2}} \cdot \Big(\sum_{j=1}^{n} |w_j|^2_{L^4(\Omega)} \Big)^{\frac{1}{2}} \qquad (6.6) \\
&\quad + \frac{1}{2} \Big(\sum_{i=1}^{n} |u_i|^2_{L^4(\Omega)} \Big)^{\frac{1}{2}} \cdot \Big(\sum_{i,j=1}^{n} |\partial_i w_j|^2_{L^2(\Omega)} \Big)^{\frac{1}{2}} \cdot \Big(\sum_{j=1}^{n} |v_j|^2_{L^4(\Omega)} \Big)^{\frac{1}{2}}. \qquad (6.7)
\end{aligned}$$

We now use an interpolation inequality for L^p norms: For $1 \leq r \leq s \leq t \leq \infty$, with $\frac{1}{r} = \frac{\theta}{s} + \frac{1-\theta}{t}$, the following inequality holds

$$|f|_{L^r} \leq |f|^{\theta}_{L^s} |f|^{1-\theta}_{L^t}.$$

Then found in [131] for the L^4 norm of a vector valued function.

$$|v|_{L^4(\Omega)} \leq 2^{\frac{1}{4}} |v|^{\frac{1}{2}}_{L^2(\Omega)} |\nabla v|^{\frac{1}{2}}_{L^2(\Omega)}, \qquad \forall v \in H^1_0(\Omega),\ \Omega \subset \mathbb{R}^2, \qquad (6.8)$$

$$|v|_{L^4(\Omega)} \leq 2^{\frac{1}{2}} |v|^{\frac{1}{4}}_{L^2(\Omega)} |\nabla v|^{\frac{3}{4}}_{L^2(\Omega)}, \qquad \forall v \in H^1_0(\Omega),\ \Omega \subset \mathbb{R}^3. \qquad (6.9)$$

Therefore, (6.8) followed by Hölder's inequality gives:

$$\begin{aligned}\sum_{i=1}^{2}|u_i|^2_{L^4(\Omega)} &\leq 2^{\frac{1}{2}}\sum_{i=1}^{2}|u_i|_{L^2(\Omega)}|\nabla u_i|_{L^2(\Omega)}\\ &\leq 2^{\frac{1}{2}}\Big(\sum_{i=1}^{2}|u_i|^2_{L^2(\Omega)}\Big)^{\frac{1}{2}}\Big(\sum_{i=1}^{2}|\nabla u_i|^2_{L^2(\Omega)}\Big)^{\frac{1}{2}}\\ &\leq 2^{\frac{1}{2}}|u|_{L^2(\Omega)}|\nabla u|_{L^2(\Omega)}, \end{aligned} \tag{6.10}$$

and similarly we find,(6.9) gives:

$$\sum_{i=1}^{3}|u_i|^2_{L^4(\Omega)} \leq 2|u|^{\frac{1}{2}}_{L^2(\Omega)}|\nabla u|^{\frac{3}{2}}_{L^2(\Omega)}, \tag{6.11}$$

Thus overall we obtain, for $n = 2$:

$$\Big|\frac{1}{2}\big(b(u,v,w) - b(u,w,v)\big)\Big| \leq 2|u|^{\frac{1}{2}}_{L^2(\Omega)}|\nabla u|^{\frac{1}{2}}_{L^2(\Omega)}|\nabla v|_{L^2(\Omega)}|w|^{\frac{1}{2}}_{L^2(\Omega)}|\nabla w|^{\frac{1}{2}}_{L^2(\Omega)}, \tag{6.12}$$

and for $n = 3$,

$$\Big|\frac{1}{2}\big(b(u,v,w) - b(u,w,v)\big)\Big| \leq 4|u|^{\frac{1}{4}}_{L^2(\Omega)}|\nabla u|^{\frac{3}{4}}_{L^2(\Omega)}|\nabla v|_{L^2(\Omega)}|w|^{\frac{1}{4}}_{L^2(\Omega)}|\nabla w|^{\frac{3}{4}}_{L^2(\Omega)}. \tag{6.13}$$

In the spatially discrete case for $b(u_h, v_h, w_h)$, we now may make use of the inverse Poincaré inequality to obtain, from (6.12):

$$\Big|\frac{1}{2}\big(b(u_h,v_h,w_h) - b(u_h,w_h,v_h)\big)\Big| \leq C(\Omega)h^{-1}|u_h|_{L^2(\Omega_h)}|\nabla v_h|_{L^2(\Omega_h)}|w_h|_{L^2(\Omega_h)},$$

and from (6.13),

$$\Big|\frac{1}{2}\big(b(u_h,v_h,w_h) - b(u_h,w_h,v_h)\big)\Big| \leq C(\Omega)h^{-\frac{3}{2}}|u_h|_{L^2(\Omega_h)}|\nabla v_h|_{L^2(\Omega_h)}|w_h|_{L^2(\Omega_h)}.$$

We denote the constants Ch^{-1} and $Ch^{-\frac{3}{2}}$ as the stability constant $S(h)$ in computations. Note that C is independent of h.

6.3.3 Bounds for the coupling operator

The operator for the coupling terms is of a very similar form to that of the convection operator. We do not use the skew symmetric form of the operator as it does not contain nice properties due to the fact that the phase field and its potential are not divergence free. We directly bound the operator $b(u, v, w)$ as follows using Hölder's inequality. Take $\frac{1}{p} = \frac{1}{2} - \frac{1}{q}$,

then:

$$\sum_{i=1}^{n} \left| \int_{\Omega} u_i \partial_i v \, w \, \mathrm{d}x \right| \leq \sum_{i=1}^{n} |u_i|_{L^p(\Omega)} |\partial_i v|_{L^2(\Omega)} |w|_{L^q(\Omega)}.$$

Applying Schwarz inequality,

$$\leq |w|_{L^q(\Omega)} \Big(\sum_{i=1}^{n} |u_i|^2_{L^p(\Omega)} \Big)^{\frac{1}{2}} \cdot \Big(\sum_{i=1}^{n} |\partial_i v|^2_{L^2(\Omega)} \Big)^{\frac{1}{2}}.$$

The form we wish the bounds to take for the coupling terms are of the form $b(u_h, v_h, w_h) \leq C(\Omega) h^{-k} |u_h|^2 |\nabla v_h|^2 |\nabla w_h|^2$ for the stability analysis. Thus we take this into account and apply the interpolation inequality (6.8) for general $\vartheta \in (0, 1)$, for $n = 2$, then the Poincaré inequality on $|w|$:

$$\sum_{i=1}^{n} |u_i|_{L^p(\Omega)} |\partial_i v|_{L^2(\Omega)} |w|_{L^q(\Omega)} \leq C(\Omega) |\nabla w|_{L^2(\Omega)} |u|^{\vartheta}_{L^2(\Omega)} |\nabla u|^{1-\vartheta}_{L^2(\Omega)} |\nabla v|_{L^2(\Omega)}. \quad (6.14)$$

In two dimensions $\vartheta > 0$ is the only condition as due to the Sobolev inequality, as $q < \infty$ is only required for the embedding with $H^1(\Omega)$. In three dimensions we require $q \leq 6$ for the embedding theorem and so we take the value $q = 6$ as our best case, this enforces $p = 3$ and then $\theta = \frac{1}{2}$. Using the interpolation inequality (6.9) for general $\vartheta \in (0, 1)$ $n = 3$, then the Poincaré inequality on $|w|$

$$\sum_{i=1}^{n} |u_i|_{L^3(\Omega)} |\partial_i v|_{L^2(\Omega)} |w|_{L^6(\Omega)} \leq C(\Omega) |\nabla w|_{L^2(\Omega)} |u|^{\frac{1}{2}}_{L^2(\Omega)} |\nabla u|^{\frac{1}{2}}_{L^2(\Omega)} |\nabla v|_{L^2(\Omega)}. \quad (6.15)$$

Finally, considering the spatially discrete setting with a finite element approximation. We consider $b(u_h, v_h, w_h)$ and from (6.14) we apply the reverse Poincaré inequality to $|u_h|^*$. This yields overall,

$$\sum_{i=1}^{2} \left| \int_{\Omega_h} u_{ih} \partial_i v_h \, w_h \, \mathrm{d}x \right| \leq C(\Omega) h^{-\theta} |u_h|_{L^2(\Omega)} |\nabla v_h|_{L^2(\Omega)} |\nabla w_h|_{L^2(\Omega)}, \quad (6.16)$$

and from (6.15):

$$\sum_{i=1}^{3} \left| \int_{\Omega_h} u_{ih} \partial_i v_h \, w_h \, \mathrm{d}x \right| \leq C(\Omega) h^{-\frac{1}{2}} |u_h|_{L^2(\Omega)} |\nabla v_h|_{L^2(\Omega)} |\nabla w_h|_{L^2(\Omega)}. \quad (6.17)$$

We denote the constants $Ch^{-\theta}$ and $Ch^{-\frac{1}{2}}$ as the stability constant $T(h)$ in computations. Note that C is independent of h.

Bibliography

[1] ABELS, H., GARCKE, H., AND GRÜN, G. Thermodynamically consistent, frame indifferent diffuse interface models for incompressible two-phase flows with different densities. *Mathematical Models and Methods in Applied Sciences 22*, 3 (2011), 1150013, 40pp.

[2] ADAMSON, A. W., AND GAST, A. P. *Physical chemistry of surfaces*. Interscience publishers New York, 1967.

[3] AFSAR-SIDDIQUI, A. B., LUCKHAM, P. F., AND MATAR, O. K. The spreading of surfactant solutions on thin liquid films. *Advances in Colloid and Interface Science 106*, 13 (2003), 183 – 236.

[4] ALKMPER, M., DEDNER, A., KLFKORN, R., AND NOLTE, M. The dune-alugrid module. *Archive of Numerical Software 4*, 1 (2016), 1–28.

[5] ALMGREN, A. S., BELL, J. B., COLELLA, P., HOWELL, L. H., AND WELCOME, M. L. A conservative adaptive projection method for the variable density incompressible navierstokes equations. *Journal of Computational Physics 142*, 1 (1998), 1 – 46.

[6] ALT, H. The entropy principle for interfaces. Fluids and solids. *Advances in Mathematical Sciences and Applications 19*, 2 (2009), 585–663.

[7] AMESTOY, P., DUFF, I. S., L'EXCELLENT, J.-Y., AND KOSTER, J. Mumps: A general purpose distributed memory sparse solver. In *Proceedings of the 5th International Workshop on Applied Parallel Computing, New Paradigms for HPC in Industry and Academia* (London, UK, UK, 2001), PARA '00, Springer-Verlag, pp. 121–130.

[8] ANDERSON, D., MCFADDEN, G., AND WHEELER, A. Diffuse–interface methods in fluid mechanics. *Annual Review of Fluid Mechanics 30*, 1 (1998), 139–165.

[9] ARNOLD, D. N., BREZZI, F., AND FORTIN, M. A stable finite element for the stokes equations. *CALCOLO 21*, 4 (1984).

[10] AYACHIT, U. *The ParaView Guide: A Parallel Visualization Application*. Kitware, Inc., USA, 2015.

[11] BALAY, S., ABHYANKAR, S., ADAMS, M. F., BROWN, J., BRUNE, P., BUSCHELMAN, K., DALCIN, L., EIJKHOUT, V., GROPP, W. D., KAUSHIK, D., KNEPLEY, M. G., MCINNES, L. C., RUPP, K., SMITH, B. F., ZAMPINI, S., ZHANG, H., AND ZHANG, H. PETSc users manual. Tech. Rep. ANL-95/11 - Revision 3.7, Argonne National Laboratory, 2016.

[12] BALAY, S., ABHYANKAR, S., ADAMS, M. F., BROWN, J., BRUNE, P., BUSCHELMAN, K., DALCIN, L., EIJKHOUT, V., GROPP, W. D., KAUSHIK, D., KNEPLEY, M. G., MCINNES, L. C., RUPP, K., SMITH, B. F., ZAMPINI, S., ZHANG, H., AND ZHANG, H. PETSc Web page, 2016.

[13] BALAY, S., GROPP, W. D., MCINNES, L. C., AND SMITH, B. F. Efficient management of parallelism in object oriented numerical software libraries. In *Modern Software Tools in Scientific Computing* (1997), E. Arge, A. M. Bruaset, and H. P. Langtangen, Eds., Birkhäuser Press, pp. 163–202.

[14] BARRETT, J. W., GARCKE, H., AND NÜRNBERG, R. Stable finite element approximations of two-phase flow with soluble surfactant. *Journal of Computational Physics 297* (2015), 530 – 564.

[15] BATCHELOR, G. K. *An introduction to fluid dynamics*. Cambridge university press, 2000.

[16] BELL, J. B., AND MARCUS, D. L. A second-order projection method for variable-density flows. *Journal of Computational Physics 101*, 2 (1992), 334 – 348.

[17] BELLETTINI, G., BRAIDES, A., AND RIEY, G. Variational approximation of anisotropic functionals on partitions. *Annali di Matematica Pura ed Applicata 184*, 1 (2005), 75–93.

[18] BETOUNES, D. Kinematics of submanifolds and the mean curvature normal. *Archive for Rational Mechanics and Analysis 96*, 1 (1986), 1–27.

[19] BOTHE, D., PRÜSS, J., AND SIMONETT, G. *Well-posedness of a Two-phase Flow with Soluble Surfactant*. Birkhäuser Basel, Basel, 2005, pp. 37–61.

[20] BOYER, F. A theoretical and numerical model for the study of incompressible mixture flows. *Computers & fluids 31*, 1 (2002), 41–68.

[21] BOYER, F., AND LAPUERTA, C. Study of a three component Cahn-Hilliard flow model. *M2AN Math. Model. Numer. Anal. 40*, 4 (2006), 653–687.

[22] BOYER, F., LAPUERTA, C., MINJEAUD, S., PIAR, B., AND QUINTARD, M. Cahn-Hilliard/Navier-Stokes model for the simulation of three-phase flows. *Transp. Porous Media 82*, 3 (2010), 463–483.

[23] BOYER, F., AND MINJEAUD, S. Hierarchy of consistent n-component Cahn-Hilliard systems. *Math. Models Methods Appl. Sci. 24*, 14 (2014), 2885–2928.

[24] BRAIDES, A. Γ-convergence for beginners. In *of Oxford Lecture Series in Mathematics and its Applications* (2002), University Press.

[25] BRENNER, S. C., AND SCOTT, L. R. *Polynomial Approximation Theory in Sobolev Spaces*. Springer New York, New York, NY, 1994, pp. 91–122.

[26] BRISTEAU, M., GLOWINSKI, R., AND PERIAUX, J. Numerical methods for the navier-stokes equations. applications to the simulation of compressible and incompressible viscous flows. *Computer Physics Reports 6*, 1 (1987), 73 – 187.

[27] BRONSARD, L., GARCKE, H., AND STOTH, B. A multi-phase Mullins-Sekerka system: matched asymptotic expansions and an implicit time discretisation for the geometric evolution problem. *Proc. Roy. Soc. Edinburgh Sect. A 128*, 3 (1998), 481–506.

[28] CAFFARELLI, L. A., AND MULER, N. E. An L^∞ bound for solutions of the Cahn-Hilliard equation. *Archive for Rational Mechanics and Analysis 133*, 2 (1995), 129–144.

[29] CAHN, J. W. On spinodal decomposition. *Acta Metallurgica 9*, 9 (1961), 795 – 801.

[30] CAHN, J. W., AND HILLIARD, J. E. Free energy of a nonuniform system. i. interfacial free energy. *The Journal of Chemical Physics 28*, 2 (1958), 258–267.

[31] CERMELLI, P., FRIED, E., AND GURTIN, M. E. Transport relations for surface integrals arising in the formulation of balance laws for evolving fluid interfaces. *J. Fluid Mech. 544* (2005), 339–351.

[32] CHEN, K.-Y., AND LAI, M.-C. A conservative scheme for solving coupled surface-bulk convectiondiffusion equations with an application to interfacial flows with soluble surfactant. *Journal of Computational Physics 257, Part A* (2014), 1 – 18.

[33] CHORIN, A. J. Numerical solution of the Navier-Stokes equations. *Mathematics of Computation 22* (1968), 745–762.

[34] CHORIN, A. J. On the convergence of discrete approximations to the Navier-Stokes equations. *Mathematics of Computation 23* (1969), 341–353.

[35] CHRISPELL, J., ERVIN, V., AND JENKINS, E. A fractional step θ-method for convectiondiffusion problems. *Journal of Mathematical Analysis and Applications 333*, 1 (2007), 204 – 218. Special issue dedicated to William Ames.

[36] CHRISPELL, J., ERVIN, V., AND JENKINS, E. A fractional step -method approximation of time-dependent viscoelastic fluid flow. *Journal of Computational and Applied Mathematics 232*, 2 (2009), 159 – 175.

[37] DAVIS, T. A. Algorithm 832: Umfpack v4.3—an unsymmetric-pattern multifrontal method. *ACM Trans. Math. Softw. 30*, 2 (June 2004), 196–199.

[38] DEDNER, A., KLÖFKORN, R., NOLTE, M., AND OHLBERGER, M. A generic interface for parallel and adaptive discretization schemes: abstraction principles and the dune-fem module. *Computing 90*, 3 (2010), 165–196.

[39] DIAMANT, H., AND ANDELMAN, D. Kinetics of surfactant adsorption at fluid–fluid interfaces. *Journal of Physical Chemistry 100* (1996), 13732–13742.

[40] DIAMANT, H., ARIEL, G., AND ANDELMAN, D. Kinetics of surfactant adsorption: the free energy approach. *Colloids and Surfaces A: Physicochemical and Engineering Aspects 183* (2001), 259–276.

[41] DING, H., SPELT, P., AND SHU, C. Diffuse interface model for incompressible two-phase flows with large density ratios. *Journal of Computational Physics 226*, 1 (2007), 2078–2095.

[42] DUNBAR, O., LAM, K. F., AND STINNER, B. Phase field modelling of surfactants in multi-phase flow. *In preperation*.

[43] EASTOE, J., AND DALTON, J. Dynamic surface tension and adsorption mechanisms of surfactants at the air–water interface. *Advances in Colloid and Interface Science 85* (2000), 103–144.

[44] EDWARDS, D. A., BRENNER, H., AND WASAN, D. T. *Interfacial transport processes and rheology*. Boston, 1991.

[45] EGGLETON, C. D., PAWAR, Y. P., AND STEBE, K. J. Insoluble surfactants on a drop in an extensional flow: a generalization of the stagnated surface limit to deforming interfaces. *Journal of Fluid Mechanics 385* (1999), 7999.

[46] ENGBLOM, S., DO-QUANG, M., AMBERG, G., AND TORNBERG, A.-K. On diffuse interface modeling and simulation of surfactants in two-phase fluid flow. *Communications in Computational Physics 14*, 4 (2013), 879–915. QC 20130819.

[47] FALGOUT, R. D., AND YANG, U. M. *hypre: A Library of High Performance Preconditioners*. Springer Berlin Heidelberg, Berlin, Heidelberg, 2002, pp. 632–641.

[48] FENG, X. Fully discrete finite element approximations of the navier–stokes–cahn-hilliard diffuse interface model for two-phase fluid flows. *SIAM Journal on Numerical Analysis 44*, 3 (2006), 1049–24.

[49] FIFE, P., AND PENROSE, O. Interfacial dynamics for thermodynamically consistent phase-field models with nonconserved order parameter. *Electronic Journal of Differential Equations 1995*, 16 (1995), 1–49.

[50] FRAIGNEAU, Y., GUERMOND, J.-L., AND QUARTAPELLE, L. Approximation of variable density incompressible flows by means of finite elements and finite volumes. *Communications in Numerical Methods in Engineering 17*, 12 (2001), 893–902.

[51] FRIBERG, S. E. Foams from non-aqueous systems. *Current Opinion in Colloid & Interface Science 15*, 5 (2010), 359 – 364.

[52] GARCKE, H. Curvature driven interface evolution. *Jahresbericht der Deutschen Mathematiker-Vereinigung 115*, 2 (2013), 63–100.

[53] GARCKE, H., HINZE, M., AND KAHLE, C. A stable and linear time discretization for a thermodynamically consistent model for two-phase incompressible flow. *Applied Numerical Mathematics 99* (2016), 151 – 171.

[54] GARCKE, H., LAM, K., AND STINNER, B. Diffuse interface modelling of soluble surfactants in two-phase flow. *Communications in Mathematical Sciences 12*, 8 (2014), 1475–1522.

[55] GARCKE, H., NESTLER, B., AND STOTH, B. On anisotropic order parameter models for multi-phase systems and their sharp interface limits. *Phys. D 115*, 1-2 (1998), 87–108.

[56] GARCKE, H., NESTLER, B., AND STOTH, B. A multiphase field concept: numerical simulations of moving phase boundaries and multiple junctions. *SIAM J. Appl. Math. 60*, 1 (2000), 295–315 (electronic).

[57] GARCKE, H., STOTH, B., AND NESTLER, B. Anisotropy in multi-phase systems: a phase field approach. *Interfaces Free Bound. 1*, 2 (1999), 175–198.

[58] GIBBON, J. D., PAL, N., GUPTA, A., AND PANDIT, R. A bkm-type theorem and associated computations of solutions of the three-dimensional cahn-hilliard-navier-stokes equations. *arXiv preprint arXiv:1608.05361* (2016).

[59] GIRAULT, V., AND RAVIART, P.-A. *Finite element methods for Navier-Stokes equations: theory and algorithms*, vol. 5. Springer Science & Business Media, 2012.

[60] GLOWINSKI, R. Finite element methods for incompressible viscous flow. In *Numerical Methods for Fluids (Part 3)*, vol. 9 of *Handbook of Numerical Analysis*. Elsevier, 2003, pp. 3 – 1176.

[61] GLOWINSKI, R., AND LE TALLEC, P. *Augmented Lagrangian and Operator-Splitting Methods in Nonlinear Mechanics*. Society for Industrial and Applied Mathematics, 1989.

[62] GRIFFIN, W. C. Calculation of hlb values of non-ionic surfactants. *Am Perfumer Essent Oil Rev 65* (1955), 26–29.

[63] GROSS, S., AND REUSKEN, A. *Numerical methods for two-phase incompressible flows*, vol. 40. Springer Science & Business Media, 2011.

[64] GUERMOND, J., MINEV, P., AND SHEN, J. An overview of projection methods for incompressible flows. *Computer Methods in Applied Mechanics and Engineering 195*, 4447 (2006), 6011 – 6045.

[65] GUERMOND, J., AND SHEN, J. A new class of truly consistent splitting schemes for incompressible flows. *Journal of Computational Physics 192*, 1 (2003), 262 – 276.

[66] GUERMOND, J.-L., AND QUARTAPELLE, L. A projection fem for variable density incompressible flows. *Journal of Computational Physics 165*, 1 (2000), 167 – 188.

[67] GURTIN, M., POLIGNONE, D., AND VIÑALS, J. Two-phase binary fluids and immiscible fluids described by an order parameter. *Mathematical Models and Methods in Applied Sciences 6*, 6 (1996), 815–831.

[68] HAMEED, M., SIEGEL, M., YOUNG, Y.-N., LI, J., BOOTY, M. R., AND PAPAGEORGIOU, D. T. Influence of insoluble surfactant on the deformation and breakup of a bubble or thread in a viscous fluid. *Journal of Fluid Mechanics 594* (2008), 307340.

[69] HARKINS, W., AND FELDMAN, A. Films. the spreading of liquids and the spreading coefficient. *Journal of the American Chemical Society 44*, 12 (1922), 2665–2685.

[70] HEYWOOD, J. G., AND RANNACHER, R. Finite-element approximation of the nonstationary navier–stokes problem. part iv: Error analysis for second-order time discretization. *SIAM Journal on Numerical Analysis 27*, 2 (1990), 353–384.

[71] HOHENBERG, P., AND HALPERIN, B. Theory of dynamic critical phenomena. *Reviews of Modern Physics 49*, 3 (1977), 435–479.

[72] HÖTZER, J., TSCHUKIN, O., SAID, M. B., BERGHOFF, M., JAINTA, M., BARTHELEMY, G., SMORCHKOV, N., SCHNEIDER, D., SELZER, M., AND NESTLER, B. Calibration of a multi-phase field model with quantitative angle measurement. *Journal of Materials Science 51*, 4 (2016), 1788–1797.

[73] JAMES, A., AND LOWENGRUB, J. A surfactant-conserving volume-of-fluid method for interfacial flows with insoluble surfactant. *Journal of Computational Physics 201* (2004), 685–722.

[74] JIAO, J., AND BURGESS, D. J. Rheology and stability of water-in-oil-in-water multiple emulsions containing span 83 and tween 80. *AAPS PharmSci 5*, 1 (Mar 2003), 62–73.

[75] JIN, F., GUPTA, N. R., AND STEBE, K. J. The detachment of a viscous drop in a viscous solution in the presence of a soluble surfactant. *Physics of Fluids 18*, 2 (2006), 022103.

[76] JOOS, P., FANG, J., AND SERRIEN, G. Comments on some dynamic surface tension measurements by the dynamic bubble pressure method. *Journal of Colloid and Interface Science 151*, 1 (1992), 144 – 149.

[77] KARNIADAKIS, G. E., ISRAELI, M., AND ORSZAG, S. A. High-order splitting methods for the incompressible Navier-Stokes equations. *Journal of Computational Physics 97*, 2 (1991), 414 – 443.

[78] KARSA, D. R., AND HOUSTON, J. *What are Surfactants?* Blackwell Publishing Ltd, 2007, pp. 1–23.

[79] KHATRI, S., AND TORNBERG, A.-K. A numerical method for two phase flows with insoluble surfactants. *Computers and Fluids 49* (2011), 150–165.

[80] KHATRI, S., AND TORNBERG, A.-K. An embedded boundary method for soluble surfactants with interface tracking for two-phase flows. *Journal of Computational Physics 256* (2014), 768 – 790.

[81] KLOUEK, P., AND RYS, F. S. Stability of the fractional step theta-scheme for the nonstationary Navier-Stokes equations. *SIAM Journal on Numerical Analysis 31*, 5 (1994), 1312–1335.

[82] KORTEWEG, D. J. Sur la forme que prennent les équations du mouvements des fluides si l'on tient compte des forces capillaires causées par des variations de densité considérables mais connues et sur la théorie de la capillarité dans l'hypothèse d'une variation continue de la densité. *Archives Néerlandaises des Sciences exactes et naturelles 6* (1901), 1–24.

[83] KRALOVA, I., AND SJBLOM, J. Surfactants used in food industry: A review. *Journal of Dispersion Science and Technology 30*, 9 (2009), 1363–1383.

[84] LAI, M.-C., TSENG, Y.-H., AND HUANG, H. An immersed boundary method for interfacial flows with insoluble surfactant. *Journal of Computational Physics 227* (2008), 7279–7293.

[85] LANGMUIR, I. A new adsorption isotherm. *J. Am. Chem. Soc 40* (1918), 1361–1403.

[86] LARSON, R. G. *The structure and rheology of complex fluids*, vol. 150. Oxford university press New York, 1999.

[87] LAUGEL, C., BAILLET, A., PIEMI, M. P. Y., MARTY, J., AND FERRIER, D. Oil-water-oil multiple emulsions for prolonged delivery of hydrocortisone after topical application: comparison with simple emulsions. *International Journal of Pharmaceutics 160*, 1 (1998), 109 – 117.

[88] LEE, J., AND POZRIKIDIS, C. Effect of surfactants on the deformation of drops and bubbles in navierstokes flow. *Computers & Fluids 35*, 1 (2006), 43 – 60.

[89] LIONS, P.-L., AND MOULDEN, T. Mathematical topics in fluid mechanics, volume 1: Incompressible models. *APPLIED MECHANICS REVIEWS 50* (1997), B81–B81.

[90] LIU, C., AND SHEN, J. A phase field model for the mixture of two incompressible fluids and its approximation by a Fourier-spectral method. *Physica D: Nonlinear Phenomena 179*, 34 (2003), 211 – 228.

[91] LIU, C., SHEN, J., AND YANG, X. Decoupled energy stable schemes for a phase-field model of two-phase incompressible flows with variable density. *Journal of Scientific Computing 62*, 2 (2015), 601–622.

[92] LIU, H., AND ZHANG, Y. Phase-field modeling droplet dynamics with soluble surfactants. *Journal of Computational Physics 229* (2010), 9166–9187.

[93] LOWENGRUB, J., AND TRUSKINOVSKY, L. Quasi-incompressible Cahn–Hilliard fluids and topological transitions. *Proceedings of the Royal Society of London. Series A: Mathematical, Physical and Engineering Sciences 454* (1998), 2617–2654.

[94] MARCHUK, G. I., AND RUZICKA, J. *Methods of numerical mathematics*, vol. 2. Springer-Verlag New York, 1975.

[95] MINJEAUD, S. An unconditionally stable uncoupled scheme for a triphasic Cahn-Hilliard/Navier-Stokes model. *Numerical Methods for Partial Differential Equations 29*, 2 (2013), 584–618.

[96] MODICA, L., AND MORTOLA, S. Un esempio di Gamma-convergenza. *Boll. Un. Mat. Ital. B 14*, 5 (1977), 285–299.

[97] MÜLLER-URBANIAK, S. *Eine Analyse dex Zweischritt-θ-Verfahrens zur Lösung der instationären Navier-Stokes-Gleichungen*. PhD thesis, University of Heidelberg, 1994.

[98] MURADOGLU, M., AND TRYGGVASON, G. A front-tracking method for computation of interfacial flows with soluble surfactants. *Journal of Computational Physics 227* (2008), 2238–2262.

[99] MYERS, D. *The Organic Chemistry of Surfactants*. John Wiley & Sons, Inc., 2005, pp. 1–79.

[100] NOCHETTO, R. H., AND PYO, J.-H. The gauge–uzawa finite element method. part i: The navier–stokes equations. *SIAM Journal on Numerical Analysis 43*, 3 (2005), 1043–1068.

[101] OSHER, S., AND FEDKIW, R. P. Level set methods: An overview and some recent results. *Journal of Computational Physics 169*, 2 (2001), 463 – 502.

[102] OSHER, S., AND SETHIAN, J. A. Fronts propagating with curvature-dependent speed: Algorithms based on hamilton-jacobi formulations. *Journal of Computational Physics 79*, 1 (1988), 12 – 49.

[103] OSHER, S., AND SETHIAN, J. A. *Foundations for Momentum Transfer*. Springer US, Boston, MA, 2007, pp. 107–158.

[104] PEACEMAN, D. W., AND H. H. RACHFORD, J. The numerical solution of parabolic and elliptic differential equations. *Journal of the Society for Industrial and Applied Mathematics 3*, 1 (1955), 28–41.

[105] POESIO, P., DAMONE, A., AND MATAR, O. K. Slip at liquid-liquid interfaces. *Phys. Rev. Fluids 2* (Apr 2017), 044004.

[106] POPESCU, M. N., OSHANIN, G., DIETRICH, S., AND CAZABAT, A.-M. Precursor films in wetting phenomena. *Journal of Physics: Condensed Matter 24*, 24 (2012), 243102.

[107] PU, W.-F., GU, J.-Y., ZHAO, T.-H., TANG, Y.-L., ZHAO, L., AND LU, L.-M. Stability and adsorption of multiphase foam system with high temperature resistance. *Journal of Dispersion Science and Technology 0*, 0 (2017), 1–9.

[108] PYO, J.-H., AND SHEN, J. Gauge-Uzawa methods for incompressible flows with variable density. *Journal of Computational Physics 221*, 1 (2007), 181 – 197.

[109] ROSEN, M. J., AND KUNJAPPU, J. T. *Characteristic Features of Surfactants*. John Wiley & Sons, Inc., 2012, pp. 1–38.

[110] ROSEN, M. J., AND KUNJAPPU, J. T. *Reduction of Surface and Interfacial Tension by Surfactants*. John Wiley & Sons, Inc., 2012, pp. 235–271.

[111] ROSEN, M. J., AND KUNJAPPU, J. T. *Wetting and Its Modification by Surfactants*. John Wiley & Sons, Inc., 2012, pp. 272–307.

[112] ROWLINSON, J. Translation of JD van der Waals' the thermodynamik theory of capillarity under the hypothesis of a continuous variation of density. *Journal of Statistical Physics 20*, 2 (1979), 197–200.

[113] ROWLINSON, J. S., AND WIDOM, B. *Molecular theory of capillarity*. Courier Corporation, 2013.

[114] RTZ, A., RIBALTA, A., AND VOIGT, A. Surface evolution of elastically stressed films under deposition by a diffuse interface model. *Journal of Computational Physics 214*, 1 (2006), 187 – 208.

[115] SHAH, D. O. *Improved oil recovery by surfactant and polymer flooding*. Elsevier, 2012.

[116] SHEN, J. A remark on the projection-3 method. *International Journal for Numerical Methods in Fluids 16* (1993), 249–253.

[117] SHEN, J., AND YANG, X. Energy stable schemes for Cahn-Hilliard phase-field model of two-phase incompressible flows. *Chinese Annals of Mathematics, Series B 31*, 5 (2010), 743–758.

[118] SHEN, J., AND YANG, X. A phase-field model and its numerical approximation for two-phase incompressible flows with different densities and viscosities. *SIAM Journal on Scientific Computing 32*, 3 (2010), 1159–1179.

[119] SHEN, J., AND YANG, X. Decoupled, energy stable schemes for phase-field models of two-phase incompressible flows. *SIAM Journal on Numerical Analysis 53*, 1 (2015), 279–296.

[120] STERNBERG, P. Vector-valued local minimizers of nonconvex variational problems. *Rocky Mountain J. Math. 21*, 2 (1991), 799–807. Current directions in nonlinear partial differential equations (Provo, UT, 1987).

[121] STINNER, B. Surface energies in multi-phase systems with diffuse phase boundaries. In *Free boundary problems*, vol. 154 of *Internat. Ser. Numer. Math.* Birkhäuser, Basel, 2007, pp. 413–423.

[122] STINNER, B., NESTLER, B., AND GARCKE, H. A diffuse interface model for alloys with multiple components and phases. *SIAM Journal on Applied Mathematics 64*, 3 (2004), 775–25.

[123] STONE, H. A. Dynamics of drop deformation and breakup in viscous fluids. *Ann. Rev. Fluid Mech. 26* (1994), 65–102.

[124] STRANG, G. On the construction and comparison of difference schemes. *SIAM Journal on Numerical Analysis 5*, 3 (1968), 506–517.

[125] TADROS, T. F. *Applied Surfactants:Principles and Applications*. Wiley-VCH Verlag GmbH & Co. KGaA, 2005.

[126] TEIGEN, K., LI, X., LOWENGRUB, J., WANG, F., AND VOIGT, A. A diffuse-interface approach for modeling transport, diffusion and adsorption/desorption of material quantities on a deformable interface. *Communications in Mathematical Sciences 7*, 4 (2009), 1009–1037.

[127] TEIGEN, K. E., SONG, P., LOWENGRUB, J., AND VOIGT, A. A diffuse-interface method for two-phase flows with soluble surfactants. *Journal of Computational Physics 230*, 2 (2011), 375 – 393.

[128] TÉMAM, R. Sur l'approximation de la solution des équations de navier-stokes par la méthode des pas fractionnaires (i). *Archive for Rational Mechanics and Analysis 32*, 2 (1969), 135–153.

[129] TÉMAM, R. Sur l'approximation de la solution des équations de navier-stokes par la méthode des pas fractionnaires (ii). *Archive for Rational Mechanics and Analysis 33*, 5 (1969), 377–385.

[130] TEMAM, R. *Navier-Stokes equations and nonlinear functional analysis*, vol. 66. Siam, 1995.

[131] TEMAM, R. *Navier-Stokes equations: theory and numerical analysis*, vol. 343. American Mathematical Soc., 2001.

[132] TIDDY, G. Surfactant-water liquid crystal phases. *Physics Reports 57*, 1 (1980), 1 – 46.

[133] TIERRA, G., AND GUILLÉN-GONZÁLEZ, F. Numerical methods for solving the Cahn-Hilliard equation and its applicability to related energy-based models. *Archives of Computational Methods in Engineering 22*, 2 (2015), 269–289.

[134] TUREK, S. A comparative study of time-stepping techniques for the incompressible Navier-Stokes equations: From fully implicit non-linear schemes to semi-implicit projection methods. *International Journal for Numerical Methods in Fluids 22*, 10 (1996), 987–1011.

[135] VILLANI, A. Another note on the inclusion $l^p(\mu) \subset l^q(\mu)$. *The American Mathematical Monthly 92*, 7 (1985), 485–487.

[136] WARD, A. F. H., AND TORDAI, L. Time-dependence of boundary tensions of solutions i. the role of diffusion in time-effects. *The Journal of Chemical Physics 14*, 7 (1946), 453–461.

[137] WONG, H., RUMSCHITZKI, D., AND MALDARELLI, C. On the surfactant mass balance at a deforming fluid interface. *Physics of Fluids (1994-present) 8*, 11 (1996), 3203–3204.

[138] XU, J., LI, Z., LOWENGRUB, J., AND ZHAO, H. A level-set method for interfacial flows with surfactant. *Journal of Computational Physics 212*, 2 (2006), 590–616.

[139] XU, K., BOOTY, M. R., AND SIEGEL, M. Analytical and computational methods for two-phase flow with soluble surfactant. *SIAM Journal on Applied Mathematics 73*, 1 (2013), 523–548.